The synthesis of bimane constrained peptides and their fluorescent and structural properties

The University of Adelaide

School of Physical Sciences

Department of Chemistry

Submitted in fulfilment of the degree

Master of Philosophy (Chemical Sci)

Presented by

Aimee Horsfall $B.Sc.$ *(MDD)*

Supervisor(s): Professor Andrew Abell
& Dr. Sabrina Heng

October 2016

Declaration

I certify that this work contains no material which has been accepted for the award of any other degree or diploma in my name, in any university or other tertiary institution and, to the best of my knowledge and belief, contains no material previously published or written by another person, except where due reference has been made in the text. In addition, I certify that no part of this work will, in the future, be used in a submission in my name, for any other degree or diploma in any university or other tertiary institution without the prior approval of the University of Adelaide and where applicable, any partner institution responsible for the joint-award of this degree.

I give consent to this copy of my thesis, when deposited in the University Library, being made available for loan and photocopying, subject to the provisions of the Copyright Act 1968.

I also give permission for the digital version of my thesis to be made available on the web, via the University's digital research repository, the Library Search and also through web search engines, unless permission has been granted by the University to restrict access for a period of time.

Aimee Jade Horsfall

31/10/2016

Abstract

Aberrant protein-protein interactions often result in disease, and as such, effective protein-protein interaction inhibitors are needed to mitigate the disease state. These interaction interfaces often involve secondary structural motifs, for example, an α-helix or β-sheet. Small molecule drugs are not well suited to inhibit protein-protein interactions however constrained peptides, have shown to have great therapeutic potential.[1-17] Short peptides display little secondary structure in aqueous solution and as such, peptide sequences derived from a protein-protein interaction interface for use as a protein-protein interaction inhibitor, must be constrained into the native secondary structure. This can be achieved by installing a linker between the side-chains of two appropriately spaced amino-acids in the sequence. Many different linker chemistries have been designed and implemented with good biological results. However, these constrained peptide therapeutics are still restricted by traditional small-molecule drug hurdles including cell permeability, protease degradation and the ability to visualise and track a molecule intracellularly. Linkers such as the all-hydrocarbon metathesis linker have shown great promise in reducing protease degradation and increasing cell permeability,[3, 7, 18-21] however a fluorescent tag is still necessary to visualise a drug candidate. Here, a bimane linker is proposed as a new peptide linker to help overcome these limitations. Dibromobimane is reacted with thiol-containing amino-acid side chains to introduce a new fluorescent constraint in a series of model peptides. The reaction conditions with dibromobimane are optimised in solution to reveal that a buffered system is required for the cyclisation to occur efficiently. Optimal reaction conditions, determined by monitoring the increase of the fluorescent product, were 0.5 mg/ml peptide in 10 mM PBS with one equivalent of dibromobimane. The reaction was shown to be facile and versatile; in this thesis an array of peptides with varied sequence length, constraint length and amino-acid composition were cyclised under the same conditions, all reaching reaction completion in under 30 minutes. Additionally, these same conditions were applied successfully to react monobromobimane with series of short peptides. Cyclisation on reaction with

dibromobimane, was also demonstrated on-resin with similar efficiency. The fluorescent properties of the resultant peptides were then explored to reveal that pH does not affect the observed fluorescence however a longer peptide length resulted in greater fluorescence intensity. Furthermore, acyclic mono-bimane-functionalised peptides displayed lower fluorescence intensity than the bimane-cyclised counterparts. The fluorescence of the bimane cyclised peptide could be detected as low as 10 nM on a plate reader, which is expected to further improve on a more sensitive instrument. The secondary structure of a series of tri- and penta-peptides were investigated through CD and NMR techniques. It was deduced that the bimane linker can induce β-strand like structure in an *i-i*+2 constrained peptide; in contrast an *i-i*+4 constrained pentapeptide with homocysteine in the 1 and 5 positions results in a 3_{10} helical like structure. β-alanine containing analogues of these peptides were also synthesised and showed minimal structure.

This work outlines the synthesis of macrocyclic peptides containing a peptide constraint, in the form of a fluorescent bimane, both in solution and on-resin to produce cyclised peptides. The fluorescent properties of the resultant peptides have been shown to be biologically compatible with great fluorescence sensitivity. Furthermore, different secondary structure can be introduced by simply alterations of the constraint length from *i-i*+2 to *i-i*+4. This work provides a foundation on which to design new fluorescent bimane-cyclised peptide-based protein-protein interaction inhibitors.

Acknowledgments

I owe a huge thanks to my supervisor Prof. Andrew Abell for his continuous support over the last couple years, both in science and my personal circumstances. I would not have been able to complete this degree without the huge assistance you have provided above and beyond what was called of you. Thank you for continually pushing me to produce work of increasing quality and never letting me settle for second best.

Thank you to Kelly Keeling, who taught me the ropes and made me feel at home in a new and rather daunting environment that is the research lab. Thank you to Sabrina Heng, for the guidance and motivational support to put things in perspective when I have needed it the most. Thank you to Denis Scanlon and Kate Wegner for allowing me to continually pick their brains and wealth of knowledge.

The last couple of years have been an absolute rollercoaster and without a huge support team both academically and socially I would not be filling in this final addition to my thesis. To Irene, there is no way I could have picked a better desk-buddy to help see me through the first year of research, thank you for all the laughs, I'm so glad our friendship has lasted since you left. To Kirby, my sanity would have been far worse off without you as a wall to sound ideas off of whether that was over a coffee, beer or test tube. To all of you whom I shared a beer with at the end of a long day, when science decided cooperating was over-rated - you are what makes me love science when I hate it the most, in particular to the regular Friday crew of Tash, Oli, Kate. Harley you earn a special mention for always turning up at the most opportune times and suffering through my drafts in the last week. To Cohen and Matt, for the

endless ~~mind numbing~~ hilarious videos, wines and knowing when its best to not ask or just nodding when you have no idea what I've started rambling about.

Pat, thank you for bearing with me on the days of little sanity, the early mornings, the even later nights, and providing an endless stream of coffee and love; and for trying to understand, even when you really don't. This would have been all the harder without your support and encouragement.

Mum and Dad, despite the cliché, I would not be here, handing up this work, without you. Thank you for supporting me in my decision to move away, and for always fuelling my fire to do better. In spite of the distance from home, this has been one of the most rewarding, yet challenging experiences I have endured. To Lachlan, thank you for the endless stream of memes (selected specifically for my current circumstance), laughs, binge TV sessions and adventures every time we catch up, if only we could make them more often.

I have learnt so much more, in the last year, about science and myself, than in the last ten and have grown so much as a result – I hope you would agree. Although this has been by far the most challenging mental experience of my life, above all else, it has highlighted what an awesome support group surrounds me and just how lucky I am for that. Thank you, to you all so much. Here's to the next four years!

Abbreviations

AAB: Ammonium acetate buffer; **Ac₂O**: Acetic anhydride; **ACN**: Acetonitrile; **dBB**: Dibromobimane; **CD:** Circular Dichroism; **DCM**: Dichloromethane; **DIPEA**: *N,N*-Diisopropylethylamine; **DMF**: *N,N'*-Dimethylformamide; **DMSO:** Dimethylsulfoxide; **DODT**: 2,2′-(Ethylenedioxy)diethanethiol; **Fmoc**: 9-Fluorenylmethoxycarbonyl; **HATU:** 1-[Bis(dimethylamino)methylene]-1H-1,2,3-triazolo[4,5-b]pyridinium 3- oxid hexafluorophosphate; **HCy:** Homocysteine; **HOBt:** 1-Hydroxybenzotriazole hydrate; **HPLC:** High Performance Liquid Chromatography; **HRMS:** High Resolution Mass Spectrometry; **LCMS**: Liquid Chromatography Mass Spectrometry; **mBB**: Monobromobimane; **Mmt:** 4-Methoxytrityl; **NMR**: Nuclear Magnetic Resonance; **Pbf**: 2,2,4,6,7-pentamethyldihydrobenzofuran-5-sulfonyl; **PBS:** Phosphate buffered saline; **PPI:** Protein-protein interaction; **PyBOP** : (Benzotriazol-1-yloxy)tripyrrolidinophosphonium hexafluorophosphate; **RP-HPLC**: Reverse-Phase High Performance Liquid Chromatography; **SPPS**: Solid-phase peptide synthesis; **TFA**: Trifluoroacetic acid; **TFE**: 2,2,2-Trifluoroethanol; **TIPS**: Triisopropylsilane; **TNBS**: 2,4,6-Trinitrobenzenesulfonic acid; **Trt:** Trityl.

Table of Contents

Chapter 1: Introduction

1.1 Protein-protein interactions in disease

A large majority of diseases are the result of protein function gone awry.[3, 7, 8, 18, 22-31] This may be a result of protein absence, over abundance, or an inability to carry out a designated role. Each protein may have many interaction partners, each related to a separate biological pathway.[22, 27] It is essential these interactions occur with a high level of specificity to allow tight regulation of each individual pathway. Protein interactions are defined by protein shape, thereby inherently linking the shape of a protein to its function.[27, 28, 32, 33] Consequently, alterations of protein shape result in modified, or loss of, function. Therefore, changes in protein structure in turn often lead to disease; however exploiting these modifications can provide an avenue to mitigate the disease state.[8, 18, 28-42] Through understanding the structure of proteins involved in disease, therapeutics can be better designed.

Traditional small-molecule drugs are not well suited to target protein-protein interactions (PPIs) as the protein-drug interface is small.[32, 37] Therefore, in a disease resultant from an overabundant protein, a small-molecule inhibitor would be readily displaced from the interaction site by the native partner protein. Furthermore, due to this small surface area of contact, it is very difficult to design a small-molecule inhibitor that can specifically target one protein site.[30, 33, 37, 42] Small-molecule PPI inhibitors target a limited area of contact, and consequently there is a low probability that the amino-acid sequence involved in the interaction is unique. Hence, small molecule PPI inhibitor specificity is inherently low, thereby lowering drug efficacy while increasing the likelihood of side-effects. It should also be noted that the exterior surface of a protein is relatively flat and featureless,[27, 28, 30, 33, 37] further increasing the difficultly to design an effective, reversible PPI inhibitor. Hence, for many years, PPIs have been considered 'undruggable'. Now, the development of PPI inhibitors has expanded dramatically through the exploration of constrained peptides.

Constrained peptides provide a large interaction surface area thereby reducing the likelihood to be readily displaced. Furthermore, by deriving the amino-acid sequence of a constrained peptide from the native partner protein, a PPI inhibitor can provide enhanced specificity, consequently reducing potential side effects.[30, 33, 42] To understand the design of these inhibitors, the nature of secondary structure must first be discussed, and its importance in PPIs.

1.2 Protein structure

There are four levels of structure that define protein shape, as depicted in Figure 1. Primary structure comprises the linear sequence of amino-acids covalently bound through amide bonds. This first level of structure also encompasses all covalent crosslinking within the sequence, for instance, disulphide bonds between cysteine residues. Secondary structure arises from hydrogen bonding interactions between backbone amides, which result in small segments of well defined structure such as an α-helix or β-sheet.[43, 44] These motifs form integral binding domains for PPIs. The third level of protein structure, tertiary structure, arises from a series of non-covalent interactions between amino-acid side chains. These secondary bonds affect the three-dimensional shape of the polypeptide. Lastly, quaternary structure describes the assembly of multiple poly-peptide subunits, associating to form a functional protein complex. In this work, the focus will be on the secondary structure.
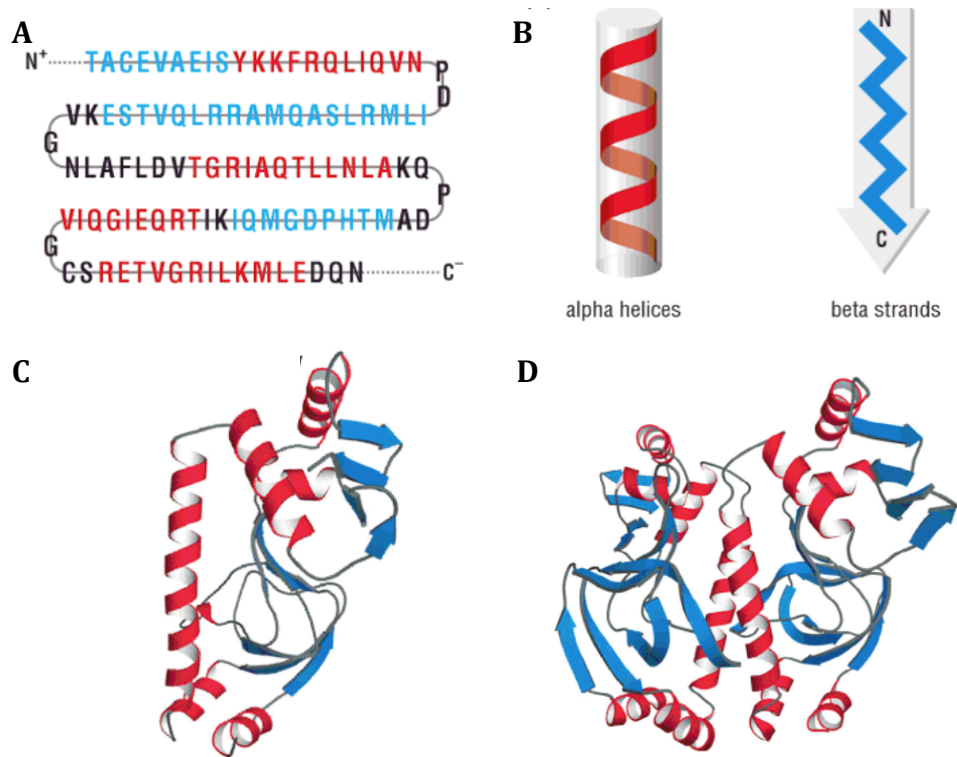
Figure 1: The four levels of protein structure which result in a functional protein complex (Ref. 26)

Secondary structural elements are of great importance in PPIs due to the defined conformation of each motif.[46] Each turn of an α-helix, comprises an average of 3.6 amino-acids, and is formed through hydrogen bonding interactions between residues two or three amino-acids apart,[47] as shown in Figure 3. These interactions are described by specific nomenclature. The initial residue in the motif is termed the ith amino-acid and the following C-terminal amino-acid the $i+1$ residue, then next the $i+2$ etc. Therefore, an α-helix is formed through hydrogen bonding of the ith carbonyl and the amine of the i+4th residue, the $i+4^{th}$ carbonyl to the $i+7^{th}$ amine, then the $i+7^{th}$ carbonyl to the $i+11^{th}$ amine and so on until the motif is terminated. Consequently, this results in the side chain of the ith residue to lie on the same face of the helix as the $i+4$, $i+7$ and $i+11$ etc. side-chain as shown in Figure 2 where the $i+7$, $i+4$, $i+11$ and i^{th} residue are adjacent on the helix face. Protein-protein interactions may occur through one or more faces of a helix. Therefore it is important to know which of the amino-acids, within the linear sequence, are positioned in proximity when in the native 3D conformation.
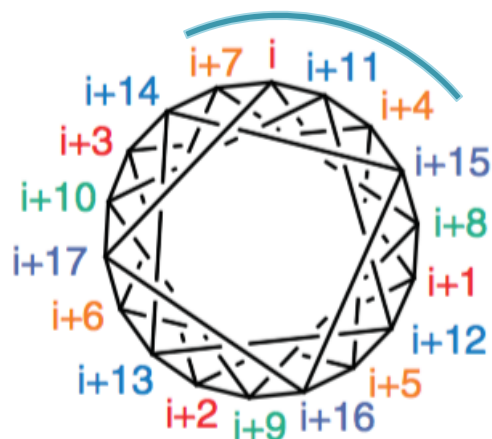
Figure 2: Wheel diagram depicting the position of each successive amino-acid side-chain when looking down the 'barrel' of an α-helix. Consequently, the *i*, *i*+4, *i*+7 and *i*+11 residues lie on the same face of the α-helix. (Ref. 48)

β-Sheets also play an important role in protein interactions.[46] Hydrogen bonds are formed between consecutive backbone amides, from different sections of the peptide, to result in a sheet-like structure,[49] as shown in Figure 3. "Pleating" of this sheet results from the tetrahedral arrangement of the α-carbon. Multiple peptide strands can associate to horizontally extend the β-sheet structure. Each of these peptide strands may be locally or distally positioned in the amino-acid sequence relative to one another, or from a separate polypeptide. Overall, this gives rise to a sheet-like structure comprised of two or more strands, where the backbone amides lie in the face of the sheet. Every second amino-acid side-chain, lies on the same side of the sheet, perpendicular to the sheet plane. That is, the *i*, *i*+2 and *i*+4 residue side-chains (etc.) will lie on the same side of the β-sheet. A β-strand is simply one-strand in the same conformation as if it were part of a β-sheet.
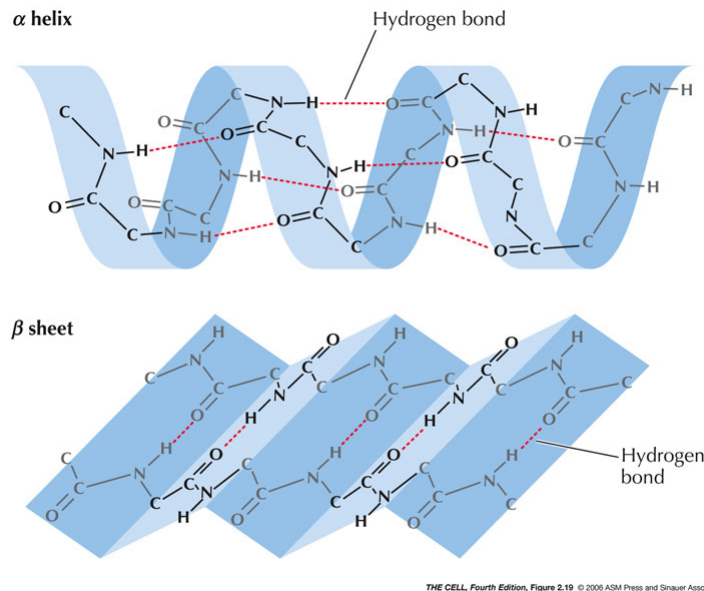
THE CELL, Fourth Edition, Figure 2.19 © 2006 ASM Press and Sinauer Associates, Inc.

Figure 3: The characteristic hydrogen bonding networks of the α-helix and β-sheet. The overall secondary structure is represented in blue, and the hydrogen bonds are shown as red dashed lines. (Ref 50)

All other secondary structural elements, including the 3_{10} helix and various turns, can all be defined in the same manner and also are characterised by specific side-chain orientations. For example, a 3_{10} helix is similar to an α-helix, however only comprises three amino-acids per turn over a rise of 2.0 Å, resulting in a much tighter helix. Therefore the side chains of the i, $i+3$, $i+6$ etc. residues lie on the same side of the helix. These structures are most commonly found at the termini of α-helices.[43, 51]

There are many types of turns just as there are many types of helices. Similarly, turns are defined by the number of amino-acids between hydrogen-bonding residues. For example, an α-turn is a result of hydrogen-bonding between the backbone of the i and $i+4$ residue (c.f. α-helix); a β-turn is formed through the hydrogen bonding of the i and $i+3$ residue; and a γ-turn describes the hydrogen-bonding of the i and $i+2$ residues.[52] These secondary structures are not extended, in contrast to a helix or sheet, and therefore do not form repeating units and only comprise one hydrogen bond. The side-chains of the amino-acids within the turn are usually positioned on the turn exterior.

In summary, secondary structural elements pre-arrange a unique sequence of amino-acid residues into a defined conformation. This specific fixed configuration of the side-chain

residues lends to the importance of these motifs in protein-interactions. Consequently as these structural elements, and the associated binding interactions, can be defined and are well characterised, they present as a good target to exploit in the design of PPI inhibitors.[30, 33, 34, 40, 46]

1.3 Methods for determining secondary structure

There have been many techniques developed, in both biology and chemistry, to determine which residues are involved at the interface of protein-protein interactions. Furthermore, the secondary structure of the participating elements can be elucidated. Consequently, an α-helix or β-strand (etc.) may be revealed at a PPI interface, and therefore identified as a lead structure to develop a new therapeutic. However to develop a peptide-based PPI inhibitor, with the same structure as this interface motif, the secondary structure of this compound needs to be fully characterised. There are many ways this can be achieved. Here circular dichroism (CD) and nuclear magnetic resonance (NMR) spectroscopy techniques will be discussed as secondary structural analysis tools.

1.3.1 Circular Dichroism

In this technique, the compound of interest is irradiated with circularly polarised light from the far-UV region of the Electromagnetic Resonance (EMR) spectrum. Peptides or proteins show characteristic maxima or minima between 195-260 nm, related to the secondary structural elements present. A helical protein will display minima at 208 and 222 nm, and a maximum at 190 nm.[53-55] It should be noted that for short peptides (< 40 residues) this second minima occurs at 215 nm, as opposed to 222 nm.[56] The ratio between these two minima ($\theta_{215 \text{ or } 222}/\theta_{208}$) can indicate the nature of the helix. A $\theta_{(215 \text{ or } 222)/208}$ of approximately 0.90 is indicative of an α-helix, whereas a ratio of 0.47 suggests 3_{10} helicity.[57] β-Sheet structure induces a minimum at 214 nm and maxima at 195 nm, compared to a random coil structure where there is a large minimum below 200 nm.[53-55] These maxima and mimima are a result of specific electronic transitions that occur in the characteristic secondary structure when irradiated with

UV light. The analyte in solution may be in equilibrium between structural states. A CD spectrum represents the 'average' of all the structures present. Consequently, a dynamic or not well defined structure may result in a uninformative or difficult to analyse spectrum.[55, 58]

1.3.2 Nuclear Magnetic Resonance Spectroscopy

Coupling constants

The defined hydrogen bonding arrays of secondary structural motifs restrict the polypeptide backbone and consequently give rise to characteristic torsional angles described as ω, ϕ and ψ as shown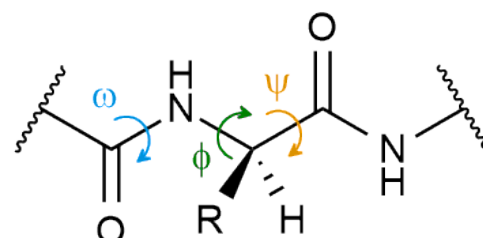 in Figure 4. These angles can be experimentally measured by NMR and are subsequently used as a diagnostic tool to resolve the secondary structure present in a

Figure 4: Torsional angles of the amide backbone defined as ω, φ and ψ.

peptide or protein. Each kink in the backbone forces both the protons directly attached, and on the side-chains into different conformations. Coupling constants describe interactions between two protons and can provide information about the similarity of the environments these protons exist in. Consequently, information about the proton position in space can be derived. The $^3J_{HNH\alpha}$ coupling can be easily determined via a well resolved 1D or 2D spectrum of the α-hydrogen or NH amide signals. This value can be related to the ϕ angle by the Karplus equation, below.[59]

$$^3J_{HNH_\alpha} = 6.4 \cos^2 \theta - 1.4 \cos \theta + 1.9$$

$$\text{Where } \theta = |\phi - 60°|$$

Therefore, a $^3J_{HNH\alpha}$ greater than 8 Hz indicates a ϕ angle corresponding to an extended β-strand like structure.[59] An α -helical structure is indicated by a ϕ value of -57° which relates to a $^3J_{HNH\alpha}$ of 3.9 Hz, however it is generally accepted that a $^3J_{HNH\alpha}$ less than 6 Hz suggests a helical structure.[60] The φ angle is more difficult to determine and most commonly requires the preparation of a ^{15}N doped sample to allow collection of a ^{15}N-^{13}C HSQC spectrum.

Nuclear Overhauser Effect NMR crosspeaks

The characteristic folding of secondary structural elements results in distinct nuclear Overhauser effect (NOE) cross-peaks in a 2D NOESY (or ROESY) spectra. For an α-helix, there are strong interactions between the α-hydrogen of the ith residue and the amide hydrogen of the $i+4$ and $i+3$ residue (referred to as $d_{\alpha N}(i,i+4)$ and $d_{\alpha N}(i,i+3)$ respectively), whereas for a 3_{10} helix the $d_{\alpha N}(i,i+4)$ is not observed. For a β-sheet structure only strong $d_{\alpha N}(i,i+1)$ interactions are evident, along with weak $d_{NN}(i,i+1)$ cross-peaks. A summary of the anticipated interactions for various secondary structural elements are shown in Figure 5.[59][61, 62]

Figure 5: The anticipated NOEs for various secondary structural elements along with the idealised $J_{HNH\alpha}$ values. The thickness of an interaction line indicates increased strength of the NOE. (Ref 59)

Chemical Shift Index

Chemical shift has also been demonstrated as a useful technique to indicate the secondary structural environment. For each individual amino-acid a standard random-coil chemical shift for the α-hydrogen, α-carbon, β-carbon and carbonyl carbon have been experimentally determined.[62-66] It was elucidated that when an amino-acid was observed in a secondary structural motif, the chemical shift would undergo a definable change. Particularly the α-hydrogen, α-carbon and carbonyl carbon shifted in a very characteristic manner.[62-66] That is, for an α-helical structure, the α-hydrogen of an amino-acid will decrease by at least 0.1 ppm,

or increase by a minimum of 0.1 ppm for a β-sheet. All these shifts are summarised in Figure 6.[64]

CHEMICAL SHIFT VALUES FOR BACKBONE ATOMS USED IN DETERMINATION OF
SECONDARY STRUCTURE[a]

Residue	α-^{1}H range	2-^{13}C range	1-^{13}C range
Ala	4.35 ± 0.10	52.2 (+0.8, −0.5)	177.6 ± 0.5
Cys	4.65 ± 0.10	56.8 (+0.8, −0.5)	174.1 ± 0.5
Asp	4.76 ± 0.10	53.9 (+0.8, −0.5)	176.8 ± 0.5
Glu	4.29 ± 0.10	56.5 (+0.8, −0.5)	176.6 ± 0.5
Phe	4.66 ± 0.10	57.9 (+0.8, −0.5)	175.5 ± 0.5
Gly	3.97 ± 0.10	45.0 (+0.8, −0.5)	173.6 ± 0.5
His	4.63 ± 0.10	55.5 (+0.8, −0.5)	174.9 ± 0.5
Ile	3.95 ± 0.10	61.2 (+0.8, −0.5)	176.5 ± 0.5
Lys	4.36 ± 0.10	56.5 (+0.8, −0.5)	176.5 ± 0.5
Leu	4.17 ± 0.10	55.0 (+0.8, −0.5)	176.9 ± 0.5
Met	4.52 ± 0.10	55.2 (+0.8, −0.5)	177.0 ± 0.5
Asn	4.75 ± 0.10	52.7 (+0.8, −0.5)	175.6 ± 0.5
Pro	4.44 ± 0.10	63.0 (+0.8, −0.5)	176.0 ± 0.5
Gln	4.37 ± 0.10	56.0 (+0.8, −0.5)	175.6 ± 0.5
Arg	4.38 ± 0.10	56.0 (+0.8, −0.5)	176.6 ± 0.5
Ser	4.50 ± 0.10	58.1 (+0.8, −0.5)	174.7 ± 0.5
Thr	4.35 ± 0.10	62.0 (+0.8, −0.5)	175.5 ± 0.5
Val	3.95 ± 0.10	62.2 (+0.8, −0.5)	176.0 ± 0.5
Trp	4.70 ± 0.10	57.6 (+0.8, −0.5)	175.6 ± 0.5
Tyr	4.60 ± 0.10	58.0 (+0.8, −0.5)	175.9 ± 0.5

[a] Data are given in ppm, relative to DSS.

Figure 6: The expected random coil chemical shifts of a peptide in aqueous solution relative to DSS for the αH (α-^{1}H), αC (2-^{13}C) and CO (1-^{13}C) carbon. Shifts which lie outside the specified variances indicate the probability of secondary structure. That is, an αH of less than -0.10 ppm different to the random coil value, αC of more than +0.8 and CO value of more than +0.5 ppm are indicative of α-helical structure, and vice versa for a β-sheet structure. At least four consecutive residues must display the same structural shift to identify a secondary structural element. (Ref 64)

Temperature Coefficients

Lastly, to establish the strength of any apparent hydrogen bonds, amide-based temperature coefficients (Δδ/T) can be calculated by conducting a variable temperature 1D ^{1}H NMR experiment. That is, if a hydrogen bond is held tightly in its conformation, directly or indirectly, the chemical shift of the amide NH participating in this bond will not change by more than -4 ppb/K.

1.4 Constrained peptides

Protein folding is a complex process that most often takes place in the presence of smaller proteins referred to as chaperones or heat shock proteins. Chaperones help mediate the folding of proteins by forcing specific side-chain interactions to occur in a controlled setting.[23, 25, 67-72] It has been shown that without these complexes a polypeptide chain can very rarely fold autonomously, in an aqueous environment, into a functional structure.[18, 23, 72-74] Furthermore, protein structure and folding is cooperative such that one section of a protein helps maintain the structure in another area.[75-77] Consequently, if a portion of the protein is excised then, in most cases, the protein will no longer fold in the same manner. Therefore the protein will display a loss of, or modified function. Similarly, if a section of an amino-acid sequence is removed from its constituent protein, it will no longer exhibit the secondary structure that is apparent when part of the parent protein. That is, an α-helical segment of a protein will not be α-helical, in an aqueous environment, when removed from the native protein.

Structure can be reintroduced into a disordered peptide by exploiting the characteristic amino-acid side chain orientations when part of a secondary structural element. By introducing an appropriate constraint between the *i* and *i*+4/7th residue of a peptide, the signature hydrogen bonding interactions of an α-helix can be reintroduced, thereby re-establishing structure (Figure 7). Constraints can be introduced by incorporating appropriate amino-acids at the required positions to allow cyclisation of the peptide. This may be through direct reaction of the two (natural or unnatural) amino-acids, or by reacting a bifunctional linker precursor with these residues. For example, an aspartic acid and lysine may be reacted to form a lactam constraint,[78] or two cysteines may be cyclised through the introduction of a perfluoro moiety.[79] Unnatural amino-acids have also been incorporated; a prime example is the introduction of terminal-olefin derivatized amino-acids which can undergo ring closing metathesis. [20, 80]
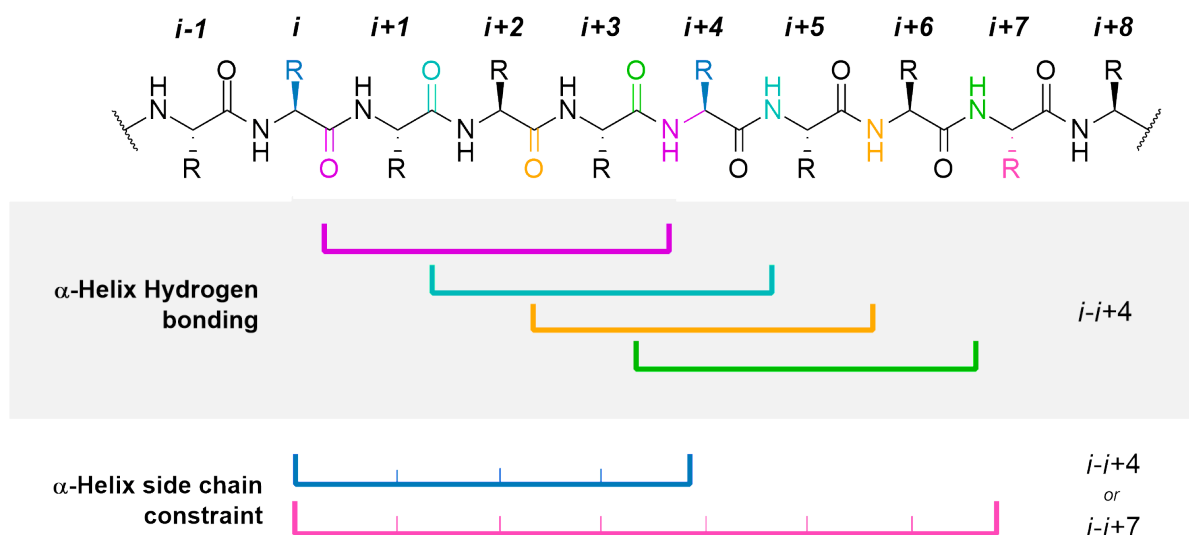
Figure 7: The hydrogen bonds of a natural α-helix form between the *i* and *i*+4 residues of a peptide sequence. These can be reintroduced by constraining between the *i* and *i*+4 or *i* and *i*+7 (or *i* and *i*+11) residue side-chains to re-establish α-helical structure in an unstructured peptide.

The cyclisation process can constrain the peptide and force the *i* and *i*+4/7 residues into close proximity such that a hydrogen bond can be re-established and α-helical geometry re-introduced. Similarly, it has been shown that links of appropriate length between the *i* and *i*+2nd residue side-chains produce β-strand structure.[81]

Conformationally constrained peptides show great promise to act as therapeutics by inhibiting or mediating PPIs related to disease. The amino-acid sequence of the peptide-based PPI inhibitor is most often derived from the aberrant interaction interface. For example, if an α-helix forms the primary interaction with a groove in the partner protein, the amino-acid sequence of the helix will form the lead compound. Constraining this sequence into its native secondary structure allows development of a new PPI inhibitor. These biologically-derived constrained peptides show potential to overcome the inherent issues in targeting PPIs through increased interface surface area, compared to small-molecule inhibitors, coupled with greater specificity introduced by utilising conserved side chain interactions.[3, 4, 7, 8, 10, 13-15, 48, 82-84]

Types of linkers

Many different linkers have been developed since the inception of this area of chemistry.[4, 9, 18, 20, 21, 35, 41, 79-81, 85-92] and many reviews have compared the respective benefits and limitations.[18, 30,

[35, 39, 48, 82, 87, 93] Here, only a few will be discussed to illustrate various factors which need to be considered in designing a PPI inhibitor.

Inspired by the natural constraints within proteins, the disulphide bridge was one of the first cross-linkers explored.[94] This cross-linker has been successfully implemented in the inhibition of the oestrogen receptor α/cofactor interaction.[95] However, the disulphide bond can be reduced in the oxidative environment of a stressed cell. This returns the cysteines to a free thiol form and the PPI inhibitor to an unconstrained form, therefore eliminating PPI inhibitor ability.

Another biologically inspired constraint, the lactam linker (Figure 8, **1**), has proved to be very effective at inducing helicity in short peptides.[17, 78, 86, 96] It is has been implemented in a number of biologically relevant peptides and shown great promise for new therapeutics.[1, 2, 5, 14] However, as the amide of the lactam linker is also a common moiety in biology, specifically in peptides, there are many mechanisms for its degradation. Therefore, similarly to the disulphide bridge, the constraint can be eliminated *in vivo* and the function of the PPI inhibitor removed. In comparison, metathesis reaction of terminal-olefin derivatized amino-acids results in a very biologically stable all hydrocarbon constraint (Figure 8, **2**). The hydrocarbon linker has also been shown to induce helicity comparable to that introduced by the lactam linker, in biologically relevant systems. [3, 21, 80, 97]

A study by de Araujo *et. al.*[86] compared six linkers commonly implemented in the literature, including the metathesis and lactam linker, on a simple alanine-rich sequence (Figure 8). This study will be discussed in more depth in chapter 3, but is a good example of the many factors at play in designing a system that can effectively induce secondary structure into a peptide. It is demonstrated that helicity is not merely dictated by the linker length but also the chemistry and position of the linker substituents as well as the flexibility and steric restrictions imposed by the constraint. This statement is true of the design of any structural peptide constraint. For example, by changing the position of the triazole within the linker of **3** can eliminate any

helicity observed. This work testifies to the inherent complexity of designing a suitable linker, and furthermore how difficult it may be to predict the effect of a linker on a relevant biologically derived peptide sequence.
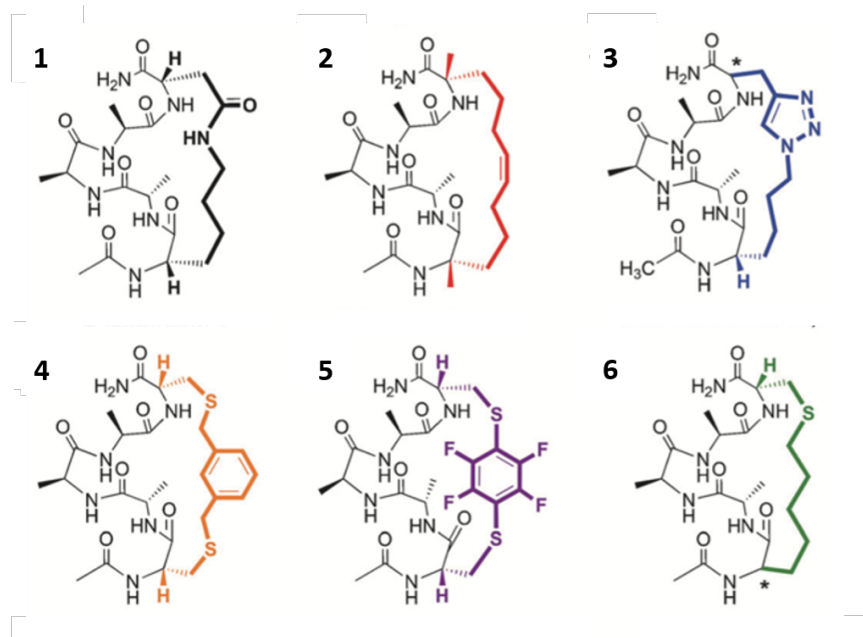

Figure 8: The six linkers above were applied to an alanine-rich pentapeptide sequence and their helicity compared by NMR and CD. The linkers included the lactam (**1**), metathesis (**2**), click/triazole (**3**), m-xylene thioether (**4**), perfluo**ro** (**5**) and an alkyl thioether staple (**6**). (Ref. 86)

Biological considerations

Though many linker chemistries have been developed, the ability to predict the exact effect of a linker, in general or on a specific sequence, is not yet possible. The position of a linker within the peptide sequence can elicit different effects on the structure. Furthermore, the position of the linker must be adjusted to allow optimal interaction with the partner protein *in vivo*.[98] As a result, when developing a new PPI inhibitor, multiple linkers may be trialled in multiple positions in the sequence.

It has been shown that the introduction of a linker, over an amino-acid combination targeted by proteases, can sterically inhibit the protease action and thereby increase the stability of a constrained peptide. However, if a functional group such as the disulphide or lactam is present in the linker, the biostability of the constrained peptide as a PPI inhibitor may be

jeopardised. In contrast, many hydrocarbon stapled peptides have shown enhanced biostability by reducing proteolysis.[3, 80] Not only does the constraint have the ability to protect the backbone from digestion by proteases but additionally the alkyl chain itself is not readily degraded.

Cell permeability, and consequently good bioavailability, is a significant hurdle that must be addressed during the drug design and development process. Peptide fragments often show very poor cell permeability due to their relatively large and polar nature.[30, 42] Some peptide linkers have been shown to enhance the permeability of the constrained peptide fragment.[4, 7, 8, 79, 99] For example, a hydrocarbon staple attached to a BH3 fragment produces a helical and cell permeable product, a significant improvement on the unstructured impermeable linear precursor.[8] The increased hydrophobicity is likely to be a contributing factor to this observation.

Cell permeability and the localisation of any drug within a cell cannot be determined without the ability to probe the molecule. That is, the compound must possess, or be attached to, a fluorescent or radioactive probe to allow tracking and visualisation of the compound. Most compounds are not themselves fluorescent or radioactive and consequently need to be attached to a "tag". Hence, although a hydrocarbon stapled peptide may address both biostability and cell permeability hurdles, further modification of these compounds would still be required to visualise intracellular localisation. Carboxyfluorescein (CF) and fluorescein isothiocyanate (FITC) are two commonly employed fluorescent tags, show in Figure 9. Despite the thorough characterisation and broad application of these substituents, the addition of a large aromatic group may influence the properties of the compound of interest. Multiple assays are often required to prove that cell permeability or biological activity is a result of the designed compound and not induced by the addition of the tag. Furthermore, the assembly of constrained peptides often requires unusual amino-acid derivatives which are often difficult to synthesise. Therefore it is desirable to avoid additional synthetic or purification steps as would be introduced when attaching a tag.
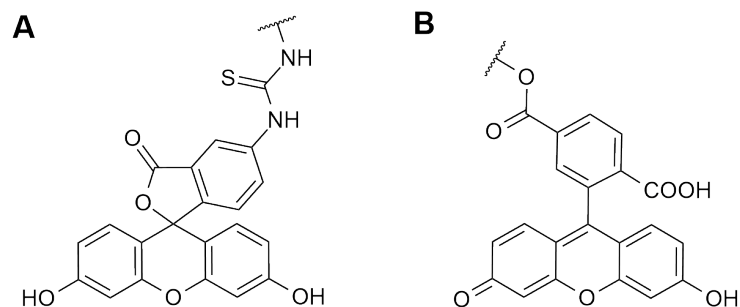
Figure 9: Two typical fluorescent tags, fluorescein isothiocyanate **A)** and carboxyfluorescein **B),** incorporated into potential therapeutics to allow cellular tracking.

Although constrained peptides provide an avenue to target otherwise undruggable PPIs, traditional drug design issues of stability to proteolysis, cell permeability and tracking ability, still apply. Proposed here is a new linker as a potential avenue to design new therapeutics and overcome these issues simultaneously.

1.5 An alternative constraint

Dibromobimane (**7**) is a thiol-selective fluorescent probe that has been utilised under physiological conditions *in vivo* for the purpose of identifying accessible sulfhydryl groups. The class of bromobimanes undergo second order reaction kinetics with thiolate anions to displace the bromine entity and form stable thioether bonds, as shown in Figure 10. [100, 101] In a biological environment this reaction most commonly occurs with hydrogen sulphide, cysteine or glutathione residues.[100-102]
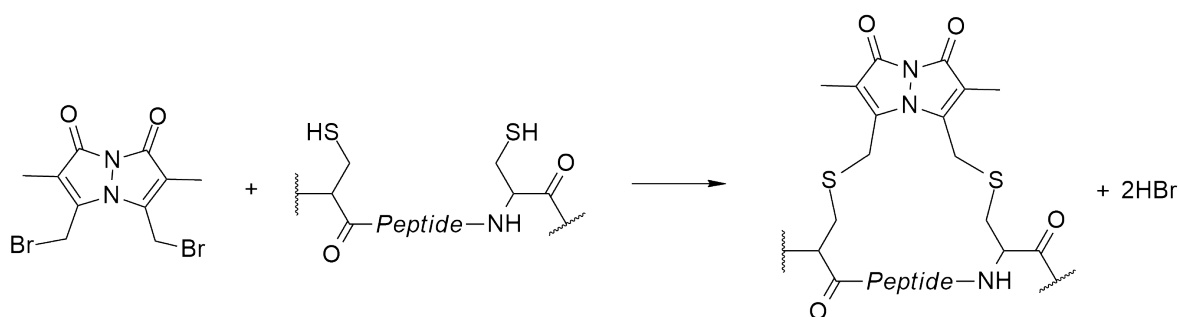

Figure 10: The reaction of dibromobimane with a generic peptide containing two peptide residues. Neither dibromobimane or the peptide on the left-hand side of the equation are fluorescent, however on alkylation the bimane-peptide entity fluoresces with an excitation of 380-390 nm and emission of 475-485 nm.

Both monobromobimane (Figure 11, **8**) and dibromobimane (Figure 11, **7**) are cell permeable[103] and therefore have been used to tag intracellular thiols.[102-106] Bromobimanes are

themselves, not fluorescent. However, upon displacement of the bromo group by a thiol nucleophile, the alkylated bimane becomes highly fluorescent with a reported emission wavelength of 475-485 nm (dependent on the substituent bound).[101, 107] It is reported that the resulting bimane bound peptide/protein displays a high quantum yield and is resistant to fluorescence bleaching upon irradiation. Furthermore it has been reported that the bromobimanes are selective to thiol groups, and do not show a tendency to react with other nucleophiles such as amines. [107]
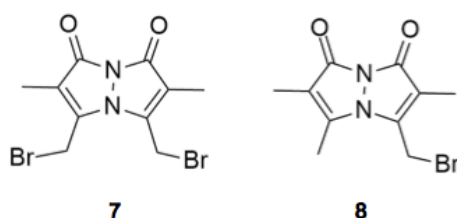

Figure 11: Bromobimanes: Dibromobimane **(7)** and monobromobimane **(8).**

1.5.1 Aims for this thesis

Bimane-constrained peptides present an opportunity to overcome the fundamental biostability, permeability and tracking issues inherent in designing an effective therapeutic. Specifically, the fluorescent nature, facile reaction and established *in vivo* application of dibromobimane define it as a good candidate to produce a simple, fluorescent and permeable peptide-based PPI inhibitor.

The initial aim was to optimise conditions for reaction of dibromobimane with short cysteine containing peptides in an aqueous environment. Simple alanine-rich model peptides incorporating the bifunctional bimane as an *i-i*+2, *i-i*+4 and *i-i*+7 cyclic constraint were synthesised via solid-phase peptide synthesis (SPPS) and the optimised solution-phase bimane-attachment conditions. Unmodified linear versions and acyclic bimane-attached peptide analogues provide controls for NMR and CD studies into the secondary structural changes induced through bimane attachment and cyclisation of the target peptides.

Analogues of alanine-rich i-i+2, i-i+4 and i-i+7 bimane cyclised peptides are also proposed, in which the central alanines are replaced with β-alanine, to investigate the effect of extended backbone length on secondary structure. Similarly, analogues in which natural cysteine is replaced by side-chain extended homocysteine are proposed to explore the effect of an extended constraint size on the backbone secondary structure. The optimised bromobimane reaction conditions were applied to longer alanine-rich 18mer peptides, and a biologically relevant αIIβ3 integrin derived peptide to better define the scope of the bimane-attachment chemistry and resultant secondary structure.

The peptides are characterised by RP-HPLC, MS, NMR, and CD, the fluorescence properties were also investigated including the excitation and emission wavelength. A detection limit was also defined, with explicit intention to prove the applicability of these structures in a biological context for future development of new PPI inhibitors.

Chapter 2: Synthesis and Fluorescent Properties

2.1 Synthesis

2.1.1 Optimisation of solution-phase reaction conditions

Bromobimanes alkylate thiolate anions via a S_N2 mechanism, and consequently generate HBr,[101] as shown in Figure 12. Therefore, it is necessary to buffer the system to allow continuous reaction of bromobimane with free thiols. Bromobimanes have been widely used for the *in vivo*, *ex vivo* and *in situ* tagging of thiols.[100-109] The conditions outlined in these procedures were used as a starting point to optimise the reaction of bromobimanes with short peptides, such as those presented here. Buffer was also employed in all the literature reactions to stabilise the constituent proteins. Therefore buffer was deemed a necessary component of the reaction mixture, and two different buffers were investigated. Other aspects of the reaction were optimised, including the concentration of peptide and equivalents of bromobimane, to develop a set of widely applicable and biologically relevant conditions for the reaction of bromobimane.
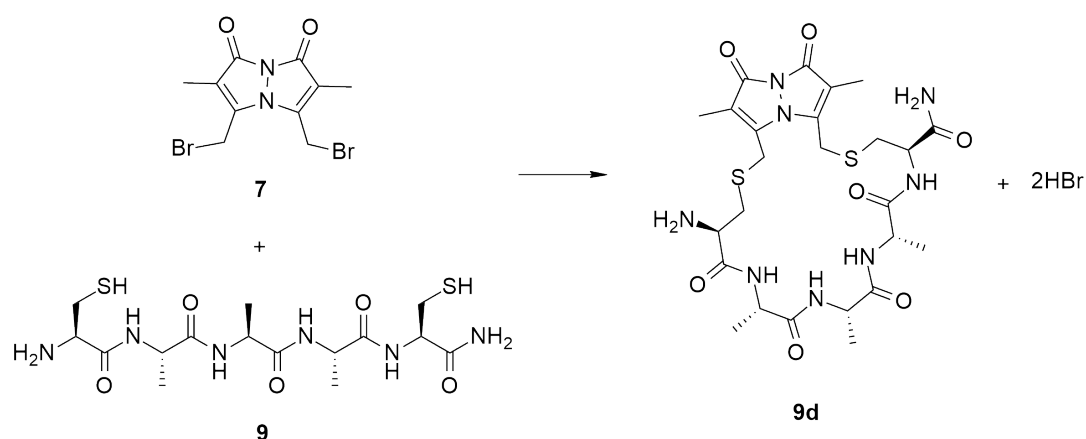

Figure 12: The reaction of the linear peptide precursor **9** to give the fluorescent bimane cyclised peptide **9d** and HBr,

The fluorescent nature of the alkylated bimane was exploited in experiments to optimise the reaction conditions. An alanine rich peptide sequence, **9** (Figure 12), was selected as a simple model peptide for optimisation. The linear peptide **9** and dibromobimane displayed negligible

fluorescence in comparison to the highly fluorescent bimane-linked peptide **9d**, as shown both qualitatively (A) and quantitatively (B) in Figure 13. Fluorescence increase was monitored for the reaction of peptide **9** with dibromobimane to produce the fluorescent **9d**. The set of conditions with maximal fluorescence were chosen as the optimum combination.
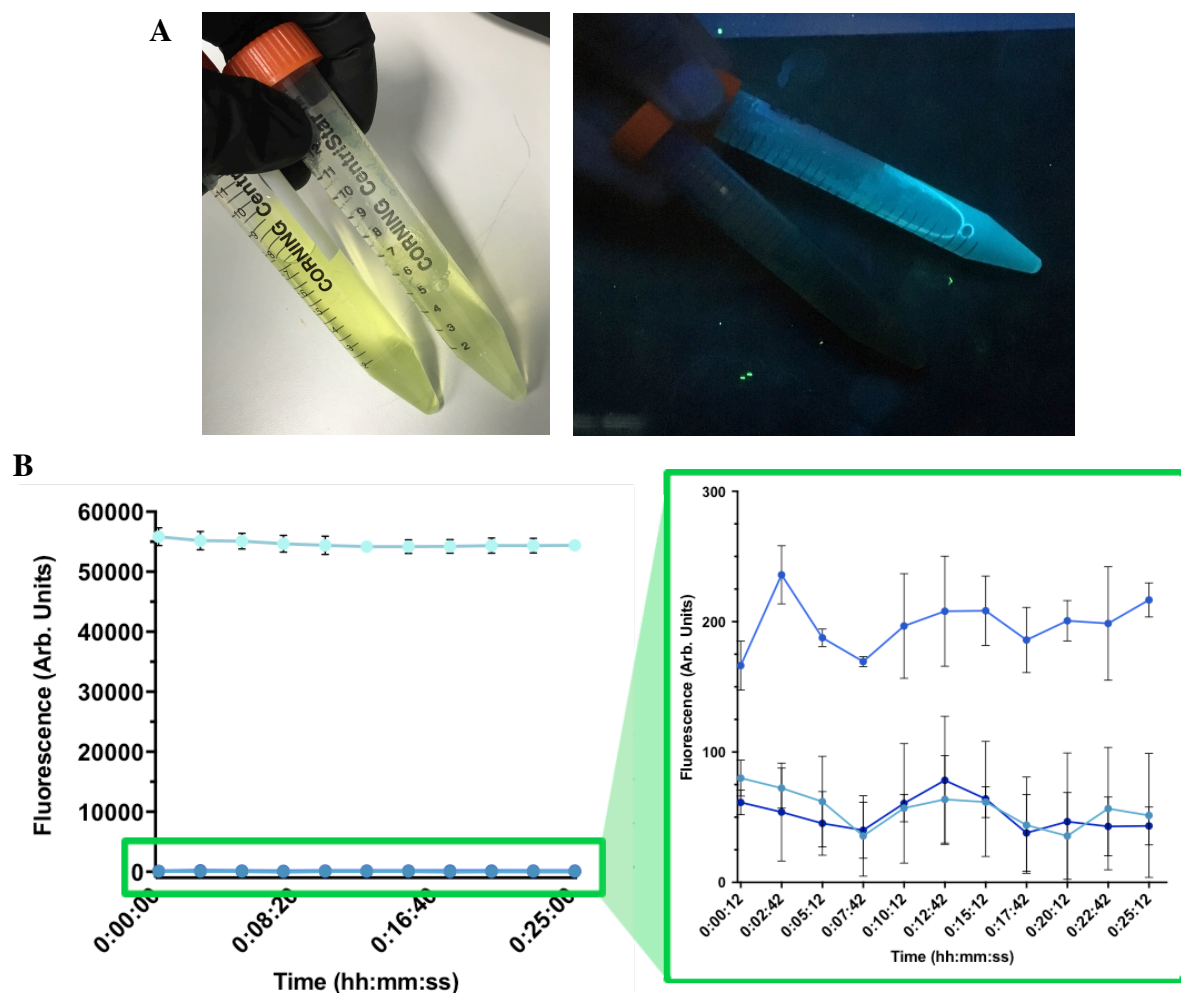

Figure 13: A) Under visible light (LHS) both a solution of dibromobimane (left tube) and solution of bimane cyclised peptide (right tube) appear similar in colour. However under UV light (RHS) the bromobimane is apparently non-fluorescent (left vial) as compared to the cyclised peptide (right vial) which glows blue. **B)** Relative fluorescence of a 1mg/ml of a bimane cyclised peptide ⎯ in 10 mM PBS at pH 7.4, compared to three sets of control wells that display negligible levels of fluorescence. Control 1 ⎯ 10 mM PBS + 1 mg/ml peptide; Control 2 ⎯ −10 mM PBS + 1 mg/ml dibromobimane; Control 3 ⎯ 10 mM PBS.

A preliminary 96-well plate experiment was designed to screen a series of reaction conditions by monitoring the change in fluorescence intensity. PBS buffer at 10 mM was used here as it is reported in literature bromobimane reactions,[101, 105, 107] and widely applied in biology. A range of peptide concentrations (1, 2, 4 and 8 mg/ml in the final reaction solution) were

examined using 1.5 equivalents of dibromobimane in each case. Three controls were also plated for each peptide concentration. These controls were 1) PBS and peptide, 2) PBS and dibromobimane, and 3) PBS alone. Control 1 was plated at 1, 2, 4 and 8 mg/ml peptide concentration, and control 2 plated with 1.5 equivalents of dibromobimane with respect to each of these peptide concentrations, all in 10 mM PBS. The plate layout is displayed in Table 1. All conditions, experimental and control, were conducted in triplicate. All reagents, 100 mM buffer stock solution, peptide stock solution in 50% aq. acetonitrile and dibromobimane stock solution in methanol, were added to the wells and diluted to the correct concentration with milliQ water. The same volume of acetonitrile and methanol was used in all cases to remove any possible influence of solvent on fluorescence. Dibromobimane solution was added last to all the wells and the fluorescence was monitored at an excitation wavelength of 385 nm and emission of 477 nm.[101, 107] Fluorescence was not observed for any of the control wells as shown in Figure 13B and qualitatively in Figure 13A. Fluorescence was observed in all experimental wells, however it was higher for 1 mg/ml reaction solution compared to the more concentrated wells. Precipitation of the peptide occurred in some wells and was especially significant at peptide concentrations of 4 and 8 mg/ml, accounting for the lower fluorescence observed in these cases. Therefore, lower peptide concentrations were examined for a more complete optimisation experiment.

Table 1: Layout of a 96 well plate for the preliminary optimisation of peptide concentration (varied between 1 and 8 mg/ml) conducted in 10 mM PBS at pH 7.4, with 1.5 equivalents of dibromobimane. The codes given within coloured cells reflect the wells for a given set of conditions. Intensity of coloured cells reflects the approximate relative fluorescence intensity observed. *Control 1*: 10 mM PBS + peptide; *Control 2*: 10 mM PBS + dibromobimane; *Control 3*: 10 mM PBS.

Concentration (mg/ml) →	1	2	4	8
Experimental	A1-3	A4-6	A7-9	A10-12
Control 1	B1-3	B4-6	B7-9	B10-12
Control 2	C1-3	C4-6	C7-9	C10-12
Control 3	D1-3	D4-6	D7-9	D10-12

A second plate experiment was conducted in which an additional buffer (ammonium acetate buffer (AAB)), four peptide concentrations and dibromobimane concentrations were compared, as shown in Table 2. AAB buffers at a higher pH range (~7-9) compared to PBS, which buffers best between pH 6 and 8. This provides an opportunity to investigate both the effect of pH and the buffering system. Peptide concentrations of 0.1, 0.2, 0.5 and 1 mg/ml were investigated, with four ratios of dibromobimane: 1.5, 1.3, 1.1 and 1 equivalent relative to the peptide concentration in each case. 10% 2,2,2-trifluoroethanol (TFE) was also included in all reactions to aid peptide folding[110, 111] and thereby reduce the likelihood of inter-peptide cross-links.

Table 2: Layout of a 96 well plate for the optimisation of peptide concentration, bromobimane equivalents and buffer type at pH 7.4. The codes given within coloured cells reflect the wells for a given set of conditions. Intensity of coloured cells reflects the approximate relative fluorescence intensity observed.

Peptide concentration (mg/ml) →		1	0.5	0.2	0.1
Dibromobimane equivalents ↓					
PBS buffer	1.5	A1-3	A4-6	A7-9	A10-12
	1.3	B1-3	B4-6	B7-9	B10-12
	1.1	C1-3	C4-6	C7-9	C10-12
	1.0	D1-3	D4-6	D7-9	D10-12
AAB buffer	1.5	E1-3	E4-6	E7-9	E10-12
	1.3	F1-3	F4-6	F7-9	F10-12
	1.1	G1-3	G4-6	G7-9	G10-12
	1.0	H1-3	H4-6	H7-9	H10-12

As before, peptide stock solutions were made up in 50% aq. acetonitrile, and the dibromobimane stocks in methanol. All combinations of buffer, peptide (**9**) concentration, and dibromobimane equivalents were plated in triplicate, and the fluorescence averaged, as shown in the plate layout in Table 2. Dibromobimane was added last over approximately three minutes and fluorescence was immediately measured by the plate reader at an emission wavelength of 477 nm (ex. 385 nm). The plate was scanned every two-minutes for a total of 1.5 hours. Samples were then taken and analysed by RP-HPLC and LCMS to confirm product

identity. The effect of each variable (peptide concentration, dibromobimane equivalents, and buffer system) on the amount of **9d** produced was examined separately as described below.

Peptide concentration

As shown in Figure 14A, maximum fluorescence intensity and hence product formation, was achieved at 0.5 mg/ml of peptide. The reaction with 1 mg/ml of peptide gave some precipitation, which is reflected in a slightly lower observed fluorescence. Some aggregation may also be occurring at the higher concentration, thereby limiting the reaction. This trend was also apparent at the other concentrations of the dibromobimane as shown in Figure 14B. Hence a reaction solution of 0.5 mg/ml of peptide provided the optimal concentration with which to conduct the dibromobimane reaction.
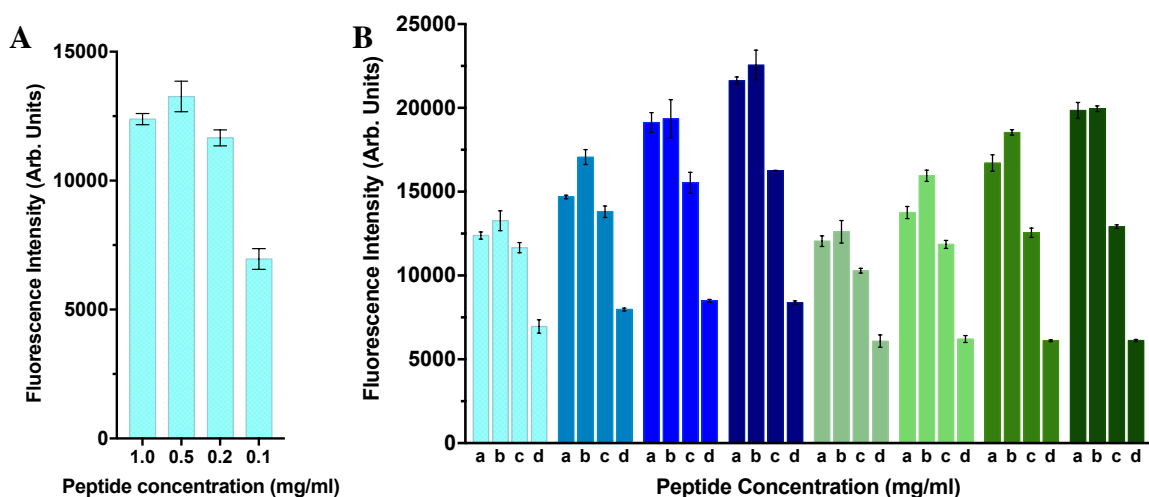
Figure 14: A) A snapshot of the relative fluorescence intensity (excitation: 385 nm, emission: 477 nm) for the reaction of **9** with dibromobimane, 46 minutes since the addition of dibromobimane (arbitrary point after reaction completion). Peptide concentration is varied (1.0, 0.5, 0.2 & 0.1 mg/ml) between reactions with 1.5 equivalents of dibromobimane relative to the peptide, in 10 mM PBS at pH 7.4. B) Snapshot of the relative fluorescence intensity (excitation: 385 nm, emission: 477 nm) for the reaction of **9** with dibromobimane (to produce **9d**) at 46 minutes since the addition of dibromobimane. All reactions are in 10 mM buffer at pH 7.4. Peptide concentration is varied within each series: a) 1 mg/ml, b) 0.5 mg/ml, c) 0.2 mg/ml and d) 0.1 mg/ml. Dibromobimane concentration is varied between series: *PBS*: ▨ 1.5 equiv; ▨ 1.3 equiv; ▨ 1.1 equiv; ▨ 1 equiv; *AAB:* ▨ 1.5 equiv, ▨ 1.3 equiv; ▨ 1.1 equiv; ▨ 1.0 equiv.

Dibromobimane concentration

An increase in fluorescence was observed when the number of dibromobimane equivalents was reduced from 1.5 to 1.3 to 1.1 to 1.0 equivalents, irrespective of the peptide concentration. This is shown in Figure 14B, moving from left to right within each series (blue or green), for a given concentration. The fluorescence is greater for reactions of lower dibromobimane concentration, therefore with a lower ratio of dibromobimane to peptide, more **9d** is produced. This fluorescence intensity trend implies that the reaction of **9** with dibromobimane may be inhibited in some way by higher concentrations of dibromobimane. Therefore to mitigate this effect, and to conserve reagent, 1.0 equivalent of dibromobimane was utilised in future reactions.

Buffer system

The fluorescence observed for the reactions conducted in PBS (blue series) was larger than for AAB (green series), see Figure 15A. A plot of fluorescence intensity vs time, as shown in Figure 15A, reveals that all the PBS reactions reach maximum fluorescence within five minutes. In comparison, the AAB reactions take approximately an hour and 30 minutes to achieve a maximum fluorescence. Reactions in PBS thus occur at a significantly faster rate compared to those in AAB. The dibromobimane reactions were conducted at pH 7.4, which better matches the buffering range of PBS. PBS is thus the optimum buffer and was used in all future reactions.
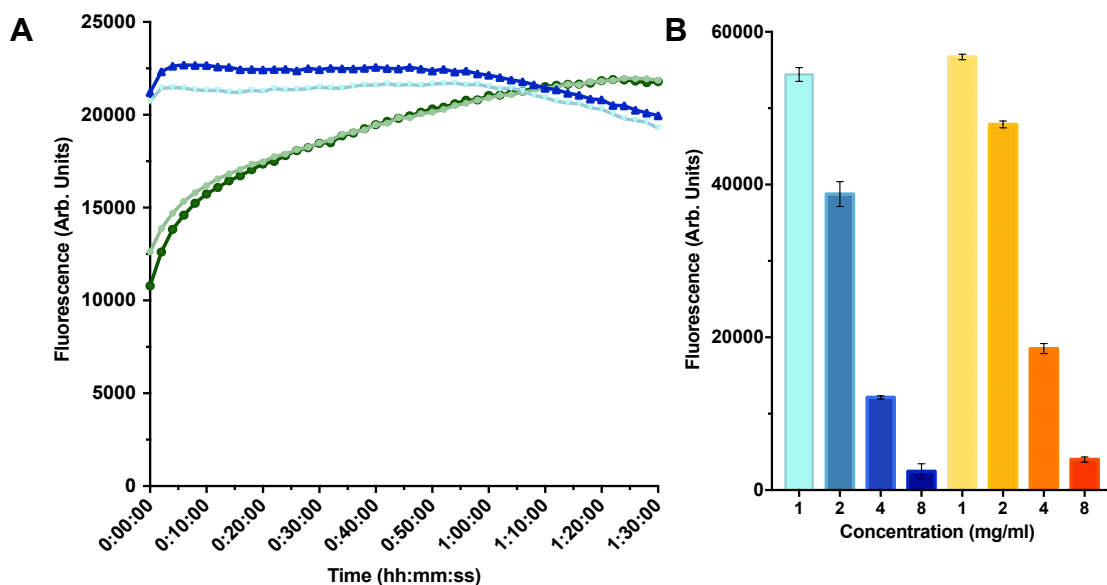
Figure 15: A) Monitoring the reaction of **9** with dibromobimane by fluorescence (excitation: 385 nm, emission: 477 nm) to yield **9d**. Reactions were conducted in 10 mM buffer at pH 7.4 and one equivalent of dibromobimane with respect to peptide **9**. ➤ **P**BS, 0.5 mg/ml peptide; ─ PBS, 1 mg/ml peptide; ● AAB, 0.5 mg/ml peptide; ● AAB, 1 mg/ml peptide. **B)** Fluorescence of **9d** taken ~10 minutes after the addition of dibromobimane to **9**. Reaction was conducted in 10 mM PBS and 1.5 equivalents of dibromobimane. *pH 7.4:* ☐ 1 mg/ml peptide; ■ 2 mg/ml peptide; ■ 4 mg/ml peptide; ■ 8 mg/ml peptide. *pH 7.8:* ☐ 1 mg/ml peptide; ■ 2 mg/ml peptide; ■ 4 mg/ml peptide; ■ 8 mg/ml peptide.

The initial plate experiment conducted at pH 7.4 (see Table 1) was repeated at pH 7.8 to assess the effect of subtle pH changes on the rate of reaction. Reactions at pH 7.4 (Figure 15B, blue series), gave slightly lower fluorescence intensity compared to the pH 7.8 (Figure 15B, orange series) reactions at the same peptide concentration. This further emphasises that the dibromobimane reaction requires a slightly basic pH, and that the reaction occurs at a more efficiently at higher pH. However the effect here is minimal.

Time dependence

A small-scale reaction of **9** (10 mg) with dibromobimane, to produce **9d**, was conducted in 10 mM AAB, at a peptide concentration of 0.5 mg/ml and 1.3 equivalents of dibromobimane and the reaction monitored over time by HPLC to observe reaction progress. These conditions were chosen, as opposed to the optimisation conditions, as this reaction occurs at a slower rate per the fluorescence data. As soon dibromobimane was added to the reaction ('time 0'), a

sample was taken and immediately analysed by analytical HPLC to observe reaction progress. Analysis by LCMS then identified which peaks corresponded to **9**, **9d,** dibromobimane or any other by-products. Further samples were taken at 30 min intervals and analysed immediately in order to monitor the progress of the reaction as shown in Figure 16.

The linear peptide **9** does not absorb at 254 nm and therefore is not observed in the spectrum presented in Figure 15A. It should be noted that dibromobimane absorbs much more strongly at 254 nm than bimane-cyclised peptide **9d**, therefore it is not valid to directly compare the peak heights to obtain a ratio of products. Instead the change in peak height is discussed.

As shown in Figure 16, the HPLC peak at 9.1 minutes corresponds to the cyclised peptide **9d,** and the peak at 14.5 min is due to dibromobimane. At 'time 0' the **9d** peak is already quite large given the sample was passed through the HPLC immediately after addition of dibromobimane to the reaction solution. This reiterates how facile the dibromobimane reaction is. As anticipated, the dibromobimane peak decreases in intensity over time, directly correlating with an increase in the **9d** peak. There is only a minimal increase in **9d** between 30 minutes and 90 minutes, and almost no further increase after 90 minutes. This same trend is revealed in the fluorescence data shown in Figure 15 for the AAB reaction which also shows that the greatest product formation occurs over the first 30 minutes and the reaction slows and reaches completion by 90 minutes. The consistency between HPLC and fluorescence data confirms that it is valid to monitor the reaction by fluorescence, and therefore it can be concluded that the PBS reactions were complete within 15 to 30 minutes.
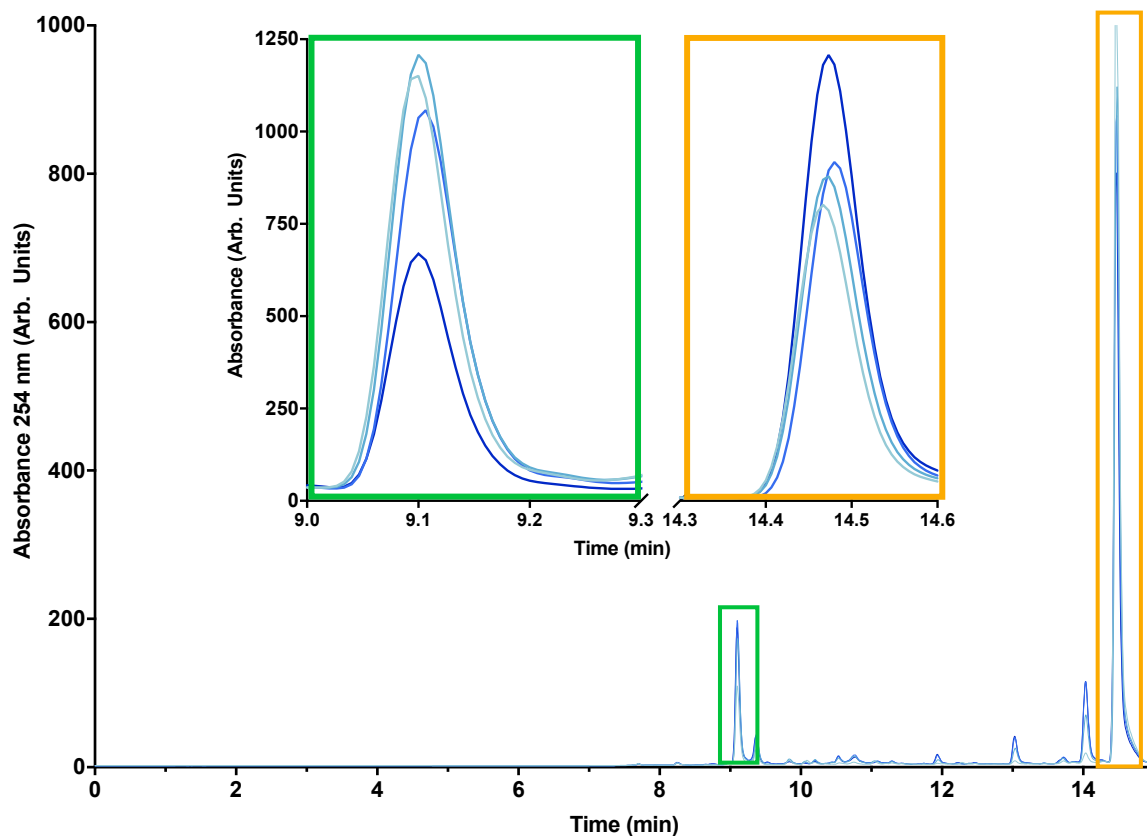
Figure 16: Analytical RP-HPLC spectrum, 0-100% aq. ACN gradient over 15 minutes on a C18 column visualised at 254 nm, for the reaction of **9** with dibromobimane to yield **9d.** Reaction was carried out in 10 mM AAB, 10% TFE, 0.5 mg/ml peptide and 1.3 equiv of dibromobimane. A sample of the reaction mixture were taken upon addition of dibromobimane to the reaction and every 30 minutes thereafter for 2 hours, and immediately analysed by HPLC. Time after addition of dibromobimane: ▬▬ 0 min; ▬▬ 30 min; ▬▬ 90 min; ▬▬ 120 min. The peak at 9.1 minutes highlighted in green indicates the cyclised peptide **9d** and the peak at 14.5 minutes correlates with unreacted dibromobimane. *Inset*: a normalised zoom in of the peaks of interest.

Optimisation conclusion

It was established that buffer is essential for the dibromobimane to occur efficiently and the reaction could be monitored via fluorescence of the bimane-cyclised product. The optimal conditions for reaction of dibromobimane with short peptides is in 10 mM PBS with 10% TFE, 0.5 mg/ml of peptide and one equivalent of dibromobimane over 30 minutes.

2.1.2 Applications of the solution-phase dibromobimane reaction
Tripeptides (i –i+2 constraint)

The optimised reaction conditions for the formation of bimane-cyclised peptides, as described above, were used to prepare a series of *i-i*+2 constrained tripeptides (Figure 17, **10d**, **11d** and **12d**). The reaction conditions were also used to react monobromobimane with single cysteine

containing peptides to give **13m** and **14m**, shown in Figure 17. TFE was deemed unnecessary in the synthesis of these five peptides, as the cysteines are not distal in **10d**, **11d** or **12d**, and only one cysteine is present in **13m** and **14m**. The successful synthesis of cyclic peptides **11d** (containing β-alanine) and **12d** (with homocysteine) demonstrate that the *i-i*+2 cyclisations are tolerant of amino-acid changes.
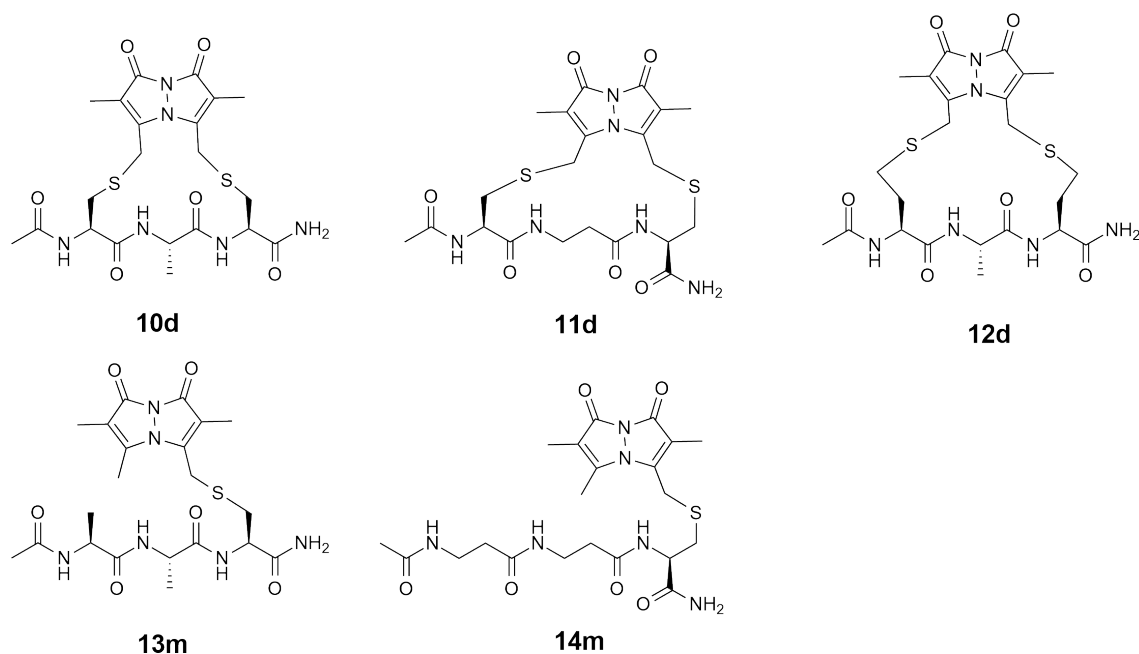

Figure 17: Tripeptides with a *i-i*+2 bimane linker (**10d, 11d, 12d**) and a bimane attached in an acyclic manner (**13m, 14m**) synthesised through the reaction of dibromobimane and monobromobimane, respectively, with linear analogues of the tripeptides.

Pentapeptides (i –i+4 constraint)

Pentapeptides, with cysteine residues at the 1 and 5 positions, were synthesised and then reacted with dibromobimane to form bimane cyclised **15d**, **16d, 18d** and **17d** (Figure 18)**.** Acyclic bimane-bound analogues were synthesised using monobromobimane under the same conditions described in section 2.1.1, with the omission of TFE, to give **19m** and **20m**. No starting peptide remained in any of these syntheses after 30 minutes, as determined by HPLC. Thus substitution of alanine at positions 2-4 in **15d** for β-alanine, to give the longer and more flexible **16d**, did not affect the reaction efficiency. The peptide **18d**, with homocysteine at the 1 and 5 positions underwent reaction as per the cysteine analogue. To investigate if the linker

could be installed as an even longer constraint, an *i-i*+7 series was also developed as discussed in the following section.
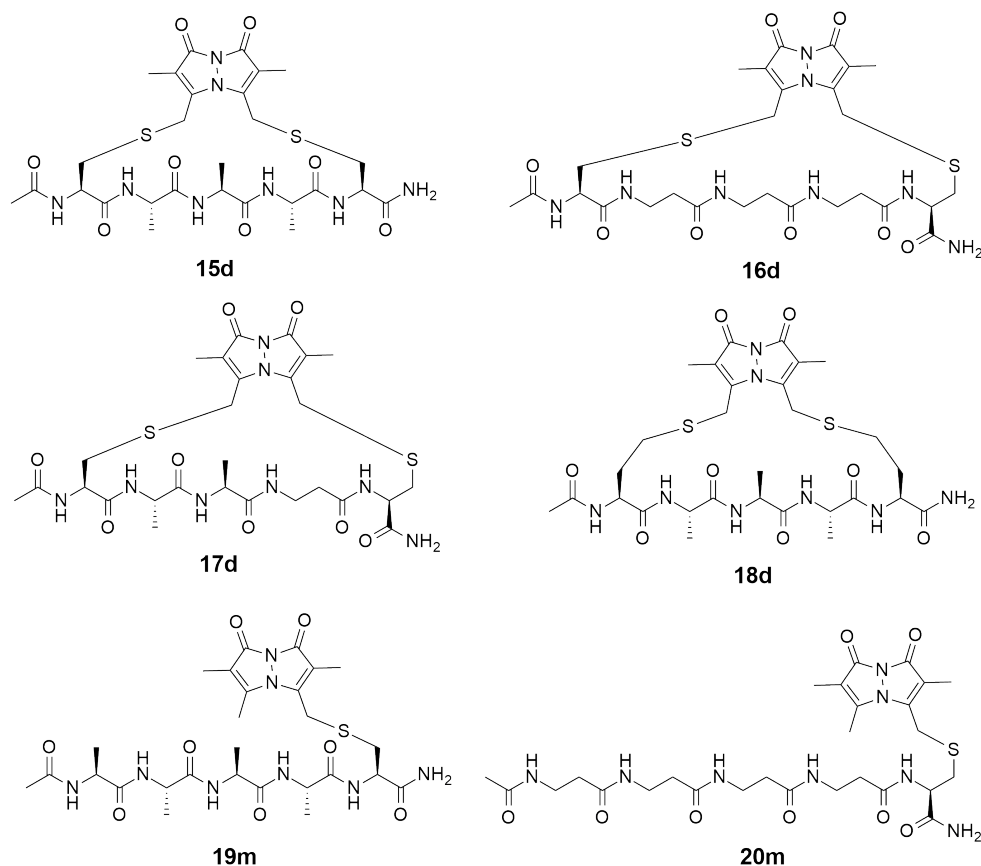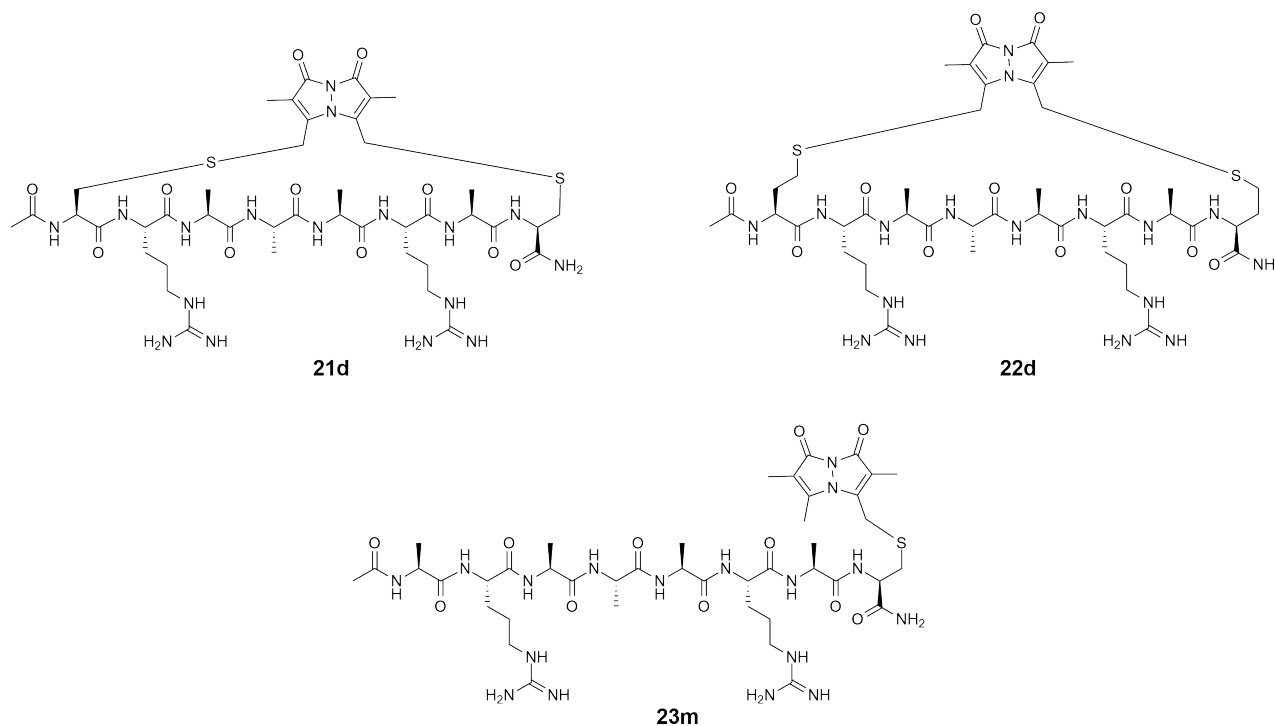

Figure 18: Pentapeptides with a *i-i*+4 bimane linker (**15d, 16d, 18d and 17d**) and a bimane attached in an acyclic manner (**19m, 20m**) synthesised through the reaction of dibromobimane and monobromobimane, respectively, with linear analogues of the pentapeptides.

Octapeptides (i –i+7 constraint)

The cyclic octapeptides with cysteine, or homocysteine, at the 1 and 8 positions were synthesised by cyclisation of the respective linear peptides with dibromobimane to give **21d** and **22d** respectively (Figure 19). Neither the peptide length nor linker length affected the synthesis. Reaction of monobromobimane with a single cysteine containing octapeptide, to form acyclic **23m**, was also performed with similar efficiency.

Figure 19: Octapeptides with an *i-i*+7 bimane linker (**21d, 22d**) and a bimane attached in an acyclic manner (**23m**) synthesised through the reaction of dibromobimane and monobromobimane, respectively, with linear analogues of the octapeptides.

Alternate sequences

Two, more hydrophobic and sterically hindered peptides (**24d** and **25d,** Figure 20), were synthesised under the same optimised conditions described in section 2.1.1, again without addition of TFE. Despite the fact that peptides **24d** and **25d** were hydrophobic, they remained freely soluble in the aqueous conditions. Again starting material was not observed after 30 minutes of reaction time, despite the fact that they contained sterically hindered amino acids.
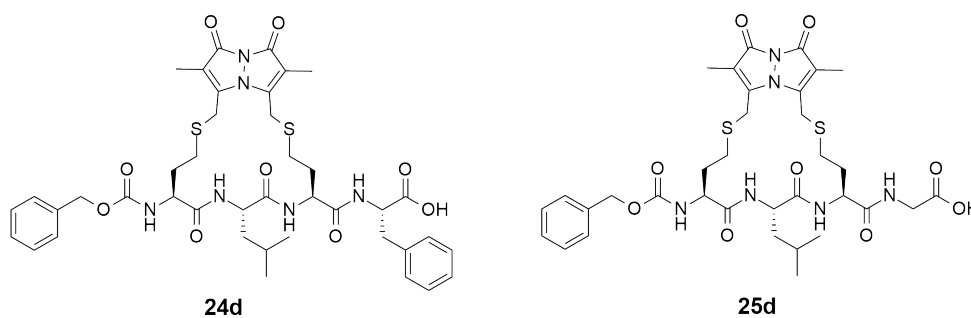
Figure 20: Hydrophobic tetrapeptides with an *i-i*+2 bimane linker synthesised by the reaction of dibromobimane with the corresponding linear precursor in solution.

Lastly, 18mer peptides, based on a sequence reported by de Araujo *et al.*[86], were similarly synthesised and cyclised with dibromobimane to form *i-i*+4 (**26d**) and *i-i*+7 (**27d**) bimane cyclised peptides (Figure 21). A peptide derived from the αIIβ3 integrin protein[98, 112, 113] was also prepared (Figure 21, **28d**) under the same conditions. All these longer peptides were cyclised with high efficiency.

Side products were not observed, even in the presence of a *C*-terminal acid or an *N*-terminal amine as in **24d** and **25d** (Figure 20) and **9d** (Figure 12A), respectively. This reinforces that the bromobimane reaction is thiol-selective.[100-102, 104] The compounds reported in this section form a basis to demonstrate the versatility of the bromobimane reaction as a means to introduce a new peptide constraint in a variety of peptide sequences and constraint lengths.

26d

27d

28d
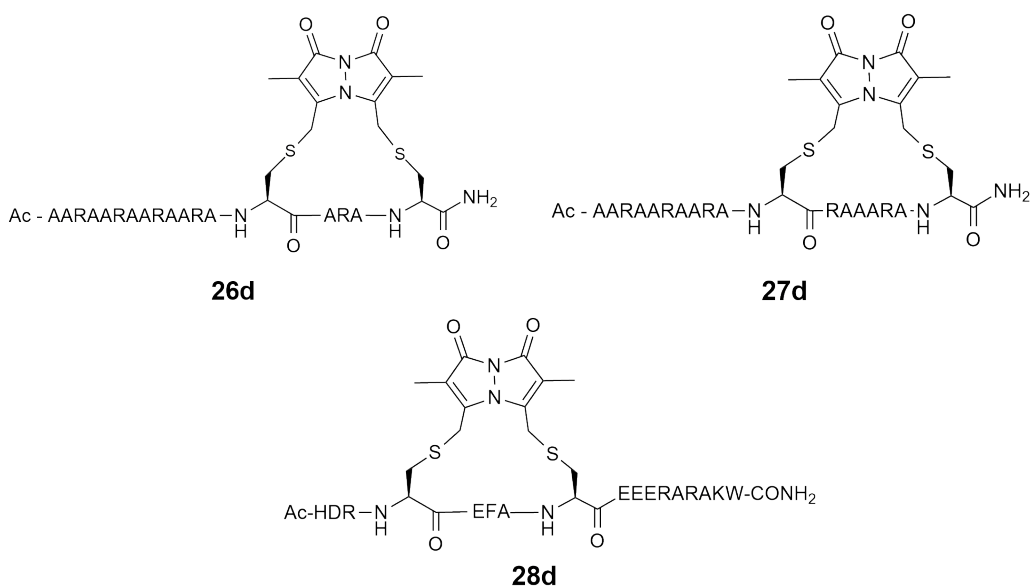
Figure 21: Extended alanine rich peptide sequences for *i-i*+4 (**26d**) and *i-i*+7 (**27d**) constraint with a bimane, as derived from a sequence used by de Araujo *et al.* Bimane introduced as an *i-i*+4 constraint in a biologically derived peptide sequence from the αIIβ3 integrin protein interaction with talin (**28d**).

2.1.3 Cyclisation on solid support

Solid-phase peptide synthesis & protecting group strategies

The linear peptides 9-23 **and** 26-28 **described in this thesis, shown in Table 3-**

Table 6, were synthesised on-resin via solid-phase peptide synthesis (SPPS) protocols , on Rink Amide PL resin, while **24** and **25** were synthesised on Wang resin. A representative

synthesis of the literature peptide **15**[86] is shown in Figure 22. All amino-acid side-chain protecting groups were removed in the final cleavage step (92.5% TFA with scavengers), which also removed the peptide from the resin. The linear precursor peptides synthesised in this way, were then reacted with bromobimane in solution, per the method outlined in section 2.1.1.

Table 3: Amino-acid sequences for the unfunctionalised linear tripeptides synthesised by SPPS.

		Residue			
Compound		**1**	**2**	**3**	
10		C	A	C	
11		C	βAla	C	
12	Ac	Hcy	A	Hcy	Am
13		A	A	C	
14		βAla	βAla	C	

Table 4: Amino-acid sequences for the unfunctionalised linear pentapeptides synthesised by SPPS

		Residue				
Compound		1	2	3	4	5
9	H₂N	C	A	A	A	C
15		C	A	A	A	C
16		C	βAla	βAla	βAla	C
17	Ac	C	A	A	βAla	C	Am
18		Hcy	A	A	A	Hcy
19		A	A	A	A	C
20		βAla	βAla	βAla	βAla	C

Table 5: Amino-acid sequences for the unfunctionalised linear octapeptides synthesised by SPPS

		Residue							
Compound		1	2	3	4	5	6	7	8
21		C	R	A	A	A	R	A	C
22	Ac	Hcy	R	A	A	A	R	A	Hcy	Am
23		A	R	A	A	A	R	A	C

Table 6: Amino-acid sequences for the unfunctionalised linear 18mer peptides synthesised by SPPS

Compound	Sequence
26	Ac-AARAARAARAARACARAC-Am
27	Ac-AARAARAARACRAAARAC-Am
28	Ac-HDRCEFACEEERARAKW-Am
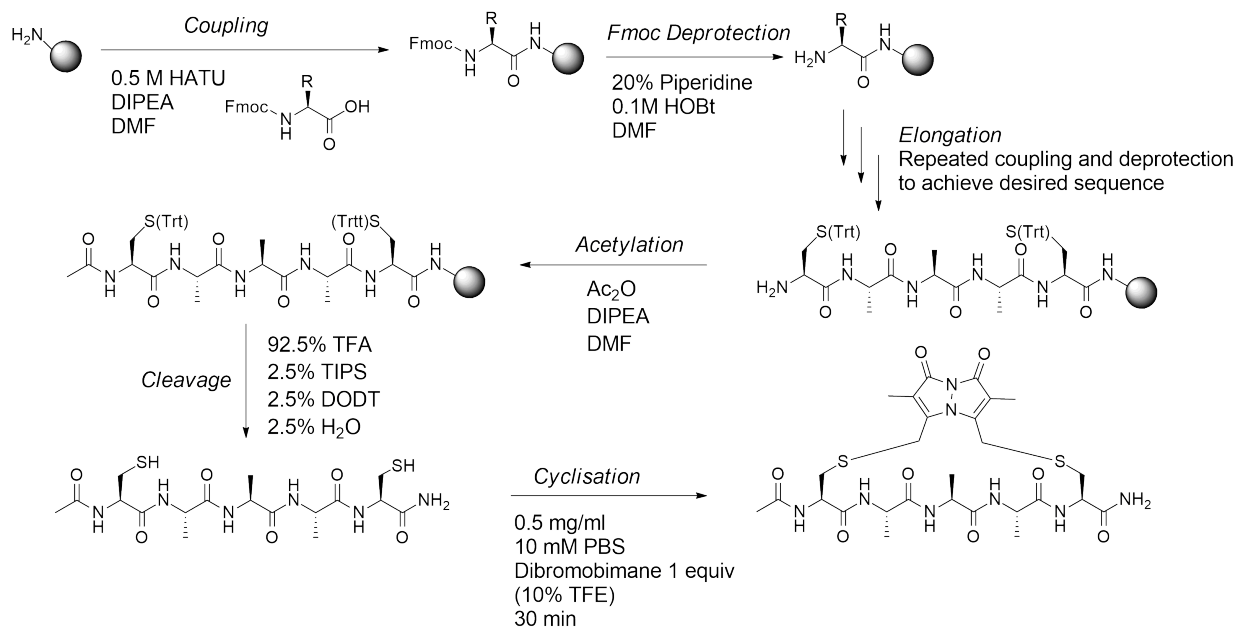
Figure 22: Reaction scheme for SPPS on Rink Amide resin of **15** using a Fmoc protecting strategy and subsequent cyclisation by reaction with dibromobimane in solution to give **15d**.

The peptides **15**, **29** and **30** were prepared by on resin cyclisation. The peptides were assembled on-resin as described above, however in these cases using Fmoc-Cys(Mmt)-OH in place of Fmoc-Cys(Trt)-OH (Figure 23A – without Fmoc) to allow on-resin deprotection of the cysteine thiol; a general scheme for the synthesis of **15/15d** is shown in Figure 25. The methoxytrityl (Mmt) protecting group, Figure 23B, was removed using multiple additions of 2% TFA in DCM. This avoids cleaving any peptide from the resin and the reaction is followed by visually monitoring the yellow colour of the liberated Mmt group (Figure 24). Resin was then thoroughly washed with DCM and DMF to remove all traces of acid prior to cyclisation. A solution of dibromobimane (2 equiv) and DIPEA (4 equiv) in DMF was added to the resin and stirred intermittently for 3 hours. This method has previously been reported by de Araujo *et al.*[86] for on-resin reaction of other

A

B
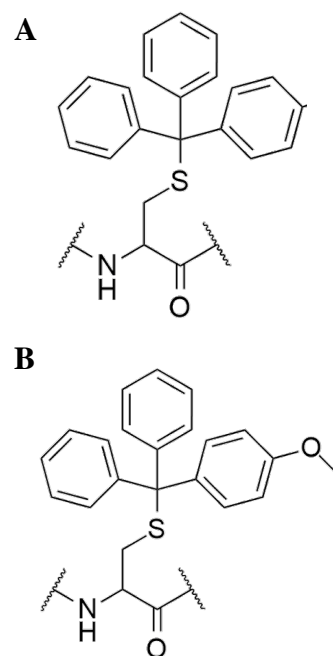
Figure 23: Sulfhydryl protecting groups: **A)** Trityl (Trt) group – deprotected by treatment with >90% TFA; **B)** Methoxytrityl (Mmt) group – deprotected by repeated treatments with 2% TFA in DCM

dibromo-functionalised compounds with resin bound **15**. After this time, the resin was washed, dried and the peptide cleaved to give the final bimane cyclised peptide, as shown in Figure 25. This synthesis was used to prepare **15d** (Figure 18), **29d** and **30d** (Figure 26), without modifications.
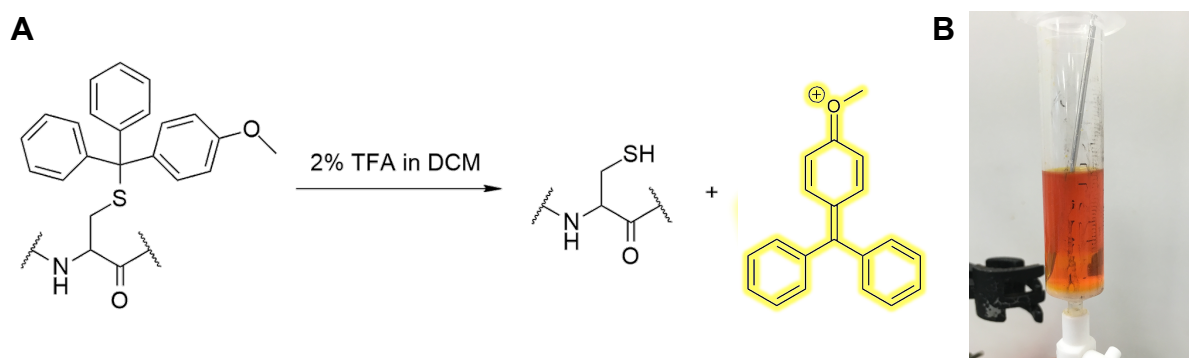
Figure 24: A) Deprotection of a methoxytrityl (Mmt) attached to a thiol can be achieved, while the peptide is attached to the solid resin support, by one minute treatments of the resin with 2% TFA in DCM. Liberation of the Mmt group to reveal a free thiol results in the production of a yellow chromophore. This allows a method by which to monitor the reaction progress. **B)** A sample of resin treated with 2% TFA in DCM when –Cys(Mmt)- is present results in an intense yellow colour.
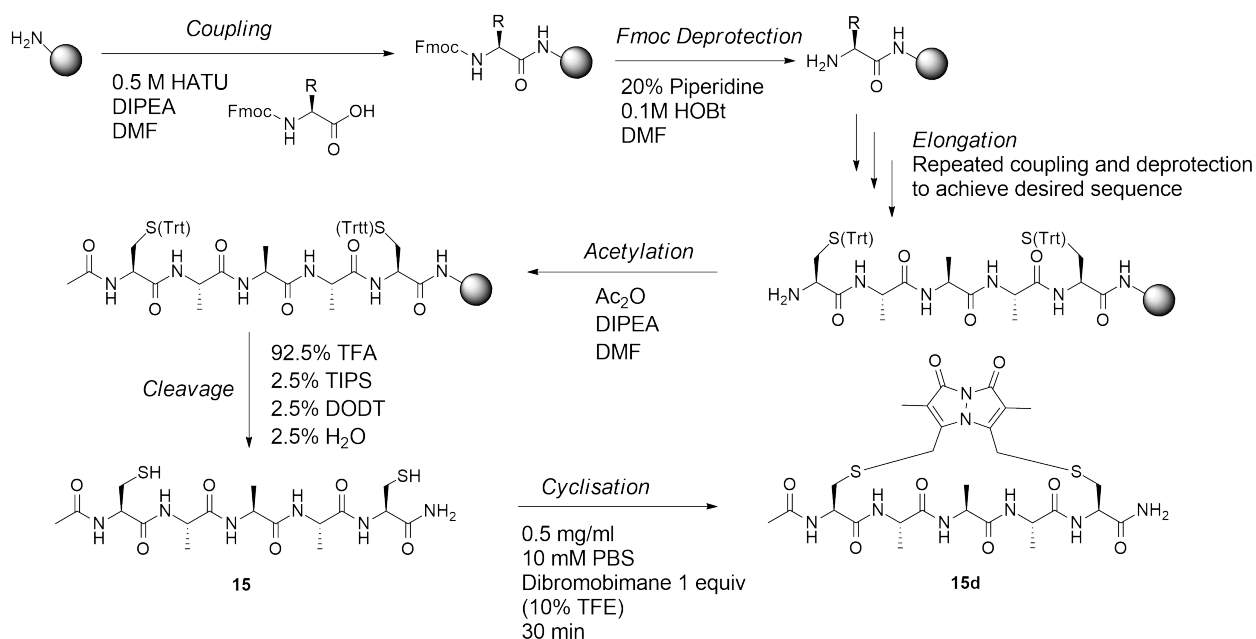
Figure 25: Reaction scheme for solid-phase peptide synthesis (SPPS) on Rink Amide resin of **15d** using a Fmoc protecting strategy to assemble the linear peptide. An alternate combination of cysteine protecting groups (Mmt in favour of Trt) allows deprotection while attached to the resin and subsequent cyclisation with a bromobimane.

The on-resin cyclisation protocol requires less isolation steps, compared to separately synthesising the linear peptide and then cyclising off-resin, thereby streamlining the route. Furthermore, the appropriate choice of protecting group allows selective deprotection of cysteines, therefore the on-resin cyclisation method will be useful in reacting peptides which contain more than one or two thiols for mono- or di-bromobimane reaction, respectively. However, the on-resin reaction must be carried out on a larger scale compared to the solution based experiments, and also requires more equivalents of bromobimane.
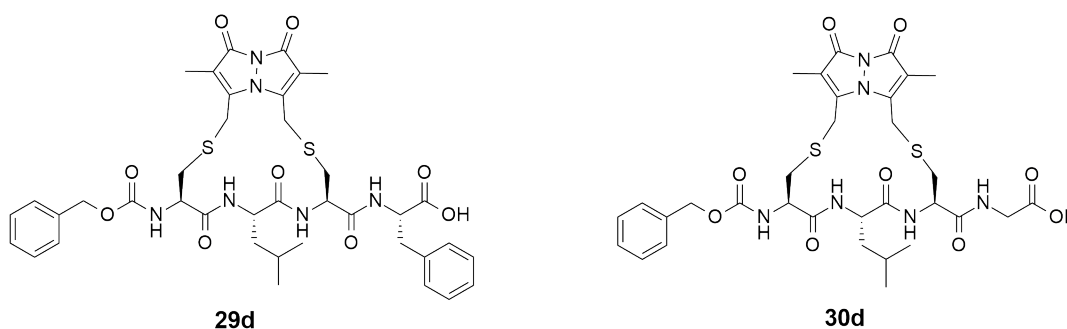
Figure 26: Two hydrophobic tetrapeptides assembled and cyclised with a bimane linker in an *i-i+2* manner on Wang resin.

2.2 Purification

The polar nature of peptides makes purification by traditional silica chromatography difficult. The unfunctionalised linear peptides **9**-**20**, **24**-**25**, dibromobimane cyclised peptides **9d-12d**, **15-18d** and **29d**-**30d**, and acyclic bimane attached peptides **13m**, **14m**, **19m**, and **20m** could not be purified by semi-preparatory RP-HPLC, despite separating well on the analytical RP-HPLC. The compounds were not retained well on the semi-preparatory column above 100 µl injections of a <1 mg/ml solution and consequently useable quantities of purified peptide could not be obtained. This may be due to a combination of the short peptide length and lack of a larger functional group to give strong interactions with the reverse-phase silica surface. As purification by semi-preparatory RP-HPLC was low yielding and not time efficient, other methods were sought.

Solid-phase extraction (SPE) columns are most commonly used to desalt compounds,[114] however here the SPE columns were implemented as a purification technique, and set up as shown in Figure 27. The purification system was placed under vacuum as the tightly packed fine silica beads severely restricted elution by gravity. The peptides were purified by eluting the compound using, a gradient of aqueous acetonitrile (5-10%, or 10-40% for **29d** and **30d**). Furthermore, a three-way tap was introduced to allow the system to be easily isolated from the vacuum source, such that a new fraction could be placed under the column as shown in Figure 27. Significantly improved yields (20-90%) and purity were achieved by SPE column purification. Figure 28A and B shows a HPLC spectrum of a crude peptide mixture, in which the desired cyclised compound **16d** and another peptide (**16d** with an alanine deletion) that are separated by less than 1 minute in the spectrum. Figure 28A and B are the HPLC spectra of column fractions in which the peptides were isolated from one another.
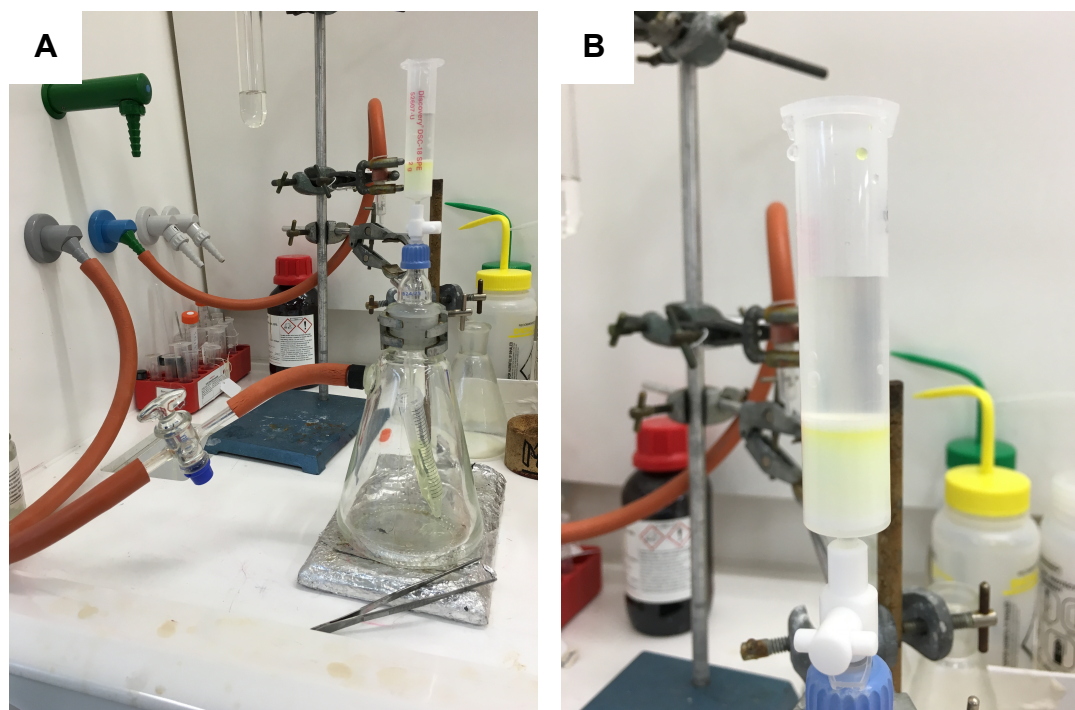
Figure 27: A) Purification set up of an RP pre-packed SPE column under vacuum. Elution is controlled by a PTFE stopcock and fractions collected in 15 mL falcon tubes. The system is easily isolated from the vacuum by the introduction of a three-way tap in the vacuum hosing. **B)** The yellow cyclised peptide can be seen loaded in a band below the top frit before an acetonitrile gradient is begun to initiate elution.
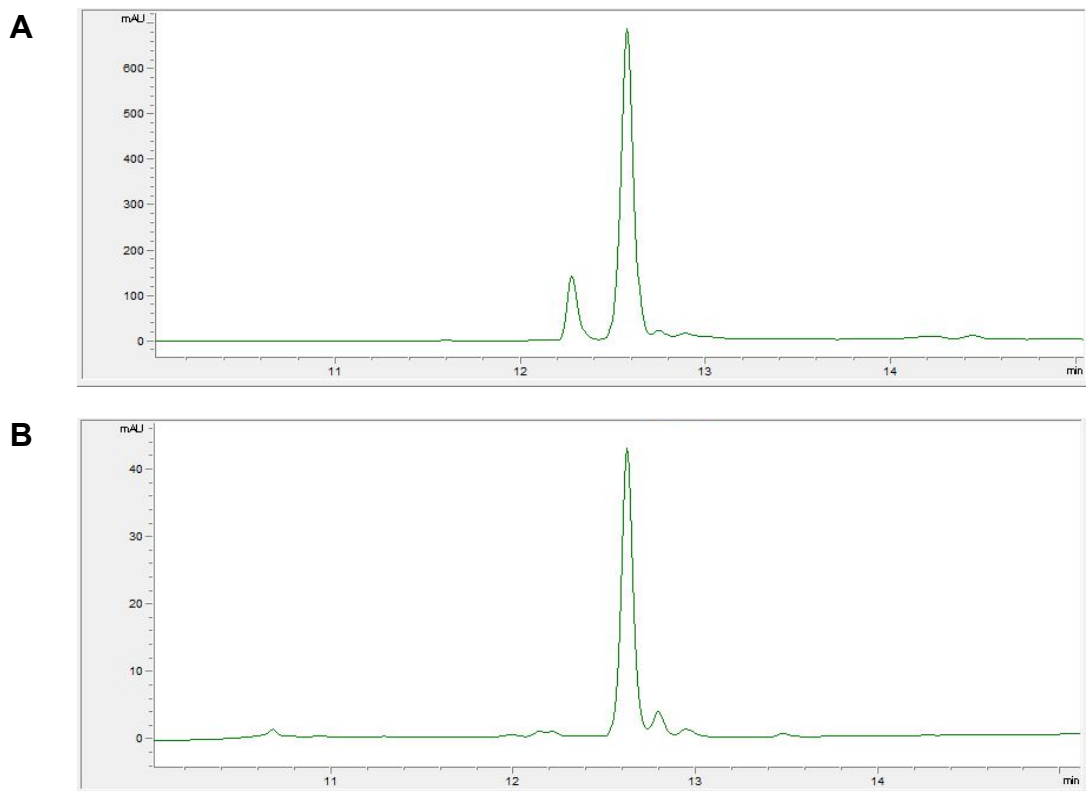
Figure 28: A) Zoomed region of the cyclised product peaks where the peak at 12.6 min is **16d** and at 12.3 min is **16d** with an alanine deletion **B) 16d** purified from the reaction mixture on an SPE C18 column eluted at 7% aq. ACN.

2.3 Fluorescent Properties

A plate experiment was designed to investigate the effect of pH on fluorescence, determine a detection limit and elucidate any differences in the fluorescent properties of bimane-cyclised peptides with an *i-i*+2 (**10d**), *i-i*+4 (**15d**), and *i-i*+7 (**21d**) constraint length. The fluorescence of these compounds was then compared to the acyclic bimane-containing peptides **13m**, **19m** and **23m**, respectively. Solutions of these peptides at 10 μM and 50 μM in 10 mM PBS at pH 7 were prepared and plated in triplicate in a 96-well plate.

Fluorescence spectra, for all six peptides, were collected by irradiating the sample with 300-450 nm light at 5 nm intervals, to determine the excitation wavelength that generated maximum fluorescence emission, as detected at 477 nm. Conversely, the samples were irradiated at 385 nm and a spectral scan from 300-700 nm was conducted to determine the wavelength at which maximum fluorescence intensity was detected, as shown Figure 29. The six peptides analysed had a maximum fluorescence excitation and emission at very similar

wavelengths, shown in Figure 29 and Table 7. These values centred around an excitation at 389 nm and emission at 479 nm. The literature reports variation in the fluorescence excitation and emission wavelengths of the bimane dependent on the substituent bound,[100, 101, 103, 107] as observed

here. However, the different excitation and emission wavelengths for each peptide here were not statistically different. As a consequence, a full fluorescence characterisation scan, such as this, should not need to be conducted prior to investigations of new bimane-bound peptides in biology. However, this observation must first be confirmed on more diverse peptide sequences.

The fluorescence intensity is lower for all acyclic bimane bound peptides (**13m**, **19m**, and **23m**) compared to the analogous bimane-cyclised peptide (**10d**, **15d**, and **21d**, respectively). For example, the fluorescence of **21d** is greater than **23m** as shown in Figure 29. This may be a result of a smaller conjugated system in the mono-functionalised bimane. Peptides of longer length resulted in greater fluorescence intensity, for example the octapeptide **21d** displayed greater fluorescence than pentapeptide **15d**, which was greater than the fluorescence of the tripeptide **10d**. This is an interesting observation that may impact precise quantification of bimane-bound peptide by fluorescence, without a robust control group. Further studies are required to confirm these two trends on more diverse sequences and elucidate the origin.

Table 7: Wavelength maxima for the fluorescence excitation (when emission is read at 477 nm) and fluorescence emission (when excited at 385 nm). The mean average and standard deviation (SD) of these values is also shown.

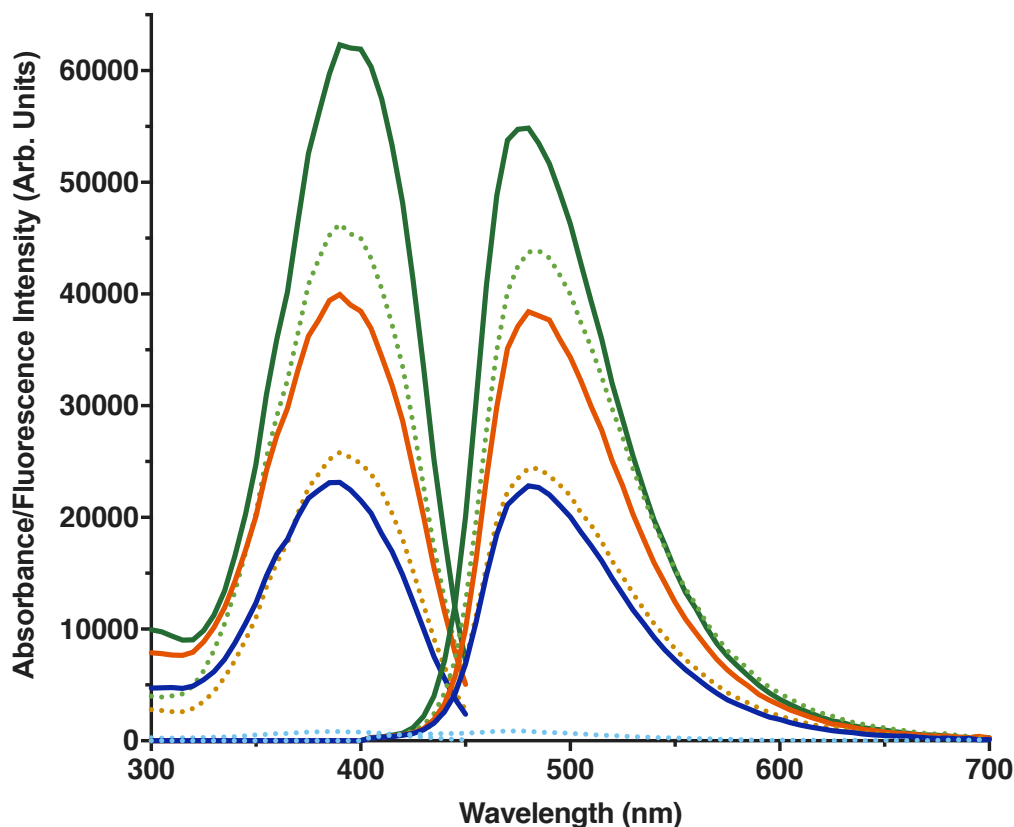|	10d	13m	15d	19m	21d	23m	Mean	SD
Excitation Wavelength (nm)	386	390	389	390	392	389	389	1.97
Emission Wavelength (nm)	482	476	482	481	474	482	479	3.56

Figure 29: Fluorescence excitation and emission curves for a series of alanine-rich peptides attached to bimane moieties at 50 μM in 10 mM PBS at pH 7. ····· **13m;** ── **10d;** ····· **19m;** ── **15d;** ····· **23m;** ── **21d**.

Effect of pH on fluorescence

Solutions of peptides **15d** and **19m** were prepared at 50 μM in 10 mM PBS at pH 6, 7 and 8 to observe any variation in fluorescence due to changes in pH, within a biologically relevant context. The fluorescence intensity did not alter between pH 6 and 8 for **15d** nor **19m**, as shown in Figure 30. Therefore it is known that any pH fluctuations within a biological system will not effect the fluorescence observed and hence will not impact the ability to quantify the amount of bimane-bound peptide present, including pH changes which may arise from a more diverse peptide sequence.
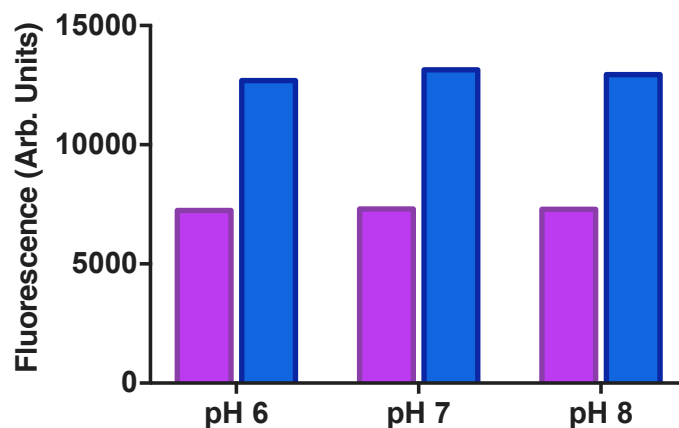
Figure 30: Fluorescence of 50 μM solutions of ▮ **19m** and ▮ **15d** in 10 mM PBS at varied pH.

Detection Limit

A fluorescent probe must be clearly distinguishable from background fluorescence at low nano- or pico- molar concentrations to be utilised as tag for potential therapeutics in a pre-clinical or clinical setting. The peptide **15d** was prepared at lower concentrations, to help establish a detection limit of the fluorescent bimane-bound peptide. As shown in Figure 31, fluorescence can still be differentiated from a PBS-only control with good accuracy at 10 nM concentration. This is a very encouraging result, as **15d** is not the most fluorescent system as shown in Figure 29, and furthermore the plate reader is not the most sensitive instrument with which to detect fluorescence. Most clinical studies, in which drug candidates are monitored within cells, are not conducted on plate readers. This is due to low sensitivity inherent in the plate reader system. Fluorescence studies with drug candidates are most often conducted via confocal microscopy or fluorescence-activated cell sorting (FACS) analysis, which incur greater sensitivity through laser excitation. Therefore, the detection limit of 10 nM on a plate reader would be expected to be significantly reduced when analysed by a more precise system. This study demonstrates the sensitivity of the bimane cyclised peptide/protein at a lower concentration that reported in the literature.[100, 103-105] Hence, there is good scope for application of bimane-bound peptides to biologically relevant peptide therapeutics.
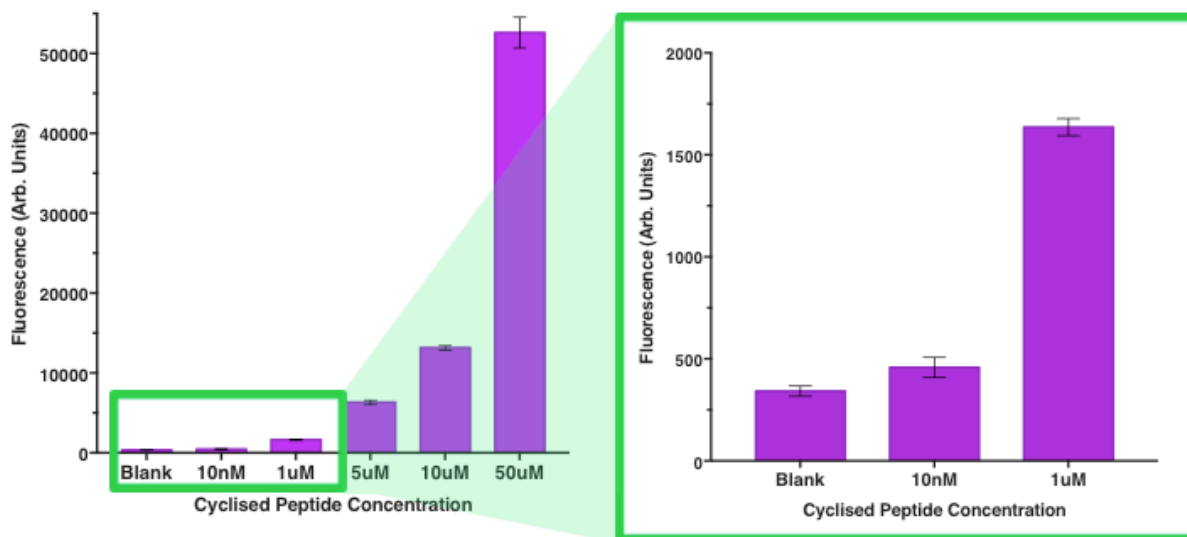
Figure 31: Fluorescence of varied concentrations of 15d in 10 mM PBS at pH 7 compared to a blank of only 10 mM PBS. Fluorescence was read at an excitation of 385 nm and emission of 477 nm using a H4 Synergy Plate reader with a Xenon source. Even greater sensitivity, and therefore lower detection limit, would be anticipated for a more sensitive and high excitation energy source such as a confocal microscope.

2.4 Chapter conclusions

The optimal conditions for reaction of dibromobimane with short peptides is in 10 mM PBS at 0.5 mg/ml of peptide and one equivalent of dibromobimane over 30 minutes. 10% TFE can be added to the solution to aid folding of the peptide and further reduce the likelihood of inter-peptide crosslinks. Alternate concentrations of peptide (0.1-8 mg/ml) and dibromobimane (1.1-1.5 equivalents) still let the reaction proceed, however the reaction will slow significantly with removal of buffer from the reaction conditions. These conditions have been utilised to react both dibromobimane and monobromobimane with a series of peptides. Furthermore the cyclisation by reaction with dibromobimane was conducted on-resin, per a literature method.[86]

The reaction conditions used here, both in solution and on-resin, are versatile and allow the preparation of a variety of peptides as per the methods described above. Peptides of varied solubility, length and constraint length were all reacted under the conditions described above without further modification.

The fluorescent properties of the alanine rich peptides were investigated to reveal that the fluorescence excitation and emission wavelengths do not change with peptide sequence.

Longer peptides fluoresce with greater intensity, and furthermore, the bimane-cyclised peptides showed greater intensity than an analogous acyclic bimane-attached peptide. pH did not effect the fluorescence of the bimane-bound peptides therefore they were determined to be applicable for use in a biological setting and furthermore the fluorescence could be detected as low as 10 nM concentration on a plate reader. This detection limit is expected to be further improved when analysed on a more sensitive instrument.

Chapter 3: Secondary structural characterisation of bimane-bound peptides

3.1 Introduction

A study by de Araujo et al.[86] directly compared six literature peptide linker types which were the configurations deemed 'the best' of the respective class of linker for an *i-i+4* constraint. 'Configuration' refers to both the linker length and position of any rigid substituents (such as the triazole or double bond). The linkers, depicted in Figure 32, include a lactam bridge, all-hydrocarbon metathesis staple, a 'click'/triazole linker, an alkyl thioether bridge, a perfluoro staple and finally a *m*-xylene thioether. The six linkers were applied to a simple pentapeptide sequence: Ac-X_1AAAX_5-NH$_2$, where X_1 and X_5 were appropriate natural or unnatural amino-acids to facilitate cyclisation, and the helical structure of the cyclised peptides (shown in Figure 32) were directly compared by CD and NMR techniques. The lactam-constrained peptide **1** (Figure 32) performed the best out of the six as indicated by two symmetrical minima at 207 and 215 nm in the CD spectra. This was accompanied by $J_{HNH\alpha}$ of less than 6 Hz for all residues except the position 5 aspartate residue, accompanied by strong ROE cross-peaks for the αN(*i-i+2*), αN(*i-i+3*) and αN(*i-i+4*) interactions, indicative of an α-helical structure. 2,2,2-Trifluoroethanol (TFE) has been shown induce helicity in aqueous-solubilised peptides,[110, 111] consequently a CD spectrum of the lactam peptide was run with 50% TFE in 10 mM PBS. This spectrum did not differ from the 10 mM PBS spectrum and thereby indicated that **1** had already reached maximal helicity. As such, the lactam-constrained peptide was defined to have 100% helicity. Relative to this, the hydrocarbon (**2**, Figure 32) and triazole-linked (**3**, Figure 32) peptides showed 62% helicity, while the thioether constrained peptide showed notably less α-helical character in the CD spectrum.

The L- or D- nature of the propargylglycine residue used to assemble **3** (Figure 32), was found to have an effect on the helicity achieved, specifically the D-Pra analogue displayed only 48% helicity as measured by CD, as compared to the L-Pra with 62% helicity.
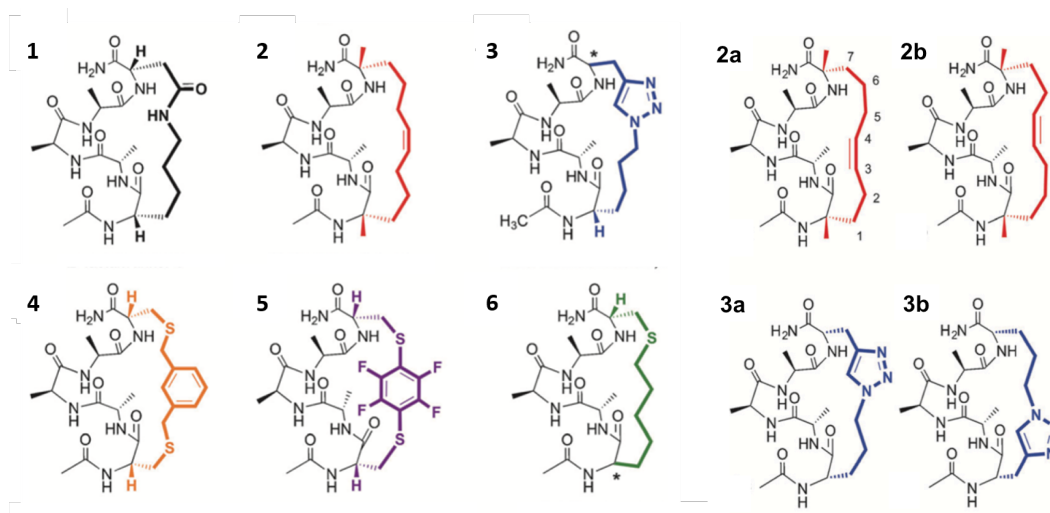
Figure 32: The alanine-rich pentapeptides constrained by a variety of linkers and linker analogues as presented by de Araujo *et al*. (Ref 86)

As the lactam linker of **1** results in maximal helicity and contains one less atom than the metathesis (**2**) and triazole linkers (**3**), the paper also detailed an investigation into the effect of linker length on helicity. Therefore, peptide analogues of the hydrocarbon and triazole linkers with only seven atoms were synthesised. The position of the double bond in the hydrocarbon staple and the location of the triazole within the linker were also investigated and revealed that helicity was eliminated in both 7-atom analogues of **3** (**3a** and **3b**, Figure 32), which was also the case for the metathesis 7-atom analogue **2a** when the double-bond was positioned in the C3-C4 position. However helicity was maintained in the 7-atom analogue of **2b** with the double bond in the C4-C5 position. This section of the study by de Araujo *et al*.[86] is a good example of the many factors at play in designing a constrained-peptide system that can effectively induce secondary structure into a peptide. It demonstrates that helicity is not merely dictated by the linker length but also the chemistry and position of the linker substituents as well as the flexibility and steric restrictions imposed by the constraint. Furthermore, the position of a linker within a peptide sequence can also drastically impact the observed structure.[98] This work testifies to the inherent complexity of designing a suitable

linker, and furthermore how difficult it may be to predict the effect of a linker on a relevant biologically derived peptide sequence, hence a comprehensive study on how a linker induces structure into a peptide must be conducted to aid the design process.

Here the secondary structure of a series of bimane-constrained peptides, in which the linker length and peptide backbone length was varied, was analysed by CD and NMR. Simple alanine-rich peptides, based on those utilised by de Araujo *et al*.,[86] were chosen for the study. β-Alanine was substituted for alanine in some of these sequences, as a means to analyse the effect of an extended backbone on secondary structure. β-Amino-acids have also proved to have many other benefits when incorporated into biologically relevant constrained-peptides. β-Amino-acids have been shown to introduce interesting structural changes in peptides that cannot be accessed by α-peptides.[115-120] Furthermore, by substituting β-amino-acids for α-amino-acids in a peptide sequence, similar chemical properties can be maintained but intra-cellular degradation can be limited as proteases are unable to recognise the isostere.[119-122]

The effect of a bimane linker on secondary structure was studied through a series of peptides to provide a good knowledge base with which to design future biologically-relevant bimane-bound compounds. The alanine-rich bimane-cyclised tripeptides (**10d-12d**) and pentapeptides (**15d-18d**), were studied by CD and NMR, in order to investigate the effect of the bimane linker on secondary structure, with a constraint distance of *i-i+2* and *i-i+4* for the tripeptides and pentapeptides, respectively. Alanine was chosen to avoid complicating the spectra. Furthermore, within each of these series, β-alanine was substituted into the sequence of **11d**, **16d** and **17d** to investigate the effect of an extended backbone length. Homocysteine replaced cysteine in **12d and 18d** to observe the effect of an increased linker length on the secondary structure. All of the bimane-cyclised peptides were analysed by CD and NMR to determine the secondary structure. Analogous acyclic bimane-attached tri-, penta- and octa- peptides (**13m, 14m**, **19m**, and **20m**), were synthesised to investigate if changes in the CD and NMR spectra are due to the macrocyclisation or the bimane entity itself. Consequently, comparisons of spectral features for the bimane-cyclised peptides, the acyclic bimane-bound peptides and

the linear precursor peptides were drawn, to deduce if changes in the CD or NMR were due to 1) *chemical* changes caused by attaching a bimane to the peptide; 2) *structural* changes in the peptide induced by *bimane* attachment; or 3) *structural* changes as a result of *cyclisation*.

3.2 Tripeptides (*i-i*+2)

The bimane-cyclised tripeptide **10d** (Figure 33) was designed to investigate the effect of an *i-i*+2 bimane linker on secondary structure. The position 2 alanine of **10** was substituted with β-alanine to give **11**, and similarly the position 1 and 3 cysteines in **10** were substituted with side-chain extended homocysteine to give **12**, as shown in Figure 33. Linear peptides **11** and **12** were then cyclised through reaction with dibromobimane as previously discussed (in section 2.1.2), to give **11d** and **12d** (Figure 33). Peptide **11d** was included to investigate the effect a longer backbone may have on the secondary structure when constrained by an *i-i*+2 bimane linker. In contrast, **12d** allows a longer bimane linker (larger macrocycle) to be investigated and its effect on secondary structure observed. Two acyclic analogues (**13m** and **14m**, Figure 33) were synthesised by the reaction of **13** and **14** (Figure 33), respectively, with monobromobimane. These analogues act as pseudo-controls, in which the effect of the bimane on the secondary structure could be observed, without cyclisation of the peptide. Therefore, conclusions can be drawn as to whether structural changes observed were an effect of the bimane itself, or the cyclisation. NMR and CD analysis is separated into two groups for simplicity, such that the effect of the amino-acid sequence changes can be individually evaluated. Specifically, **10d** and **12d** are compared directly to **13m** and **10**, then **11d** is compared to **14m** and **11**.
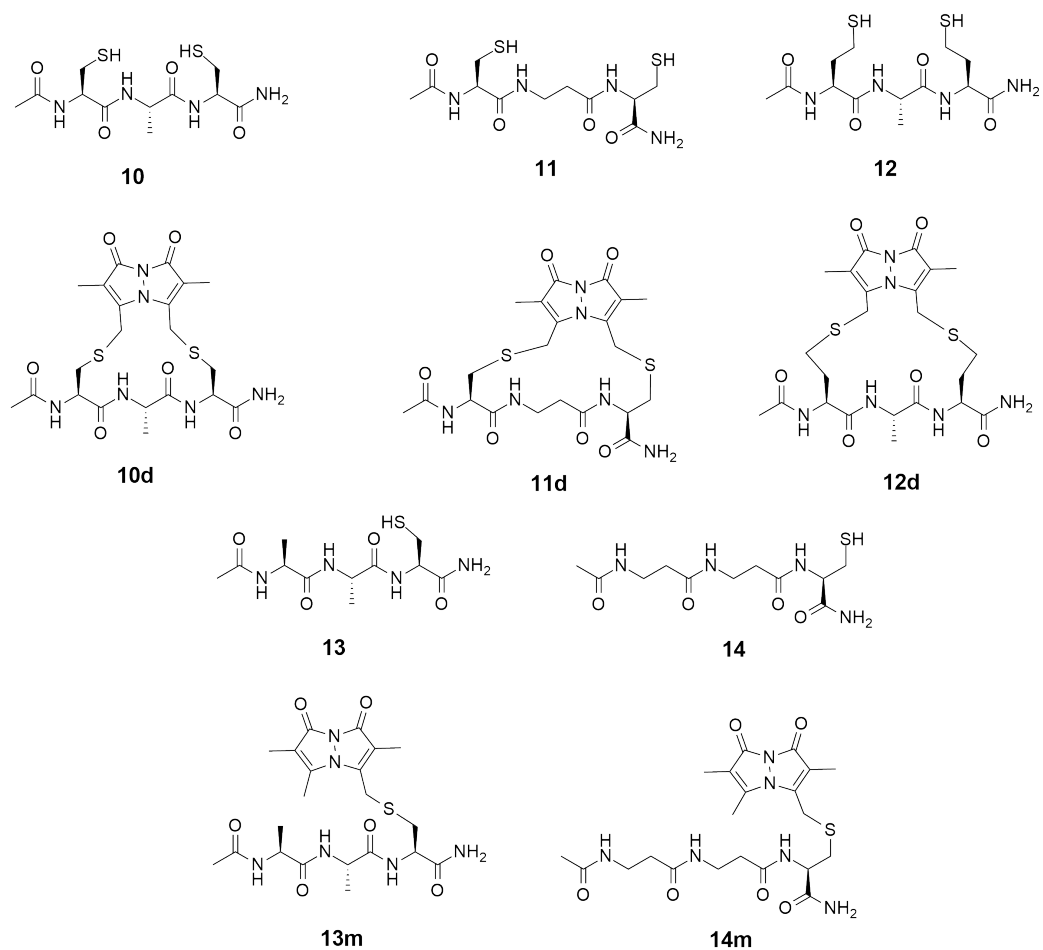
Figure 33: Chemical structures of the linear tripeptides, the acyclic bimane-attached counterparts and the cyclic bimane tripeptides.

CD was conducted using samples of 150 μM concentration in 10 mM aq. PBS at pH 7.2 NMR spectroscopy was conducted in d_6-DMSO and $J_{HNH\alpha}$ coupling constants were extracted from NH splitting, and chemical shifts of key residues compared to literature values.[62-64]

3.2.1 The effect of bimane cyclisation and increased linker length: A study of 10d and 12d

Circular Dichroism

The CD spectrum of the linear peptide **10** (Figure 34) shows a single large minimum at 197 nm (Figure 35) suggesting a lack of secondary structure. The acyclic peptide **13m** (Figure 34) with a bimane bound at position 3 exhibited a near identical CD spectrum (to **10**) with a minimum at 196 nm, and it was therefore inferred that introduction of the bimane did not dramatically influence the secondary structure of **10**. Neither the spectra of **10** or **13m** display any maxima, further supporting the conclusion that significant secondary structure is not present in these peptides.

It was anticipated that the bimane itself may display additional absorbance in the far-UV region analysed in CD, as reported for the perfluoro linker.[79] However, no additional maxima or minima were observed in the spectrum of bimane-attached **13m** compared to the linear **10** over the range of 190-260 nm, therefore it can be concluded that the bimane does not complicate the CD analysis.

The CD spectrum for bimane cyclised **10d** showed minima at 221 and 199 nm, and maximum at 186 nm (Figure 35, Table 8). The presence of the minimum at 221 nm suggests some secondary structure is induced in the peptide when cyclised, specifically β-strand type structure. The CD of peptide **12d** was similar to that of **10d**, however the minimum at 226 nm in **12d** is greater in intensity (more negative) than the 221 nm minimum of **10d**, which is consistent with enhanced β-strand like structure in **12d**, which is further supported by a strong maximum at 186 nm.
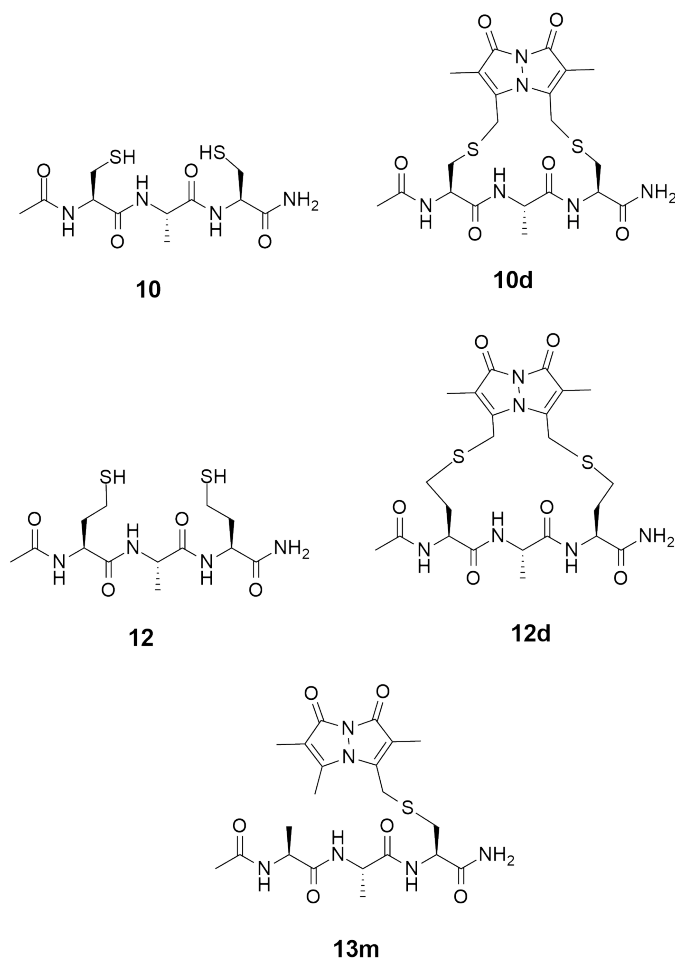
Figure 34: The tripeptide **10d** allowed investigation of bimane-cyclisation on the effect on secondary structure, **12d** allowed investigation into an extended linker length. These structures are presented here compared to the analogous unfunctionalised linear and acyclic bimane-attached peptides
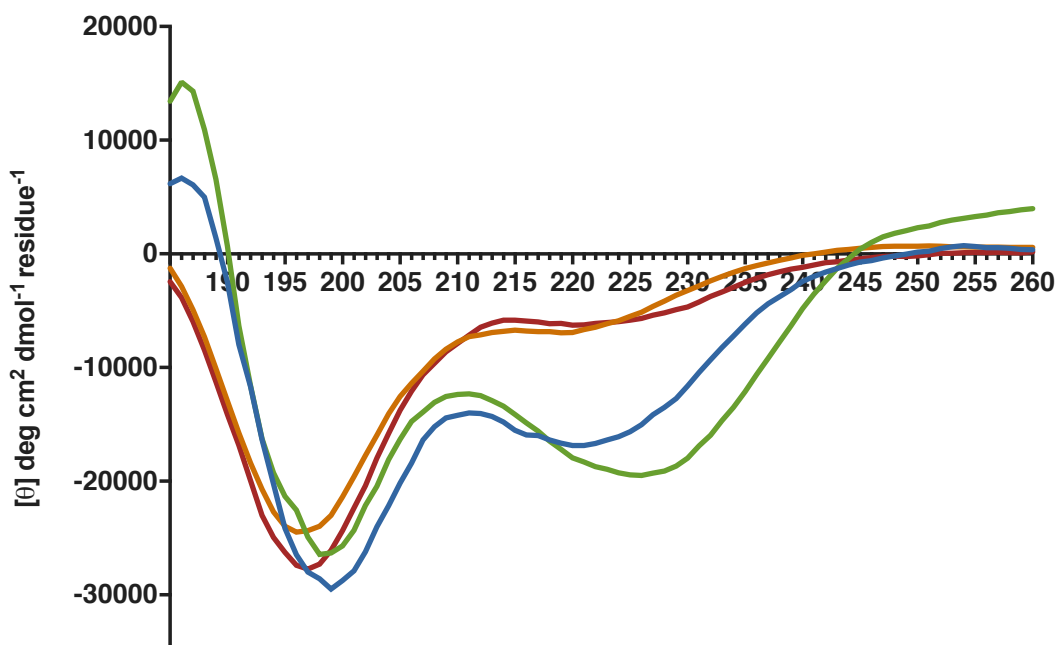
Figure 35: CD spectra for ▬ **10,** ▬ **13m,** ▬ **10d** and ▬ **12d** collected on a Jasco J-810 spectropolarimeter at 150 μM in 10 mM PBS at pH 7.2.

Table 8: Summary of the maxima and minima observed in the CD spectra presented in **Figure 35**.

	10	10d	12d	13m
Minima	197	199	198	196
		221	226	
Maximum	-	186	186	-

$J_{HNH\alpha}$ Coupling constants

The $J_{HNH\alpha}$ coupling constants for **10** all lie within the random coil region of 6-8 Hz, as shown in Figure 36, which supports the CD observations. This is also the case for **12** and **13m** in which only one $J_{HNH\alpha}$, in each peptide, lies just outside of the random coil region. The bimane-cyclised peptide **10d** shows increased $J_{HNH\alpha}$ values relative to **10**. However this observed increase only places one $J_{HNH\alpha}$ for **10d** within the β-strand region. The $J_{HNH\alpha}$ values for bimane-cyclised peptide **12d,** similarly, are larger than those of the linear **12** $J_{HNH\alpha}$ values. This difference places the two modified-cysteine residues of **12d** within the β-strand region (>8 Hz), implying increased β-strand character compared to **10**, which is consistent with the CD data.
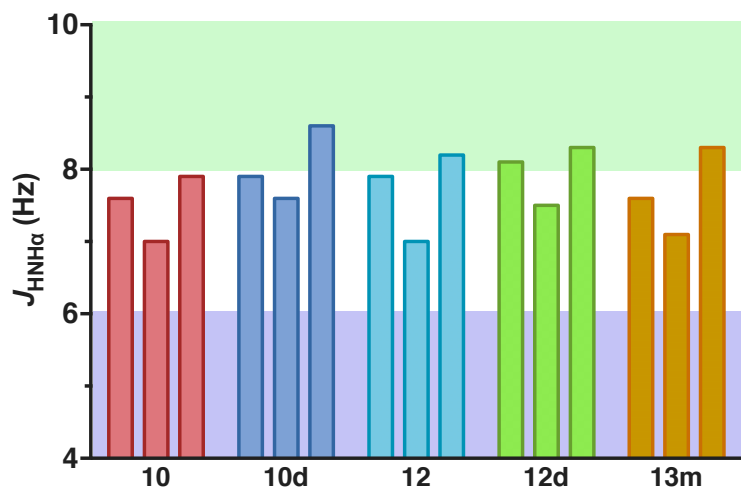
Figure 36: The $J_{HNH\alpha}$ for a series of bimane-bound tripeptides and the acyclic analogues, determined from a H^1 NMR spectra in d_6-DMSO. ▮ β-strand region (>8 Hz), ▮ helical region (< 6 Hz).

NMR Chemical Shift

Defined secondary structure gives rise to characteristic NMR chemical shifts of key residues relative to random coil literature values.[62-66] The change in chemical shift relative to random coil literature values ($\Delta\delta$, where $\Delta\delta = \delta_{exp} - \delta_{lit}$), were calculated for **10**, **12**, **10d**, **12d** and **13m**, as displayed graphically in Figure 37-Figure 39. All cysteines in **10**, **12**, **10d**, **12d** and **13m** show notably negative α-proton $\Delta\delta$, particularly in comparison to the position 2 alanines, and therefore the cysteine $\Delta\delta$ were discounted from structural analysis. This shift is less prominent when the cysteine is bound to a bimane, i.e. the $\Delta\delta$ is less negative in **10d**, **12d** and **13m** compared to **10** and **12**. In the linear peptides **10** and **12**, the position 2 alanine also shows a negative shift, but this is still within the random coil window, in agreement with the CD data discussed above.

The α-proton $\Delta\delta$ values for acyclic bimane-bound **13m** all lie well within the random coil window of 6-8 Hz, indicating a random coil structure, in line with the $J_{HNH\alpha}$ values (Figure 37). The $\Delta\delta$ values calculated relative to the linear **10** ($\Delta\delta_{linear} = \delta_{cyclised} - \delta_{linear}$), for the position 3 modified-cysteine α-proton of **13m** shows a significantly larger change than the position 1 and 2 alanines. This implies that attachment of a bimane to an amino-acid induces a notable chemical shift change in these resonances, independent of any secondary structural changes observed in the peptide. The $\Delta\delta$ of the α-carbon (Figure 38) for the modified cysteine

(position 3) of **13m**, is larger than the two alanines. This $\Delta\delta$ is more pronounced when observing the position 3 $\Delta\delta_{linear}$ which lies well within the β-strand region, further confirming that bimane attachment leads to a change in chemical shift. The $\Delta\delta$ values are much less significant or conclusive for the carbonyl carbon (Figure 39).

The alanine α-proton $\Delta\delta$ for the bimane cyclised peptide **10d** is positive – suggesting enhanced β-strand structure, in agreement with the $J_{HNH\alpha}$ and CD. However the $\Delta\delta$ does not lie within the defined β-strand region. Both the α-carbon and carbonyl carbon $\Delta\delta$ for the **10d** position 2 alanine residue are quite negative, suggesting β-strand structure. However, the $\Delta\delta_{linear}$ (relative to **10**) for the position 2 alanine residue shows a much smaller value such that the $\Delta\delta_{linear}$ lies within the random coil region. This implies that some of the observed structure is likely defined by the peptide sequence.

The $\Delta\delta$ for the position 2 alanine α-proton of **12d** is positive, representing a shift toward β-strand This shift is more prominent when the α-proton $\Delta\delta_{linear}$ is calculated, relative to **12**, in which the alanine $\Delta\delta_{linear}$ lies within the β-strand region, as shown in Figure 37. Similarly, the α-carbon and carbonyl carbons $\Delta\delta$ for the alanine of **12d** show a strong negative $\Delta\delta$ (see Figure 38 and 39) indicating a β-strand like structure.

Both bimane cyclised peptides **11d** and **12d** show evidence of β-strand like structure. The CD spectra suggest that **12d** is slightly more structured that **10d** due to the greater intensity of the maximum at 186 nm and 226 nm minimum. That is, a *i-i*+2 bimane linker within a tripeptide induces β-strand like structure.

Table 9: Sequence summaries for the α-alanine tripeptides, where Ac indicates an acetyl group and Am indicates an amide. Residues with a '*' are bimane bound.

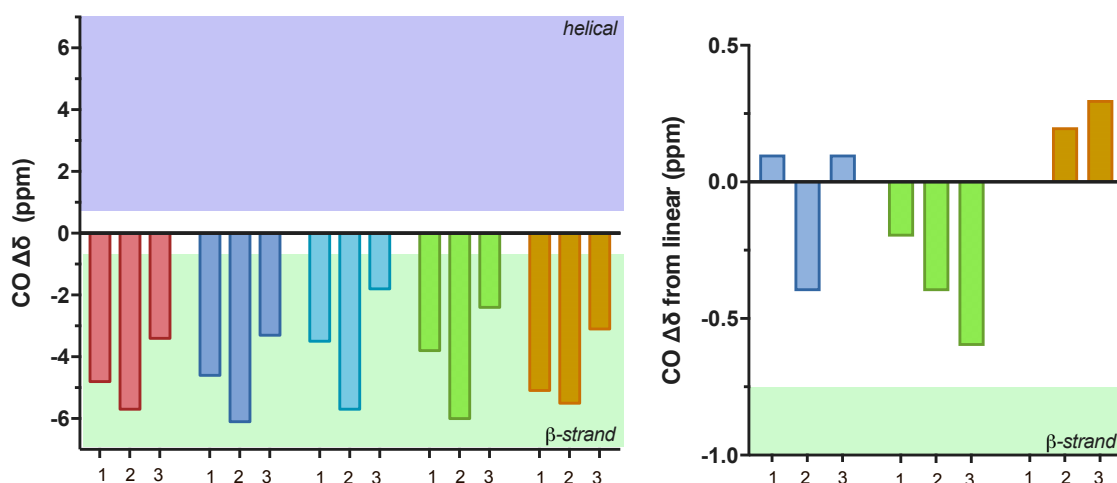|		Residue			
Compound		1	2	3	
10		C	A	C	
10d		C*	A	C*	
12	Ac	Hcy	A	Hcy	Am
12d		Hcy*	A	Hcy*	
13m		A	A	C*	
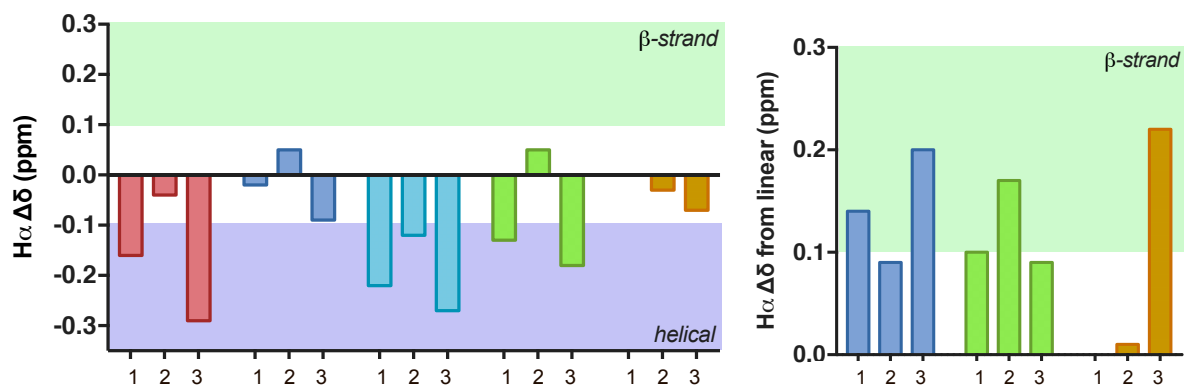
Figure 37: α-Protons chemical shifts relative to literature random coil values (left) for a series of tripeptides and relative to the linear unfunctionalised peptide **10** (right). ▉**10**, ▉**10d**, ▉**12**, ▉**12d**, ▉**13m**; ▉ β-strand region (> 0.1 Hz), ▉ helical region (< -0.1 Hz).
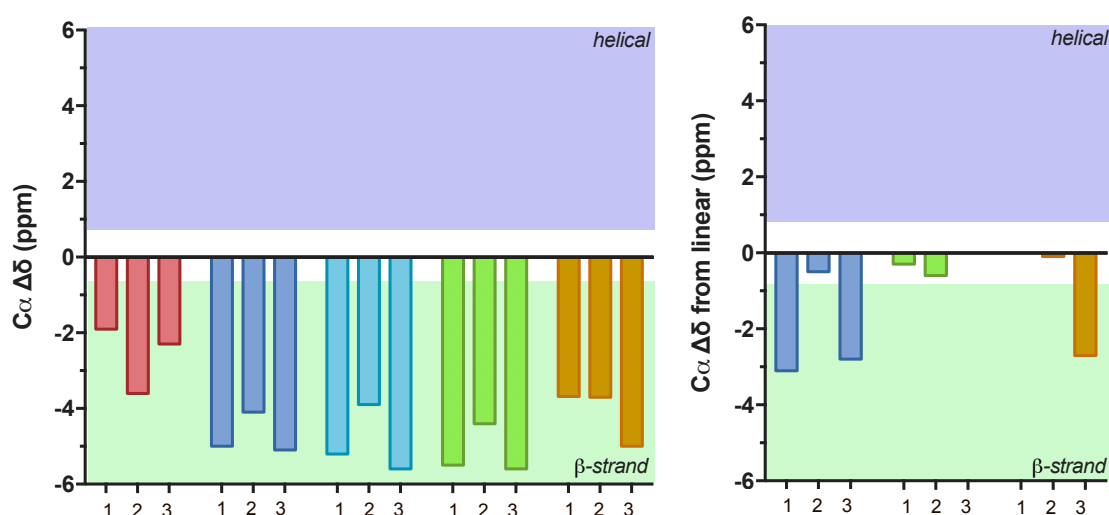
Figure 38: α-Carbon chemical shifts relative to literature random coil values (left) for a series of tripeptides and relative to the linear unfunctionalised peptide **10** (right). ▉**10**, ▉**10d**, ▉**12**, ▉**12d**, ▉**13m**; ▉ β-strand region (< -0.7 Hz), ▉ helical region (> 0.7 Hz).

Figure 39: Carbonyl chemical shifts relative to literature random coil values (left) for a series of tripeptides and relative to the linear unfunctionalised peptide **10** (right). ▉**10**, ▉**10d**, ▉**12**, ▉**12d**, ▉**13m**; ▉ β-strand region (< -0.7 Hz), ▉ helical region (> 0.7 Hz).

3.2.2 The effect of increased backbone length: A study of 11d

The effect of an increased backbone length on an *i-i+2* bimane-constrained tripeptide, as compared to **10** (all standard α-amino-acids), was investigated through structural studies of β-alanine peptide **11d**, shown in Figure 40. The acyclic peptide **14m** (Figure 40), with a bimane at position 3, was also investigated and compared to the unfunctionalised linear peptide **11**, such that any chemical or structural effects incurred by the bimane itself could be elucidated.
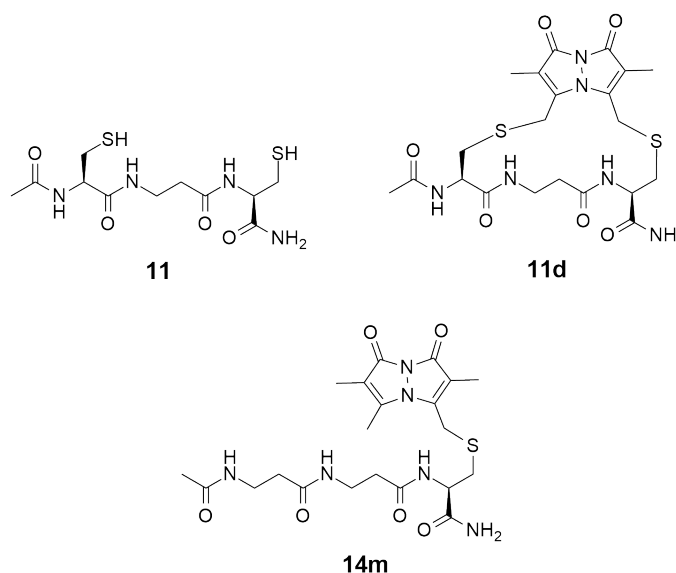
Figure 40: Chemical structure of the three β-alanine containing tripeptides which were studied to investigate the effect of a longer backbone in an *i-i+2* bimane constrained peptide.

Circular dichroism

The CD spectra presented in Figure 41 were collected in 10 mM PBS at pH 7.2. The observed minima and maxima are summarised in Table 10. The combination of a minimum at 196 nm and the absence of a maximum, in the CD spectrum of the linear unfuctionalised peptide **11**, coupled with the weak intensity of the spectrum indicates that there is very little to no secondary structure in the peptide. The acyclic bimane-bound peptide **14m** shows only one intense minimum at 198 nm, characteristic of a random coil structure. The β-alanine bimane-cyclised peptide **11d** similarly shows a very intense minimum at 194 nm, however plateaus between 215 and 220 nm before forming a distinct maximum at 237 nm. This spectrum is somewhat similar to a poly-Glu CD spectrum reported in literature,[123] which infers the structure adopts a conformation similar to a Poly-Pro II helix.

53
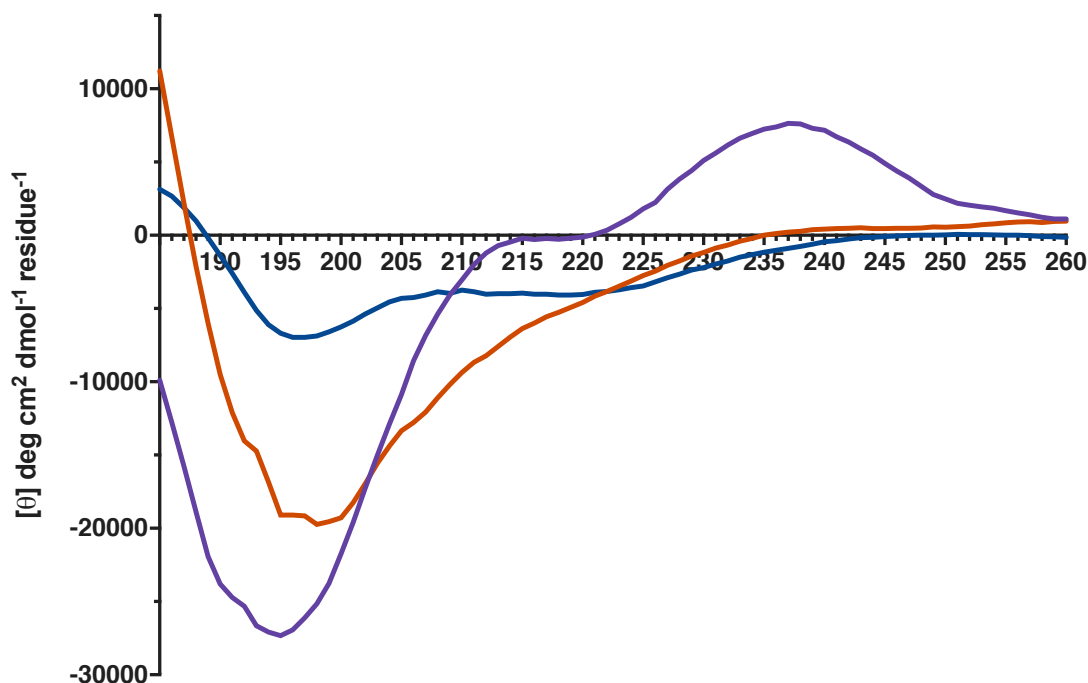
Figure 41: CD spectra for ── **11,** ── **11d** and ── **14m** collected on a Jasco J-810 spectropolarimeter at 150 μM in 10 mM PBS at pH 7.2.

Table 10: Summary of the wavelengths of the CD maxima and minima shown in Figure 41.

	11	11d	14m
Minimum (nm)	196	194	198
Maximum (nm)	-	237	-

Coupling constants

NMR structural studies for the tripeptides were carried out in d_6-DMSO, the $J_{HNH\alpha}$ were determined and are displayed in Figure 42. The $J_{HNH\alpha}$ for **11** could not be determined as the NH resonances all overlapped, which was also the case for the α-protons. The position 1 and 2 alanine $J_{HNH\alpha}$ for **14m** are well below 6 Hz and suggest a helical structure, unlike the CD data. The position 3 modified-cysteine $J_{HNH\alpha}$ is anomalously large. The position 2 alanine $J_{HNH\alpha}$ for bimane-cyclised **11d** lies within the random coil region, and the bimane-bound cysteine residues at position 1 and 3 are slightly higher and lie within the β-strand region. This data does not correlate with the observations made in the CD. New H^1 NMR data in 10% D_2O in water were collected and $J_{HNH\alpha}$ extracted in order to determine if the solvent induced a structural change in the peptides to account for the disparity between the NMR and CD data.

The NH and α-proton NMR resonances for the three tripeptides **11**, **11d** and **14m** in water were shifted notably compared to the spectrum in d$_6$-DMSO. The $J_{HNH\alpha}$ in 10% aq. D$_2$O are also presented in Figure 42. The position 1 and 2 β-alanine $J_{HNH\alpha}$ values in 10% D$_2$O in water, for the linear peptide **11**, lie within the helical region which agrees with the observations made in the CD. The β-alanine $J_{HNH\alpha}$ for **14m** are significantly larger in 10% aq. D$_2$O such that all $J_{HNH\alpha}$ lie within the random coil region of 6-8 Hz, better matching the CD data. However, the $J_{HNH\alpha}$ for bimane-cyclised **11d** are smaller in 10% aq. D$_2$O compared to those in DMSO. The position 2 alanine $J_{HNH\alpha}$ for **11d** lies below 6 Hz and is therefore in the helical region, although the position 1 and 3 modified-cysteine $J_{HNH\alpha}$ values still lie within the random coil region, in comparison to the **11d** $J_{HNH\alpha}$ values in 10% D$_2$O in water are much smaller and indicate slight helical structure. This $J_{HNH\alpha}$ in water matches the CD data much more closely than the DMSO $J_{HNH\alpha}$ values. This is a good example of the effect solvent can induce on secondary structure, here bimane-cyclised **11d** appears somewhat β-strand like in DMSO, however takes on a helical or turn-type structure 10% D$_2$O in water. The remaining NMR chemical shift data discussed was conducted in DMSO, and as such, cannot be compared to the CD.
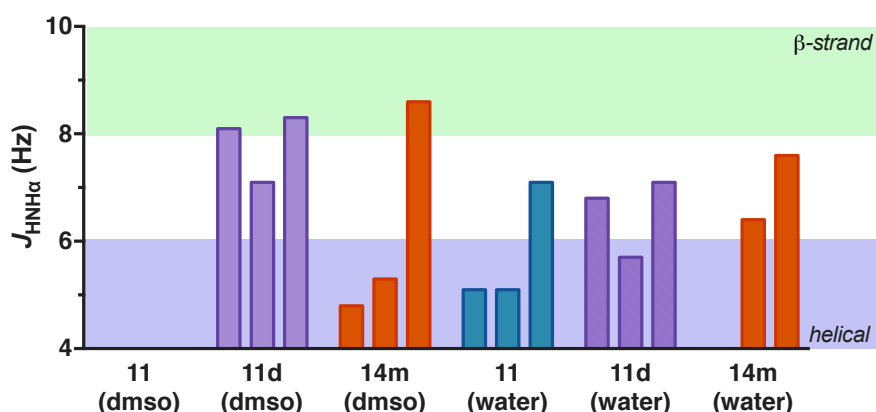
Figure 42: $J_{HNH\alpha}$ coupling constants for a series of tripeptides **11, 11d** and **14m** (**Figure 40**), determined in d$_6$-DMSO and 10% D$_2$O in water at pH ~5. ▨ β-strand region (> 8 Hz), ▨ helical region (< 6 Hz).

NMR Chemical shift

The change in chemical shift (Δδ) for the cysteine α-protons and the β-alanine α- and β-protons are collectively referred to as proton Δδ in this section, as opposed to α-proton Δδ. A

reliable literature source for ^{13}C chemical shifts of β-alanine in a known random-coil structure could not be found, therefore carbon Δδ relative to literature sources could not be calculated. As such the α-carbon and carbonyl-carbon Δδ are only calculated relative to the linear peptide **11** ($\Delta\delta_{linear}$). Furthermore, as discussed above, the cysteine Δδ cannot be included in the structural analysis due to the bimane altering the observed resonances, independent of structural changes. The amino-acid sequences for **11**, **11d** and **14m** are summarised in Table 11.

The linear peptide **11** shows negative proton Δδ for all residues, as shown in Figure 43, which suggests helical structure. The proton Δδ of the acyclic bimane-bound **14m**, are all negative and lie within the helical region. However, the $\Delta\delta_{linear}$ are small for **14m**, implying that there is limited secondary structure in **14m** and any observed structure is likely a characteristic of the analogous linear peptide **11**. This is supported by the α-carbon and carbonyl-carbon $\Delta\delta_{linear}$ which shows very small $\Delta\delta_{linear}$ values indicating that the structure of **14m** is very similar to **11**. This implies that introduction of the bimane into **14m** does not alter the secondary structure of the tripeptide.

The observable proton Δδ for bimane-cyclised peptide **11d** are also negative, suggesting a slight tendency toward helical structure. However the Δδ are quite small, which implies very little secondary structure present which is further supported by very small $\Delta\delta_{linear}$ (Figure 43). The α-carbon $\Delta\delta_{linear}$ are negative, indicating β-strand like structure, however only one of the two β-alanine carbons lie within the β-strand region. Conversely, the observable position 2 β-alanine carbonyl-carbon $\Delta\delta_{linear}$ (Figure 44) lies within the random coil region (position 1 cysteine is excluded). This NMR data is inconclusive and suggests that, in DMSO, **11d** does not exist in any defined secondary structure. The NMR spectrum itself however is quite intriguing, every proton (except the bimane and acetyl methyls) in the structure appears as a separate resonance, that is there are no signals which integrate for more than one proton. Furthermore, only two resonances overlap – this is shown by the signal at ~2.75 ppm which represents two 1H signals, correlated to one bimane methylene proton from each side of the

bridge. The splitting pattern of all these resonances suggest that the **11d** structure is in a restricted conformation induced by the bimane in a way which isolates each proton to a separate chemical environment. However it is not clear from the NMR chemical shift exactly what this structure is and further studies are needed to elucidate this.

Table 11: Sequence summaries for the β-alanine tripeptides, where Ac indicates and acetyl group and Am indicates an amide. Residues with a * are bimane bound

		Residue		
Compound		**1**	**2**	**3**	
11		C	βAla	C	
11d	Ac	C*	βAla	C*	Am
14m		βAla	βAla	C*	
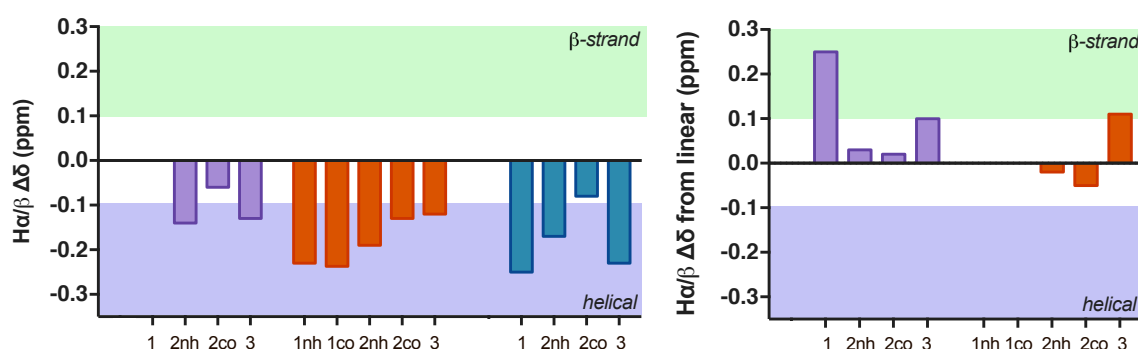
Figure 43: The change in α-proton (left) relative to literature values[124] and the relative to the unfunctionalised linear peptide **11** (right). ▮ **11**, ▮ **11d**, ▮ **14m**; ▮ β-strand region (> 0.1 Hz), ▮ helical region (< -0.1 Hz).
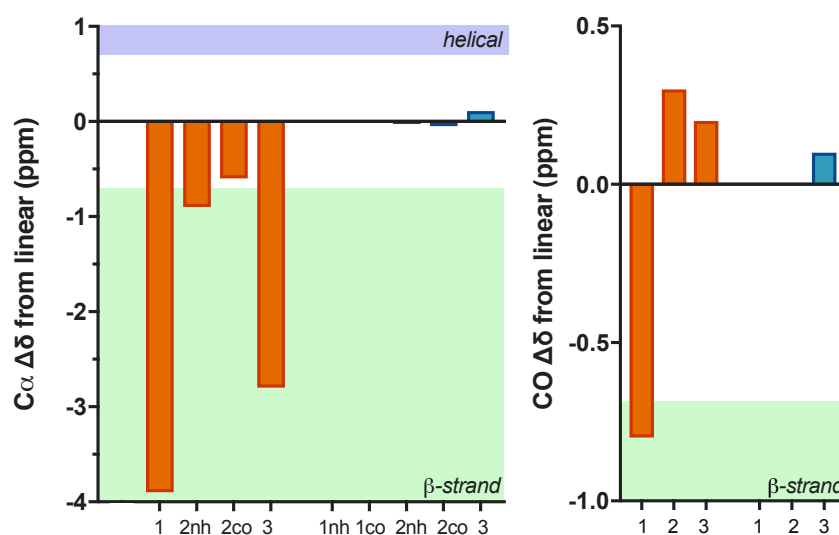
Figure 44: The change in α-carbon (left) and carbonyl carbon (right) chemical shift relative to the unfunctionalised linear peptide **11.** ▮ **11d**, ▮ **14m**; ▮ β-strand region (< -0.7 Hz), ▮ helical region (> 0.7 Hz).
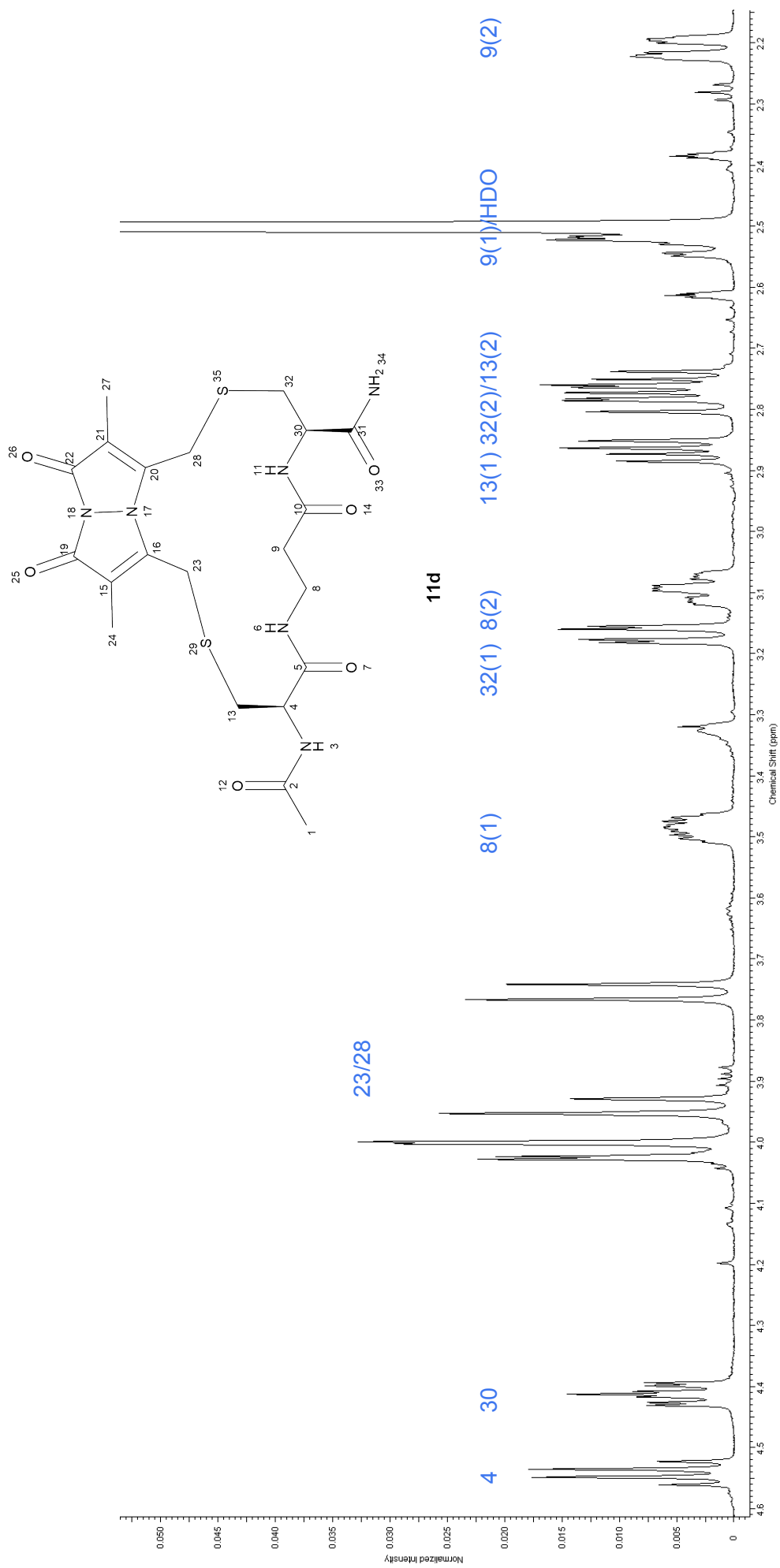
Figure 45: The aliphatic region of a 500 MHz NMR spectrum of **11d** in d$_6$-DMSO.

3.3 Pentapeptides (*i-i*+4)

The linear pentapeptide **15**,[86] which contains cysteines at position 1 and 5, was cyclised on reaction with dibromobimane to give **15d** (Figure 46). Studies on the secondary structure of this compound form a base for an extended investigation into the use of a bimane linker as an *i-i*+4 constraint. β-alanine and homocysteine were substituted into the sequence of **15** to give **16**, **17** and **18**, which were then cyclised on reaction with dibromobimane to give **16d**, **17d** and **18d** respectively, shown in Figure 46. Peptide **16d** contains β-alanine at positions 2-4, in place of alanines at these positions in **15d**. This provides an opportunity to investigate the effect of a longer, more flexible backbone on the secondary structure of an *i-i*+4 linked bimane peptide. Bimane-cyclised peptide **17d** with a single β-alanine at position 4 provides an intermediate backbone length to allow comprehensive investigation into the effect of increasing backbone length. The peptide **16d** has bimane-modified homocysteine at position 1 and 5 to provide an opportunity to investigate the effect that a longer linker has on secondary structure.

Peptide **19m** contains α-alanines at position 1-4 and a bimane functionalised cysteine at position 5, in contrast peptide **20m** employs β-alanine at positions 1-4. The acyclic bimane-bound peptides, **19m** and **20m** (Figure 46) were synthesised to determine if introducing the bimane alone into a pentapeptide induced a chemical change, independent of any structural changes, as discussed at the beginning of this chapter. The CD and NMR data of **19m** and **20m** were compared to the linear precursor peptides **19** and **20** (Figure 46), respectively, to achieve this. Once it was determined if the bimane had induced a chemical shift in the acyclic pentapeptides **19m** and **20m**, these peptides were then compared to the cyclised peptides **15d** and **16d** respectively. The bimane-cyclised peptide **18d**, with central α-alanines and homocysteines at positions 1 and 5, was deemed more similar to **15d** (than **16d**) and was therefore also compared to **19** and **19m**. It was concluded peptide **17d** was more similar to the β-alanine containing peptides (on inspection of the CD and NMR data) and was therefore

compared to **20** and **20m**. The CD and NMR data for these two sets of peptides [**15**, **15d**, **18d**, **19m**] and [**16**, **16d**, **17d**, **20m**] were evaluated separately to simplify the analysis.
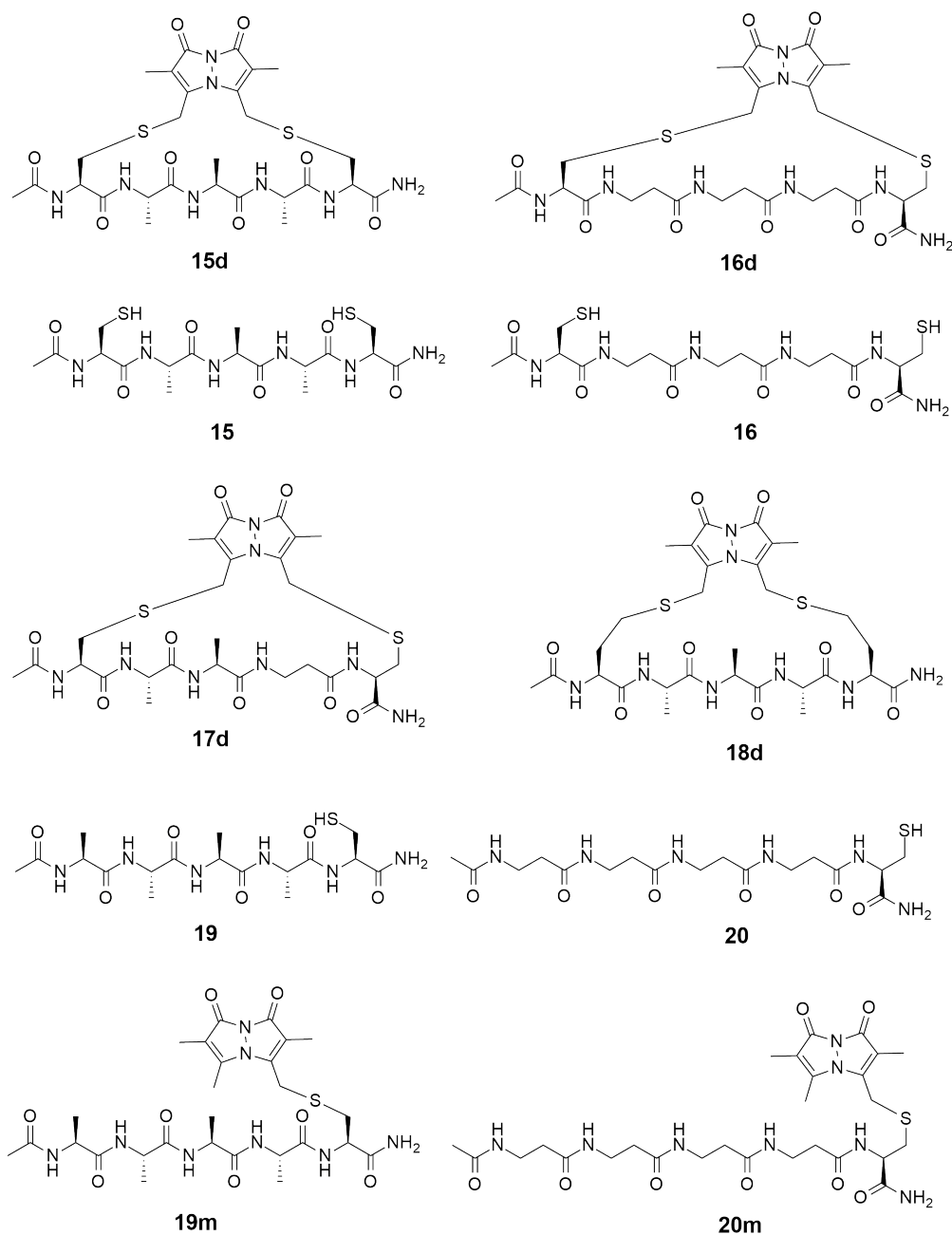
Figure 46: Chemical structures of the linear peptides, the acyclic bimane attached counterparts and the cyclic bimane pentapeptides.

CD was conduced with samples at 150 μM concentration in 10 mM PBS at pH 7.2. NMR spectroscopy was conducted in 10% D_2O in H_2O at pH ~5, and referenced to DSS. $J_{HNH\alpha}$ coupling constants were extracted, and chemical shifts of key residues compared to literature values where applicable.

3.3.1 The effect of bimane cyclisation and increased linker length: A study of 15d and 18d

$J_{HNH\alpha}$ Coupling constants

The $J_{HNH\alpha}$ coupling constants, extracted from the ^{1}H 1D NMR, for the alanine rich peptides **15**, **15d**, **18d** and **19m** (Figure 47) are represented in Figure 48. The linear pentapeptide **15** appears to adopt a helical structure as the position 2 and 3 alanine $J_{HNH\alpha}$ coupling constants are below 6 Hz and the position 4 alanine is only 6.1 Hz. Alanine is known to enhance α-helical structure[74, 125-127], and as 3 of 5 residues in **15** are alanine, it is not surprising this linear peptide naturally displays some helical structure. The $J_{HNH\alpha}$ for the 1 and 5 position cysteines of **15** are larger in magnitude compared to the central alanine residues, which may imply some flexibility at the peptide termini. A $J_{HNH\alpha}$ could not be determined for all residues in **15d** and **19m** due to overlapping NH resonances and overlap of the α-protons resonances with the broad D_2O/HDO peak.

The cysteine $J_{HNH\alpha}$ for **15**, **15d** and **18d** are all notably higher than other alanine residues, which suggests the bimane may influence the $J_{HNH\alpha}$. The acyclic bimane-bound peptide **19m**, appears to adopt some helical structure with the position 1 and 2 alanine $J_{HNH\alpha}$ coupling constants well below 6 Hz. Furthermore, the observable $J_{HNH\alpha}$ for position 2 and 3 alanines of **15d** are also within the helical region. The position 1 cysteine and position 2 and 4 alanines in **18d** are also below 6 Hz, similarly implying the presence of some helical structure.
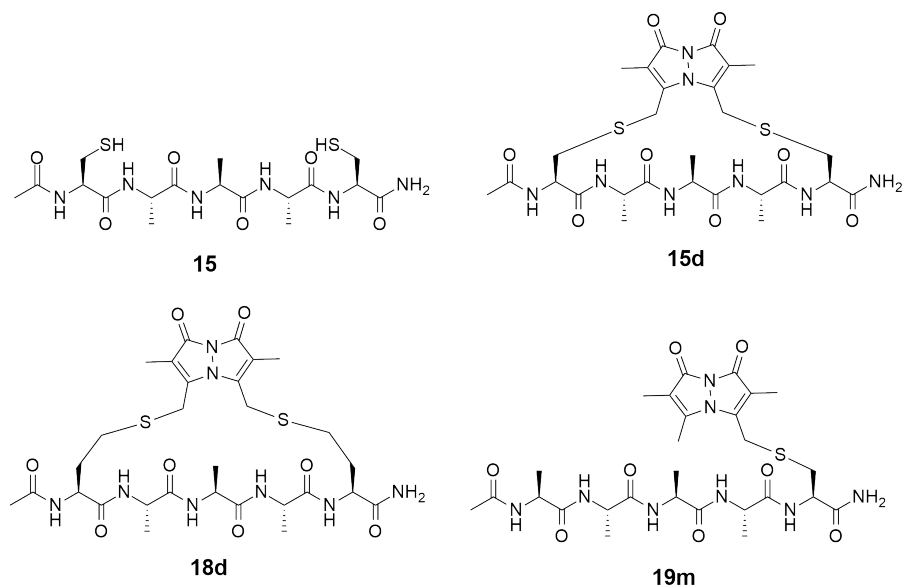
Figure 47: The pentapeptides structures which were analysed by CD and NMR in section 3.3.1
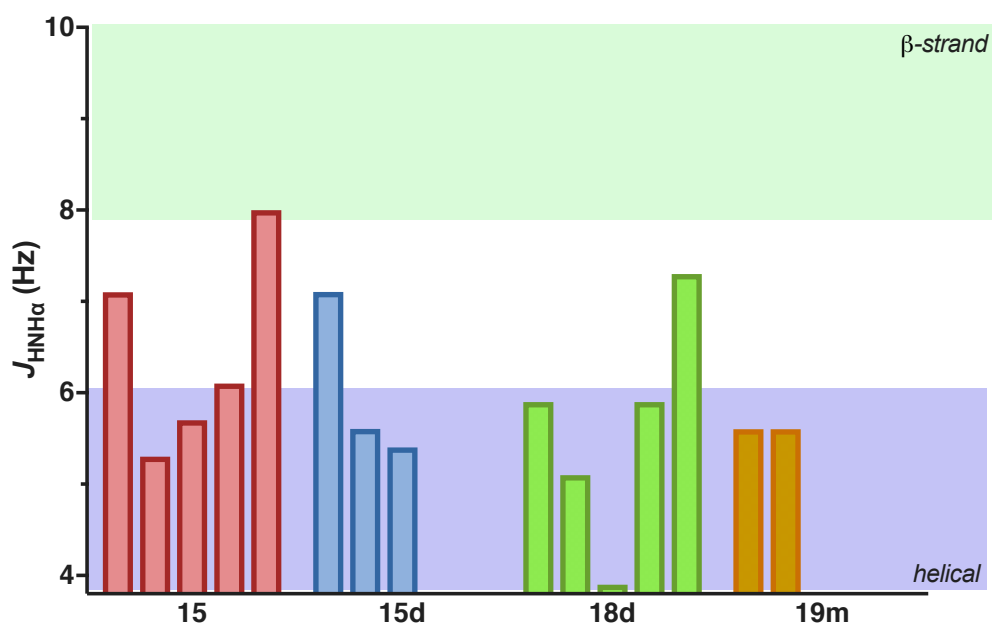
Figure 48: $J_{HNH\alpha}$ coupling constants for a series of pentapeptides **15, 15d, 18d** and **19m,** determined in 10% D_2O in water at pH ~5; β-strand region (> 8 Hz), helical region (< 6 Hz).

NMR Chemical Shift

The change in chemical shift (Δδ) relative to random coil literature values was calculated for **15**, **15d**, **18d** and **19m**, and these are displayed graphically in Figure 49 and Figure 50. The amino-acid sequences of **15**, **15d**, **18d** and **19m** are summarised in Table 12. As seen for the tripeptides discussed above, the bimane-bound cysteines show a dramatically different Δδ compared to the alanine residues, which is likely due to the attachment of the bimane itself. Therefore the cysteine Δδ are discounted from the structural analysis.

The linear peptide **15** shows negative $\Delta\delta$ for all five residues (Figure 50A), in which two have shifted enough to lie within the helical region, therefore suggesting a somewhat helical structure, in agreement with the $J_{HNH\alpha}$. A ^{13}C 1D spectrum of **15** was not obtained, as **15** could not be solubilised in D_2O in sufficient concentration.

The α-proton $\Delta\delta$ of all residues in the acyclic bimane-bound **19m** have shifted negatively, however all $\Delta\delta$ are still within the random coil region. The α-proton $\Delta\delta_{linear}$ plot for **19m** (Figure 49B) shows a very small $\Delta\delta_{linear}$, which implies that the bimane attachment has not significantly altered the peptide structure. Both the α-carbon and carbonyl carbon $\Delta\delta$ (excluding the position 5 cysteine) are very small, reinforcing that **19m** has little to no secondary structure.

The $\Delta\delta$ for the α-protons in the bimane-cyclised **15d** are slightly negative and well within the random coil window. Furthermore the $\Delta\delta_{linear}$, relative to **15**, are also within the random coil range suggesting that there is very minimal secondary structure in **15d**. The alanine α-carbon $\Delta\delta$ (Figure 50A) for **15d** are all at least 0.7 ppm which suggests a somewhat helical structure, however the $\Delta\delta$ for the position 2-4 alanine carbonyl-carbons are well within the random coil range. Therefore it is concluded that although there may be a slight tendency for helical structure, there is no strong, regular secondary structure in **15d**.

Compound **18d**, cyclised with a bimane through the position 1 and 5 homocysteines, shows negative α-proton $\Delta\delta$ values, of which the alanine residues 3 and 5 have shifted by at least -0.1 ppm, therefore suggesting helical structure. However, when the α-proton $\Delta\delta_{linear}$ are calculated, relative to the linear **15**, the $\Delta\delta_{linear}$ is very small. This implies some or all of the structure observed in **18d** may be inherent in the linear amino-acid sequence and not a result of the cyclisation. The $\Delta\delta$ for the alanine α-carbons (Figure 50A) is positive, also implying helical structure in line with the $J_{HNH\alpha}$, however only the position 2 alanine lies in the helical region. The carbonyl $\Delta\delta$ are strongly positive, reinforcing the suggestion of helical structure in **18d**. Therefore it can be said that the NMR data for **18d** suggests this bimane-cyclised homocysteine peptide is somewhat helical.

Table 12: Summary of the peptide sequence for **15, 15d, 18d** and **19m**. Ac represents an acetylated *N*-terminus, and Am indicates a *C*-terminal amide. Hcy represents a homocysteine residue and * indicates attachment to a bimane.

		Residue				
Compound		**1**	**2**	**3**	**4**	**5**
15		C	A	A	A	C	
15d	Ac	C*	A	A	A	C*	Am
18d		Hcy*	A	A	A	Hcy*	
19m		A	A	A	A	C*	
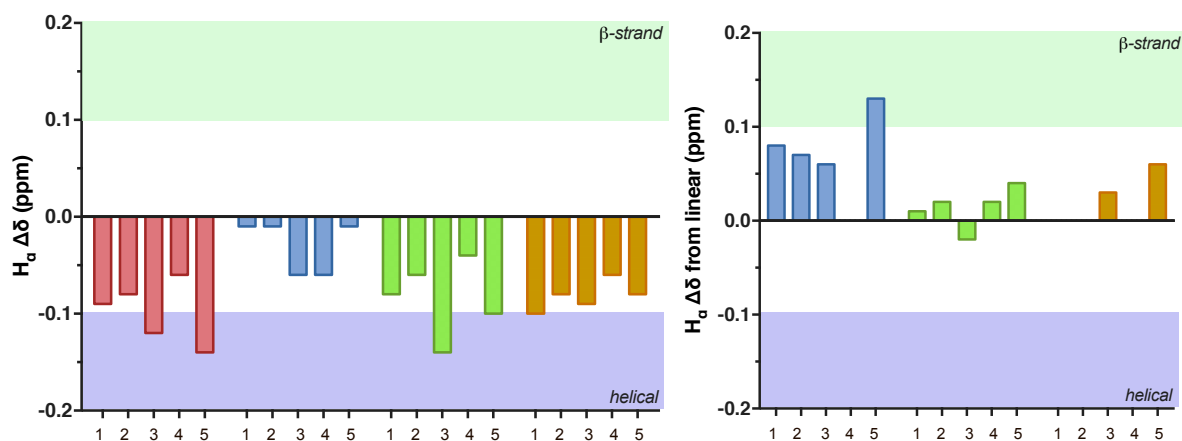
Figure 49: α-Protons chemical shifts relative to literature random coil values (left) for a series of pentapeptides and relative to the linear unfunctionalised peptide **15** (right). ■**15**, ■**15d**, ■**18d**, ■**19m,** ■ β-strand region (> 0.1), ■ helical region (< -0.1 Hz). .
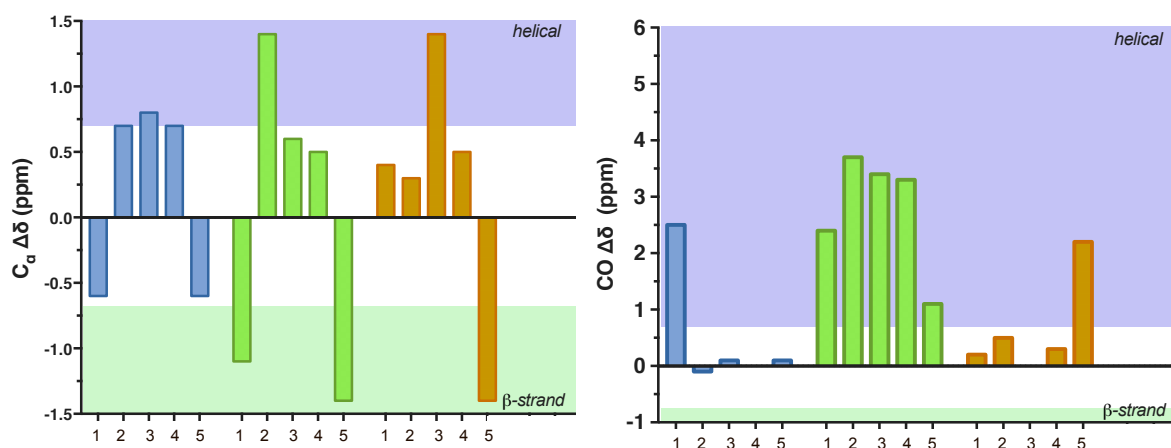
Figure 50: The change in α-carbon (left) and carbonyl carbon (right) chemical shift relative to literature random coil values. ■ **15d**, ■ **18d**, ■ **19m**, ■ β-strand region (< -0.7 Hz), ■ helical region (> 0.7 Hz). .

Circular Dichroism

The CD spectrum of the linear peptide **15,** shown Figure 51, reveals a distinct minimum at 198 nm accompanied by a minimum at 222 nm, which suggests the formation of some helical structure, in agreement with the NMR data. However the weak intensity of this spectrum

suggests that the helical structure is not very prominent, that is, **15** is not structured. The acyclic bimane bound peptide **19m,** with a bimane attached to position 5, similarly shows a large minimum at 197 nm and a slight plateau near 222 nm. This indicates that the bimane itself does not induce any secondary structure. The minimum at 197 nm in **19m** is at significantly greater intensity than in **15** which suggests that **19m** has no secondary structure, in line with the NMR data.

The CD spectrum of the bimane-cyclised peptide **15d** (Figure 51) shows a large minimum at 199 nm. There is a plateau at 218 nm, as for acyclic bimane-bound **19m**, and at low wavelengths (186 nm) the intensity has increased suggesting the formation of a maximum outside the observed wavelength range. This combination of maxima and minima may indicate weak helical structure, however interestingly there is also a maximum at 242 nm present. This combination of maxima and minima does not represent any of the CD spectra reported in literature.[54, 55, 123] The NMR and CD data combined suggest that there is not a defined secondary structure present in **15d**, however it may be hypothesised that the bimane linker has contorted the peptide into a restricted irregular structure.

A large minimum is shown at 200 nm in the CD spectrum for the bimane-cyclised peptide with homocysteine at positions 1 and 5 (**18d**). This minimum has shifted to a higher wavelength and therefore nearer to the 208 nm minimum expected for helical structure, as compared to linear **15** and acyclic bimane-bound **19m**, in agreement with the NMR data. A maximum at 186 nm further supports the formation of a helical secondary structure. There is a slight inflection in the spectrum around 221 nm, where the plateau is observed in **15** and **19m**. Therefore the combined CD and NMR data predict the presence of helical structure in bimane-cyclised **18d**. The relative ratio of this slight plateau at 221 nm and the minimum at 200 nm suggest the formation of a 3_{10} helical structure (as opposed to α-helical structure).
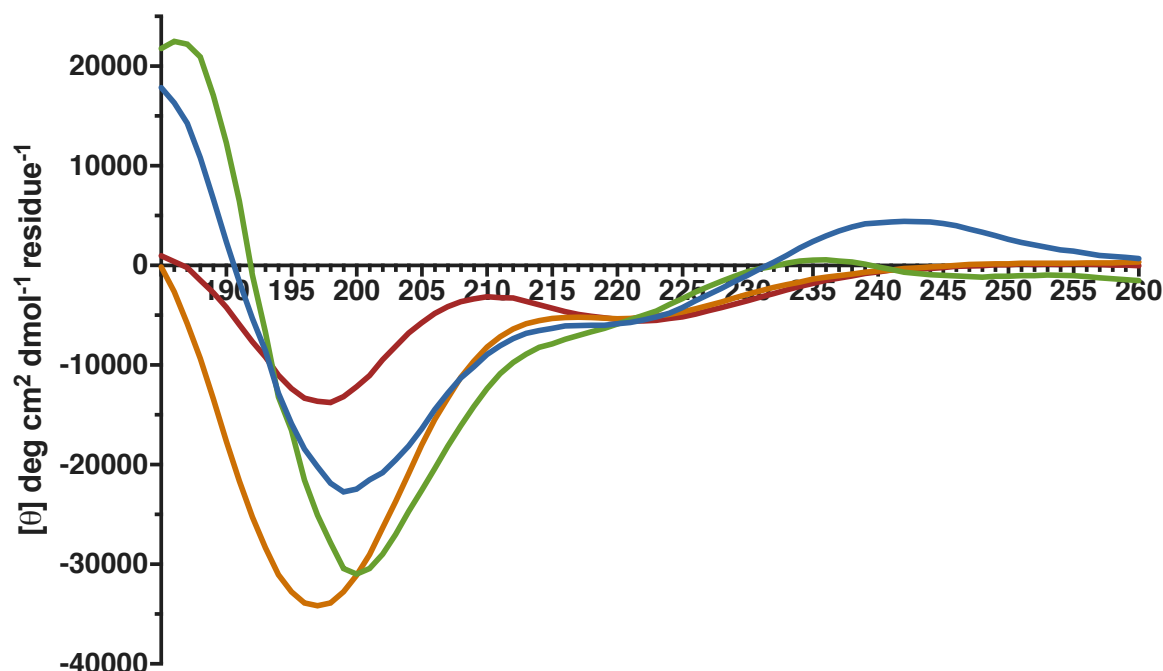
Figure 51: CD spectra for ── **15,** ── **15d,** ── **18d** and ── **19m** collected on a Jasco J-810 spectropolarimeter at 150 μM in 10 mM PBS at pH 7.2.

Table 13: Summary of CD maxima and mimima as shown in Figure 51, accompanied by %helicity calculated from the MRE intensity at 215 nm.

	15	15d	18d	19m
Minima	198	199	-	-
	222		200	197
Maximum	-	242	186	-
215/208	1.18	0.56	0.49	0.47
% α-Helicity[128]	29	42	52	35

In conclusion, CD and NMR data revealed that the bimane-attached acyclic peptide **19m** and linear peptide **15** showed no distinct secondary structure, therefore implying that introduction of the bimane into a peptide does not significantly alter the pentapeptide structure. The structure of bimane-cyclised peptide **15d** appeared to be restricted (i.e. not freely flexible), however this restriction did not result in a defined secondary structure. In comparison, the homocysteine-bimane linker of **18d** appeared to induce 3_{10} helicity in the pentapeptide, a 38% increase in helicity compared to the unmodified **15**.

3.3.2 The effect of bimane cyclisation and increased backbone length: A study of 16d and 17d

*J*_{HNHα} *coupling constants*

The $J_{HNH\alpha}$ coupling constants for all alanine residues in peptides **16**, **16d**, **17d** (positions 2-4), and **20m** (positions 1-4) were below 6 Hz (except for position 2 in **16** at 6.1 Hz), which suggests some helical structure in all four peptides. The $J_{HNH\alpha}$ for both **16** and **16d** at the position 1 and 5 cysteine residues were larger in comparison to the central alanine residues, which may suggest some flexibility at the peptide termini. The $J_{HNH\alpha}$ of the linear **16** and bimane-cyclised **16d** are very similar suggesting that introduction of the bimane linker did not induce a significant effect on the secondary structure of the peptide.
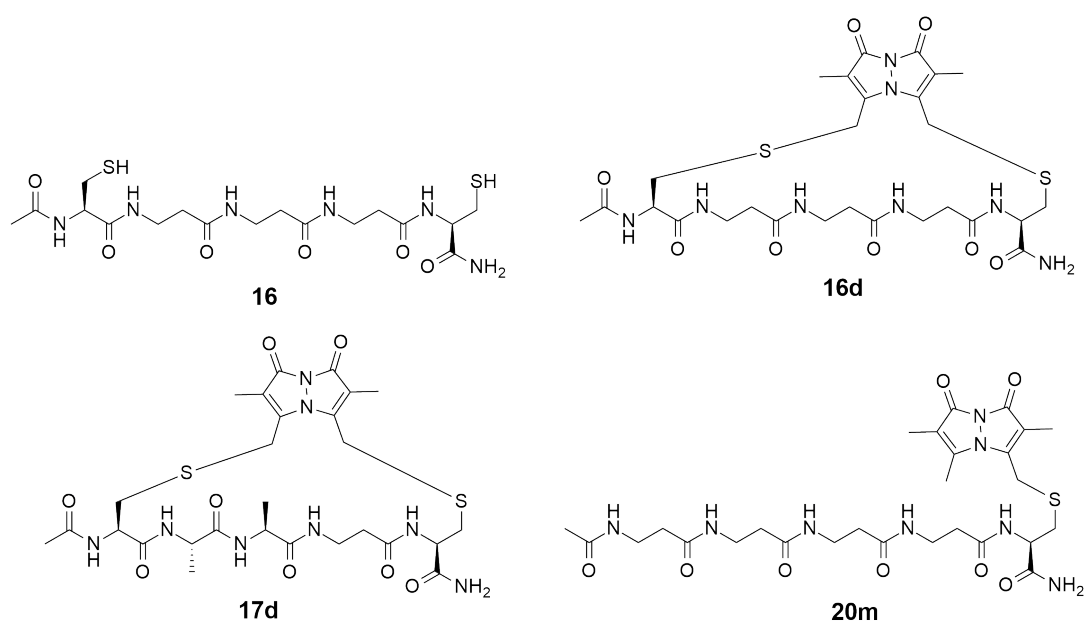
Figure 52: The structures of pentapeptides **16, 16d, 17d** and **20m** which were analysed by CD and NMR techniques in section 3.3.2
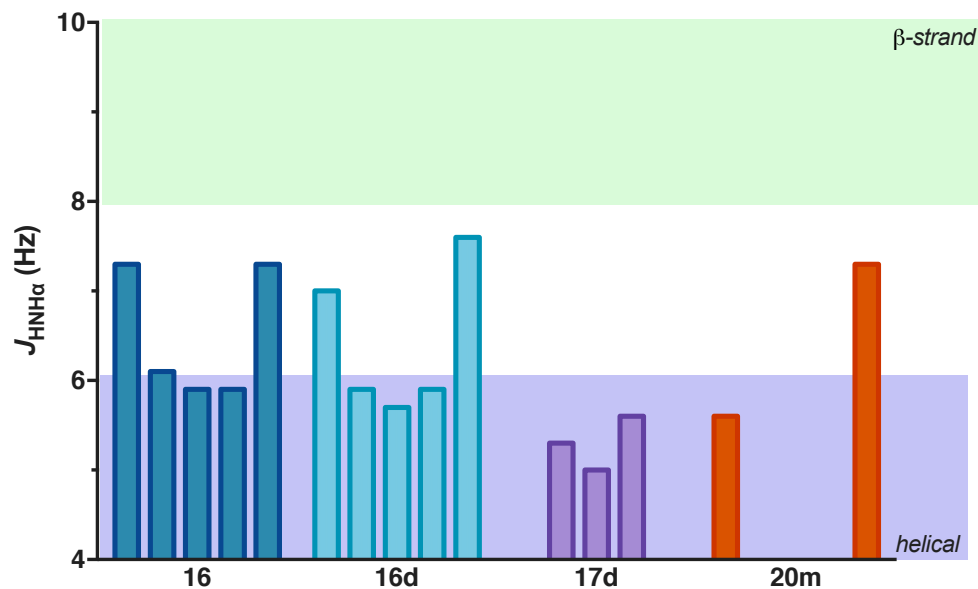
Figure 53: $J_{HNH\alpha}$ coupling constants for a series of pentapeptides **16, 16d, 17d** and **20m,** determined in 10% D_2O in water at pH ~5. ▉ β-strand region (> 8 Hz), ▉ helical region (< 6 Hz).

NMR Chemical shift

The change in carbon chemical shift, shown in Figure 57, are $\Delta\delta_{linear}$ calculated relative to **16**. As discussed in the Tripeptides section, a reliable literature source for β-alanine carbon chemical shifts could not be found and as such only $\Delta\delta_{linear}$ are discussed here. Furthermore, as both the α- and β-protons in β-alanine are located in the peptide backbone, and therefore structurally relevant, proton $\Delta\delta$ (as opposed to α-proton $\Delta\delta$) is discussed in this section. Proton $\Delta\delta$ encompasses the cysteine α-protons and all β-alanine protons.

The proton $\Delta\delta$ for linear **16**, shown in Figure 55, transitions from negative *N*-terminal values through to positive $\Delta\delta$ values at the *C*-terminal. The lack of a trend in the proton $\Delta\delta$ suggests random coil type structure. Similarly for bimane-cyclised **16d** and **17d**, a wide variety of $\Delta\delta$ values are observed with no trend, thereby indicating no secondary structure. However in the acyclic bimane-bound **20m**, all bar one resonance shifts negatively as shown in the proton $\Delta\delta$ in Figure 55A. This same trend is observed for the $\Delta\delta_{linear}$ (relative to **16**) of **20m**. This suggests a tendency toward helical structure induced by attachment of the bimane linker, however, all these values still lie within the random coil window. Hence the proton $\Delta\delta$ suggests that none of the four peptides, **16**, **16d**, **17d**, or **20m**, display any secondary

structure. β-Alanine is quite flexible due to the sp^3-hybridised carbons in comparison to the sp^2-hybridised α-carbons in α-amino-acids, accounting for the very random Δδ for these peptides.

The acyclic bimane-bound **20m** shows one negative α-carbon Δδ$_{linear}$ (excluding the cysteine at position 5) (Figure 13) in the position 2 β-alanine. The remainder of the residues show very small Δδ, indicating random coil structure. Similarly, the carbonyl-carbon Δδ$_{linear}$ (Figure 14) show almost no change. This suggests that **20m** is in a random coil state, the same as **16**, and therefore that the bimane does not incur any structural changes in the peptide, in agreement with the observable $J_{HNH\alpha}$.

The α-carbon Δδ$_{linear}$ for bimane-cyclised peptide **17d**, with mixed α/ β-alanine backbone, are all quite negative (Figure 57) suggesting β-strand structure. The Δδ$_{linear}$ for the carbonyl-carbons are instead positive, and this inconsistency between the different Δδ suggests that there is no defined secondary structure for **17d**.

The β-alanine bimane cyclised peptide **16d** shows α-carbon Δδ$_{linear}$ values which all lie within the random coil window (excluding the position 1 and 5 cysteines). This is also the case for the carbonyl-carbon Δδ$_{linear}$. Therefore the NMR data suggests that **16d** is not structured.

Table 14: Sequence summaries for the β-alanine pentapeptides, where Ac indicates and acetyl group and Am indicates an amide. Residues with a * are bimane bound

Compound		Residue					
		1	2	3	4	5	
16		C	βAla	βAla	βAla	C	
16d	Ac	C*	βAla	βAla	βAla	C*	Am
17d		C*	A	A	βAla	C*	
20m		βAla	βAla	βAla	βAla	C*	
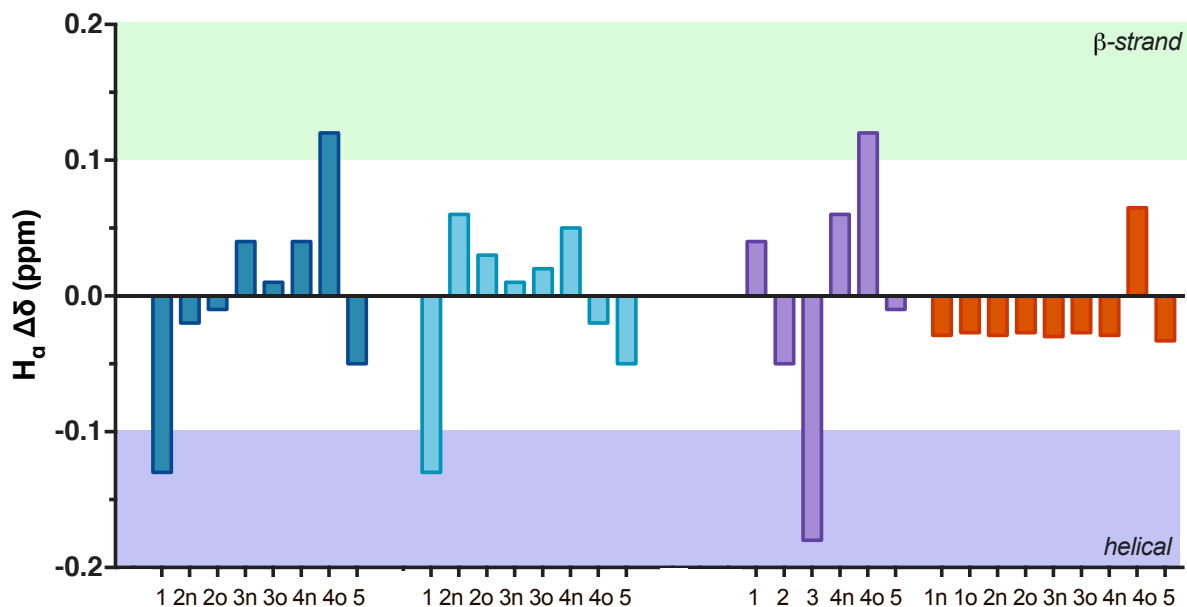
Figure 54: Backbone proton chemical shifts relative to literature random coil values[124] for a series of β-alanine containing pentapeptides. The residues are labelled on the x-axis where 2n represents the protons on the β-alanine carbon neighbouring the NH, and 2o represents the protons on the β-alanine carbon next to the CO etc. ■**16**, ■**16d**, ■**17d**, ■**20m**; ▊ β-strand region (> 0.1 Hz), ▊ helical region (< -0.1 Hz).
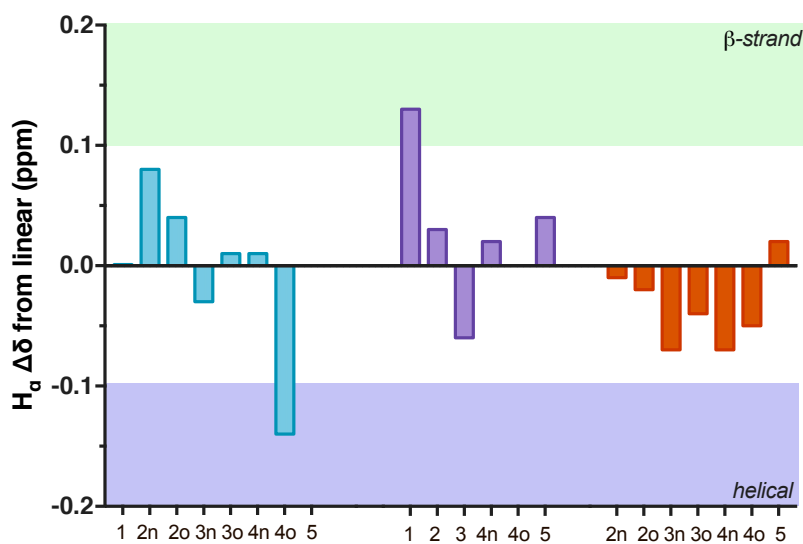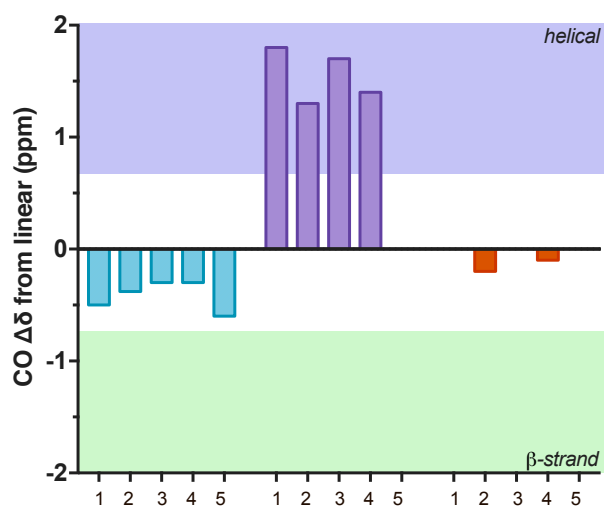

Figure 55: Backbone proton chemical shifts relative to the unfunctionalised linear peptide **16**, for a series of β-alanine containing pentapeptides. The residues are labelled on the x-axis where 2n represents the protons on the β-alanine carbon neighbouring the NH, and 2o represents the protons on the β-alanine carbon next to the CO etc. ■ **16d**, ■**17d**, ■ **20m**; ▊ β-strand region (> 0.1 Hz), ▊ helical region (< -0.1 Hz).
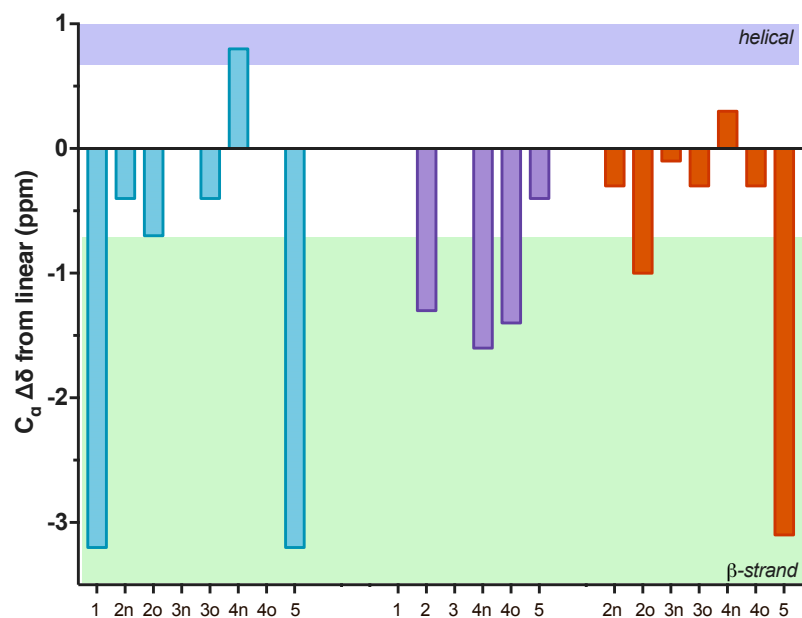
Figure 56: Backbone carbon chemical shifts relative to the unfunctionalised linear peptide **16**, for a series of β-alanine containing pentapeptides. The residues are labelled on the x-axis where 2n represents the protons on the β-alanine carbon neighbouring the NH, and 2o represents the protons on the β-alanine carbon next to the CO etc. ▬ **16d**, ▬ **17d**, ▬ **20m**; ▬ β-strand region (< -0.7 Hz), ▬ helical region (> 0.7 Hz).

Figure 57: Backbone carbonyl carbonchemical shifts relative to the unfunctionalised linear peptide **16**, for a series of β-alanine containing pentapeptides. The residues are labelled on the x-axis where 2n represents the protons on the β-alanine carbon neighbouring the NH, and 2o represents the protons on the β-alanine carbon next to the CO etc. ▬ **16d**, ▬ **17d**, ▬ **20m**; ▬ β-strand region (< -0.7 Hz), ▬ helical region (> 0.7 Hz).

Circular Dichroism

The CD spectrum for the linear peptide **16** shows only a very weak minimum at 196 nm, strongly suggesting that this compound is not structured, in agreement with the NMR chemical shift data. The spectrum of the acyclic bimane-bound β-alanine pentapeptide **20m** shows two minima, one at 199nm and another at 215 nm. This suggests some helical structure apparent in the peptide, confirming the observations made in the proton Δδ data.

The β-alanine bimane-cyclised peptide **16d** has a CD spectrum which shows minima at similar wavelengths to **20m**, at 198 and 209 nm. However these minima have shifted further away from the 208 and 215 nm minima expected for helical structure and furthermore the 198 nm minimum is greater in intensity than the corresponding minimum (199 nm) in **20m** indicating that **16d** is more random-coil like than **20m**. This agrees with the chemical shift data, which showed very small Δδ. However a maximum at 242 nm in the CD spectrum of **16d**, in combination with the 209 minimum somewhat resembles a Poly-Pro II type helix reported in literature.[123] Poly-Pro type helices are very tight turns, which would support the low $J_{HNH\alpha}$ observed.

The mixed α/ β-alanine bimane-cyclised peptide **17d**, a minimum at 198 nm and a notable maximum 238 nm suggest slightly less structured Poly-Pro II helix.[123] However, it must be noted for all four peptides, **16**, **16d**, **17d,** and **20m** the MRE intensity is quite low which implies any structure observed is quite weak. This is reflected in the percentage helicity values shown in Table 2.

In conclusion, the β-alanine bimane-attached peptides, **16**, **16d**, **17d** and **20m** show much more flexible structure than the α-alanine analogues, **15**, **15d**, **16d** and **19m**. This is reflected in both the NMR and CD data, and although **16** and **20m** are all quite disordered, the CD data for **16d** and **17d** shows similarities to a Poly-Pro II helix which suggests a tight coiled structure.
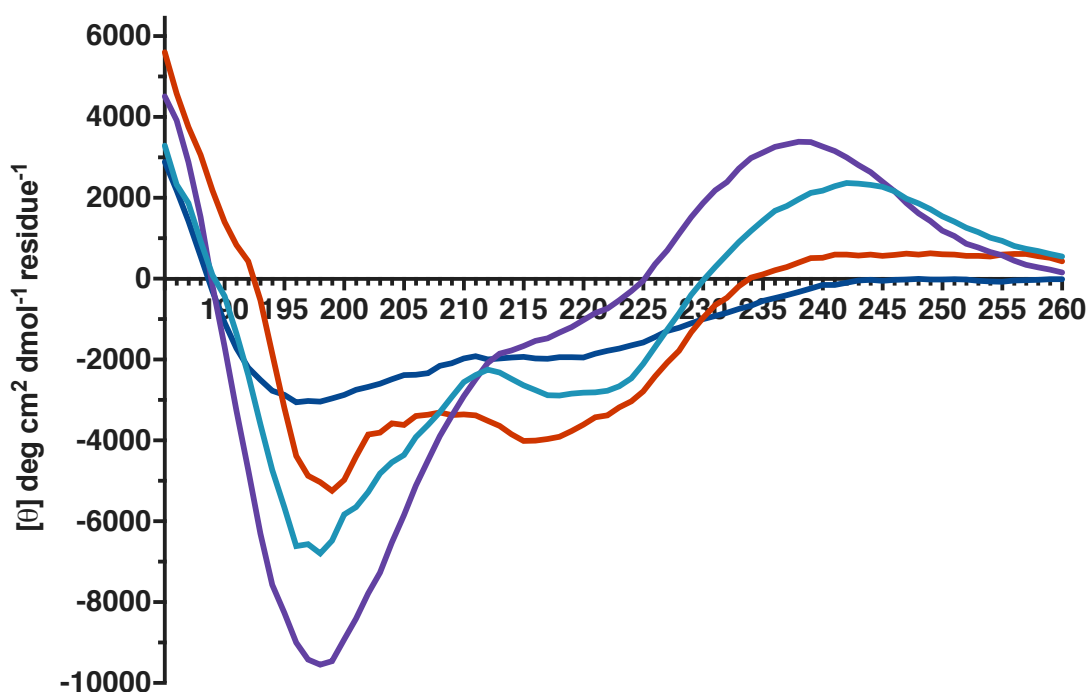
Figure 58: CD spectra for — **16,** — **16d,** — **17d** and — **20m** collected on a Jasco J-810 spectropolarimeter at 150 μM in 10 mM PBS at pH 7.2.

Table 15: A summary of the observed maxima and minima observed in the CD, and %helicity values calculated from the CD spectrum shown in Figure 58.

	16	**16d**	**17d**	**20m**
Minima	196	209	198	215
		198		199
Maximum	-	242	238	-
215/208	0.90	0.80	0.43	1.21
% α-Helicity[128]	13	17	11	27

3.4 Chapter conclusions

The secondary structure of a series of bimane cyclised tri- and penta- peptides were investigated through CD and NMR techniques. It was determined that by introducing a bimane *i-i*+2 linker, β-strand structure could be induced in a tripeptide. In a pentapeptide the *i-i*+4 bimane linker did not induce any defined secondary structure, however when the cysteines were replaced by homocysteines at the 1 and 5 positions, to give a longer bimane linker, a somewhat 3_{10} helical structure was observed. β-Alanine was also substituted in the

peptide backbone in place of the central alanines, particularly the β-alanine bimane-cyclised pentapeptides displayed very little secondary structure. Although the CD spectrum somewhat resembled that of a poly-pro II helix implying a tightly coiled structure, this structure is likely flexible and transient.

It should be noted that no distinct NOE patterns were observed for any of the peptides discussed in Chapter 3, which suggests that any secondary structure observed is somewhat transient. However, as these are quite short peptides there is a limited number of NOEs which could be observed in a peptide with secondary structure. Furthermore, amide-derived temperature coefficients (shown in the Appendix) were all above -4 ppb/K which further supports the hypothesis that the secondary structure is slightly fluid.

The structure of alanine-rich octapeptides i-i+7 bimane-cyclised peptides **21d** and **22d** were also studied by NMR and CD however the analysis was only partially complete by the time of submission so were omitted. However preliminary results suggest a somewhat helical structure for **21d** in aqueous solution.

This study demonstrates that the bimane-cyclisation can induce secondary structure in short peptides, in which an i-i+2 constraint results in β-strand structure and an extended bimane linker (through use of homocysteine) in a i-i+4 conformation can lead to a helical structure.

Chapter 4: Thesis conclusions & future directions

This work demonstrates that the reaction of dibromobimane with short peptides can be carried out on a wide variety of peptide sequences, constraint lengths and on peptides of varied length in a facile manner. Monitoring the fluorescence increase over time allowed optimisation of the solution phase reaction conditions, to show that 0.5 mg/ml of peptide in 10 mM PBS with one equivalent of dibromobimane gives a complete reaction in under 30 minutes. This revealed that buffer is essential for the reaction to occur efficiently and furthermore that high peptide concentrations, or more than one equivalent of dibromobimane, can limit the reaction efficiency. These conditions were also applied to react monobromobimane with peptides with similar efficacy. This method was applied to cyclise a variety of peptides which varied from 3 to 18 amino-acids in length, with constraint distances of i-i+2, i-i+4 and i-i+7, and a wide array of amino-acid combinations to show that the reaction is not limited by the peptide.

Furthermore, cyclisation on reaction with dibromobimane was carried out while the peptide was attached to a resin-support. This reaction route allows a method with which to selectively deprotect and react a specific cysteine with a bromobimane in a sequence which may contain additional thiols.

The fluorescent properties of a set of alanine-rich peptides (**10d**, **13m**, **15d**, **19m**, **21d** and **23m**) were investigated through 96-well plate experiments. It was determined that these six peptides, although of varying length and different constraint distances, displayed the same maximum excitation and emission wavelength. The i-i+2 bimane-cyclised peptide displayed lower fluorescence than the i-i+4 cyclised peptide that in turn showed lower intensity than the i-i+7 constrained peptide, furthermore, the bimane-cyclised peptides displayed greater fluorescence intensity than the analogous mono-functionalised bimane peptide. A detection limit for the fluorescence of a representative bimane-peptide **15d** was determined to be 10 nM, as detected by a plate reader. This limit is expected to be further improved upon when analysed on a more sensitive instrument such as a confocal microscope. Additionally,

75

variations in pH around a physiological range did not affect the observed fluorescence, therefore the bimane-cyclised peptides have been shown to be well suited to use in a biologically relevant setting, specifically in the application to PPI inhibitors.

The secondary structure of bimane-attached tri- and penta- peptides were analysed through CD and NMR techniques. It was revealed that by implementing a bimane linker, in an *i-i*+2 fashion into a tripeptide, in which the central atom was alanine, β-strand structure could be induced, shown by **10d** and **12d**. However, if the position 2 residue is instead the backbone-extended β-alanine, as in **11d**, a restricted turn-like structure is produced in which every proton in the structure appears as a separate resonance in the NMR spectrum. Helical structure was induced in **18d** which was cyclised in an *i-i*+4 manner through the 1 and 5 position homocysteine residues.

This work lays a foundation to allow bimane-cyclised peptides to be implemented as protein-protein interaction inhibitors. The bimane linker can be readily installed in a variety of sequences, and the facile nature of this reaction can allow a variety of analogues to be efficiently synthesised when probing the best linker position in a protein-protein interaction. It has been shown that the fluorescence of these compounds can be detected at suitably low concentration to establish biological applicability and the pH does not influence the fluorescence therefore reinforcing that it will be simple and effective to implement bimane-attached peptides in a biological setting, thereby providing an avenue to begin overcoming one of the traditional small molecule hurdles, and avoid introducing an additional fluorescent tag into a potential therapeutic.

Along with further secondary structural optimisation, future work would include examining how well a bimane linker can inhibit protease degradation of a set of biologically relevant peptides. Furthermore, as dibromobimane has been implemented *ex vivo* and *in vivo* it is hypothesised that the bimane moiety may aid cell-permeability of the bimane-attached peptide. Demonstrating increased permeability of a biologically-relevant bimane-attached peptide *in vitro* would be the first step in fulfilling this third drug-design hurdle.

Lastly, the bimane fluoresces in the blue-region of the spectrum, in which cell-auto-fluorescence also emits. It is desirable to chemically modify the bimane moiety to red-shift the fluorescence such that it is more easily distinguishable from the background fluorescence. However, this modification would have to be carefully considered.

Through this work we have proven the usefulness of a fluorescent bimane-linker as a means to begin to overcome some of the inherent issues in designing an effective constrained-peptide PPI inhibitor and provided good data with which to begin this process.

Chapter 5: Experimental Methods

5.1 Materials:

All reagents and solvents were obtained from Sigma Aldrich unless specifically listed below. All Fmoc-protected amino-acids and coupling agents (HATU, HCTU & PyBOP) used were obtained from Chem-Impex International. Dibromobimane and monobromobimane were purchased from Frontier Scientific. The solvents *N,N*-dimethylformamide (DMF), dichloromethane (DCM), acetic anhydride (Ac$_2$O) and piperidine were obtained from Merck & Co. Inc.; methanol was obtained from Scharlau; and acetone & ethyl acetate from Chem Supply. *N,N'*-Diisopropylethylamine (DIPEA) was obtained from Alfa Aesar. Compounds for buffer solutions, disodium hydrogen phosphate dihydrate and sodium dihydrogen orthophosphate were obtained from Merck & Co. Inc. and Univar respectively.

5.2 Methods:

5.2.1 Stock Solutions

Solution A (Deprotection: 20% piperidine with 0.1 M HOBt in DMF)

Piperidine (10 mL) and 0.72 g HOBt in DMF (10 mL) were combined with DMF (30 mL).

Solution B (Coupling: 0.5 M HATU in DMF)

HATU (1.9 g, 0.5 M) was dissolved in DMF (10 mL).

Solution C (Cleavage: Acidolysis – TFA with scavengers)

TFA (9.25 mL) was combined with DODT (250 μL), TIPS (250 μL) and H$_2$O (250 μL).

Solution D (Capping: Acetylation)

Ac$_2$O (870 μL) and DIPEA (470 μL) were combined with DMF (10 mL).

Solution E$_1$ (TNBS/Free amine Test)

5% aq. TNBS (200μL, 50 μg/mL) was added to DMF (800 μL).

Solution E₂ (TNBS/Free amine Test)

DIPEA (50 μL) was added to DMF (950 μL).

5.2.2 General Method 1a: Coupling of standard amino-acids

Rink amide PL resin (500 mg, 0.4 mequiv/g) was combined with 1:1 DCM/DMF (10 mL) and stirred intermittently for 15 min to allow swelling. The solution was removed by filtration and the resin washed with DMF (3 x 10 mL). The *N*-terminal Fmoc group was removed by addition of solution A (10 mL) to the resin and stirred intermittently for 15 min. The mixture was again filtered and the resin washed with DMF (5 x 10 mL), DCM (2 x 10 mL) and DMF (5 x 10 mL). Fmoc-Protected amino acid (5 equiv) for coupling was dissolved in a mixture of DIPEA (10 equiv, 348 μL), solution B (5 equiv, 2 mL) and DMF (8 mL). The mixture was added to the resin and stirred intermittently for 1 h. The resin was isolated by filtration and washed with DMF (5 x 10 mL), DCM (2 x 10 mL) and DMF (5 x 10 mL). This sequence was repeated using the appropriate Fmoc protected amino-acid to give the final peptide sequence. The *N*-terminal Fmoc was removed by addition of solution A (10 mL) to the resin and stirred intermittently for 15 min. The solution was removed and the resin was washed with DMF (5 x 10 mL), DCM (2 x 10 mL) and DMF (5 x 10 mL).

After each deprotection and coupling step, a small amount of resin (micro spatula-full) was transferred from the bulk reaction and tested for the presence of a free amine by addition of solution E₁ (50 μL) and solution E₂ (50 μL). Free amine is indicated by the resin undergoing a colour change to red within 1 min.[129]

5.2.3 General Method 1b: Coupling of unusual amino-acids

Fmoc-Protected amino acid (2 equiv) was dissolved in a mixture of DIPEA (4 equiv, 138 μL), solution B (2 equiv, 0.8 mL) and DMF (8 mL). The mixture was added to the resin and stirred intermittently for 16 h. The solution was then removed and the resin washed with DMF (5 x 10 mL), DCM (2 x 10 mL) and DMF (5 x 10 mL).

5.2.4 General Method 2: Acetylation

Solution D (10 mL) was added to the *N*-terminal deprotected peptide on resin and stirred intermittently for 15 min. The solution was removed and the resin washed with DMF (5 x 10 mL), DCM (2 x 10 mL) and DMF (5 x 10 mL). A small amount of the resin (micro spatula-full) was transferred from the bulk reaction and tested for the presence of a free amine by addition of solution E_1 (50 µL) and solution E_2 (50 µL). Free amine is indicated by the resin undergoing a colour change to red within 1 min

5.2.5 General Method 3: Cleavage of peptide from the resin

The resin with attached peptide was dried by washing with DMF (5 x 10 mL), DCM (2 x 10 mL), DMF (2 x 10 mL), DCM (5 x 10 mL) and diethyl ether (3 x 10 mL); any remaining ether was allowed to evaporate overnight. The resin was added to solution C (10 mL) and agitated on a rocker for 2 h. The TFA solution was removed from the resin by pipette and then concentrated to ~1-0.5 mL under a N_2 stream. Diethyl ether (10 mL) was added, and the solution refrigerated overnight at 4°C. The mixture was spun down (7800 rpm, 10 min) and the supernatant decanted from the precipitate. The precipitate was dried under a stream of N_2, dissolved in 50% aq. ACN (~5 mg/mL) and then lyophilised to give the crude product as a white fluffy solid. The process was repeated for a further 4 h to improve the yield in some cases as specified below.

5.2.6 Method 4: On resin cyclisation[86]

Mmt protecting groups were removed from cysteine sulfhydryl groups from *N*-terminally protected peptides attached to resin by the addition of 2% TFA in DCM (5 mL) with standing for 1 min. Following each treatment with 2% TFA the resin was washed with DCM (3 x 5 mL), and the treatments repeated until the solution no longer turned yellow on addition to the resin. The resin was washed successively with DCM (3 x 10 mL) and DMF (5 x 10 mL). The peptide was reacted with dibromobimane (2 equiv, 140 mg) and DIPEA (4 equiv. 138 µL) in DMF (10 mL) for 3 h, the resin was then washed with DMF (5 x 10 mL), DCM (2 x 10 mL) and DMF (5 x 10 mL) to give the cyclic peptide.

5.2.7 Method 5a: Off resin cyclisation with dibromobimane

Linear peptide (10 mg, 22.9 μmol, 5.73 mM) in 50% aq. ACN (4 mL) and dBB (8.01 mg, 1 equiv., 22.9 μmol, 5.73 mM) in MeOH (4 mL) was combined with 100mM pH 7.2-7.8 phosphate buffer solution (2 mL), TFE (2 mL) and milliQ water (8 mL) and agitated on a rocker for 45 min. The solution was diluted with milliQ water and lyophilised to give the crude product as a fluffy yellow solid.

5.2.8 Method 5b: Off resin cyclisation with monobromobimane

Linear peptide (10 mg, 22.9 μmol, 5.73 mM) in 50% aq. ACN (4 mL) and monobromobimane (6.22 mg, 1 equiv., 22.9 μmol, 5.73 mM) in MeOH (4 mL) was combined with 100mM PBS (2 mL), TFE (2 mL) and milliQ water (8 mL) and the mixture agitated on a rocker for 20 min. The solution was diluted with milliQ water and lyophilised to give the crude product as a fluffy yellow solid.

5.2.9 Method 6: Automated Purification

Purification was carried out on a Gilson Semi-preparatory RP-HPLC using a Phenomenex Luna C18(2) column.

Linear peptides were purified using a gradient of 0-60% aq. ACN over 20 min. Appropriate fractions were combined and lyophilised to give the purified product as a white fluffy solid.

Bromobimane cyclised peptides were purified using a gradient of 20-50% aq. ACN over 15 min. Appropriate fractions were combined and lyophilised to give the purified product as a pale yellow fluffy solid.

The peptides **28** and **28d** were purified using a gradient of 25-50% aq. ACN over 20 min. Appropriate fractions were combined and lyophilised to give the purified product as a pale yellow fluffy solid.

5.2.10 Method 7: Manual Purification

A DSC SPE-C18 2 g column was activated with methanol (10 mL) for 15 min and then washed with water (5 x 10 mL). Crude cyclised peptide (4 mL, 5 mg/ml) in aq. ACN (< 5%)

was loaded onto the column, and the products eluted over a gradient of 5-50% aq. ACN. Desired fractions were identified by analytical RP-HPLC and the appropriate fractions combined and lyophilised to give product as a pale yellow fluffy solid.

5.3 Analysis

5.3.1 Analytical Methods

Product purity was confirmed by RP-HPLC on a Phenomenex Luna C18(2) column over a gradient of 0-100% aq. ACN over 15 min. Product identity was confirmed by High Resolution mass spectrometry on an Agilent 6230 ESI-TOF LCMS.

5.3.2 NMR Spectroscopy

Characterisation spectra were acquired on an Agilent 500 MHz spectrometer or Oxford 600 MHz Spectrometer as specified in the appropriate compound experimental detailed as follows. All 2D structural characterisation data for the penta- and octa-peptides was acquired in 10% D_2O in H_2O at ~pH 5 and 298 K on a Oxford 600 MHz spectrometer using ES suppression sequences unless otherwise specified.

5.3.3 Circular Dichroism

Samples were prepared from aqueous peptide stock solutions of concentration determined by NMR. Concentration was determined using the "Determine Concentration" function in Agilent VnmrJ software using a caffeine reference standard. Final concentrations of the CD samples were confirmed by analytical HPLC and readjusted as necessary. CD samples were prepared at 150 μM concentration at pH 7.2 in a) 10 mM phosphate buffer or b) 10 mM phosphate buffer in 50% TFE. Circular dichroism spectra were acquired on a Jasco J-810 spectropolarimeter at the UniSA Biophysical Characterisation Lab. Spectra were recorded at 298 K in a 1 mm quartz cell over a wavelength range of 260-185 nm. A scan rate of 20 nm/min was employed, with a bandwidth of 1.0 nm, D.I.T. of 1 sec and data pitch of 1.0 nm, excepting the 8-mers in which a 0.5 nm data pitch was used. All spectra presented represent

the averaging over 5 accumulations and then processed using the associated Spectral Analysis program and smoothed using the 'Savitzy-Golay' function.

5.3.4 Plate Reader Experiments

All fluorescence values were measured (from the bottom) at an excitation wavelength of 385 nm and emission wavelength of 477 nm unless otherwise specified, on a H4 Synergy Plate Reader, with Xenon light source and a slit width of 9.0. Gain was varied dependent on the concentration of the samples analysed.

Optimisation Experiments

Peptide stock solutions were prepared in 50% aq. ACN, and dibromobimane stock solutions prepared in methanol with 10% the volume of the final reaction solution. A stock solution of 100 mM PBS or 100 mM AAB was prepared. The reagents were added in the required ratio, however dibromobimane was always the final reagent added to each well and the 96-well plate scanned by the plate reader immediately after addition of dibromobimane to the last well. The fluorescence was measured as described above with a gain of 60.

Fluorescence Experiments

Bimane cyclised peptides were prepared at the desired concentration in 10 mM PBS at pH 7, and the fluorescence measured at 477 nm, with an excitation wavelength of 477 nm. Gain was varied from 50 to 80 dependent on the concentration of wells analysed.

5.4 Syntheses

Compound 9 – H₂N-CAAAC-NH₂

9
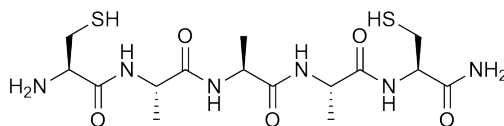
The peptide was synthesised with Fmoc-Cys(Trt)-OH and Fmoc-Ala-OH as per Method 1a, and then cleaved off the resin by Method 3 to give **9** as a white fluffy solid. Analytical HPLC: 0-100% over 15 min, R_t = 6.1 min; HRMS (ESI+) [M+H]⁺ calculated for [$C_{15}H_{28}N_6O_5S_2$]: 436.1562; observed: m/z 437.1676; ¹H NMR (500 MHz, 10% aq. D₂O) δ 4.48 (dd, J = 5.62, 6.85 Hz, 1H), 4.18 - 4.40 (m, 4H), 3.01 - 3.17 (m, 2H), 2.86 - 2.99 (m, 2H), 1.34 - 1.46 (m, 6H) ppm.

Compound 10 – Ac-CAC-NH₂
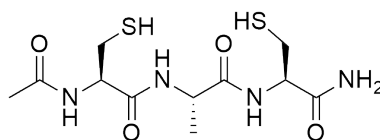
10

The peptide was synthesised with Fmoc-Cys(Trt)-OH incorporated at the 1 and 3 positions. The peptide was synthesised per Method 1a, capped per Method 2; then cleaved off the resin by Method 3., to give **10** as a white fluffy solid. Analytical HPLC: 0-100% over 15 min, R_t = 7.1 min; HRMS (ESI+) [M+H]⁺ calculated for [$C_{11}H_{20}N_4O_4S_2$]: 337.1006; observed: m/z 337.1015; ¹H NMR (500 MHz, DMSO-d₆) δ 8.28 (d, J = 6.85 Hz, 1H), 8.11 (d, J = 7.82 Hz, 1H), 7.85 (d, J = 8.07 Hz, 1H), 7.33 (br. s., 1H), 7.20 (br. s., 1H), 4.38 (dt, J = 5.62, 7.58 Hz, 1H), 4.30 (dt, J = 5.01, 7.64 Hz, 1H), 4.25 (dq, J = 7.09, 7.10 Hz, 1H), 2.60 - 2.87 (m, 4H), 2.36 (t, J = 8.10 Hz, 1H), 2.25 (t, J = 7.30 Hz, 1H), 1.87 (s, 3H), 1.24 (d, J = 6.85 Hz, 3H) ppm; ¹³C NMR (151 MHz, DMSO-d₆) δ 171.9, 171.2, 169.8, 169.4, 54.9, 54.5, 48.6, 26.1, 26.0, 22.4, 17.4 ppm.

Compound 10d– Ac-(cyclo-1,3-dBB)CAC-NH₂
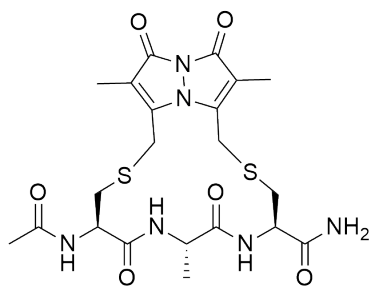
10d

The linear peptide precursor was prepared as detailed in 'Compound **10**'. The crude linear peptide **10** was cyclised by Method 5a. The peptide was also synthesised with Fmoc-Cys(Mmt)-OH in place of Fmoc-Cys(Trt)-OH and cyclised per Method 6. The crude cyclised peptide was purified per Method 7 and eluted at 7% aq. ACN over a gradient of 6-9% aq. ACN increasing in 1% increments to give **10d** as a yellow fluffy solid. Analytical HPLC: 0-100% over 15 min, R_t = 7.9 min; HRMS (ESI+) [M+H]$^+$ calculated for [$C_{21}H_{28}N_6O_6S_2$]: 525.1592; observed: m/z 525.1582; ^{1}H NMR (599 MHz, DMSO-d$_6$) δ 8.68 (d, J = 7.56 Hz, 1H), 8.18 (d, J = 7.92 Hz, 1H), 7.77 (d, J = 8.58 Hz, 1H), 7.34 (s, 1H), 7.23 (s, 1H), 4.52 (dt, J = 6.24, 7.96 Hz, 1H), 4.45 (dt, J = 4.03, 8.36 Hz, 1H), 4.38 (dq, J = 7.20, 7.20 Hz, 1H), 3.87 - 4.04 (m, 4H), 2.91 - 3.03 (m, 4H), 1.83 (s, 3H), 1.82 (s, 3H), 1.79 (s, 3H), 1.20 (d, J = 7.04 Hz, 3H) ppm; ^{13}C NMR (151 MHz, DMSO-d$_6$) δ 171.5, 171.3, 170.0, 168.8, 160.1, 159.9, 148.9, 148.3, 113.8, 113.7, 51.8, 51.7, 48.1, 34.8, 34.7, 25.6, 25.4, 22.2, 16.9, 7.1, 6.8 ppm.
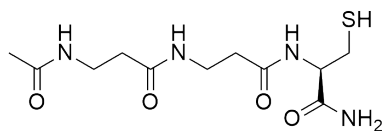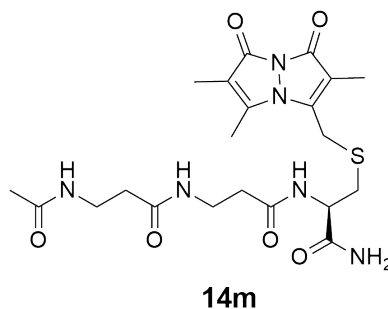
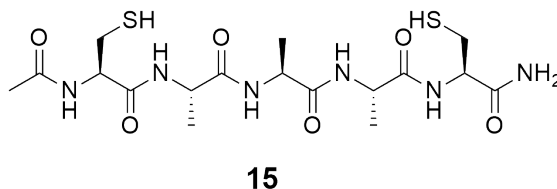## Compound 11 – Ac-CβAlaC-NH₂
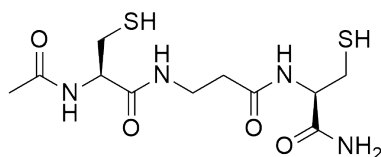
11

The peptide was synthesised using Fmoc-Cys(Trt)-OH and Fmoc-β-alanine-OH as per Method 1a, capped per Method 2; then cleaved off the resin by Method 3, to give **11** as a white fluffy solid. Analytical HPLC: 0-100% over 15 min, R_t = 6.5 min; HRMS (ESI+) [M]$^+$

calculated for [$C_{11}H_{20}N_4O_4S_2$]: 336.0926; observed: m/z 336.0888; ^{1}H NMR (500 MHz, 10% aq. D$_2$O) δ 8.39 (d, J = 7.34 Hz, 1H), 8.30 (d, J = 7.34 Hz, 1H), 8.22 (t, J = 5.62 Hz, 1H), 7.72 (br. s., 1H), 7.19 (br. s., 1H), 3.44 - 3.57 (m, 2H), 2.84 - 2.94 (m, 4H), 2.50 - 2.63 (m, 2H), 2.06 (s, 3H) ppm; ^{13}C NMR (126 MHz, DMSO-d$_6$) δ 171.7, 170.5, 169.7, 169.4, 55.0, 54.7, 35.3, 35.0, 26.1, 26.1, 22.5 ppm.

### Compound 11d– Ac-(cyclo-1,3-dBB)CβAlaC-NH$_2$

11d
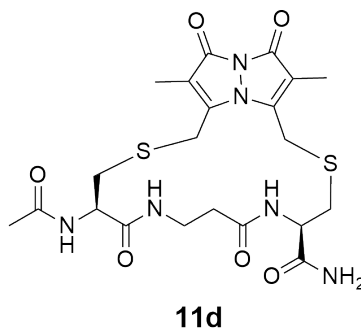
The linear peptide precursor was prepared as detailed in 'Compound **11**'. The crude linear peptide **11** was cyclised by Method 5a. The crude cyclised peptide was purified per Method 7 and eluted at 8% aq. ACN over a gradient of 5-10% aq. ACN increasing in 1% increments to give **11d** as a yellow fluffy solid. Analytical HPLC: 0-100% over 15 min, R$_t$ = 7.6 min; HRMS (ESI+) [M+H]$^+$ calculated for [$C_{21}H_{28}N_6O_6S_2$]: 525.1592; observed: m/z 525.1581; ^{1}H NMR (599 MHz, DMSO-d$_6$) δ 8.26 (dd, J = 5.03, 7.08 Hz, 1H), 8.10 (d, J = 8.29 Hz, 1H), 8.06 (d, J = 8.14 Hz, 1H), 7.41 (s, 1H), 7.16 (s, 1H), 4.54 (q, J = 7.60 Hz, 1H), 4.41 (ddd, J = 2.93, 8.18, 10.97 Hz, 1H), 4.01 (d, J = 14.97 Hz, 0H), 4.01 (d, J = 14.31 Hz, 1H), 3.94 (d, J = 14.38 Hz, 1H), 3.75 (d, J = 14.97 Hz, 1H), 3.48 (dtd, J = 3.81, 7.24, 9.85 Hz, 1H), 3.17 (dd, J = 2.97, 13.09 Hz, 1H), 3.06 - 3.12 (m, 1H), 2.87 (dd, J = 7.15, 13.02 Hz, 1H), 2.78 (dd, J = 10.82, 13.09 Hz, 1H), 2.75 (dd, J = 7.59, 13.02 Hz, 1H), 2.21 (ddd, J = 2.49, 4.22, 15.81 Hz, 1H), 1.83 (s, 2H), 1.81 (s, 3H), 1.81 (s, 3H) ppm; ^{13}C NMR (151 MHz, DMSO-d$_6$) δ 171.9, 170.8, 169.9, 168.9, 160.1, 159.9, 149.0, 148.0, 113.0, 112.9, 51.9, 51.1, 35.5, 35.0, 34.4, 34.4, 25.4, 24.7, 22.3, 7.0, 6.7 ppm.

Compound 12 – Ac-HcyAHcy -NH$_2$
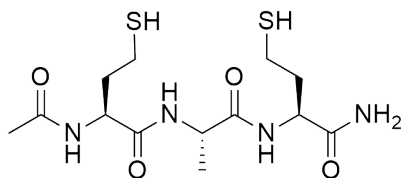
12

The peptide was synthesised using Fmoc-Hcy(Trt)-OH and Fmoc-Ala-OH as per Method 1a, however the Hcy residue at position 1 and 3 were coupled as follows per Method 1b. After coupling the final amino-acid, the deprotected peptide was capped per Method 2; then cleaved off the resin by Method 3 to give **12** as a white fluffy solid. Analytical HPLC: 0-100% over 15 min, R$_t$ = 7.6 min; HRMS (ESI+) [M+H]$^+$ calculated for [C$_{13}$H$_{24}$N$_4$O$_4$S$_2$]: 365.1319; observed: m/z 365.1639; ^{1}H NMR (599 MHz, DMSO-d$_6$) δ 8.14 (d, J = 7.04 Hz, 1H), 8.08 (d, J = 7.92 Hz, 1H), 7.81 (d, J = 8.22 Hz, 1H), 7.26 (s, 1H), 7.08 (s, 1H), 4.32 (dt, J = 5.58, 8.07 Hz, 1H), 4.27 (dt, J = 4.70, 8.66 Hz, 1H), 4.21 (dq, J = 7.00, 7.00 Hz, 1H), 2.40 - 2.50 (m, 4H), 1.69 - 1.95 (m, 7H), 1.22 (d, J = 7.04 Hz, 3H) ppm; ^{13}C NMR (151 MHz, DMSO-d$_6$) δ 172.8, 171.9, 171.1, 169.4, 51.6, 51.2, 48.3, 36.4, 36.4, 22.4, 20.3, 20.2, 17.4 ppm.

Compound 12d– Ac-(cyclo-1,3-dBB)HCyAHCy-NH$_2$
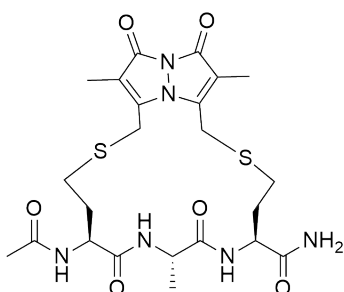
12d

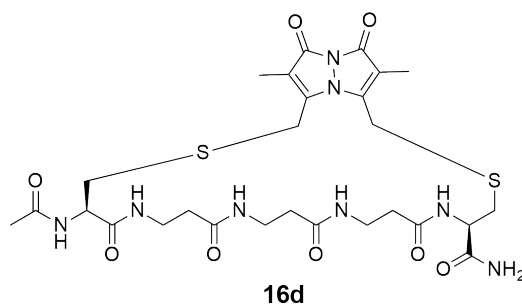The linear peptide precursor was prepared as detailed in 'Compound **12**'. The crude linear peptide **12** was cyclised by Method 5a. The crude cyclised peptide was purified per Method 7 and eluted at 10% aq. ACN over a gradient of 7-11% aq. ACN increasing in 1% increments to give **12d** as a yellow fluffy solid. Analytical HPLC: 0-100% over 15 min, R$_t$ = 8.5 min; HRMS (ESI+) [M+Na]$^+$ calculated for [C$_{23}$H$_{32}$N$_6$O$_6$S$_2$]: 575.1723; observed: m/z 575.1710; ^{1}H

NMR (599 MHz, DMSO-d_6) δ 8.52 (d, J = 7.56 Hz, 1H), 8.07 (d, J = 8.07 Hz, 1H), 7.92 (d, J = 8.29 Hz, 1H), 7.47 (s, 1H), 7.17 (s, 1H), 4.41 (td, J = 6.40, 7.90 Hz, 1H), 4.34 - 4.40 (m, 2H), 4.10 (d, J = 12.62 Hz, 1H), 4.02 (d, J = 12.76 Hz, 1H), 3.97 (d, J = 12.98 Hz, 1H), 3.96 (d, J = 12.62 Hz, 1H), 2.60 - 2.79 (m, 4H), 1.85 (s, 3H), 1.79 (s, 6H), 1.70 - 2.06 (m, 4H), 1.19 (d, J = 6.97 Hz, 3H) ppm; ^{13}C NMR (151 MHz, DMSO-d_6) δ 172.2, 171.6, 170.8, 169.0, 159.7, 159.6, 146.2, 146.1, 113.5, 113.4, 51.3, 51.2, 47.8, 32.6, 32.0, 29.1, 28.5, 25.0, 24.4, 22.4, 16.5, 6.5, 6.5 ppm.

Compound 13 – Ac-AAC-NH$_2$
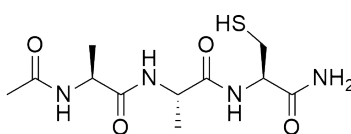
13

The peptide was synthesised with Fmoc-Cys(Trt)-OH and Fmoc-Ala-OH as per Method 1a, capped per Method 2; then cleaved off the resin by Method 3, to give the **13** as a white fluffy solid. Analytical HPLC: 0-100% over 15 min, R_t = min; 6.4; HRMS (ESI+) [M]$^+$ calculated for [304.1205]; observed: m/z 327.1122; ^{1}H NMR (500 MHz, DMSO-d_6) δ 8.13 (d, J = 6.85 Hz, 1H), 8.08 (d, J = 7.09 Hz, 1H), 7.77 (d, J = 8.07 Hz, 1H), 7.30 (br. s., 1H), 7.20 (br. s., 1H), 4.14 - 4.32 (m, 3H), 2.57 - 2.86 (m, 2H), 2.20 - 2.31 (m, 1H), 1.19 (d, J = 7.09 Hz, 3H) ppm; ^{13}C NMR (126 MHz, DMSO-d_6) δ 172.6, 172.1, 171.4, 169.3, 54.6, 48.5, 48.3, 26.0, 22.5, 17.9, 17.5 ppm.

Compound 13m – Ac-AAC(3-mBB)-NH$_2$
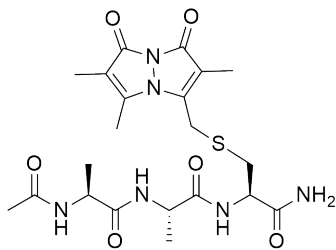
13m

The linear peptide precursor was prepared as detailed in 'Compound **13**'. The crude linear peptide **13** was cyclised by Method 5b. The crude cyclised peptide was purified per Method 7 and eluted at 7% aq. ACN over a gradient of 6-9% aq. ACN increasing in 1% increments to give **13m** as a yellow fluffy solid. Analytical HPLC: 0-100% over 15 min, R_t = min; HRMS (ESI+) [M+Na]$^+$ calculated for [C$_{21}$H$_{30}$N$_6$O$_6$S]: 517.1846; observed: m/z 517.1826; ^{1}H NMR (500 MHz, 10% aq. D$_2$O) d 8.19 (d, J = 7.09 Hz, 1H), 8.17 (d, J = 7.58 Hz, 1H), 8.04 (d, J = 8.31 Hz, 1H), 7.45 (s, 1H), 7.34 (br. s., 1H), 4.47 (dt, J = 5.87, 8.10 Hz, 1H), 4.24 - 4.37 (m, 2H), 4.03 (s, 2H), 3.08 (dd, J = 5.50, 13.33 Hz, 2H), 2.89 (dd, J = 8.19, 13.33 Hz, 2H), 1.92 (s, 3H), 1.89 (s, 3H), 1.82 (s, 3H), 1.31 (d, J = 7.09 Hz, 3H), 1.28 (d, J = 6.85 Hz, 3H) ppm; ^{13}C NMR (126 MHz, 10% aq. D$_2$O) d 172.5, 172.1, 171.5, 169.3, 147.6, 146.9, 110.7, 66.2, 53.3, 51.8, 48.5, 48.3, 33.6, 22.4, 17.9, 17.7, 11.2, 6.7, 6.4 ppm.

Compound 14 – Ac-βAlaβAlaC-NH$_2$

14

The peptide was synthesised with Fmoc-Cys(Trt)-OH and Fmoc-Ala-OH as per Method 1a, capped per Method 2; then cleaved off the resin by Method 3, to give the **14** as a white fluffy solid. Analytical HPLC: 0-100% over 15 min, R_t = min; HRMS (ESI+) [M]$^+$ calculated for [C$_{11}$H$_{20}$N$_4$O$_4$S$_1$]: 304.1205; observed: m/z 304.1179.

Compound 14m – Ac-βAlaβAlaC(3-mBB)-NH₂

14m

The linear peptide precursor was prepared as detailed in 'Compound **14**'. The crude linear peptide **14** was cyclised by Method 5b. The crude cyclised peptide was purified per Method 7 and eluted at 7% aq. ACN over a gradient of 6-9% aq. ACN increasing in 1% increments to give **14m** as a yellow fluffy solid. Analytical HPLC: 0-100% over 15 min, R_t = 6.4 min; HRMS (ESI+) [M]⁺ calculated for [$C_{21}H_{30}N_6O_6S_1$]: 494.1948; observed: m/z 494.1948.

Compound 15 – Ac-CAAAC-NH₂

15

The peptide was synthesised with Fmoc-Cys(Trt)-OH and Fmoc-Ala-OH as per Method 1a, capped per Method 2; then cleaved off the resin by Method 3, to give **15** as a white fluffy solid. Analytical HPLC: 0-100% over 15 min., R_t = 7.5 min; HRMS (ESI+) [M+Na]+ calculated for [$C_{17}H_{30}N_6O_6S_2$]: 501.1566; observed: m/z 461.1618; 1H NMR (599 MHz, 50% d_3-ACN/D₂O) δ 8.20 (d, J = 5.35 Hz, 1H), 7.97 (d, J = 7.13 Hz, 1H), 7.90 (br. s., 1H), 7.85 (d, J = 6.06 Hz, 1H), 7.77 (d, J = 8.02 Hz, 1H), 7.24 (br. s., 1H), 6.91 (br. s., 1H), 2.80 - 2.99 (m, 4H), 2.01 - 2.01 (m, 3H, under solvent), 1.33 - 1.43 (m, 9H) ppm.

Compound 15d – Ac-(cyclo-1,5-dBB)CAAAC-NH₂

15d
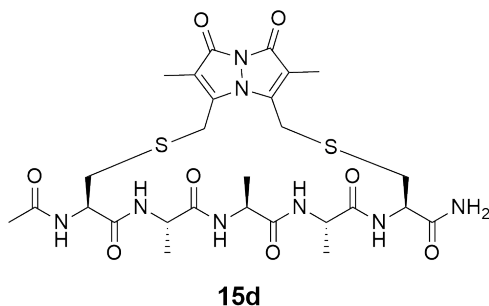
Off resin cyclisation: The linear peptide precursor **15** was prepared as detailed above. The crude linear peptide was cyclised by Method 5a.

On resin cyclisation: The linear peptide precursor **15** was synthesised per Method 1a using Fmoc-Cys(Mmt)-OH, and capped by Method 2. Following this the peptide was cyclised with dibromobimane per Method 4 and cleaved per Method 3.

The crude cyclised peptide was purified by Method 7 and eluted at 11% aq. ACN over a gradient of 5-12% aq. ACN increasing in 1% increments. The final product was isolated as a fluffy pale yellow solid. Analytical HPLC: 0-100% over 15 min., $R_t = 8.0$ min; HRMS (ESI+) [M+H]⁺ calculated for [$C_{27}H_{38}N_8O_8S_2$]: 667.2334; observed: m/z 667.2332; ¹H NMR (500 MHz, 10% aq. D₂O) δ 8.58 (d, J = 5.62 Hz, 1H), 8.44 (d, J = 7.09 Hz, 1H), 8.12 - 8.16 (m, 2H), 8.08 (d, J = 5.38 Hz, 1H), 7.54 (s, 1H), 7.28 (s, 1H), 4.51 - 4.55 (m, 1H), 4.23 - 4.35 (m, 4H), 3.90 - 4.11 (m, 4H), 3.21 (dd, J = 5.14, 13.94 Hz, 1H), 3.09 - 3.17 (m, 2H), 3.02 (dd, J = 7.34, 14.18 Hz, 1H), 2.03 (s, 3H), 1.89 (s, 3H), 1.87 - 1.89 (m, 3H), 1.35 - 1.48 (m, 9H) ppm; ¹³C NMR (151 MHz, 10% aq. D₂O) d 177.7, 177.6, 177.5, 177.1, 176.8, 174.7, 165.7, 165.4, 165.4, 165.1, 159.6, 151.7, 151.7, 121.9, 118.0, 117.5, 117.3, 110.1, 57.0, 56.2, 56.0, 53.0, 52.9, 52.9, 43.2, 36.4, 36.3, 28.4, 24.4, 21.8, 19.1, 18.4, 18.4, 9.1, 9.1, 9.0, 3.6 ppm.

Compound 16 – Ac-CβAlaβAlaβAlaC-NH₂

16
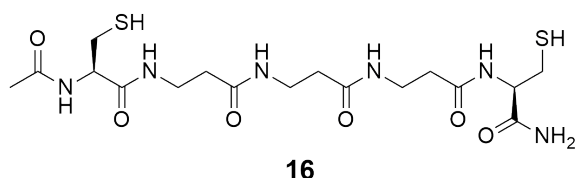
The peptide was synthesised per Method 1a using Fmoc-Cys(Trt)-OH and Fmoc-β-alanine, capped per Method 2; and cleaved off the resin by Method 3 to give **16** as a white fluffy solid. Analytical HPLC: 0-100% over 15 min, R_t = 5.7 min; HRMS (ESI+) [M]$^+$ calculated for [$C_{17}H_{30}N_6O_6S_2$]: 478.1668; observed: m/z 478.1620; ^{1}H NMR (500 MHz, 10% aq. D$_2$O) δ 8.40 (d, J = 7.09 Hz, 1H), 8.30 (d, J = 6.85 Hz, 1H), 8.21 (t, J = 5.38 Hz, 1H), 8.05 (t, J = 5.38 Hz, 1H), 8.00 (t, J = 5.26 Hz, 1H), 7.73 (br. s., 1H), 7.19 (br. s., 1H), 3.37 - 3.53 (m, 6H), 2.82 - 2.99 (m, 4H), 2.49 - 2.61 (m, J = 6.00, 6.00, 6.00 Hz, 2H), 2.43 (s, 4H), 2.06 (s, 3H) ppm; ^{13}C NMR (126 MHz, 10% aq. D$_2$O) δ 177.7, 177.4, 177.3, 176.9, 176.8, 174.9, 58.9, 58.5, 39.1, 39.1, 38.8, 38.4, 38.3, 38.0, 28.5, 24.8 ppm.

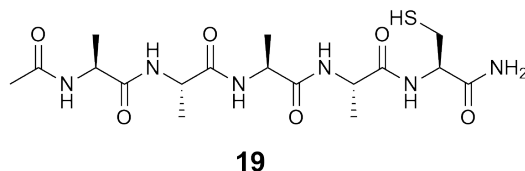### Compound 16d – Ac-(cyclo-1,5-dBB)CβAlaβAlaβAlaC-NH₂

16d

The linear peptide precursor was prepared as detailed in 'Compound **16**'. The crude linear peptide **16** was cyclised by Method 5a. The crude cyclised peptide was purified as per Method 7 and eluted at 9% aq. ACN over a gradient of 5-10% aq. ACN increasing in 1% increments to give **16d** as a fluffy pale yellow solid. Analytical HPLC: 0-100% over 15 min, R_t = 7.4 min; HRMS (ESI+) [M+H]$^+$ calculated for [$C_{27}H_{38}N_8O_8S_2$]: 667.2334; observed: m/z 667.2325; ^{1}H NMR (500 MHz, 10% aq. D$_2$O) δ 8.51 (d, J = 7.58 Hz, 2H), 8.37 (d, J = 7.09 Hz, 2H), 8.29 (t, J = 5.38 Hz, 2H), 8.08 (t, J = 5.38 Hz, 2H), 8.04 (t, J = 5.38 Hz, 2H), 7.71

(br. s., 1H), 7.20 (br. s., 2H), 4.50 - 4.56 (m, 1H), 4.44 - 4.49 (m, J = 7.10 Hz, 1H), 3.93 - 4.09 (m, 4H), 3.35 - 3.64 (m, 6H), 3.17 (dd, J = 4.03, 13.82 Hz, 1H), 3.03 (dd, J = 7.09, 13.94 Hz, 1H), 2.87 - 2.97 (m, 2H), 2.39 - 2.64 (m, 6H), 2.03 (s, 3H), 1.89 (s, 3H), 1.87 (s, 3H) ppm; ^{13}C NMR (151 MHz, 10% aq. D$_2$O) δ 177.1, 177.1, 176.6, 176.5, 176.4, 174.4, 165.1, 165.1, 150.9, 150.8, 117.3, 117.3, 55.8, 55.3, 39.0, 38.8, 38.7, 38.4, 38.1, 37.9, 35.5, 27.8, 27.6, 24.4, 9.1, 9.0 ppm.

Compound 17d – Ac-CAAβAlaC(5-mBB)-NH$_2$

17d
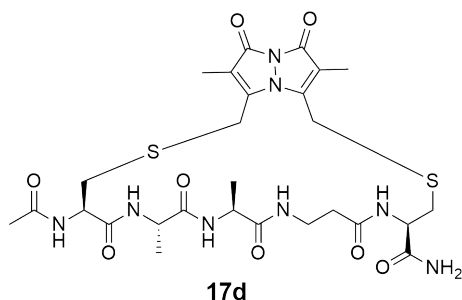
The peptide was synthesised using Fmoc-Cys(Trt)-OH and Fmoc-β-alanine as per Method 1a, capped per Method 2; and finally cleaved off the resin by Method 3 to give the linear precursor as a white fluffy solid. This material was cyclised per Method 5a and the crude cyclised peptide purified per Method 7 and eluted at 9% aq. ACN over a gradient of 5-10% aq. ACN increasing in 1% increments, to give **17d** as a fluffy pale yellow solid. Analytical HPLC: 0-100% over 15 min, R_t = 7.7 min; HRMS (ESI+) [M]$^+$ calculated for [C$_{27}$H$_{38}$N$_8$O$_8$S$_2$]: 666.2254; observed: m/z 666.2220; ^{1}H NMR (599 MHz, 10% aq. D$_2$O) δ 8.60 (d, J = 5.28 Hz, 1H), 8.40 (d, J = 7.34 Hz, 1H), 8.09 (d, J = 4.99 Hz, 1H), 7.79 (t, J = 5.58 Hz, 1H), 7.73 (br. s., 1H), 7.23 (br. s., 1H), 4.56 - 4.60 (m, 1H), 4.50 - 4.55 (m, 1H), 4.25 - 4.32 (m, 1H), 4.12 - 4.18 (m, 1H), 3.90 - 4.09 (m, 4H), 3.29 - 3.67 (m, 2H), 3.19 (dd, J = 5.14, 13.65 Hz, 1H), 3.11 (s, 1H), 2.99 (dd, J = 6.46, 14.09 Hz, 1H), 2.38 - 2.61 (m, 2H), 2.03 (s, 3H), 1.88 (s, 6H), 1.42 (d, J = 7.04 Hz, 3H), 1.36 (d, J = 7.34 Hz, 3H) ppm; ^{13}C NMR (151 MHz, 10% aq. D$_2$O) δ 176.4, 176.3, 176.0, 175.8, 175.6, 173.6, 150.5, 150.2, 116.4, 116.4, 54.9, 54.6, 52.0, 51.8, 37.4, 36.7, 35.1, 35.1, 27.3, 18.1, 18.0, 8.0, 7.9 ppm.

Compound 18 – Ac-HcyAAAHcy -NH₂
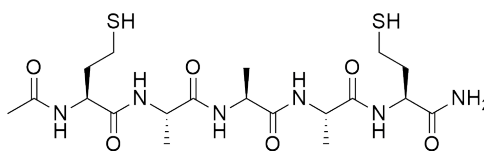
18

The peptide was synthesised with Fmoc-Hcy(Trt)-OH and Fmoc-Ala-OH as per Method 1a, however the Hcy residues at positions 1 & 5 were coupled per Method 1b. After coupling the final amino-acid the deprotected peptide was capped per Method 2; then cleaved off the resin by Method 3 to give **18** as a white fluffy solid. Analytical HPLC: 0-100% over 15 min, R_t = min; 7.1, HRMS (ESI+) [M]⁺ calculated for [$C_{19}H_{34}N_6O_6S_2$]: 506.1981; observed: m/z 506.1957; ¹H NMR (500 MHz, 10% aq. D₂O) δ 8.15 (d, *J* = 5.62 Hz, 1H), 8.09 (d, *J* = 6.60 Hz, 1H), 7.98 (d, *J* = 5.62 Hz, 1H), 7.94 (d, *J* = 6.11 Hz, 1H), 7.90 (d, *J* = 7.58 Hz, 1H), 7.29 (br. s., 1H), 6.93 (br. s., 1H), 4.10 - 4.22 (m, 1H), 2.36 - 2.71 (m, 4H), 1.80 - 2.02 (m, 5H), 1.19 - 1.35 (m, 9H) ppm.

Compound 18d – Ac-(cyclo-1,5-dBB)HcyAAAHcy -NH₂
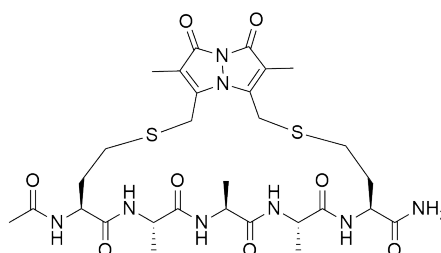
18d

The linear peptide precursor was prepared as detailed in 'Compound **18**'. The crude linear peptide **18** was cyclised by Method 5a. The crude cyclised peptide was purified per Method 7 and eluted at 18% aq. ACN over a gradient of 12-21% aq. ACN increasing in 3% increments to give **18d** as a yellow fluffy solid. Analytical HPLC: 0-100% over 15 min, R_t = 8.7 min; HRMS (ESI+) [M]⁺ calculated for [$C_{29}H_{42}N_8O_8S_2$]: 694.256706; observed: m/z 694.2523; ¹H NMR (500 MHz, 10% aq. D₂O) δ 8.32 (d, *J* = 5.87 Hz, 1H), 8.16 (s, 2H), 8.01 (d, *J* = 5.62 Hz, 1H), 7.98 (d, *J* = 6.85 Hz, 1H), 7.37 (br. s., 1H), 7.20 (br. s., 1H), 4.46 (d, *J* = 6.11 Hz,

1H), 4.28 (td, J = 6.21, 12.29 Hz, 3H), 4.10 - 4.24 (m, 1H), 3.83 - 4.08 (m, 4H), 2.80 - 2.94 (m, 3H), 2.73 (td, J = 6.94, 13.76 Hz, 1H), 2.15 - 2.27 (m, 2H), 1.95 - 2.09 (m, 5H), 1.88 (s, 3H), 1.87 (s, 3H), 1.40 (s, 9H) ppm; ^{13}C NMR (151 MHz, 10% aq. D$_2$O) δ 178.5, 178.0, 177.9, 177.0, 177.0, 165.3, 152.1, 152.0, 151.3, 55.7, 55.4, 53.6, 52.8, 52.7, 49.9, 33.3, 32.9, 31.1, 30.6, 28.2, 27.9, 24.2, 19.3, 18.6, 18.5, 9.0, 8.8 ppm.

Compound 19 – Ac-AAAAC-NH$_2$

19

The peptide was synthesised with Fmoc-Cys(Trt)-OH and Fmoc-Ala-OH as per Method 1a, and capped per Method 2. The linear peptide was cleaved from the resin by Method 3 to give **19** as a white fluffy solid. Analytical HPLC: 0-100% over 15 min, R_t = 7.0 min; HRMS (ESI+) [M]$^+$ calculated for [C$_{17}$H$_{30}$N$_6$O$_6$S]: 446.1948; observed: m/z 446.1966.

Compound 19m – Ac-AAAAC(5-mBB)-NH$_2$

19m
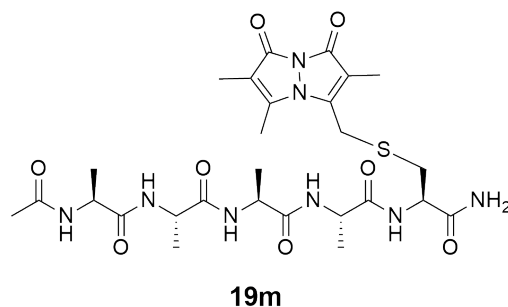
The linear peptide precursor was prepared as detailed in 'Compound **19**'. The crude linear peptide **19** was cyclised by Method 5b. T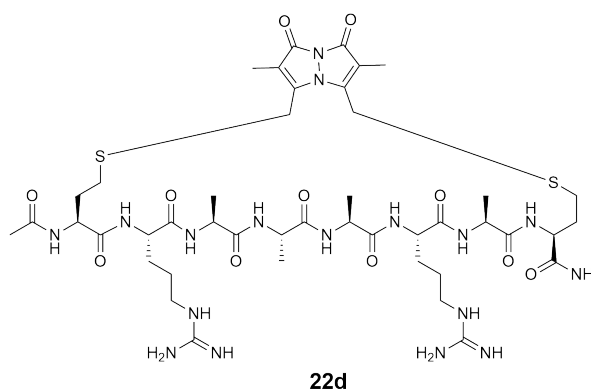he crude cyclised peptide was purified as per Method 7 over a gradient of 5-10% aq. ACN increasing in 1% increments to give **19m** which was isolated as a fluffy pale yellow solid. Analytical HPLC: 0-100% over 15 min, R_t = 8.1 min; HRMS (ESI+) [M+H]$^+$ calculated for [C$_{27}$H$_{40}$N$_8$O$_8$S]: 637.2770; observed: m/z 637.2784; ^{1}H NMR (599 MHz, 10% aq. D$_2$O) δ 8.31 (d, J = 5.58 Hz, 2H), 8.26 (d, J = 5.58 Hz, 1H), 8.14 - 8.21 (m, 3H), 7.46 (s, 1H), 7.23 (s, 1H), 4.46 (dt, J = 5.58, 7.60 Hz, 1H), 4.17 - 4.34 (m, 4H),

3.94 (d, J = 14.97 Hz, 1H), 3.91 (d, J = 14.97 Hz, 1H), 3.19 (dd, J = 5.28, 13.79 Hz, 1H), 2.98 (dd, J = 8.80, 14.09 Hz, 1H), 2.43 (s, 3H), 2.02 (s, 3H), 1.86 (s, 3H), 1.78 (s, 3H), 1.33 - 1.43 (m, 12H) ppm; ^{13}C NMR (151 MHz, 10% aq. D$_2$O) δ 8.3, 8.8, 13.8, 18.8, 18.8, 18.9, 19.1, 24.3, 27.5, 35.6, 52.5, 55.4, 114.2, 116.2, 150.8, 152.4, 165.0, 165.7, 176.8, 176.9, 177.5, 177.7, 177.8, 178.0 ppm.

Compound 20 – Ac-βAlaβAlaβAlaβAlaC-NH₂

20
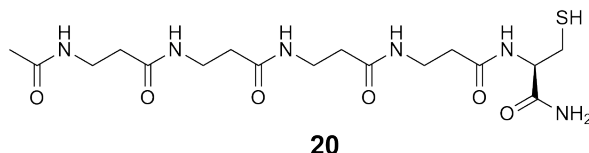
The peptide was synthesised using Fmoc-Cys(Trt)-OH and Fmoc-β-alanine per Method 1a, capped per Method 2; and cleaved off the resin by Method 3 to give **20** as a white fluffy solid. Analytical HPLC: 0-100% over 15 min, R_t = 6.5 min; HRMS (ESI+) [M+H]$^+$ calculated for [C$_{17}$H$_{30}$N$_6$O$_6$S]: 447.4720; observed: m/z 447.2021; ^{1}H NMR (500 MHz, 10% aq. D$_2$O) δ 8.06 (d, J = 7.09 Hz, 1H), 7.69 - 7.84 (m, 4H), 7.46 (br. s., 1H), 6.92 (br. s., 1H), 3.55 - 3.79 (m, 2H), 3.28 - 3.45 (m, 8H), 2.61 - 2.96 (m, 4H), 2.49 (t, J = 6.11 Hz, 2H), 2.32 - 2.40 (m, J = 6.50, 6.50 Hz, 6H), 1.91 (s, 3H) ppm.

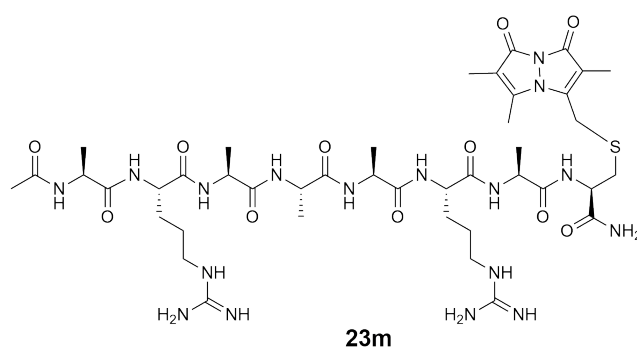### Compound 20m – Ac-βAlaβAlaβAlaβAlaC(5-mBB)-NH₂

20m
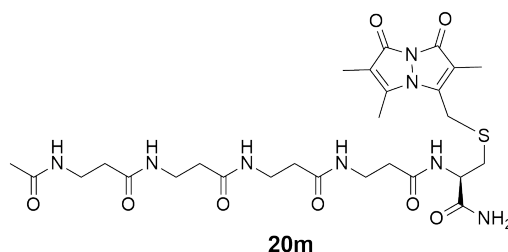
The linear peptide precursor was prepared as detailed in 'Compound **20**'. The crude linear peptide **20** was cyclised by Method 5b. The crude cyclised peptide was purified per Method 7 and eluted at 8% aq. ACN over a gradient of 5-9% aq. ACN increasing in 1% increments. The final product **20m** was isolated as a fluffy pale yellow solid. Analytical HPLC: 0-100% over 15 min, R_t = 7.6 min; HRMS (ESI+) [M+H]$^+$ calculated for [C$_{27}$H$_{40}$N$_8$O$_8$S]: 637.2770;

observed: m/z 637.2768; ^{1}H NMR (599 MHz, 10% aq. D_2O) δ 8.49 (d, J = 7.63 Hz, 1H), 8.00

- 8.07 (m, 3H), 7.97 (br. s., 1H), 7.72 (br. s., 1H), 7.21 (br. s., 1H), 4.51 (dt, J = 4.84, 7.85 Hz,

1H), 3.94 (d, J = 14.97 Hz, 1H), 3.90 (d, J = 14.67 Hz, 1H), 3.31 - 3.51 (m, 8H), 3.15 (dd, J =

5.28, 13.79 Hz, 1H), 3.09 - 3.20 (m, 1H), 2.94 (dd, J = 8.66, 13.94 Hz, 1H), 2.49 (t, J = 6.60

Hz, 2H), 2.43 - 2.45 (m, 3H), 2.37 - 2.42 (m, 6H), 1.95 (s, 3H), 1.86 (s, 3H), 1.76 - 1.80 (m,

3H) ppm; ^{13}C NMR (151 MHz, 10% aq. D_2O) δ 177.2, 176.8, 176.7, 176.6, 176.6, 176.5,

165.8, 165.1, 152.5, 150.8, 116.3, 114.3, 55.4, 38.8, 38.7, 38.6, 38.1, 38.1, 38.0, 37.8, 35.9,

27.6, 24.6, 13.9, 8.8, 8.4 ppm.

Compound 21 – Ac-CRAAARAC-NH₂
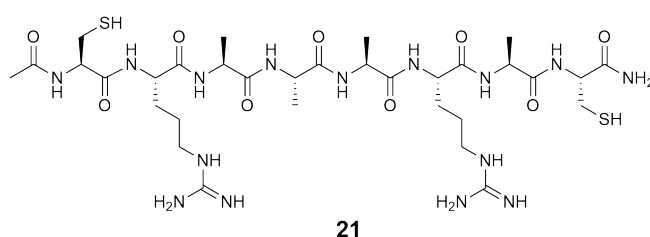
21

The peptide was synthesised with Fmoc-Cys(Trt)-OH, Fmoc-Arg(Pbf)-OH and Fmoc-Ala-

OH as per Method 1a, capped per Method 2; then cleaved off the resin by Method, to give **21**

as a white fluffy solid. Analytical HPLC: 0-100% over 15 min, R_t = 6.9 min; [HRMS (ESI+)

[M+H]$^+$ calculated for [$C_{32}H_{59}N_{15}O_9S_2$]: 862.414164; observed: m/z 862.4052.

Compound 21d – Ac-(cyclo-1,8-dBB)CRAAARAC-NH₂

21d
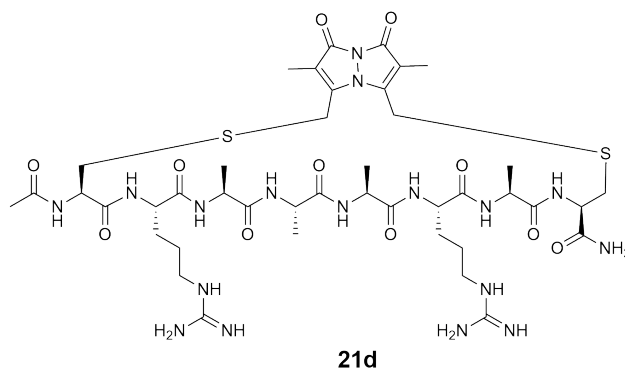
The linear peptide precursor was prepared as detailed in 'Compound **21**'. The crude linear

peptide **21** was cyclised by Method 5a. The crude cyclised peptide was purified per Method 6

to give **21d** as a fluffy pale yellow solid. Analytical HPLC: 0-100% over 15 min, R_t = 7.3 min; HRMS (ESI+) [M+2H]$^{2+}$ calculated for [$C_{42}H_{67}N_{17}O_{11}S_2$]: 526.2444; observed: m/z 526.237.

Compound 22 – Ac-HcyRAAARAHcy-NH$_2$

22
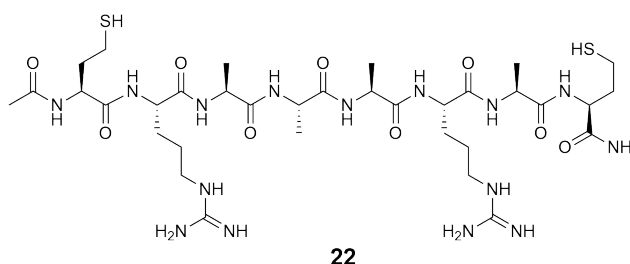
The peptide was synthesised with Fmoc-Hcy(Trt)-OH, Fmoc-Arg(Pbf)-OH and Fmoc-Ala-OH as per Method 1a, however the Hcy residues at positions 1 & 5 were coupled per Method 1b. After coupling the final amino-acid the deprotected peptide was capped per Method 2; then cleaved off the resin by Method 3 to give **22** as a white fluffy solid. HRMS (ESI+) [M+H]$^+$ calculated for [$C_{34}H_{63}N_{15}O_9S_2$]: 890.4455; observed: m/z 890.4424.

Compound 22d – Ac-(cyclo-1,8-dBB)HcyRAAARAHcy-NH$_2$

22d

The linear peptide precursor was prepared as detailed in 'Compound **22**'. The crude linear peptide **22** was cyclised by Method 5a. The crude cyclised peptide was purified per Method 6 to give **22d** as a fluffy pale yellow solid. Analytical HPLC: 0-100% over 15 min, R_t = 7.8 min; HRMS (ESI+) [M+H]$^+$ calculated for [$C_{44}H_{71}N_{17}O_{11}S_2$]: 1077.4960; observed: m/z 1077.4861.

Compound 23 - Ac-ARAAARAC-NH$_2$

23
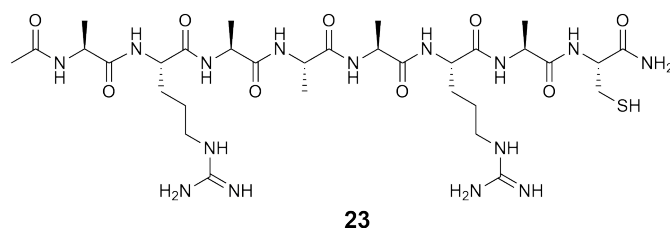
The peptide was synthesised with Fmoc-Cys(Trt)-OH, Fmoc-Arg(Pbf)-OH and Fmoc-Ala-OH per Method 1a, capped per Method 2; then cleaved off the resin by Method 3., to give **23** as a white fluffy solid. Analytical HPLC: 0-100% over 15 min, R_t = 7.0 min; HRMS (ESI+) [M+H]$^+$ calculated for [C$_{32}$H$_{59}$N$_{15}$O$_9$S$_1$]: 829.4341; observed: m/z 829.4254.

Compound 23m – Ac-ARAAARAC(8-mBB)-NH$_2$

23m

The linear peptide precursor was prepared as detailed in 'Compound **23**'. The crude linear peptide **23** was cyclised by Method 5a. The crude cyclised peptide was purified per Method 6 to give **23m** as a fluffy pale yellow solid. Analytical HPLC: 0-100% over 15 min, R_t = 7.6 min; HRMS (ESI+) [M]$^+$ calculated for [C$_{42}$H$_{69}$N$_{17}$O$_{11}$S$_1$]: 1019.5083; observed: m/z 1019.4972.

Compound 24d - Z-(cyclo-1,3-dBB)HcyLHcyF-OH

24d
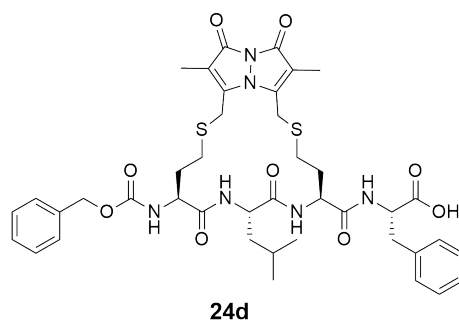
Wang resin (2 g) was loaded with Fmoc-Phe-OH (5 equiv) by reacting with HATU (5 equiv.) and DIPEA (10 equiv) for 2 h. The resin was then washed with DMF (5 x 10 mL), DCM (2 x 10 mL), and DMF (5 x 10 mL). A sample of the Wang resin (500 mg, 0.33 mequiv/g) was then reacted with Fmoc-Hcy(Trt)-OH at position 1 & 3 using Method 1b and Method 1a to attach Fmoc-Leu-OH at position 2. The *N*-terminally deprotected linear peptide was Cbz-protected by reaction with benzyl chloroformate (5 equiv, 121 µL) and DIPEA (10 equiv, 294 µL) in DMF (10 mL) for 30 min. The linear peptide was then cleaved per Method 3 and the crude peptide then cyclised per Method 5a. The crude cyclised peptide was purified per Method 6 to give **24d** as a yellow fluffy solid. Analytical HPLC: 0-100% over 15 min, $R_t =$ 13.6 min; HRMS (ESI+) [M]$^+$ calculated for [$C_{41}H_{50}N_6O_9S_2$]: 834.3045; observed: m/z 834.3081.
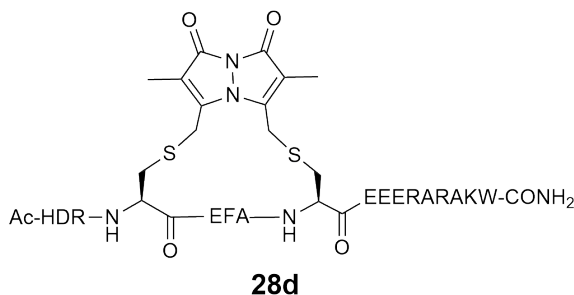
Compound 25d – Z-(cyclo-1,3-dBB)HcyLHcyG-OH

25d
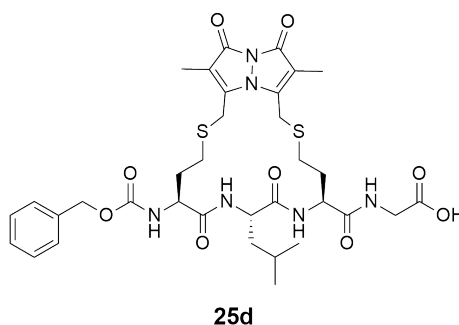
Wang resin (2 g) was loaded with Fmoc-Gly-OH (5 equiv) by reacting with HATU (5 equiv) and DIPEA (10 equiv) for 2 h. The resin was then washed with DMF (5 x 10 mL), DCM (2 x 10 mL), and DMF (5 x 10 mL). A sample of the Wang resin (500 mg, 0.33 mequiv/g) was

then reacted with Fmoc-Hcy(Trt)-OH at position 1 & 3 using Method 1b and Method 1a to attach Fmoc-Leu-OH at position 2. The *N*-terminally deprotected linear peptide was Cbz-protected by reaction with benzyl chloroformate (5 equiv, 121 μL) and DIPEA (10 equiv, 294 μL) in DMF (10 mL) for 30 min. The linear peptide was then cleaved per Method 3 and the crude peptide then cyclised per Method 5a. The crude cyclised peptide was purified per Method 6 to give **25d** as a yellow fluffy solid. HRMS (ESI+) [M]$^+$ calculated for [C$_{34}$H$_{44}$N$_6$O$_9$S$_2$]: 744.2611; observed: m/z 744.2573.

Compound 26 – Ac-AARAARAARAARACARAC-NH$_2$
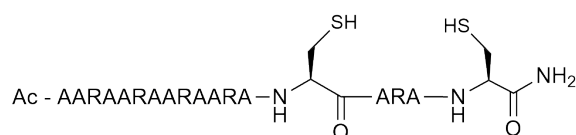
26

Rink amide resin (250 mg, 0.4 mequiv/g) was loaded with Fmoc-Cys(Trt)-OH per Method 1a. The peptide strand was assembled on this resin by a CEM Liberty Microwave Synthesiser, with Fmoc-Cys(Trt)-OH, Fmoc-Ala-OH and Fmoc-Arg(Pbf)-OH. The final capping step was carried out per Method 2 and cleaved per Method 3 to give **26** as a white fluffy solid. Analytical HPLC: 0-100% over 15 min, R$_t$ = 8 min; HRMS (ESI+) [M]$^+$ calculated for [C$_{71}$H$_{130}$N$_{34}$O$_{19}$S$_2$]: 1826.9693; observed: m/z 1826.9691.

Compound 26d – Ac(cyclo-14,18-dBB)-AARAARAARAARACARAC-NH$_2$
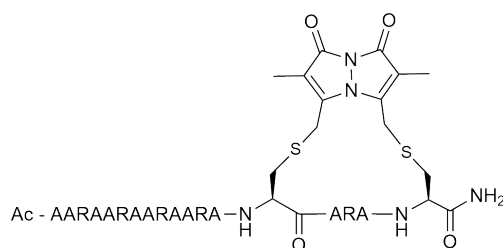
26d

The linear peptide precursor was prepared as detailed in 'Compound **26**'. The crude linear peptide was cyclised by Method 5a. The crude cyclised peptide was purified per Method 6 to give **26** as a fluffy pale yellow solid. Analytical HPLC: 0-100% over 15 min, R$_t$ = 7.8 min;

HRMS (ESI+) [M+H]$^+$ calculated for [C$_{81}$H$_{138}$N$_{36}$O$_{21}$S$_2$]: 2015.0278; observed: m/z 2015.0288.

Compound 27– Ac-AARAARAARACRAAARAC-NH$_2$
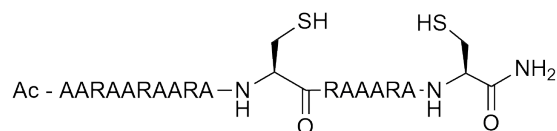
27

Rink amide resin (250 mg, 0.4 mequiv/g) was loaded with Fmoc-Cys(Trt)-OH per Method 1a. The peptide strand was assembled on this resin by a CEM Liberty Microwave Synthesiser, with Fmoc-Cys(Trt)-OH, Fmoc-Ala-OH and Fmoc-Arg(Pbf)-OH. The final capping step was carried out per Method 2 and cleaved per Method 3 to give **27** as a white fluffy solid. Analytical HPLC: 0-100% over 15 min, R$_t$ = 7.2 min; HRMS (ESI+) [M+H]$^+$ calculated for [C$_{71}$H$_{130}$N$_{34}$O$_{19}$S$_2$]: 1826.9693; observed: m/z 1826.9678.

Compound 27d– Ac-(cyclo-11,18-dBB)-AARAARAARACRAAARAC-NH$_2$
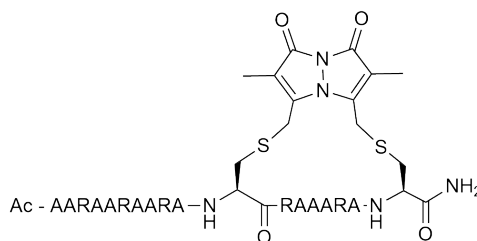
27d

The linear precursor was prepared as detailed in 'Compound **27**'. The crude linear peptide was cyclised by Method 5a. The crude cyclised peptide was purified per Method 6 to give **27d** as a pale yellow fluffy solid. Analytical HPLC: 0-100% over 15 min, R$_t$ = 7.8 min; HRMS (ESI+) [M+H]$^+$ calculated for [C$_{81}$H$_{138}$N$_{36}$O$_{21}$S$_2$]: 2015.0278; observed: m/z 2015.0272.

Compound 28 – H₂N-HDRCEFACFEEERARAKW-NH₂

28
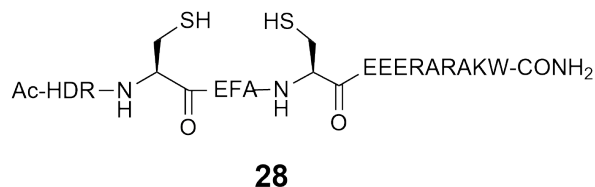
Rink amide resin (250 mg, 0.4 mequiv/g) was loaded with Fmoc-Trp(Boc)-OH per Method 1a. The peptide strand was assembled on this resin by a CEM Liberty One Microwave Synthesiser, with Fmoc-Cys(Trt)-OH, Fmoc-Ala-OH, Fmoc-Arg(Pbf)-OH, Fmoc-Glu(OtBu)-OH, and Fmoc-Phe-OH up until position 16. The final two amino acids were coupled manually per Method 1a. The final capping step was carried out per Method 2 and cleaved per Method 3 to give **28** as a white fluffy solid. Analytical HPLC: 0-100% over 15 min, R_t = 8.4 min; HRMS (ESI+) [M+4H]$^{4+}$ calculated for [$C_{98}H_{144}N_{32}O_{28}S_2$]: 571.2647; observed: m/z 571.2688.

Compound 28d - H₂N-(cyclo-4,8-dBB)HDRCEFACFEEERARAKW-NH₂

28d

The linear precursor was prepared as detailed in 'Compound **28**' The crude peptide was then cyclised per Method 5a and cleaved per Method 3. The crude cyclised peptide was purified per Method 6 to give **28d** as a pale yellow fluffy solid. Analytical HPLC: 0-100% over 15 min, R_t = 8.2 min; HRMS (ESI+) [M+4H]$^{4+}$ calculated for [$C_{108}H_{152}N_{34}O_{30}S_2$]: 618.6830; observed: m/z 618.6842.

Compound 29d – Z-(cyclo-1,3-dBB)CLCF-OH

29d
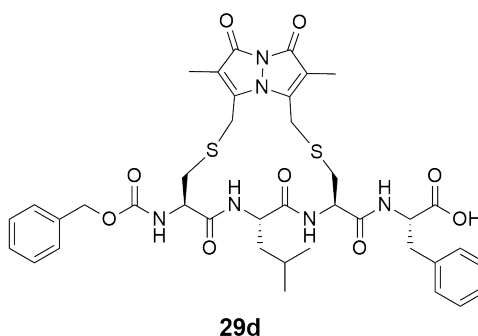
Wang resin (2 g) was loaded with Fmoc-Phe-OH (5 equiv) but reacting with HATU (5 equiv) and DIPEA (10 equiv) for 2 h. The resin was then washed with DMF (5 x 10 mL), DCM (2 x 10 mL), and DMF (5 x 10 mL). The linear peptide was assembled on Wang resin (500 mg, 0.33 mequiv/g) using the same coupling/deprotection protocol as in Method 1a with Fmoc-Cys(Mmt)-OH and Fmoc-Leu-OH. The N-terminal deprotected linear peptide was Cbz-protected by reaction with benzyl chloroformate (5 equiv, 121 μL) and DIPEA (10 equiv, 294 μL) in DMF (10 mL) for 30 min. The linear peptide was cyclised per Method 4 and cleaved per Method 3. The crude peptide was purified per Method 6 over a gradient of 35-45% aq. ACN to give the **29d** as a pale yellow solid. Analytical HPLC: 0-100% over 15 min, R_t = min; HRMS (ESI+) [M]$^+$ calculated for [$C_{39}H_{46}N_6O_9S_2$]: 806.2767; observed: m/z 806.2786.

Compound 30d– Z-(cyclo-1,3-dBB)CLCG-OH

30d
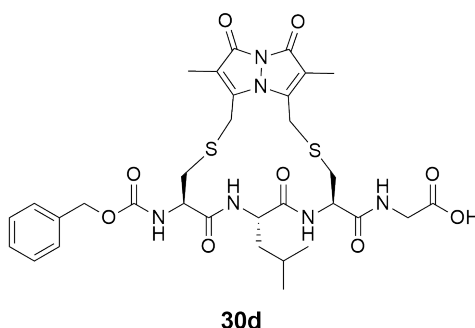
The linear peptide was assembled on Wang-Gly-Fmoc resin (500 mg, 0.33 mequiv/g) using the same coupling/deprotection protocol as in Method 1a with Fmoc-Cys(Mmt)-OH and Fmoc-Leu-OH. The N-terminal deprotected linear peptide was Cbz-protected by reaction with benzyl chloroformate (5 equiv, 121 μL) and DIPEA (10 equiv, 294 μL) in DMF (10 mL) for

30 min. The linear peptide was cyclised per Method 4 and cleaved per Method 3. The crude peptide was purified per Method 6 over a gradient of 35-45% aq. ACN to give **30d** as a pale yellow solid. Analytical HPLC: 0-100% over 15 min, R_t = min; HRMS (ESI+) [M]$^+$ calculated for [$C_{32}H_{40}N_6O_9S_2$]: 716.2298; observed: m/z 716.2236.

References

1. B. Yang, C. Zhang, X. Li, *et al*., Design, synthesis, and biological evaluation of novel peptide Gly(3) -MC62 analogues as potential antidiabetic agents, *Chem*. *Biol*. *Drug Des*., **2015**, 86, 979-989.

2. G. Philippe, Y. H. Huang, O. Cheneval, *et al*., Development of cell-penetrating peptide-based drug leads to inhibit MDMX:p53 and MDM2:p53 interactions, *Biopolymers*, **2016**, 106, 853-863.

3. P. M. Cromm, J. Spiegel, P. Kuchler, *et al*., Protease-Resistant and Cell-Permeable Double-Stapled Peptides Targeting the Rab8a GTPase, *ACS Chem*. *Biol*., **2016**, 11, 2375-2382.

4. A. Muppidi, Z. Wang, X. Li, *et al*., Achieving cell penetration with distance-matching cysteine cross-linkers: a facile route to cell-permeable peptide dual inhibitors of Mdm2/Mdmx, *Chem*. *Commun*., **2011**, 47, 9396-9368.

5. F. L. Alves, V. X. Oliveira, Jr. and A. Miranda, Angiotensin II analogues with N-terminal lactam bridge cyclization: an overview on AT1 receptor activation and tachyphylaxis, *Chem*. *Biol*. *Drug Des*., **2016**, 88, 677-682.

6. B. D. Blasio, E. Benedetti, V. Pavone, *et al*., Bicyclic Peptides: Solid State Conformation of cyclo(Glu- Leu-Pro-Gly-Lys-Leu-Pro-Gly)cyclo(1y-5e)Gly, *Biopolymers*, **1990**, 30, 509-551.

7. H. Zhang, Q. Zhao, S. Bhattacharya, *et al*., A cell-penetrating helical peptide as a potential HIV-1 inhibitor, *J*. *Mol*. *Biol*., **2008**, 378, 565-580.

8. G. L. Verdine and L. D. Walensky, The challenge of drugging undruggable targets in cancer: lessons learned from targeting BCL-2 family members, *Clinical cancer*

research : an official journal of the American Association for Cancer Research, **2007**, 13, 7264-7270.

9. Maria Pellegrini, Miriam Royo, Michael Chorev and D. F. Mierke, Conformation consequnces for i, i+3 cystine linkages: nucleation for alpha-helicity?, *J. Pept. Res.*, **1997**, 49, 404-414.

10. S. A. Kawamoto, A. Coleska, X. Ran, *et al.*, Design of triazole-stapled BCL9 alpha-helical peptides to target the beta-catenin/B-cell CLL/lymphoma 9 (BCL9) protein-protein interaction, *J. Med. Chem.*, **2012**, 55, 1137-1146.

11. Y. H. Lau, P. de Andrade, N. Skold, *et al.*, Investigating peptide sequence variations for 'double-click' stapled p53 peptides, *Org. Biomol. Chem.*, **2014**, 12, 4074-4077.

12. Z. Biron, S. Khare, A. O. Samsom, *et al.*, A Monomeric 310-Helix Is Formed in Water by a 13-Residue Peptide Representing the Neutralizing Determinant of HIV-1 on gp41, *Biochemistry*, **2002**, 41, 12687-12696.

13. A. Muppidi, K. Doi, S. Edwardraja, *et al.*, Rational design of proteolytically stable, cell-permeable peptide-based selective Mcl-1 inhibitors, *J. Am. Chem. Soc.*, **2012**, 134, 14734-14737.

14. H. N. Hoang, K. Song, T. A. Hill, *et al.*, Short Hydrophobic Peptides with Cyclic Constraints Are Potent Glucagon-like Peptide-1 Receptor (GLP-1R) Agonists, *J. Med. Chem.*, **2015**, 58, 4080-4085.

15. A. Iyer, D. Van Lysebetten, Y. Ruiz Garcia, *et al.*, Stapling monomeric GCN4 peptides allows for DNA binding and enhanced cellular uptake, *Org. Biomol. Chem.*, **2015**, 13, 3856-3862.

16. D. P. Fairlie and A. D. de Araujo, Stapling peptides using cysteine crosslinking, *Biopolymers*, **2016**, 106, 843-852.

17. P. Luo, D. T. Braddock, R. M. Subramanian, *et al.*, Structural and Thermodynamic Characterization of a Bioactive Peptide Model of Apolipoprotein E: Side-Chain Lactam Bridges To Constrain the Conformation, *Biochemistry*, **1994**, 33, 12367-12377.

18. L. K. Henchey, A. L. Jochim and P. S. Arora, Contemporary strategies for the stabilization of peptides in the alpha-helical conformation, *Curr. Opin. Chem. Biol.*, **2008**, 12, 692-697.

19. S. Y. Shim, Y. W. Kim and G. L. Verdine, A new i, i + 3 peptide stapling system for alpha-helix stabilization, *Chem. Biol. Drug Des.*, **2013**, 82, 635-642.

20. H. E. Blackwell, J. D. Sadowsky, R. J. Howard, *et al.*, Ring-Closing Metathesis of Olefinic Peptides: Design, Synthesis, and Structural Characterisation of Macrocyclic Helical Peptides, *J. Org. Chem.*, **2001**, 66, 5291-5302.

21. Y. W. Kim, T. N. Grossmann and G. L. Verdine, Synthesis of all-hydrocarbon stapled alpha-helical peptides by ring-closing olefin metathesis, *Nat. Protoc.*, **2011**, 6, 761-771.

22. H. Ruffner, A. Bauer and T. Bouwmeester, Human protein-protein interaction networks and the value for drug discovery, *Drug Discov. Today*, **2007**, 12, 709-716.

23. D. Balchin, M. Hayer-Hartl and F. U. Hartl, In vivo aspects of protein folding and quality control, *Science*, **2016**, 353, aac4354.

24. T. A. Edwards and A. J. Wilson, Helix-mediated protein--protein interactions as targets for intervention using foldamers, *Amino Acids*, **2011**, 41, 743-754.

25. M. A. Arslan, P. Csermely and C. Soti, Protein homeostasis and molecular chaperones in aging, *Biogerontology*, **2006**, 7, 383-389.

26. T. L. Blundell, B. L. Sibanda, R. W. Montalvao, *et al*., Structural biology and bioinformatics in drug design: opportunities and challenges for target identification and lead discovery, *Philos. Trans. R. Soc. B*, **2006**, 361, 413-423.

27. S. Jones and J. M. Thornton, Principles of protein-protein interactions, *Proc. Natl. Acad. Sci. U. S. A.*, **1996**, 93, 13-20.

28. D. E. Scott, M. T. Ehebauer, T. Pukala, *et al*., Using a fragment-based approach to target protein-protein interactions, *ChemBioChem*, **2013**, 14, 332-342.

29. C. G. Cummings and A. D. Hamilton, Disrupting protein-protein interactions with non-peptidic, small molecule alpha-helix mimetics, *Curr. Opin. Chem. Biol.*, **2010**, 14, 341-346.

30. N. Tsomaia, Peptide therapeutics: Targeting the undruggable space, *Eur. J. Med. Chem.*, **2015**, 94, 459-470.

31. A. Jamieson and N. Robertson, Regulation of protein-protein interactions using stapled peptides, *Reports in Organic Chemistry*, **2015**, 5, 65-74.

32. L. M. Meireles, A. S. Domling and C. J. Camacho, ANCHOR: a web server and database for analysis of protein-protein interaction binding pockets for drug discovery, *Nucleic Acids Res.*, **2010**, 38, W407-411.

33. A. M. Watkins and P. S. Arora, Structure-based inhibition of protein-protein interactions, *Eur. J. Med. Chem.*, **2015**, 94, 480-488.

34. B. N. Bullock, A. L. Jochim and P. S. Arora, Assessing helical protein interfaces for inhibitor design, *J. Am. Chem. Soc.*, **2011**, 133, 14220-14223.

35. J. Garner and M. M. Harding, Design and synthesis of alpha-helical peptides and mimetics, *Org. Biomol. Chem.*, **2007**, 5, 3577-3585.

36.   H. Jo, N. Meinhardt, Y. Wu, *et al.*, Development of alpha-helical calpain probes by mimicking a natural protein-protein interaction, *J. Am. Chem. Soc.*, **2012**, 134, 17704-17713.

37.   M. C. Smith and J. E. Gestwicki, Features of protein-protein interactions that translate into potent inhibitors: topology, surface area and affinity, *Expert Reviews in Molecular Medicine*, **2012**, 14, e16.

38.   S. M. Biros, L. Moisan, E. Mann, *et al.*, Heterocyclic alpha-helix mimetics for targeting protein-protein interactions, *Bioorg. Med. Chem. Lett.*, **2007**, 17, 4641-4645.

39.   V. Azzarito, K. Long, N. S. Murphy and A. J. Wilson, Inhibition of alpha-helix-mediated protein-protein interactions using designed molecules, *Nature Chem.*, **2013**, 5, 161-173.

40.   A. P. Higueruelo, H. Jubb and T. L. Blundell, Protein-protein interactions as druggable targets: recent technological advances, *Curr. Opin. Pharmacol.*, **2013**, 13, 791-796.

41.   J. M. Davis, L. K. Tsou and A. D. Hamilton, Synthetic non-peptide mimetics of alpha-helices, *Chem. Soc. Rev.*, **2007**, 36, 326-334.

42.   H. Hennemann, S. Wirths and C. Carl, Cell-based peptide screening to access the undruggable target space, *Eur. J. Med. Chem.*, **2015**, 94, 489-496.

43.   D. J. Barlow and J. M. Thronton, Helix Geometry in Proteins, *J. Mol. Biol.*, **1988**, 201, 601-619.

44.   L. Pauling and R. B. Corey, Configuration of Polypeptide Chains with Favored Orientation around Single Bonds: Two New Pleated Sheets, *Proc. Natl. Acad. Sci. U. S. A.*, **1951**, 37, 729-740.

45.   G. A. Petsko and D. Ringe, *Protein Structure and Function*, New Science Press Ltd. , London, 2004.

46. M. Guharoy and P. Chakrabarti, Secondary structure based analysis and classification of biological interfaces: identification of binding motifs in protein-protein interactions, *Bioinformatics*, **2007**, 23, 1909-1918.

47. L. Pauling and R. B. Corey, Atomic Coordinates and Structure Factors for Two Helical Configurations of Polypeptide Chains, *Proceedings of the National Academy of Sciences*, **1951**, 37, 235-240.

48. K. Estieu-Gionnet and G. Guichard, Stabilized helical peptides: overview of the technologies and therapeutic promises, *Expert Opinion Drug Discovery*, **2011**, 6, 937-936.

49. L. Pauling and R. B. Corey, Configurations of Polypeptide Chains with Favored Orientations around Single Bonds: Two New Pleated Sheets, *Chemistry*, **1951**.

50. *The Cell*, ASM Press and Sinauer associates, 4th ed. edn., 2006.

51. E. Benedetti, B. D. Blasio, V. Pavone, *et al.*, Characterization at Atomic Resolution of Peptide Helical Structures, *Biopolymers*, **1992**, 32, 453-456.

52. C. Toniolo and E. Benedetti, Intramolecularly Hydrogen-Bonded Peptide Conformation, *Critical Reviews in Biochemistry*, **2008**, 9, 1-44.

53. N. Sreerama, S. Y. Venyaminov and R. W. Woody, Estimation of the number of alpha-helical and beta-strand segments in proteins using circular dichroism spectroscopy, *Protein Sci.*, **1999**, 8, 370-380.

54. S. M. Kelly and N. C. Price, The Use of Circular Dichroism in the Investigation of Protein Structure and Function, *Curr. Protein Pept. Sci.*, **2000**, 1, 349-384.

55. S. M. Kelly, T. J. Jess and N. C. Price, How to study proteins by circular dichroism, *Biochim. Biophys. Acta*, **2005**, 1751, 119-139.

56. N. E. Shepherd, H. N. Hoang, G. Abbenante and D. P. Fairlie, Single Turn Peptide Alpha Helices with Exceptional Stability in Water, *J. Am. Chem. Soc.*, **2005**, 127.

57. R. W. Woody and A. Koslowski, Recent developments in the electronic spectroscopy of amides and a-helical polypeptides, *Biophys. Chem.*, **2002**, 101-102, 535-551.

58. M. C. Manning, Underlying assumptions in the estimation of secondary structure content in proteins by circular dichroism spectroscopy - a critical review, *J. Pharm. Biomed. Anal.*, **1989**, 7, 1103-1119.

59. K. Wuthrich, *NMR of Proteins and Nucleic Acids*, John Wiley & Sons, Canada, 1986.

60. A. Pardi, M. Billeter and K. Wuthrich, Calibration of the Angular Dependence of the Amide Proton-Ca Proton Coupling Constants, 3JHNa, in a Globular Protein, *J. Mol. Biol.*, **1984**, 180, 741-751.

61. G. Wagner, D. Neuhaus, E. Worgotter, *et al.*, Nuclear Magnetic Resonance Identification of "Half-turn" and 310-Helix Secondary Structure in Rabbit Liver Metallothionein-2, *J. Mol. Biol.*, **1986**, 187, 131-135.

62. D. S. Wishart and B. D. Sykes, The 13C Chemical-Shift Index: A simple method for the identification of protein secondary structure using 13C chemical shift data, *J. Biomol. NMR*, **1994**, 4, 171-180.

63. D. S. Wishart, B. D. Sykes and F. M. Richards, The Chemical Shift Index: A Fast and Simple Method for the Assignment of Protein Secondary Structure through NMR Spectroscopy, *Biochemistry*, **1992**, 31, 1647-1651.

64. D. S. Wishart and B. D. Sykes, Chemical Shifts as a Tool for Structure Determination, *Methods Enzymol.*, **1994**, 239, 363-392.

65. T. Asakura, K. Taoka, M. Demura and M. P. Williamson, The relationship between amide proton chemical shifts and secondary structure in proteins, *J. Biomol. NMR*, **1995**, 6, 227-236.

66. M. P. Williamson, Secondary-Structure Dependent Chemical Shifts in Proteins, *Biopolymers*, **1990**, 29, 1423-1431.

67. C. Soti and P. Csermely, Molecular chaperones and the aging process, *Biogerontology*, **2000**, 1, 225-233.

68. A. Yu, Y. Shibata, B. Shah, *et al.*, Protein aggregation can inhibit clathrin-mediated endocytosis by chaperone competition, *Proc. Natl. Acad. Sci. U. S. A.*, **2014**, 111, E1481-E1490.

69. P. L. Clark and A. H. Elcock, Molecular chaperones: providing a safe place to weather a midlife protein-folding crisis, *Nat. Struct. Mol. Biol.*, **2016**, 23, 621-623.

70. Y. Bar-Lavan, N. Shemesh and A. Ben-Zvi, Chaperone families and interactions in metazoa, *Essays Biochem.*, **2016**, 60, 237-253.

71. S. Horowitz, L. Salmon, P. Koldewey, *et al.*, Visualizing chaperone-assisted protein folding, *Nat. Struct. Mol. Biol.*, **2016**, 23, 691-697.

72. A. Strauch and M. Haslbeck, The function of small heat-shock proteins and their implication in proteostasis, *Essays Biochem.*, **2016**, 60, 163-172.

73. J. M. Scholtz and R. L. Baldwin, The Mechanism of a-helix formation by peptides, *Annu. Rev. Biophys. Biomol. Struct.*, **1992**, 21, 95-118.

74. S. Merquee, V. H. Robbins and R. L. Baldwin, Unusually stable helix formation in short alanine-based peptides, *Proc. Natl. Acad. Sci. U. S. A.*, **1989**, 86, 5286-5290.

75. E. Freire, D. T. Haynie and D. Xie, Molecular Basis of Cooperativity in Protein Folding IV. CORE: A General Cooperative Folding Model, *Proteins: Structure, Function and Genetics*, **1993**, 17, 111-123.

76. H. S. Chan, S. Bromberg and K. A. Dill, Models of cooperativity in protein folding, *Philos. Trans. R. Soc. B*, **1995**, 348, 61-70.

77. P. Malhotra and J. B. Udgaonkar, How cooperative are protein folding and unfolding transitions?, *Protein Sci.*, **2016**, Published Online

78. J. W. Taylor, The Synthesis and Study of Side-Chain Lactam-Bridged Peptides, *Peptide Science*, **2002**, 66, 49-75.

79. A. M. Spokoyny, Y. Zou, J. J. Ling, *et al.*, A perfluoroaryl-cysteine S(N)Ar chemistry approach to unprotected peptide stapling, *J. Am. Chem. Soc.*, **2013**, 135, 5946-5949.

80. C. E. Schafmeister, J. Po and G. L. Verdine, An All-Hydrocarbon Cross-Linking System for Enhancing the Helicity and Metabolic Stability of Peptides, *J. Am. Chem. Soc.*, **2000**, 122, 5891-5892.

81. *Proteases in Health and Disease*, Springer, New York, 2013.

82. T. A. Hill, N. E. Shepherd, F. Diness and D. P. Fairlie, Constraining cyclic peptides to mimic protein structure motifs, *Angew. Chem. Int. Ed. (English)*, **2014**, 53, 13020-13041.

83. M. D. Cummings, C. Schubert, D. J. Parks, *et al.*, Substituted 1,4-benzodiazepine-2,5-diones as alpha-helix mimetic antagonists of the HDM2-p53 protein-protein interaction, *Chem. Biol. Drug Des.*, **2006**, 67, 201-205.

84. A. Gori, C. Peri, G. Quilici, *et al.*, Flexible vs Rigid Epitope Conformations for Diagnostic- and Vaccine-Oriented Applications: Novel Insights from the Burkholderia pseudomallei BPSL2765 Pal3 Epitope, *ACS Infect. Dis.*, **2016**, 2, 221-230.

85. Y. H. Lau, Y. Wu, P. de Andrade, *et al.*, A two-component 'double-click' approach to peptide stapling, *Nat. Protoc.*, **2015**, 10, 585-594.

86. A. D. de Araujo, H. N. Hoang, W. M. Kok, *et al.*, Comparative alpha-helicity of cyclic pentapeptides in water, *Angew. Chem. Int. Ed. (English)*, **2014**, 53, 6965-6969.

87. Y. H. Lau, P. de Andrade, Y. Wu and D. R. Spring, Peptide stapling techniques based on different macrocyclisation chemistries, *Chem. Soc. Rev.*, **2015**, 44, 91-102.

88.   J. C. Phelan, N. J. Skelton, A. C. Braisted and R. S. McDowell, A General Method for Constraining Short Peptides to an Alpha-Helical Conformation, *J. Am. Chem. Soc.*, **1997**, 119, 455-460.

89.   M. J. Kelso, R. L. Beyer, H. N.Hoang, *et al.*, Alpha-Turn Mimetics: Short Peptide alpha-Helices Composed of Cyclic Metallopentapeptide Modules, *J. Am. Chem. Soc.*, **2004**, 126, 4828-4842.

90.   F. Zhang, O. Sadovski, S. J. Xin and G. A. Woolley, Stabilization of Folded Peptide and Protein Structures via Distance Matching with a Long, Rigid Cross-Linker, *J. Am. Chem. Soc.*, **2007**, 129.

91.   Y. V. Schlippe, M. C. Hartman, K. Josephson and J. W. Szostak, In vitro selection of highly modified cyclic peptides that act as tight binding inhibitors, *J. Am. Chem. Soc.*, **2012**, 134, 10469-10477.

92.   Y. Wang and D. H.-C. Chou, A Thiol–Ene Coupling Approach to Native Peptide Stapling and Macrocyclization, *Angew. Chem. Int. Ed. (English)*, **2015**, 54, 10931-10934.

93.   V. Haridas, From Peptides to Non-Peptide Alpha-Helix Inducers and Mimetics, *Eur. J. Org. Chem.*, **2009**, 2009, 5112-5128.

94.   D. Y. Jackson, D. S. King, J. Chimielewski, *et al.*, General Approach to the Synthesis of Short a-Helical Peptides, *J. Am. Chem. Soc.*, **1991**, 113, 9391-9392.

95.   A.-M. Leduc, J. O. Trent, J. L. Wittliff, *et al.*, Helix-stabilized cyclic peptides as selective inhibitors of steroid receptor– coactivator interactions, *Biochemistry*, **2003**, 100, 11273-11278.

96.   H. N. Hoang, R. W. Driver, R. L. Beyer, *et al.*, Helix Nucleation by the Smallest Known alpha-Helix in Water, *Angew. Chem. Int. Ed. (English)*, **2016**, 55, 8275-8279.

97. L. D. Walensky, A. L. Kung, I. Escher, *et al.*, Activation of Apoptosis in vivo by a Hydrocarbon-Stapled BH3 Helix, *Science*, **2004**, 305, 1466-1470.

98. K. L. Keeling, O. Cho, D. B. Scanlon, *et al.*, The key position: influence of staple location on constrained peptide conformation and binding, *Org. Biomol. Chem.*, **2016**, 14, 9731-9735.

99. Q. Chu, R. E. Moellering, G. J. Hilinski, *et al.*, Towards understanding cell penetration by stapled peptides, *MedChemComm*, **2015**, 6, 111-119.

100. A. E. Radkowsky and E. M. Kosower, Bimanes. 17. (Haloalky1)- 1,5-diazabicyclo[3.3.0loctadienediones (Halo-9,lO-dioxabimanes): Reactivity toward the Tripeptide Thiol, Glutathione, *J. Am. Chem. Soc.*, **1986**, 108, 4527-4531.

101. E. M. Kosower and N. S. Kosower, Bromobimane Probes for Thiols, *Methods Enzymol.*, **1995**, 251, 133-148.

102. L. A. Montoya, X. Shen, J. J. McDermott, *et al.*, Mechanistic investigations reveal that dibromobimane extrudes sulfur from biological sulfhydryl sources other than hydrogen sulfide, *Chem. Sci.*, **2015**, 6, 294-300.

103. N. S. Kosower, G. L. Newton, E. M. Kosower and H. M. Ranney, Bimane Fluorescent Labels - Characterization of the Bimane Labeling of Human Hemoglobin, *Biochim. Biophys. Acta*, **1980**, 622, 201-209.

104. N. S. Kosower, E. M. Kosower, G. L. Newton and H. M. Ranney, Bimane fluorescent labels: Labeling of normal human red cells under physiological conditions, *Proc. Natl. Acad. Sci. U. S. A.*, **1979**, 76, 3382-3386.

105. P. Danielsohn and A. Nolte, Bromobimanes- fluorescent labeling agents for histochemical detection of sulfur containing neuropeptides in semithin sections, *Histochemistry*, **1987**, 86, 281-285.

106. X. Shen, C. B. Pattillo, S. Pardue, *et al.*, Measurement of plasma hydrogen sulfide in vivo and in vitro, *Free Radical Biol. Med.*, **2011**, 50, 1021-1031.

107. J.-S. Kim and R. T. Raines, Dibromobimane as a Fluorescent Crosslinking Reagent, *Anal. Biochem.*, **1994**, 225, 174-176.

108. X. Shen, E. A. Peter, S. Bir*, et al.*, Analytical measurement of discrete hydrogen sulfide pools in biological specimens, *Free Radical Biol. Med.*, **2012**, 52, 2276-2283.

109. T. D. Dunham and D. L. Farrens, Conformational Changes in Rhodopsin, *J. Biol. Chem.*, **1999**, 274, 1683-1690.

110. P. Luo and R. L. Baldwin, Mechanism of Helix Induction by Triflouroethanol: A Framework for Extrapolating the Helix-Forming Properties of Peptides from Trifluoroethanol/Water Mixtures Back to Work, *Biochemistry*, **1997**, 36, 8413-8421.

111. A. Kentsis and T. R. Sosnick, Trifluoroethanol Promotes Helix Formation by Destabilizing Backbone Exposure: Desolvation Rather than Native Hydrogen Bonding Defines the Kinetic Pathway of Dimeric Coiled Coil Folding, *Biochemistry*, **1998**, 37, 14613-14622.

112. K. L. Wegener, A. W. Partridge, J. Han, *et al.*, Structural basis of integrin activation by talin, *Cell*, **2007**, 128, 171-182.

113. O. Vinogradova, A. Velyvis, A. Velyviene*, et al.*, A Structural Mechanism of Integrin aIIbB3 "Inside-Out" Activation as Regulated by Its Cytoplasmic Face, *Cell*, **2002**, 110, 587-597.

114. S. Aldrich, Discovery DSC-18 SPE tubes, http://www.sigmaaldrich.com/catalog/, Accessed 2016.

115. D. H. Appella, L. A. Christianson, I. L. Karle, *et al.*, Beta-Peptide Foldamers: Robust Helix Formation in a New Family of beta-Amino Acid Oligomers, *J. Am. Chem. Soc.*, **1996**, 118, 13071-13072.

116. B. R. Huck, J. D. Fisk and S. H. Gellman, Promotion of Sheet Formation in a-Peptide Strands by a beta-Peptide Reverse Turn, *Org. Lett.*, **2000**, 2, 2607-2610.

117. M. A. Schmitt, S. H. Choi, I. A. Guzei and S. H. Gellman, Residue Requirements for Helical Folding in Short a/beta-Peptides: Crystallographic Characterization of the 11-Helix in an Optimized Sequence, *J. Am. Chem. Soc.*, **2005**, 127, 13130-13131.

118. R. D. Blasio, A. Lombardi, G. D'Auria, *et al.*, Beta-Alanine Containing Peptides: Gamma-Turns in Cyclotetrapeptides, *Biopolymers*, **1993**, 33, 621-631.

119. V. Pavone, A. Lombardi, G. D'Auria, *et al.*, Beta-Alanine Containing Peptides, *Biopolymers*, **1992**, 32, 173-183.

120. D. Seebach and J. Gardiner, Beta-Peptidic Peptidomimetics, *Acc. Chem. Res.*, **2008**, 41, 1366-1375.

121. J. A. Kritzer, O. M. Stephens, D. A. Guarracino, *et al.*, beta-Peptides as inhibitors of protein-protein interactions, *Bioorg. Med. Chem.*, **2005**, 13, 11-16.

122. R. P. Cheng, S. H. Gellman and W. F. DeGrado, Beta-Peptides: From Structure to Function, *Chem. Rev.*, **2001**, 101, 3219-3232.

123. R. W. Woody, The development and current state of protein circular dichroism, *Biomed. Spectrosc. Imaging*, **2015**, 4, 5-34.

124. J. D. Glickson and J. Applequist, The Conformation of Poly-B-alanine in Aqueous Solution from Proton Magnetic Resonance and Deuterium Exchange Studies, *J. Am. Chem. Soc.*, **1970**, 93, 3276-3281.

125. S. Costantini, G. Colonna and A. M. Facchiano, Amino acid propensities for secondary structures are influenced by the protein structural class, *Biochem. Biophys. Res. Commun.*, **2006**, 342, 441-451.

126. K. Fujiwara, H. Toda and M. Ikeguchi, Dependence of α-helical and β-sheet amino acid propensities on the overall protein fold type, *BMC Structural Biology*, **2012**, 12, 1-15.

127. C. N. Pace and J. M. Scholtz, A Helix Propensity Scale Based on Experimental Studies of Peptides and Proteins, *Biophys. J.*, **1998**, 75, 422-427.

128. N. E. Shepherd, H. N. Hoang, G. Abbenante and D. P. Fairlie, Single Turn Peptide Alpha Helices with Exceptional Stability in Water, *J. Am. Chem. Soc.*, **2005**, 127, 2974-2983.

129. W. S. Hancock and J. E. Battersvy, A new micro-test for the detection of incomplete coupling reactions in solid-phase peptide synthesis using 2,4,6-trinitrobenzene-sulphonic acid, *Anal. Biochem.*, **1976**, 71, 260-264.

Appendices

Appendix 1: Calculations

Statistical Difference in Maximum excitation and emission wavelengths

Table S1: Fluorescence excitation and emission wavelengths and the standard deviation (SD) from the mean of those values

	10d	13m	15d	19m	21d	23m	Mean	SD (σ)
Excitation Wavelength (nm)	386	390	389	390	392	389	388.67	2.65
Emission Wavelength (nm)	482	476	482	481	474	482	477.56	5.61

99% confidence interval:

$$99\%\ confidence\ interval = \bar{x} \pm 2.567\left(\frac{\sigma}{\sqrt{n}}\right)$$

where

$\bar{x}$= mean average

σ= standard deviation

n = number of samples

95% confidence interval:

Excitation wavelength: 386.4-390.9 nm

Emission wavelength: 472.8-482.4 nm

All compounds lie within these ranges therefore are not significantly different

% Helicity

$$MRE = \frac{millidegrees}{C * P * N}$$

where,

C= concentration in dM

P = cell pathlength in cm

N = number of amino-acid residues

From N. E. Shepherd, H. N. Hoang, G. Abbenante and D. P. Fairlie, Single Turn Peptide Alpha Helices with Exceptional Stability in Water, *J. Am. Chem. Soc.*, **2005**, 127, 2974-2983.

$$MRE_{100\% \, \alpha-\text{helicity}}(@215nm) = (-44000 + 250T) \times \left(1 - \frac{k}{N}\right)$$

where,

T = temperature in °C

k = 3 for carboxyamidated peptides

N = number of amino-acid residues

Therefore the maximum intensity MRE at 215 nm, for a carboxyamidated peptide with 100% α-helicity consisting of 5 amino-acids at 25°C is -15100 mdeg dmol^{-1} residue^{-1}

$$\% \, \alpha - \text{helicity} = \frac{MRE@215nm}{MRE_{100\% \, \alpha-\text{helicity}}(@215nm)} \times 100$$

Appendix 2: NMR Data

Table S 2: NMR Chemical shift (ppm) for tripeptides **10**-**14m** analysed in section 3.2.

Hα		Change in shift Relative to Linear sequence (ppm)					
		d₆-DMSO					
		10d	12d	13m		11d	14m
	1	0.14	0.10	-	1	0.25	-
	2	0.09	0.17	.01	2nh	0.03	-0.02
	3	0.20	0.09	.22	2co	0.02	-0.05
					3	0.10	0.11

Cα		Change in shift Relative to Linear sequence (ppm)					
		d₆-DMSO					
		10d	12d	13m		11d	14m
	1	-3.1	-0.3	-	1	-3.9	-
	2	-0.5	-0.6	-0.1	2nh	-0.9	0.0
	3	-2.8	0.0	-2.7	2co	-0.6	0.2
					3	-2.8	-3.1

CO		Change in shift Relative to Linear sequence (ppm)					
		d₆-DMSO					
		10d	12d	13m		11d	14m
	1	0.1	-0.2	-		-0.8	-
	2	-0.4	-0.4	0.2		0.3	0.0
	3	0.1	-0.6	0.3		0.2	0.1

NH		Change in shift Relative to Linear sequence (ppm)					
		d₆-DMSO					
		10d	12d	13m		11d	14m
	1	0.06	-0.01	-		0.02	-
	2	0.39	0.38	-0.099		0.24	-0.17
	3	-0.09	0.11	0.179		0.07	0.14

Table S3: NMR chemical shift data (ppm) for pentapeptides **15-20m** analysed in section 3.3. For β-alanine containing peptides, 'nh' next to the residue number represents the methylene neighbouring the NH, and 'co' next to the residue number represents the methylene neighbouring the CO. In the case where the β-alanine methylene split into 2 1H resonances the middle of those two resonances is quoted.

Chemical Shift (ppm)

Hα

	15	15d	18d	19m	10% D₂O in water	16	16d	17d	20m
1	4.45	4.53	4.46	4.23	1	4.41	4.41	4.58	3.40
					1co	-	-	-	2.40
2	4.25	4.32	4.27	4.25	2nh	3.41	3.49	4.28	3.40
					2co	2.42	2.46	-	2.40
3	4.21	4.27	4.19	4.24	3nh	3.47	3.44	4.15	3.40
					3co	2.44	2.45	-	2.40
4	4.27	4.27	4.29	4.27	4nh	3.47	3.48	3.49	3.40
					4co	2.55	2.41	2.55	2.50
5	4.40	4.53	4.44	4.46	5	4.49	4.49	4.53	4.51

Cα

	15	15d	18d	19m	10% D₂O in water	16	16d	17d	20m
1	Identifiable spectrum cannot be collected	56.2	55.7	52.6	1	58.9	55.8	54.5	38.8
					1co	-	-	-	38.1
2		52.9	53.6	52.5	2nh	39.1	38.7	51.9	38.8
					2co	39.1	38.4	-	38.1
3		53.0	52.8	53.6	3nh	38.8	38.8	51.8	38.7
					3co	38.4	37.9	-	38.0
4		52.9	52.7	52.7	4nh	38.3	39.0	37.4	38.6
					4co	38.0	38.1	36.7	37.8
5		56.2	55.4	55.4	5	58.5	55.3	54.9	55.4

CO

	15	15d	18d	19m	10% D₂O in water	16	16d	17d	20m
1		177.1	177.0	177.8	1	174.9	174.4	173.6	176.6
2		177.5	178.3	178.1	2	176.8	176.4	176	176.6
3		177.7	178.0	177.6	3	176.8	176.5	176.4	176.5
4		177.6	177.9	177.9	4	177.3	177.0	175.8	176.7
5	-	174.7	178.7	176.8	5	177.7	177.1	176.3	177.2

Table S4: Change in chemical shift (ppm) relative to literature values from Wishart et. al. (Ref 58 & 64) for pentapeptides

Hα	Change in shift relative to Random coil shifts (ppm)								
	15	15d	18d	19m		16	16d	17d	20m
1	-0.09	-0.01	-0.08	-0.10	1	-0.13	-0.13	0.04	-0.029
2	-0.08	-0.01	-0.06	-0.08		-	-	-	-0.027
3	-0.12	-0.06	-0.14	-0.09	2n	-0.02	0.06	-0.05	-0.029
4	-0.06	-0.06	-0.04	-0.06	2o	-0.01	0.03	-	-0.027
5	-0.14	-0.01	-0.1	-0.08	3n	0.04	0.01	-0.18	-0.030
					3o	0.01	0.02	-	-0.027
					4n	0.04	0.05	0.06	-0.029
					4n	0.12	-0.02	0.12	0.065
					5	-0.05	-0.05	-0.01	-0.033

Cα	Change in shift relative to Random coil shifts (ppm)								
	15	15d	18d	19m		16	16d	17d	20m
1	-56.8	-0.6	-1.1	0.4	1	2.1	-1.0	-2.3	
2		0.7	1.4	0.3	2n				
3		0.8	0.6	1.4	2o				
4		0.7	0.5	0.5	3n				
5		-0.6	-1.4	-1.4	3o				
					4n				
					4n				
					5	1.7	-1.5	-1.9	-1.9

CO	Change in shift relative to Random coil shifts (ppm)							
	15	15d	16	16d	17d	18d	19m	20m
1	-2.8	2.5	0.3	-0.2	-1.0	2.4	0.2	
2	-2.9	-0.1				3.7	0.5	
3	-2.9	0.1				3.4	0	
4	-3.2	0.0				3.3	0.3	
5		0.1		-0.5	-1.3	1.1	2.2	-0.4

Table S5: Change in chemical shift (ppm) for **10d**-**14m** relative to the corresponding linear peptide as described in section 3.2.

Hα		Change in shift Relative to Linear sequence (ppm)						
				d₆-DMSO				
		10d	**12d**	**13m**			**11d**	**14m**
	1	0.14	0.10	-	**1**		0.25	-
	2	0.09	0.17	.01	**2nh**		0.03	-0.02
	3	0.20	0.09	.22	**2co**		0.02	-0.05
					3		0.10	0.11

Cα		Change in shift Relative to Linear sequence (ppm)						
				d₆-DMSO				
		10d	**12d**	**13m**			**11d**	**14m**
	1	-3.1	-0.3	-	**1**		-3.9	-
	2	-0.5	-0.6	-0.1	**2nh**		-0.9	0.0
	3	-2.8	0.0	-2.7	**2co**		-0.6	0.2
					3		-2.8	-3.1

CO		Change in shift Relative to Linear sequence (ppm)						
				d₆-DMSO				
		10d	**12d**	**13m**			**11d**	**14m**
	1	0.1	-0.2	-			-0.8	-
	2	-0.4	-0.4	0.2			0.3	0.0
	3	0.1	-0.6	0.3			0.2	0.1

NH		Change in shift Relative to Linear sequence (ppm)						
				d₆-DMSO				
		10d	**12d**	**13m**			**11d**	**14m**
	1	0.06	-0.01	-			0.02	-
	2	0.39	0.38	-0.099			0.24	-0.17
	3	-0.09	0.11	0.179			0.07	0.14

Table S6: Change in chemical shift (ppm) for **15d**-**20m** relative to the corresponding linear peptide as described in section 3.3.

Hα	Change in shift Relative to Linear sequence (ppm)						
	15d	18d	19m		16d	17d	20m
1	0.08	0.01	-	1	0.001	0.13	-
2	0.07	0.02	0.00	1co	-	-	-
3	0.06	-0.02	0.03	2n	0.08	0.03	-0.01
4	0.00	0.02	0.00	2o	0.04		-0.02
5	0.13	0.04	0.06	3n	-0.03	-0.06	-0.07
				3o	0.01	-	-0.04
				4n	0.01	0.02	-0.07
				4n	-0.14	0.00	-0.05
				5	0.00	0.04	0.02

Cα	Change in shift Relative to Linear sequence (ppm)						
	15d	18d	19m		16d	17d	20m
1	-	-	-	1	-3.2	-1.3	-
2	-	-	-	1co			-
3	-	-	-	2n	-0.4	-	-0.3
4	-	-	-	2o	-0.7		-1.0
5	-	-	-	3n	0.0	-	-0.1
				3o	-0.4		-0.3
				4n	0.8	-1.6	0.3
				4n	0.0	-1.4	-0.3
				5	-3.2	-0.4	-3.1

CO	Change in shift Relative to Linear sequence (ppm)						
	15d	16d	17d	18d	19m	20m	
1		-0.5	1.8			-	
2		-0.3786	1.3			-0.2	
3		-0.3	1.7			-0.3	
4		-0.3	1.4			-0.1	
5		-0.6	-			-0.5	-

NH	Change in shift Relative to Linear sequence (ppm)						
	15d	16d	17d	18d	19m	20m	
1	0.51	0.08	0.47	0.38	-	-	
2	0.42	0.08	0.44	0.00	0.15	-0.18	
3	0.24	0.05	0.24	0.30	0.33	0.03	
4	0.34	0.04	-0.25	0.20	0.35	-0.02	
5	0.42	0.12	0.00	0.26	0.47	0.09	

Table S7: The $J_{HNH\alpha}$ values (Hz) for tripeptides **10-14m** in d$_6$-DMSO and 10% aq. D$_2$O.

	J values (Hz)										
	d$_6$-DMSO								10% D$_2$O in water		
	10	10d	11	11d	12	12d	13m	14m	11	11d	14m
1	7.6	7.9		8.1	7.9	8.1	7.6	4.8	5.1	6.8	
2	7.0	7.6		7.1	7.0	7.5	7.1	5.3	5.1	5.7	6.4
3	7.9	8.6		8.3	8.2	8.3	8.3	8.6	7.1	7.1	7.6

Table S8: The $J_{HNH\alpha}$ values (Hz) for pentapeptides **15-20-m** in 10% aq. D$_2$O.

	J values (Hz)							
	10% D$_2$O in water							
	15	15d	16	16d	17d	18d	19m	20m
1	7.1	7.1	7.3	7.0		5.9	5.6	5.6
2	5.3	5.6	6.1	5.9	5.3	5.1 *	5.6	
3	5.7	5.4	5.9	5.7	5.0	3.9 *	-	
4	6.1	-	5.9	5.9	5.6	5.9	-	
5	8.0	-	7.3	7.6		7.3		7.3

Table S9: The amide-derived temperature coefficients (from 25-50 °C) for pentapeptides **15d-20m**.

	Amide-derived temperature coefficients (ppb/K)					
	15d	16	16d	18d	19m	20m
1	-8.03	-7.30	-8.23	-7.64	-6.57	-6.88
2	-7.13	-6.91	-7.46	-4.21	-9.14	
3	-4.03	-7.09	-7.49	-8.43	-5.41	
4	-7.66	-7.26	-7.91	-5.10	-6.91	-7.39
5	-7.27	-7.63	-8.43	-4.60	-7.37	-7.95

Appendix 3: Characterisation

1D NMR Spectra
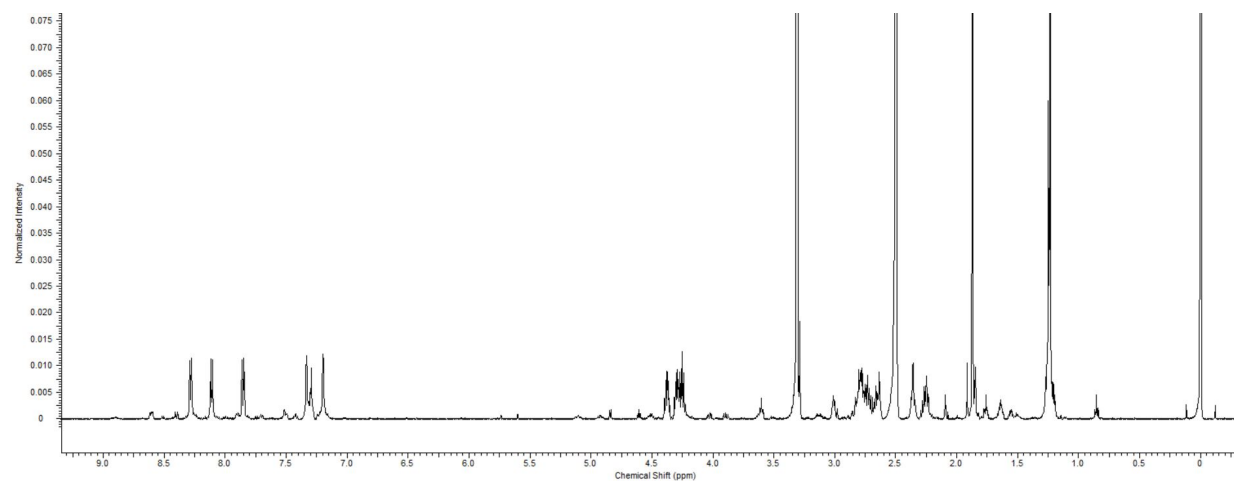
Figure S1: 500 MHz spectrum of **10** in d$_6$-DMSO.
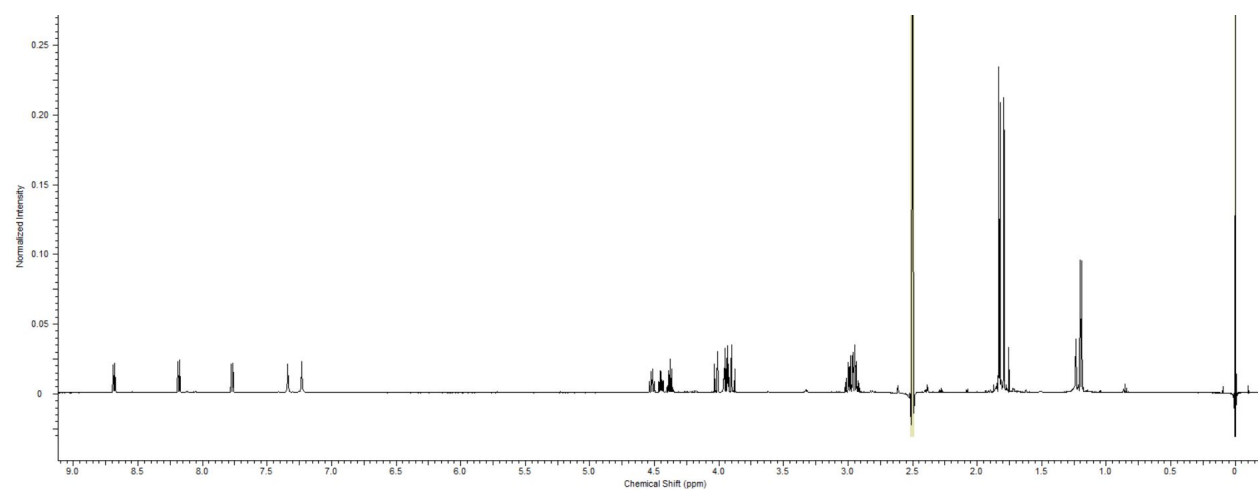
Figure S2: 600 MHz spectrum of **10d** in d$_6$-DMSO.
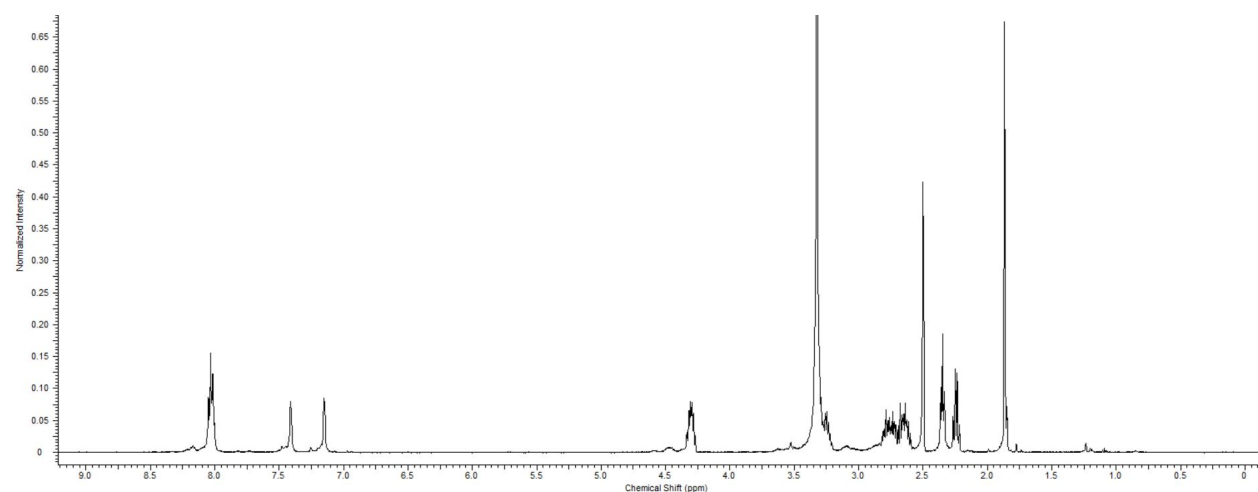
Figure S3: 500 MHz spectrum of **11** in d$_6$-DMSO.
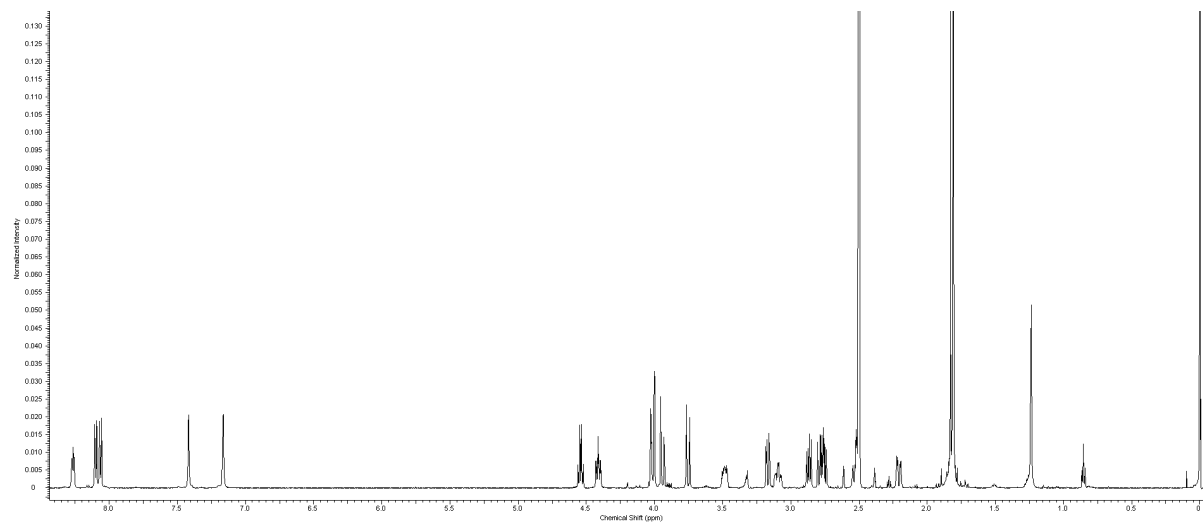
Figure S4: 500 MHz spectrum of **11d** in d_6-DMSO.
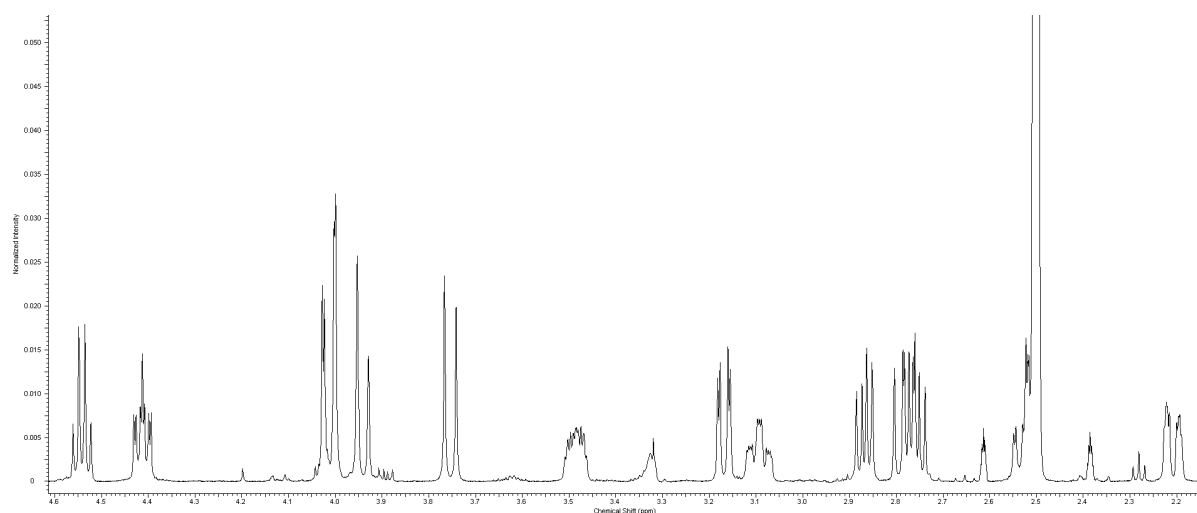
Figure S5: 500 MHz spectrum of **11d i**n d_6-DMSO between 2.1 and 4.6 ppm.
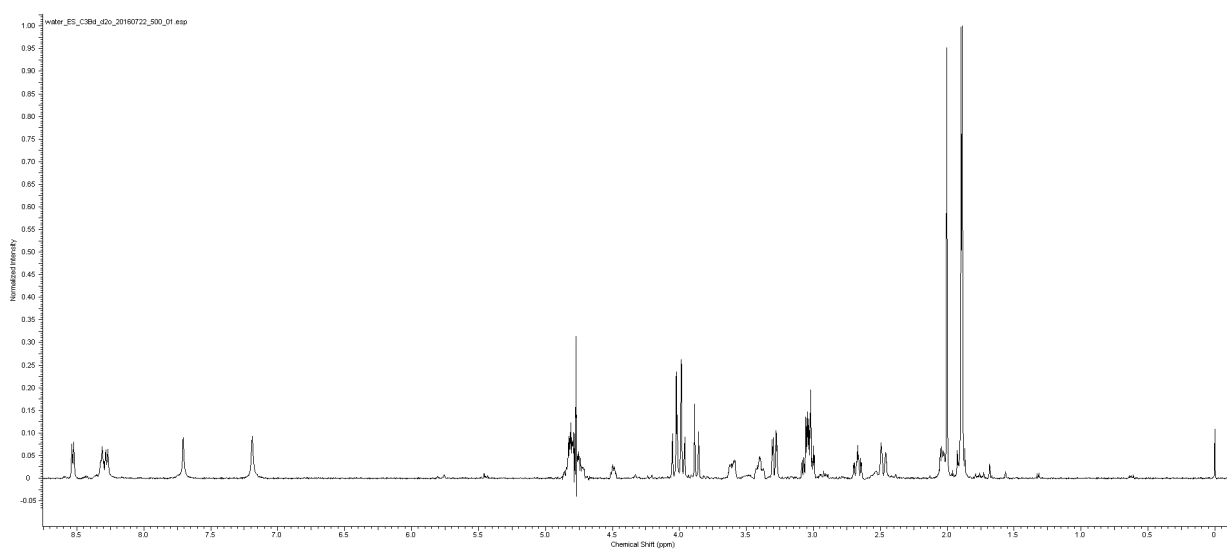
Figure S6: 500 MHz spectrum of **11d** in 10% D_2O in water.
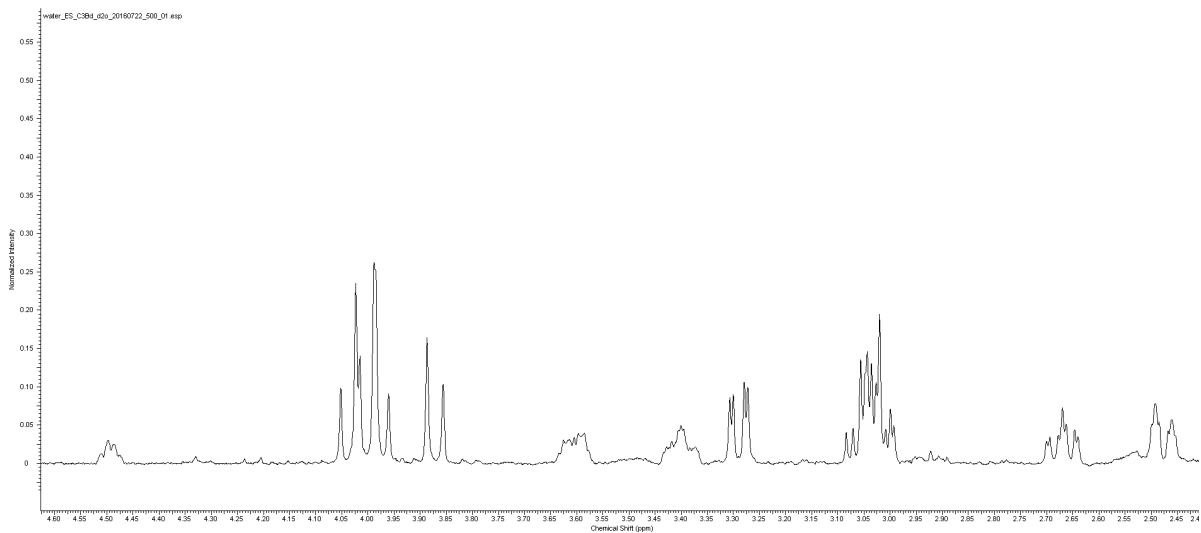
Figure S7: 500 MHz spectrum of **11d** in 10% D_2O in water between 2.4 and 4.6 ppm.
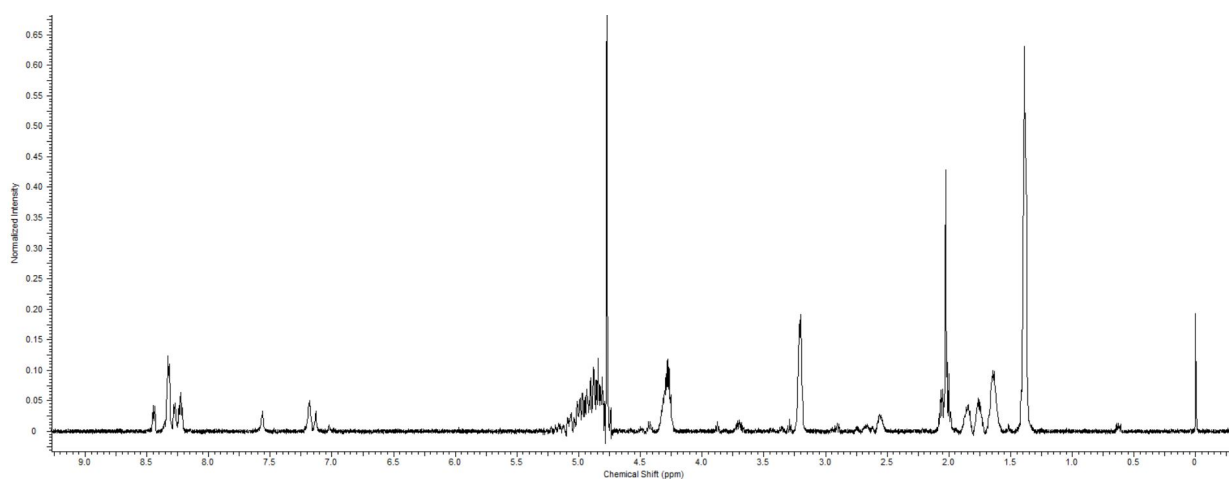
Figure S8: 600 MHz spectrum of **12** in d_6-DMSO.
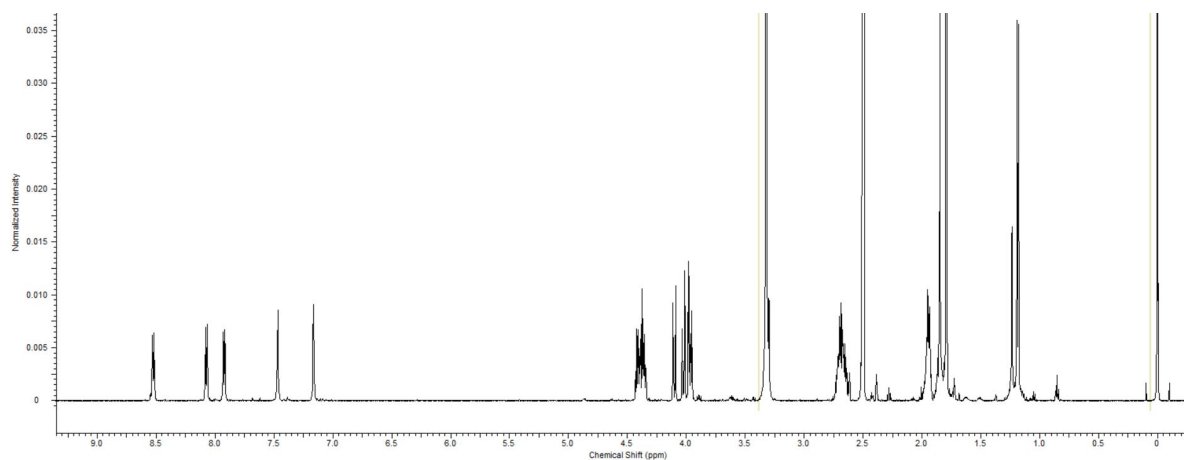
Figure S9: 600 MHz spectrum of **12d** in d_6-DMSO.
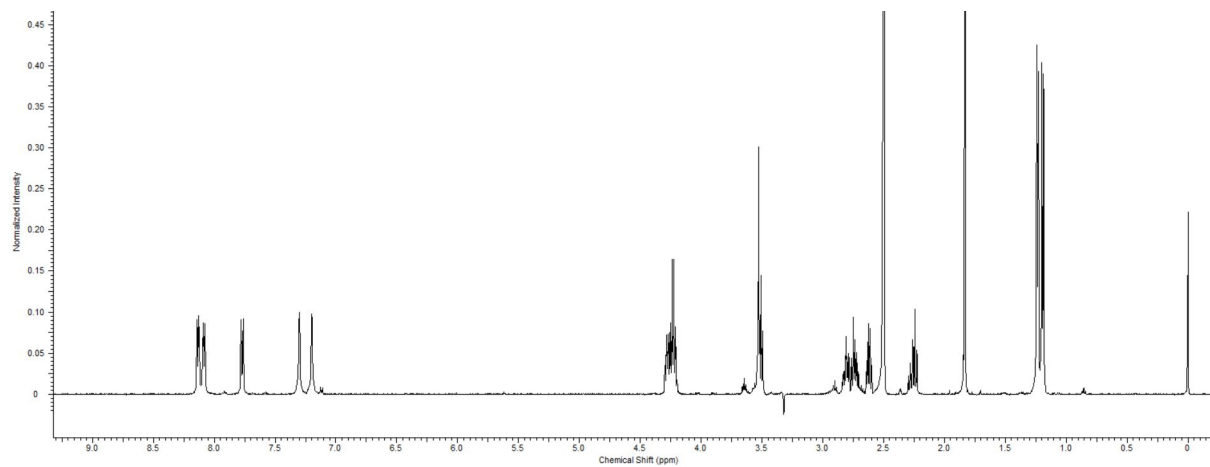
Figure S10: 500 MHz spectrum of **13** in d$_6$-DMSO.
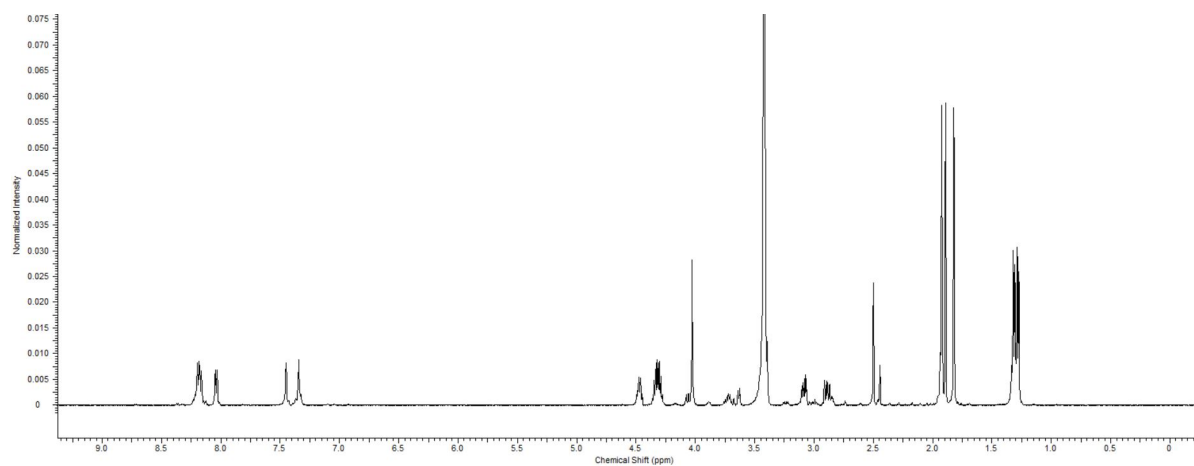
Figure S11: 500 MHz spectrum of **13m** in d$_6$-DMSO.
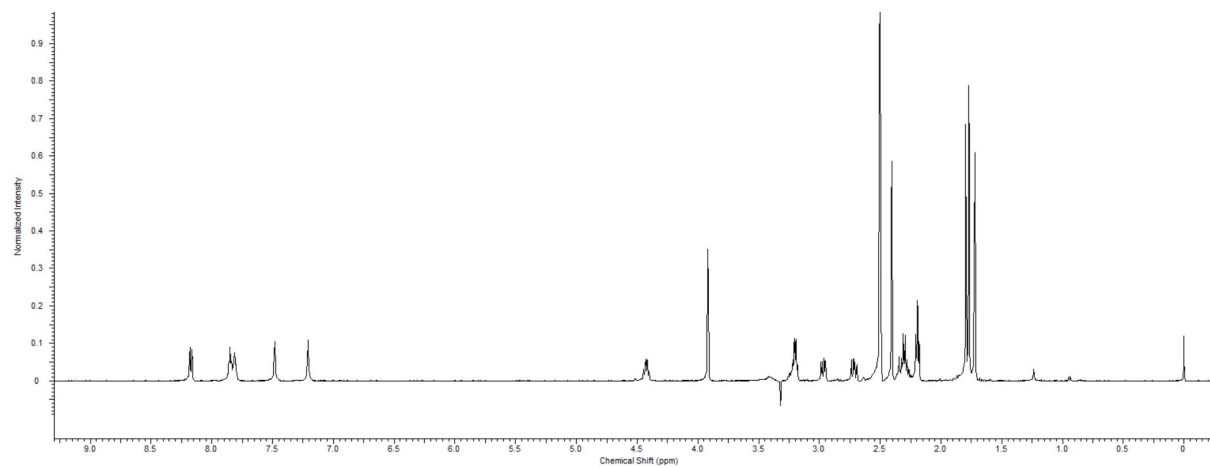
Figure S12: 500 MHz spectrum of **14m** in d$_6$-DMSO.
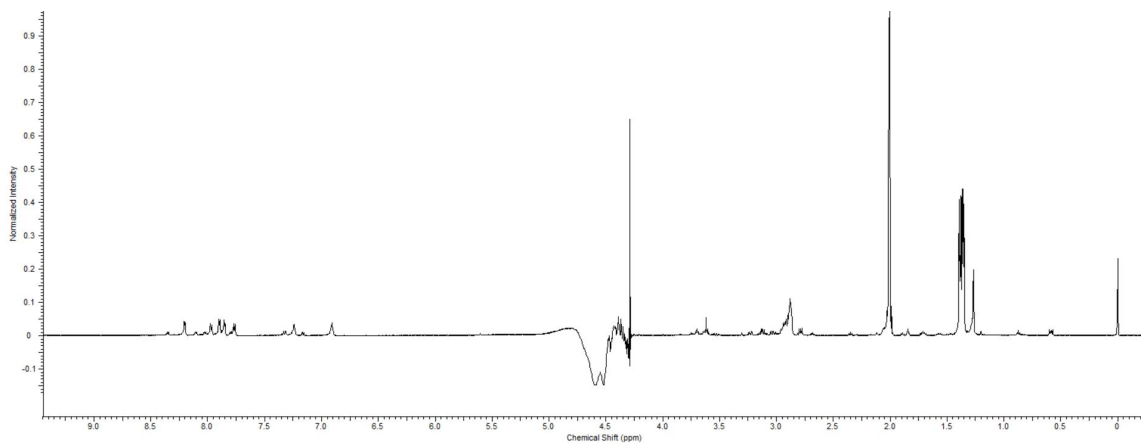
Figure S13: 600 MHz spectrum of **15** in 50% CD₃CN and 10% D₂O in water.
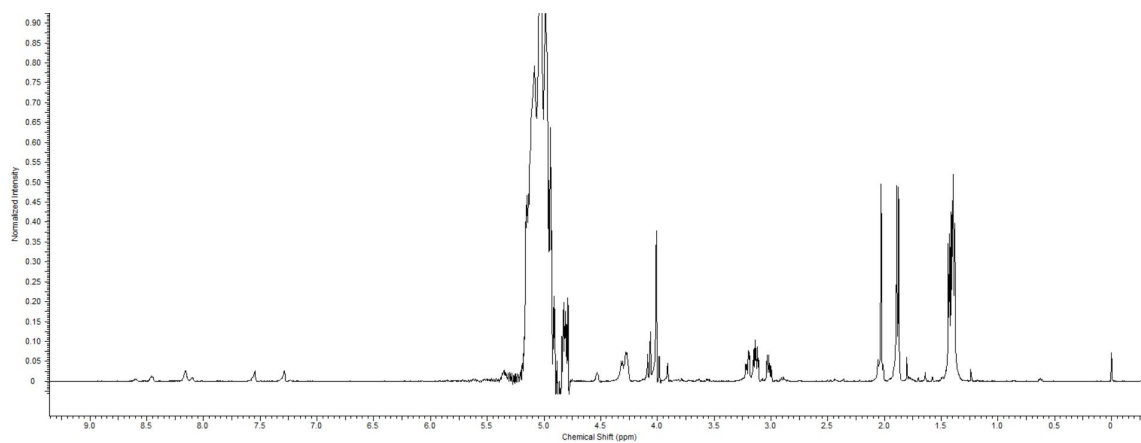
Figure S14: 600 MHz spectrum of **15d** in 10% D₂O in water.
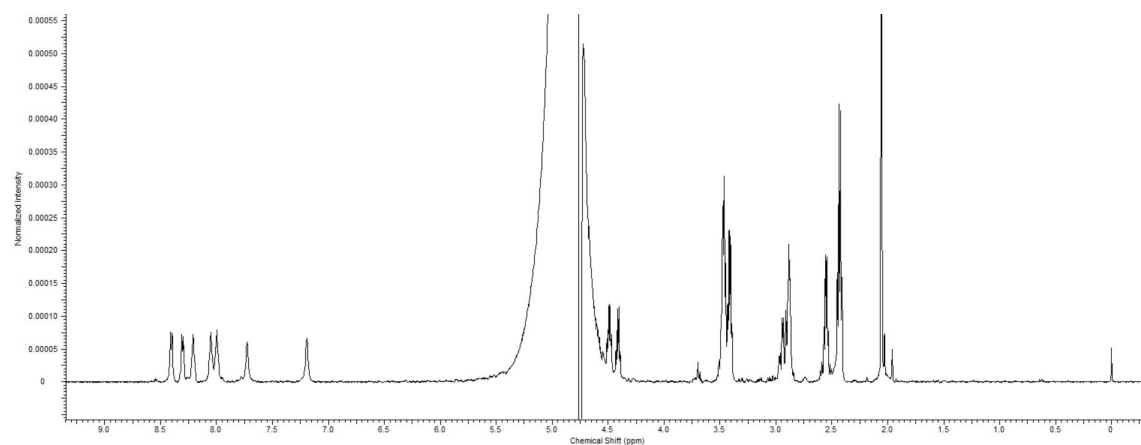
Figure S15: 500 MHz spectrum of **16** in 10% D₂O in water.
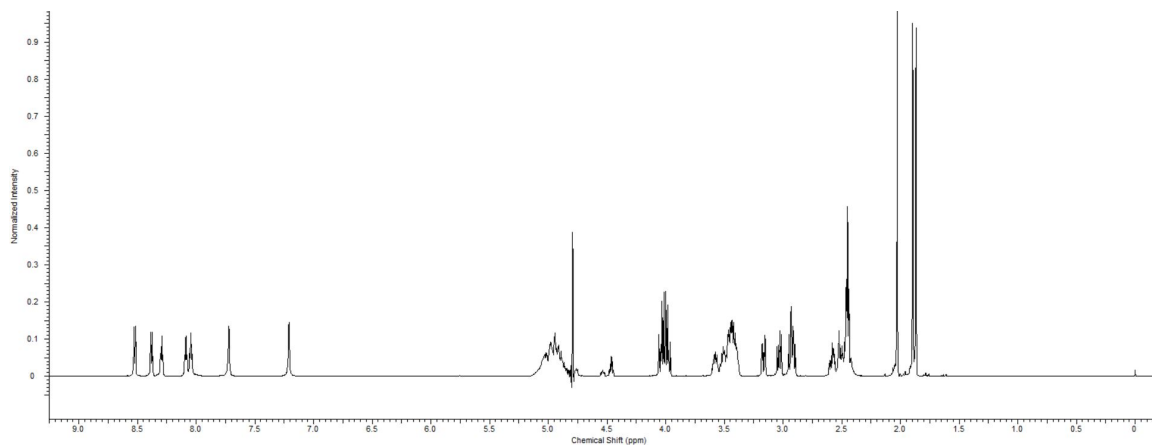
Figure S16: 600 MHz spectrum of **16d** in 10% D$_2$O in water.
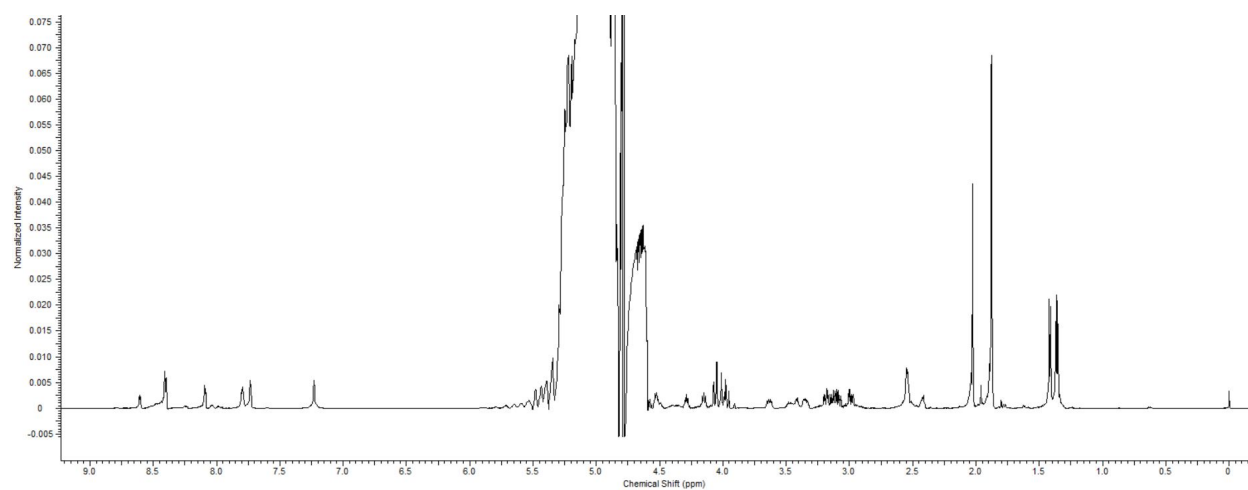
Figure S17: 600 MHz spectrum of **17d** in 10% D$_2$O in water.
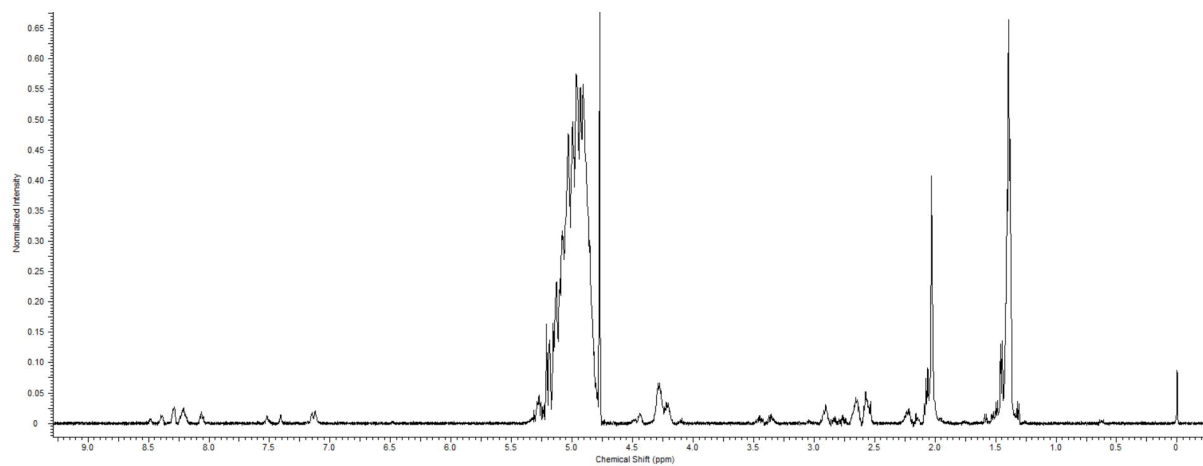
Figure S18: 500 MHz spectrum of **18** in 10% D$_2$O in water.
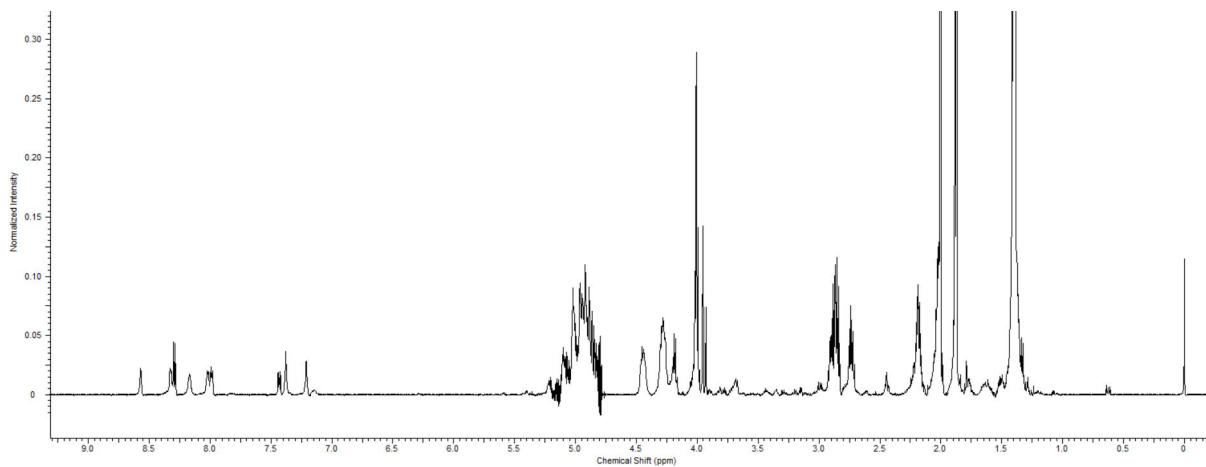
Figure S19: 600 MHz spectrum of **18d** in 10% D$_2$O in water.
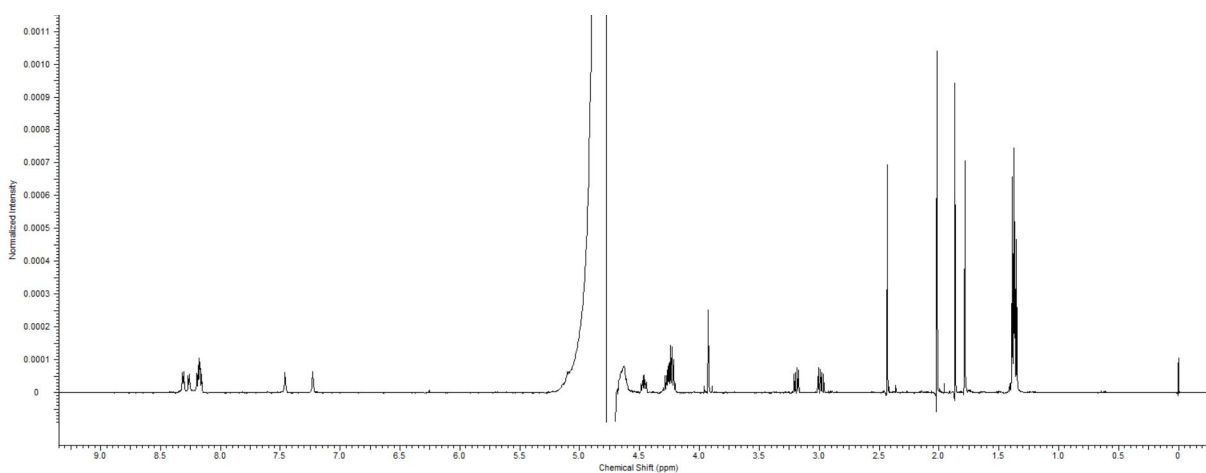
Figure S20: 500 MHz spectrum of **19m** in 10% D$_2$O in water.
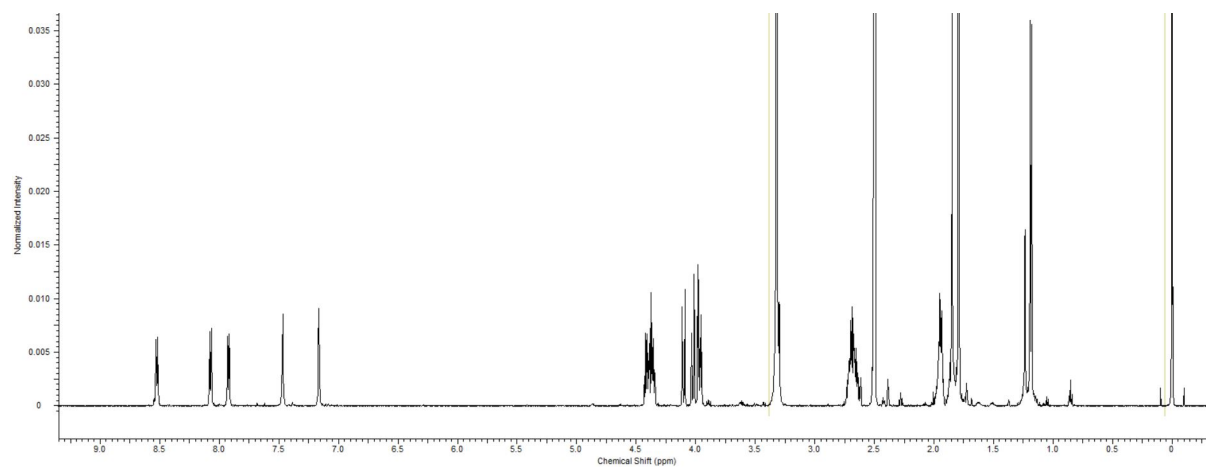
Figure S21: 500 MHz spectrum of **20** in 10% D$_2$O in water.
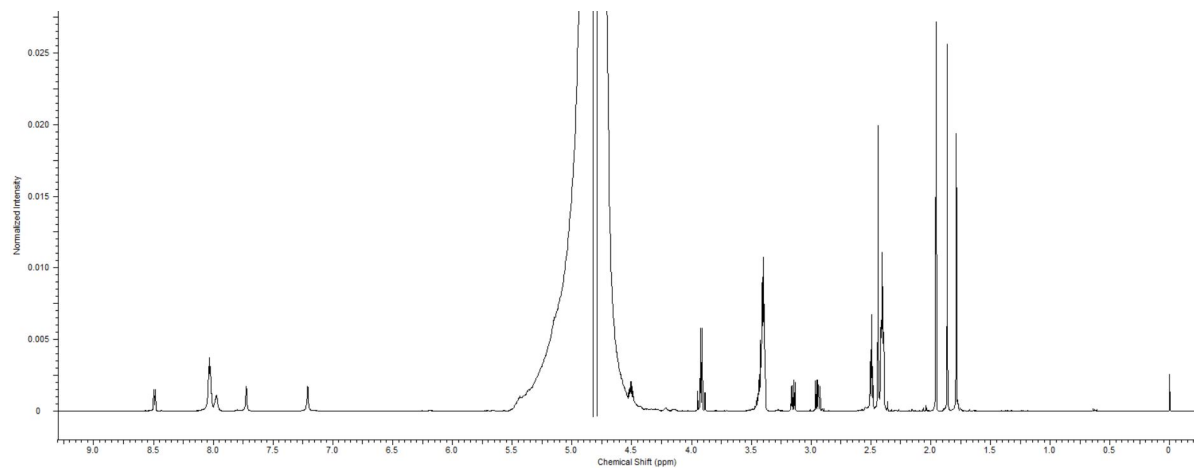
Figure S22: 600 MHz spectrum of **20m** in 10% D_2O in water.
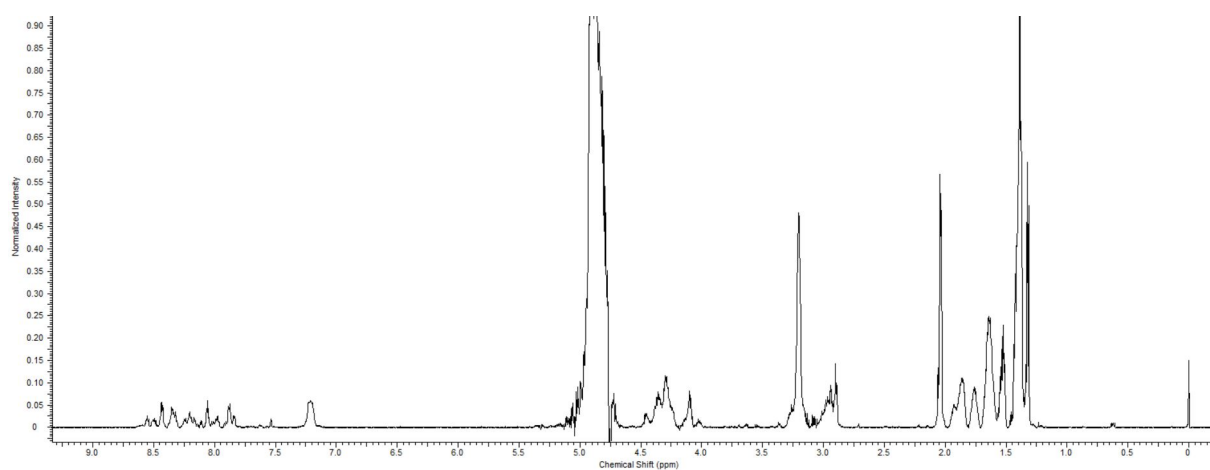
Figure S23: 600 MHz spectrum of **21** in 10% D_2O in water.
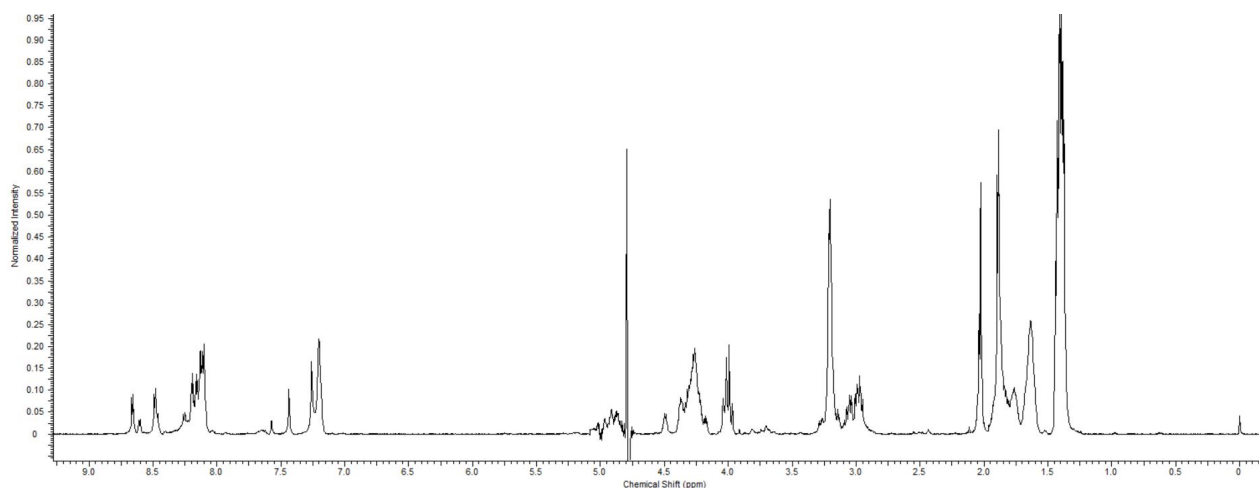
Figure S24: 600 MHz spectrum of **21d** in 10% D_2O in water.
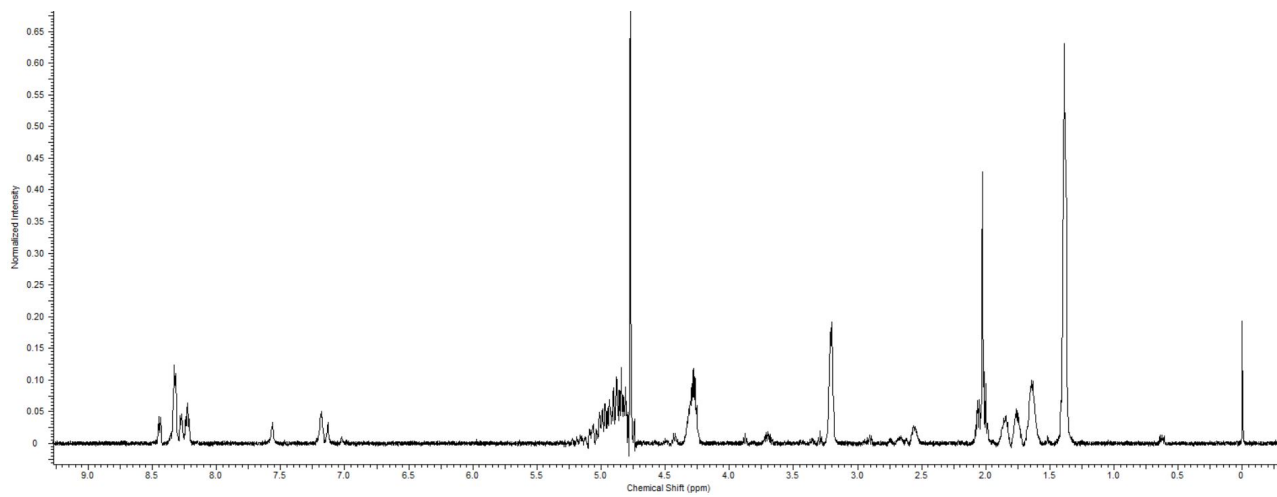
Figure S25: 500 MHz spectrum of **22** in 10% D$_2$O in water.
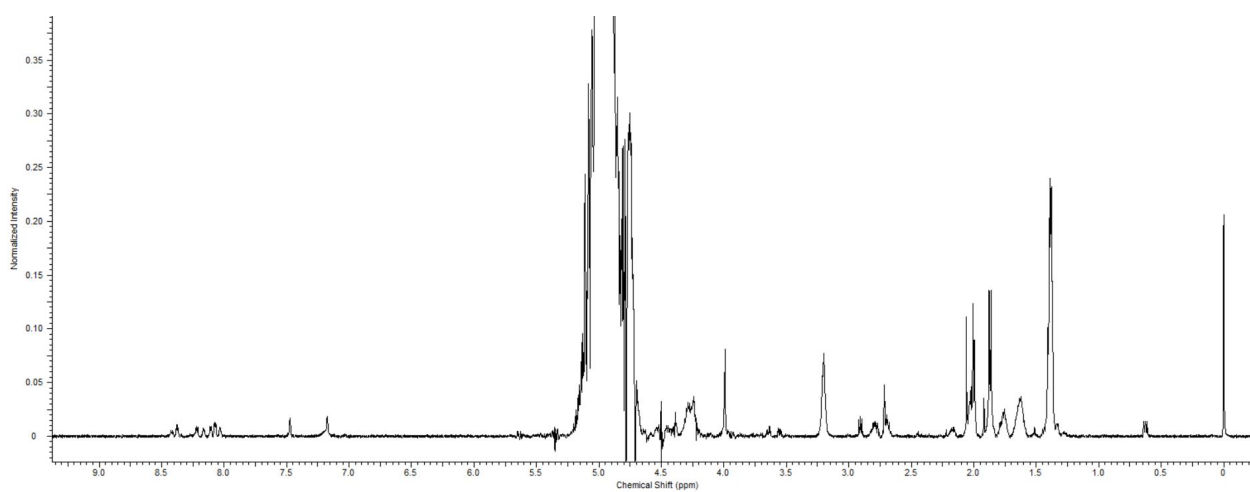
Figure S26: 600 MHz spectrum of **22d** in 10% D$_2$O in water.
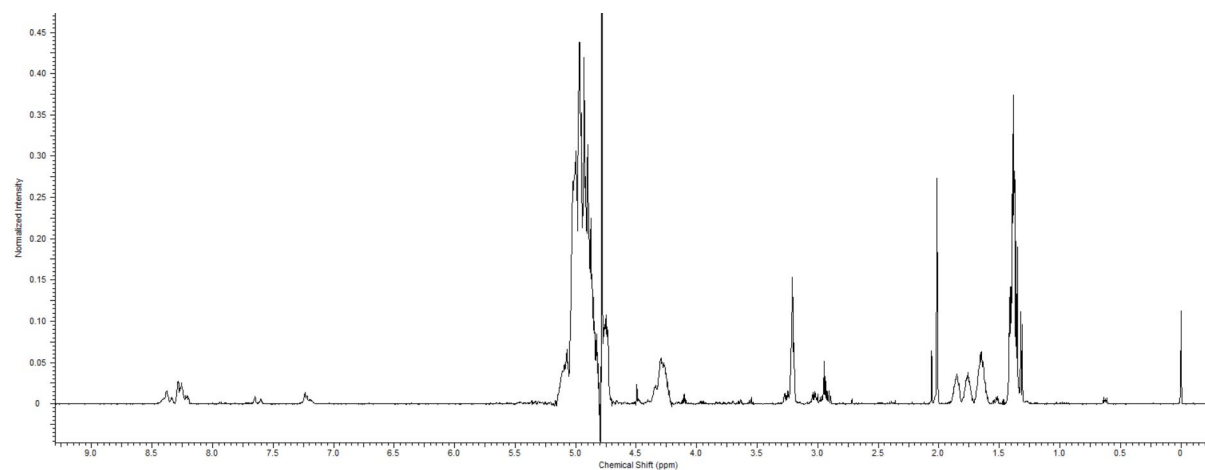
Figure S27: 600 MHz spectrum of **23** in 10% D$_2$O in water.
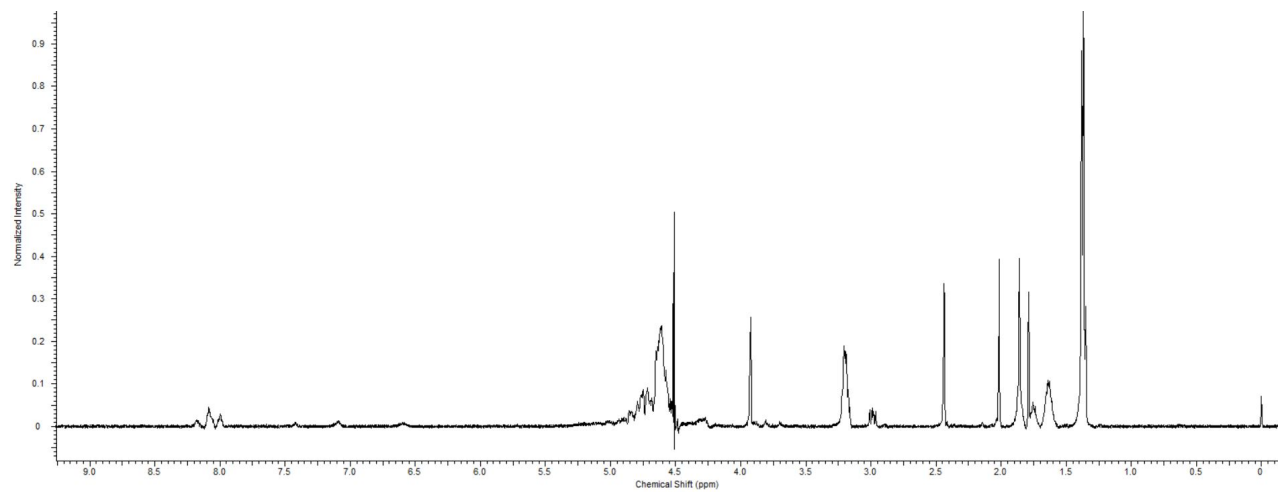
Figure S28: 500 MHz spectrum of **23m** in 10% D$_2$O in water.
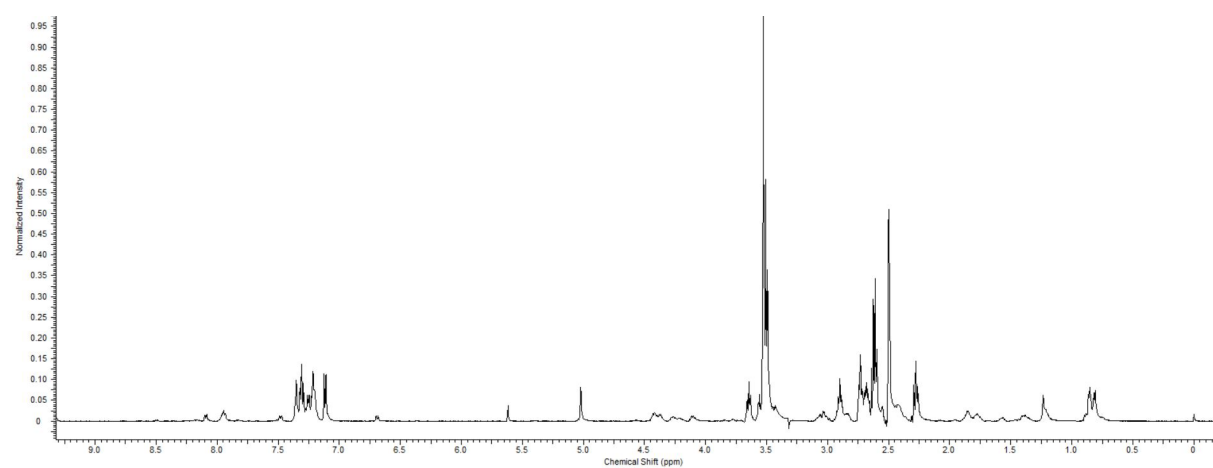
Figure S29: 500 MHz spectrum of **24** in d$_6$-DMSO.
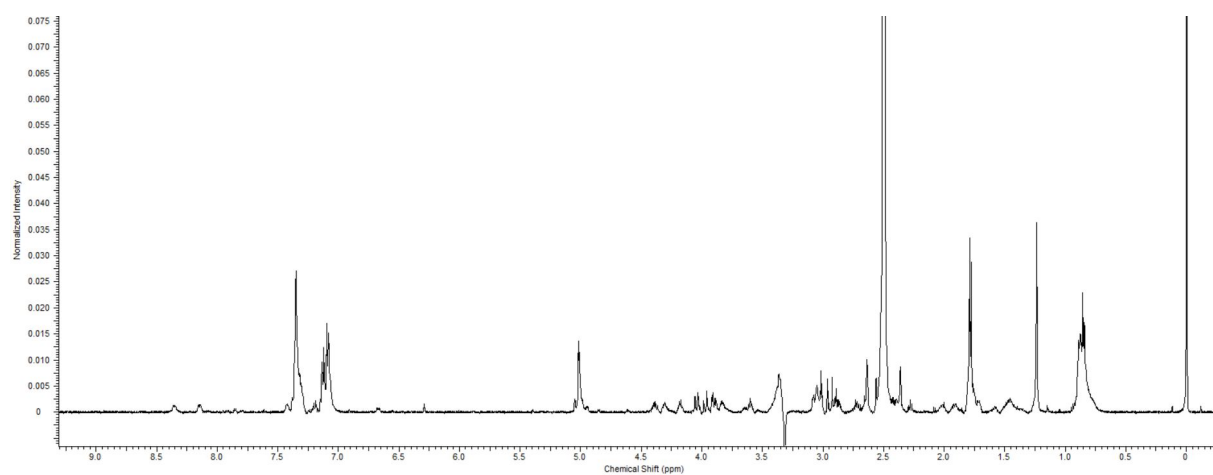
Figure S30: 500 MHz spectrum of **24d** in d$_6$-DMSO.
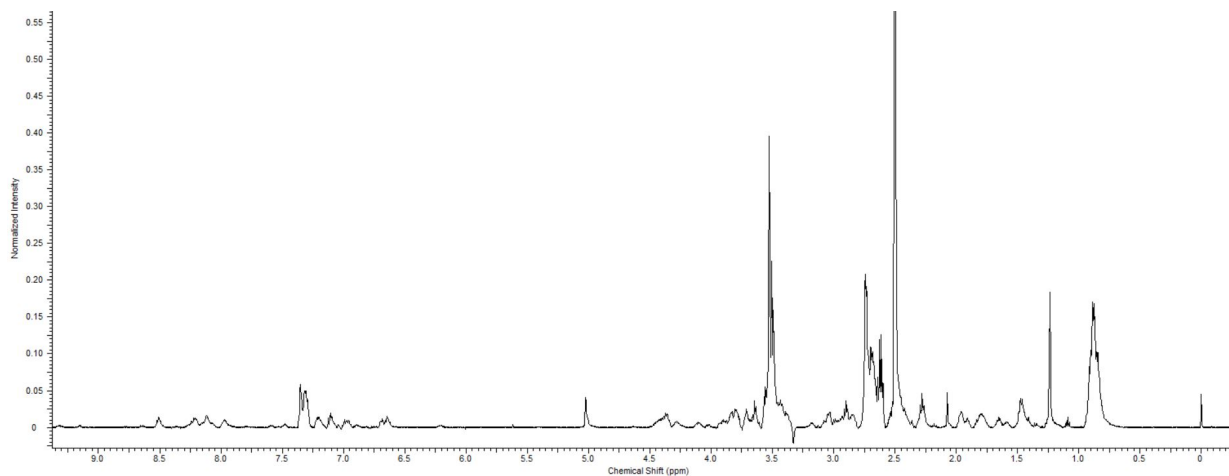
Figure S31: 500 MHz spectrum of **25** in d.₆-DMSO
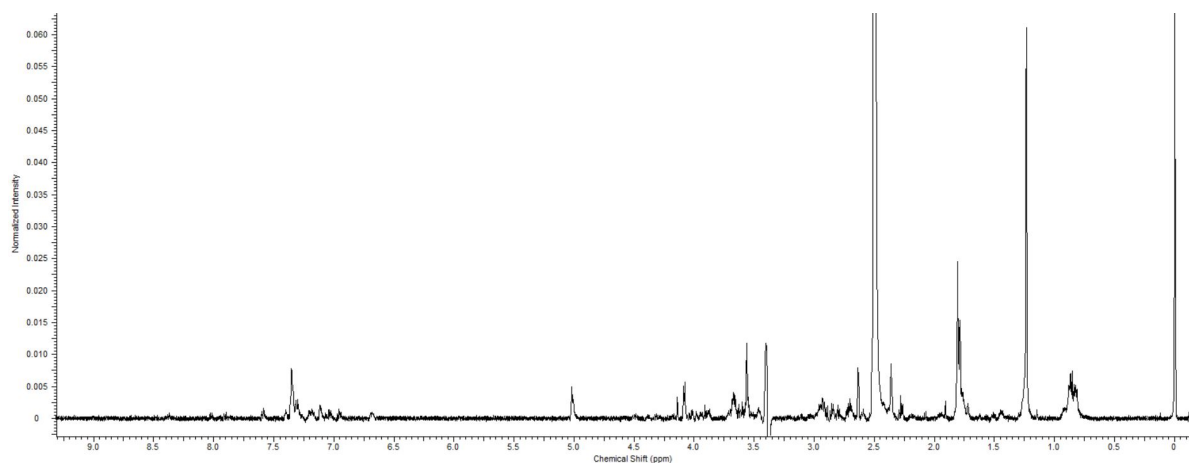
Figure S32: 500 MHz spectrum of **25d** in d₆-DMSO.
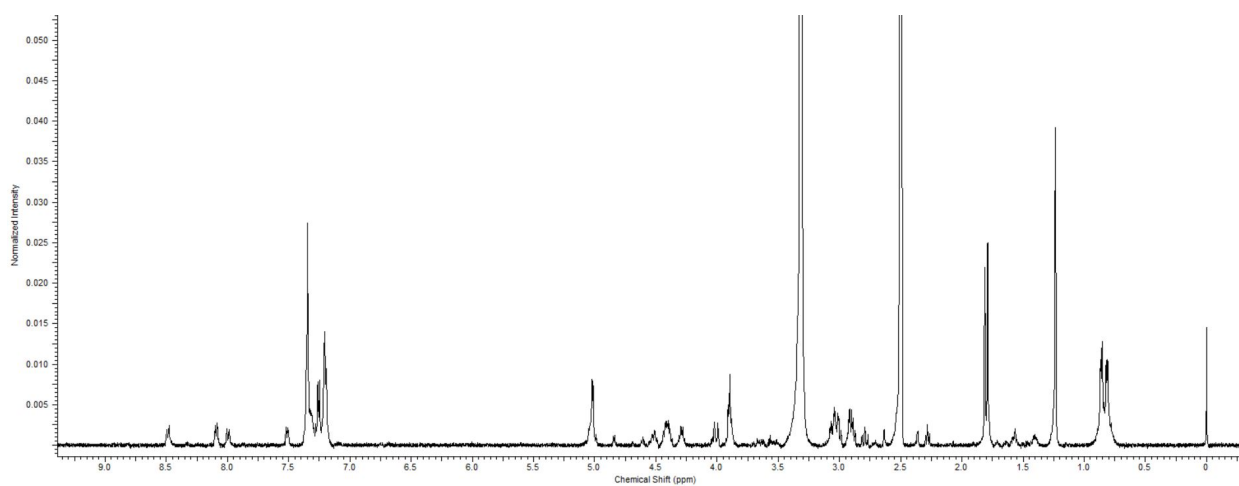
Figure S33: 500 MHz spectrum of **29d** in d₆-DMSO.
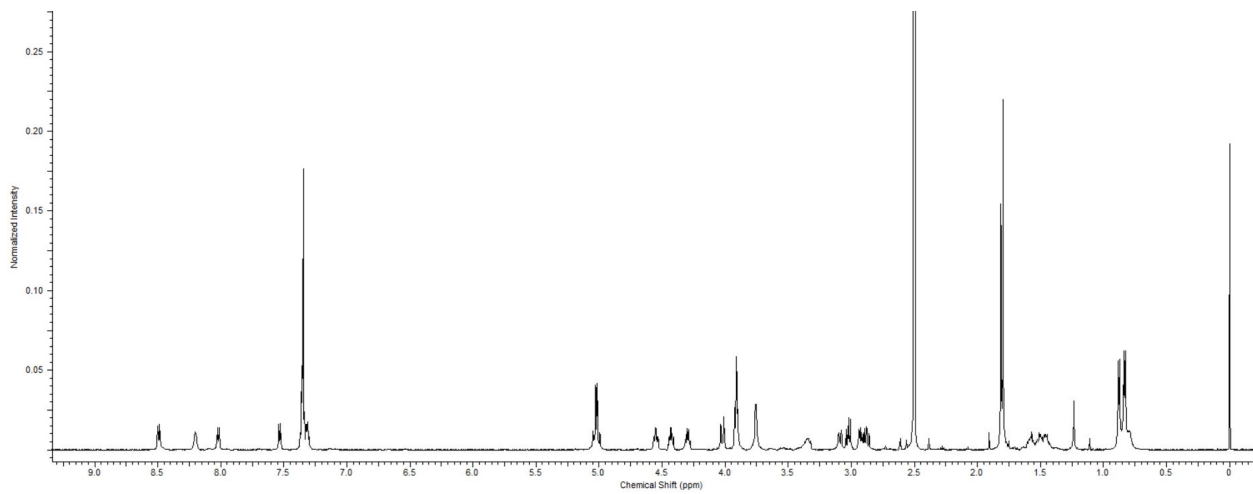
Figure S34: 600 MHz spectrum of **30d** in d$_6$-DMSO.

2D NMR Spectra

Figure S35: zTOCSY 500MHz in 10% aq. D$_2$O pf **11d**
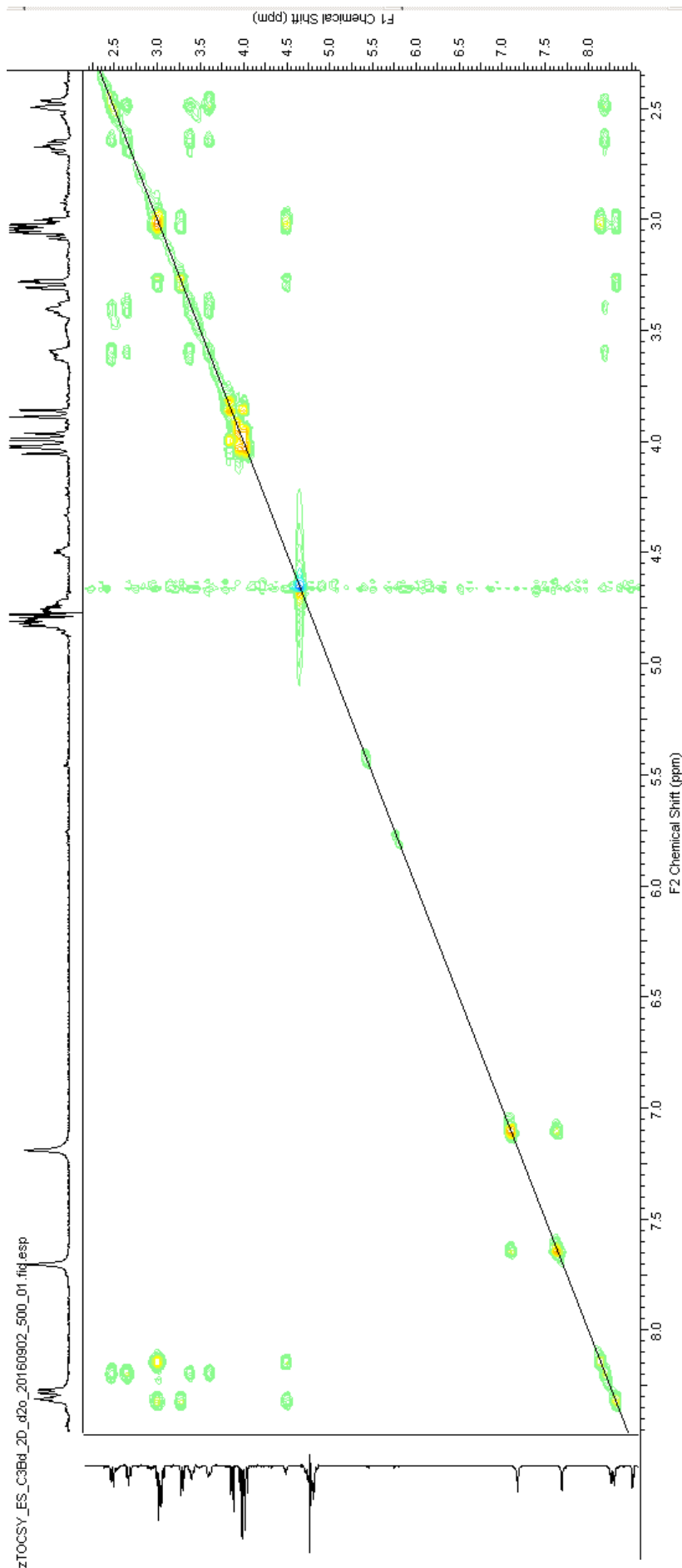
Figure S 36: zTOCSY 500MHz in d$_6$-DMSO of **11d**.

zTOCSY_C3Bd_dmso_20160517_600_01.fid.esp
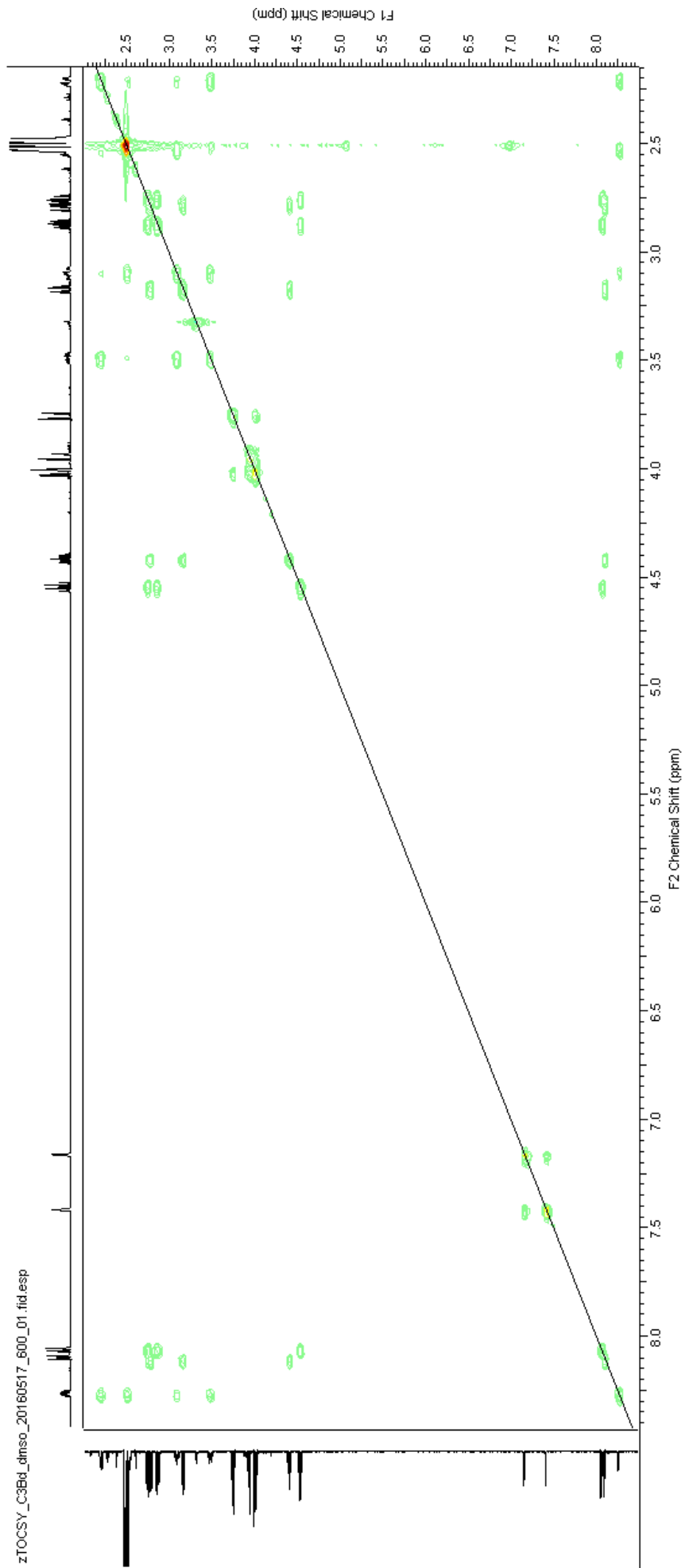
Figure S 37:ROESY 500MHz in d$_6$-DMSO of **11d.**

ROESYAD_C3Bd_dmso_2016050 _600_01.fid.esp
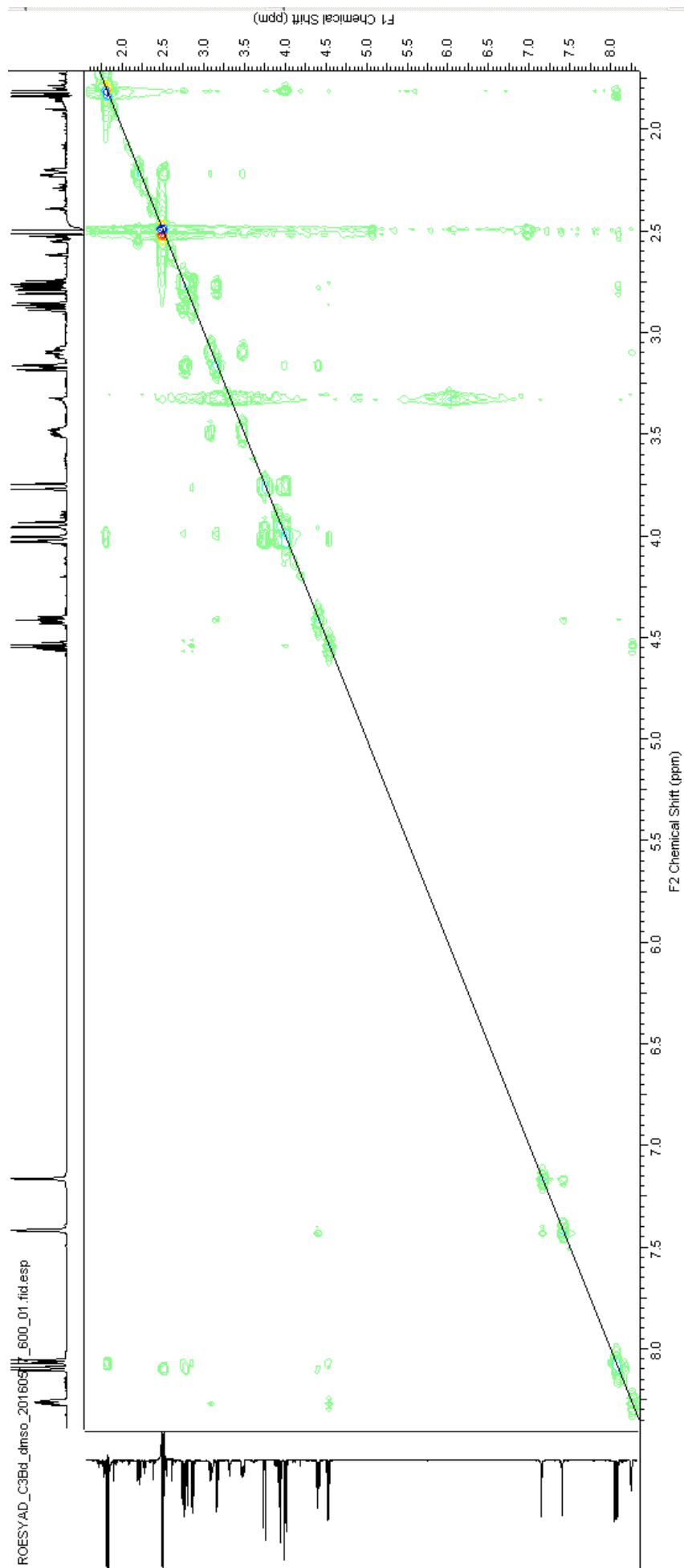
HPLC Spectra
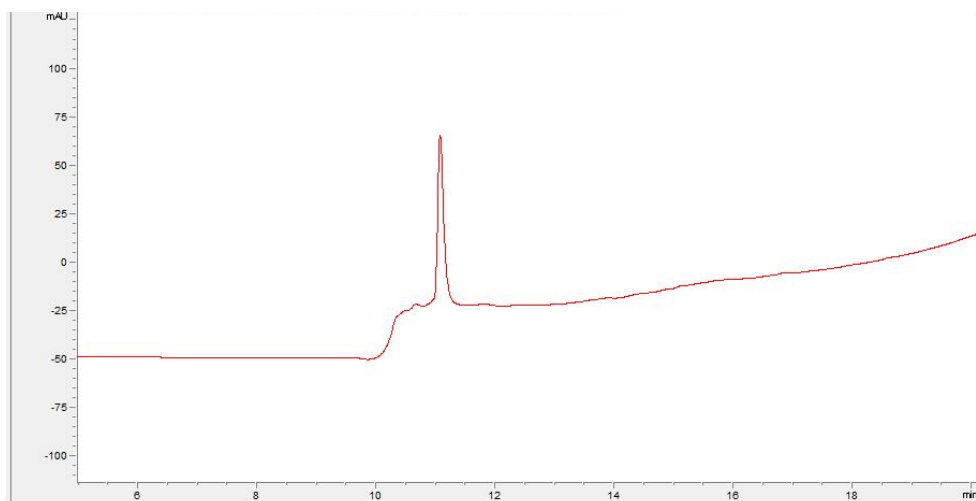
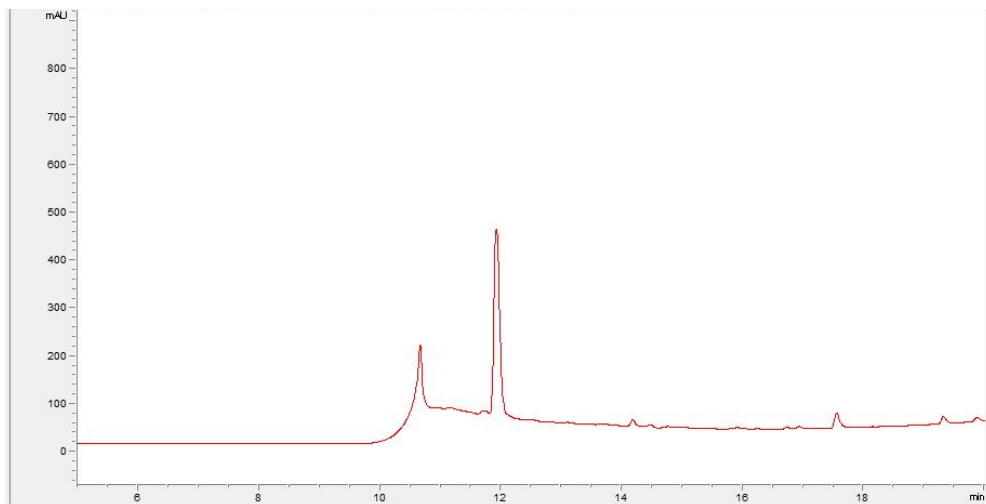**Figure S38:** Analytical RP-HPLC C18 spectrum for **9**, 0-100% over 15 minutes (from 5-20 min) visualised at 220 nm.
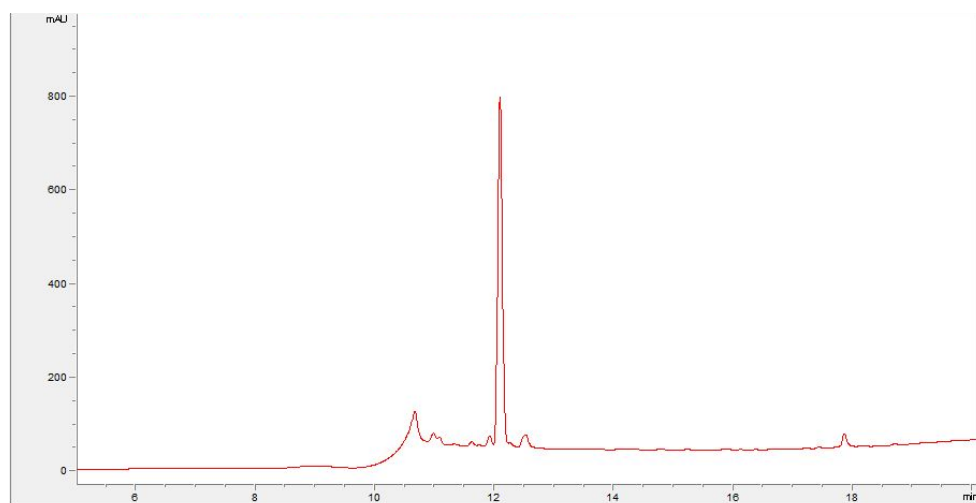
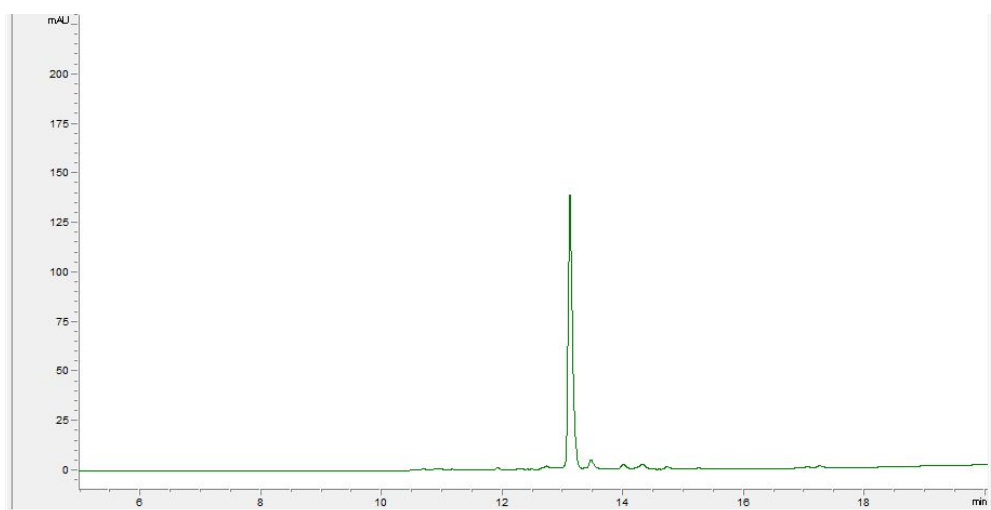**Figure S39:** Analytical RP-HPLC C18 spectrum for **10**, 0-100% over 15 minutes (from 5-20 min) visualised at 220 nm.
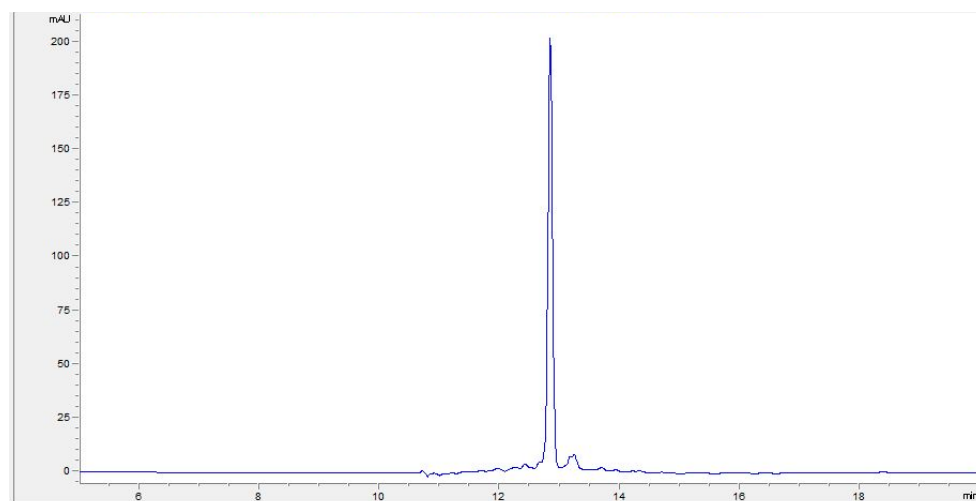
Figure S40: Analytical RP-HPLC C18 spectrum for **10d**, 0-100% over 15 minutes (from 5-20 min) visualised at 254 nm.
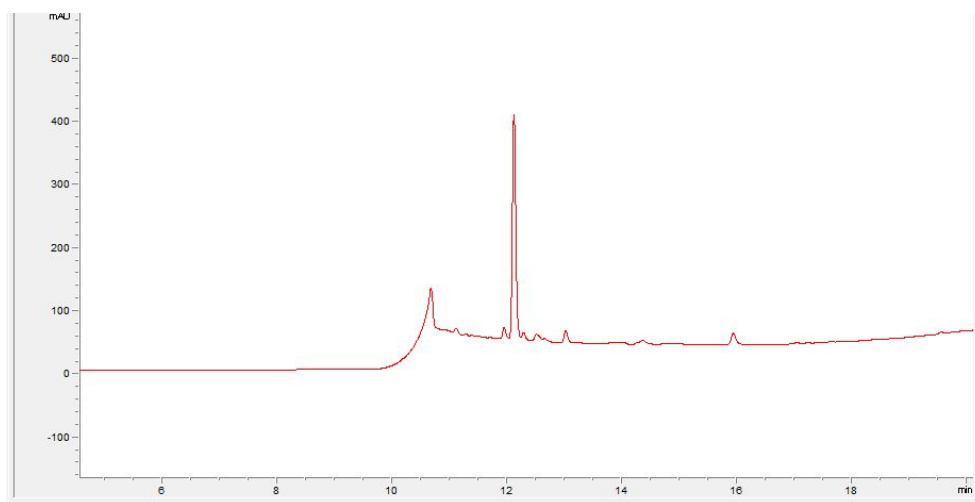
Figure S41: Analytical RP-HPLC C18 spectrum for 11, 0-100% over 15 minutes (from 5-20 min) visualised at 220 nm.
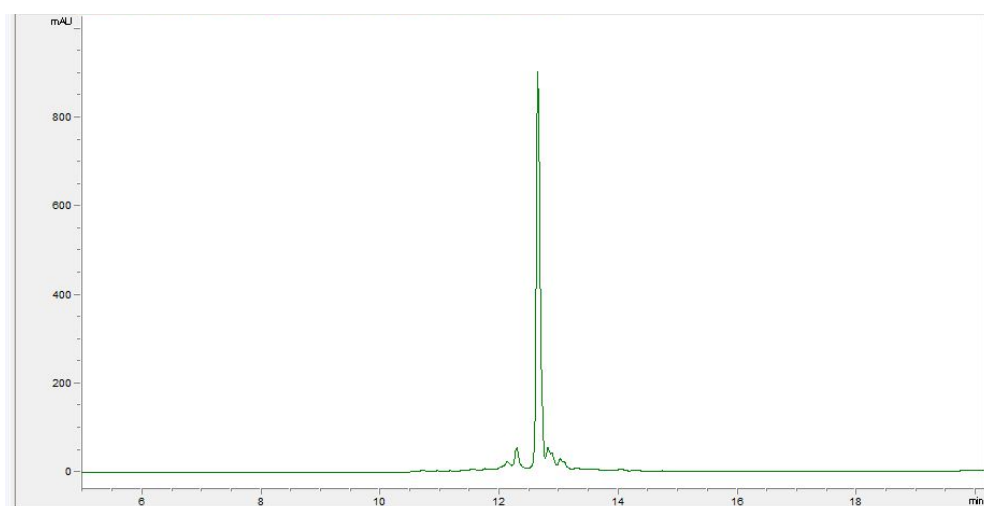
Figure S42: Analytical RP-HPLC C18 spectrum for **11d**, 0-100% over 15 minutes (from 5-20 min) visualised at 254 nm.
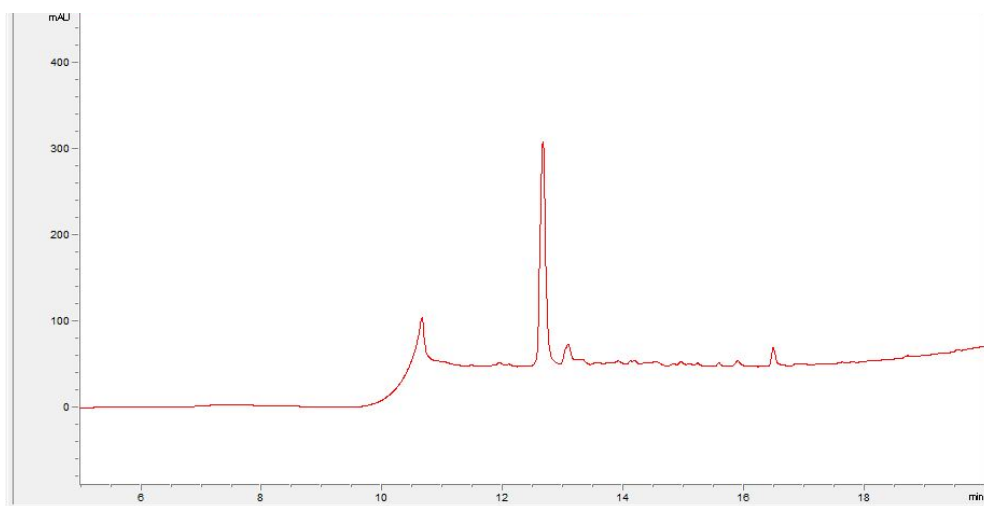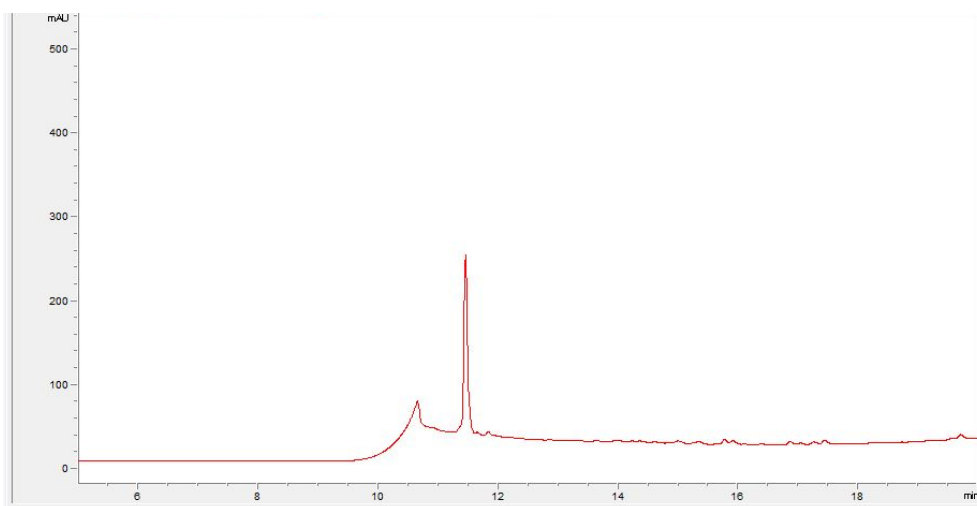

Figure S43: Analytical RP-HPLC C18 spectrum for **12**, 0-100% over 15 minutes (from 5-20 min) visualised at 220 nm.
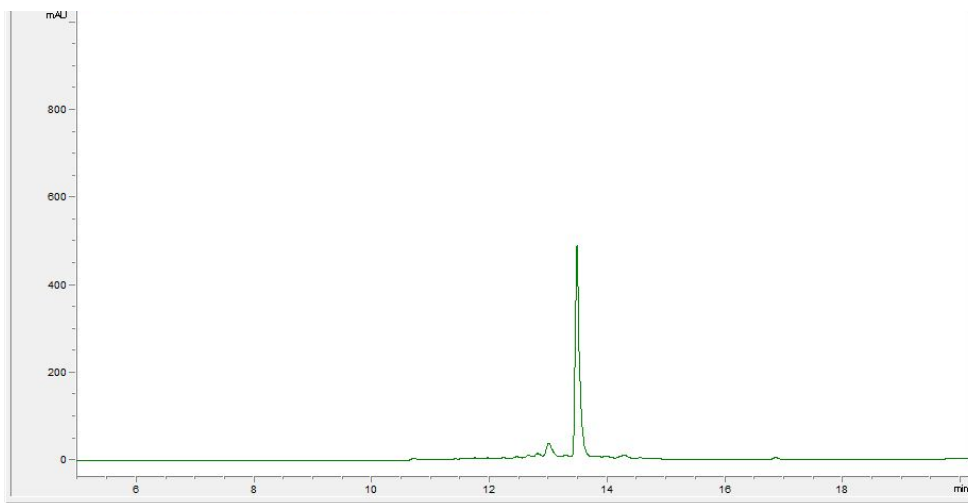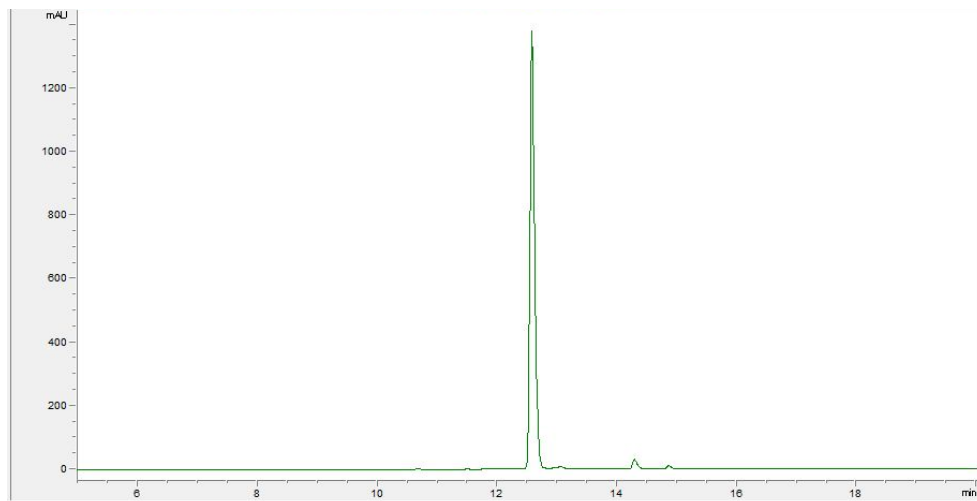
Figure S44: Analytical RP-HPLC C18 spectrum for **12d**, 0-100% over 15 minutes (from 5-20 min) visualised at 254 nm.
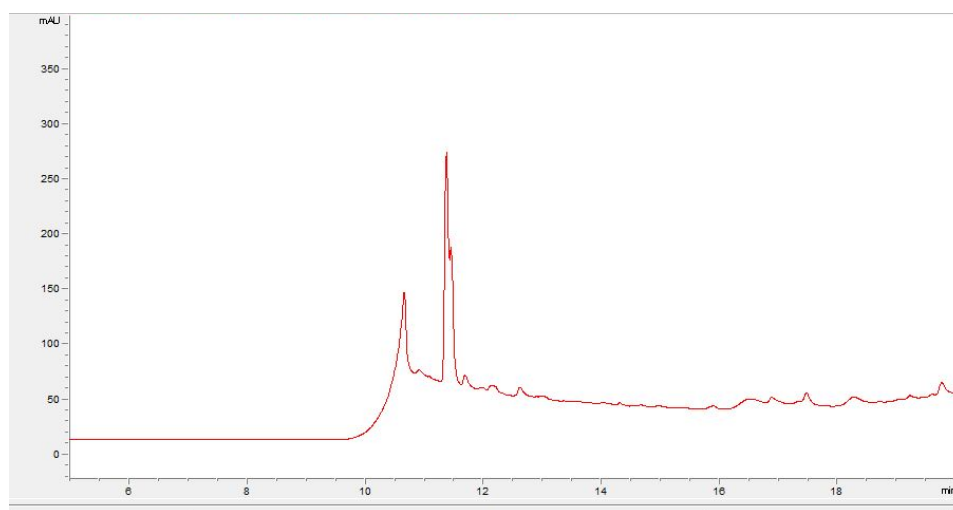
Figure S45: Analytical RP-HPLC C18 spectrum for **13**, 0-100% over 15 minutes (from 5-20 min) visualised at 220 nm.
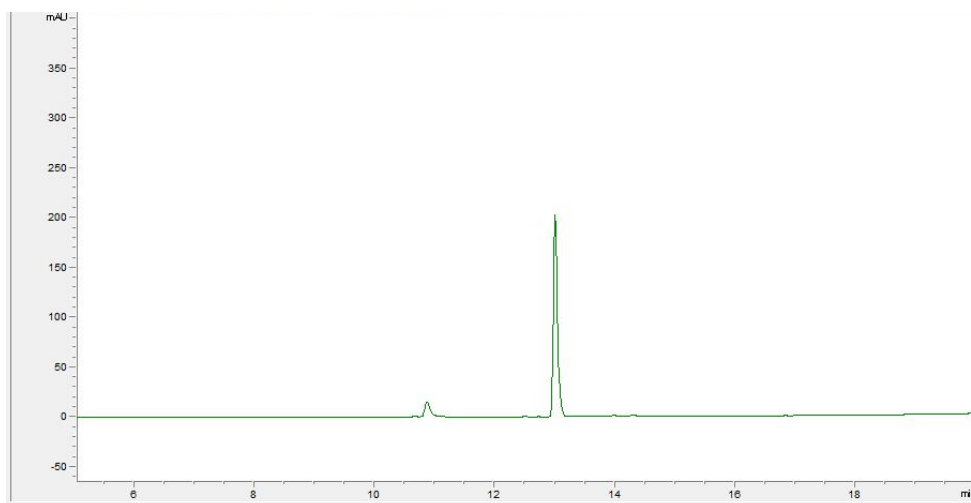
Figure S46: Analytical RP-HPLC C18 spectrum for **13m**, 0-100% over 15 minutes (from 5-20 min) visualised at 254 nm.
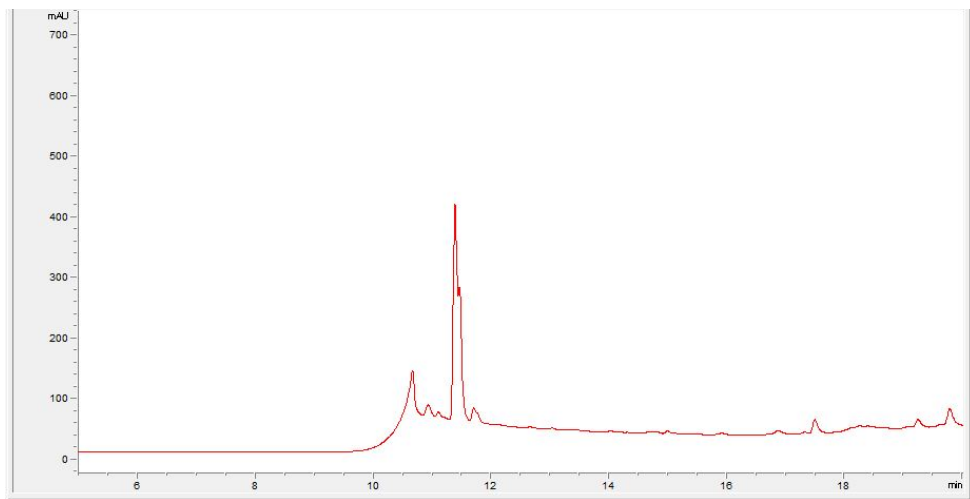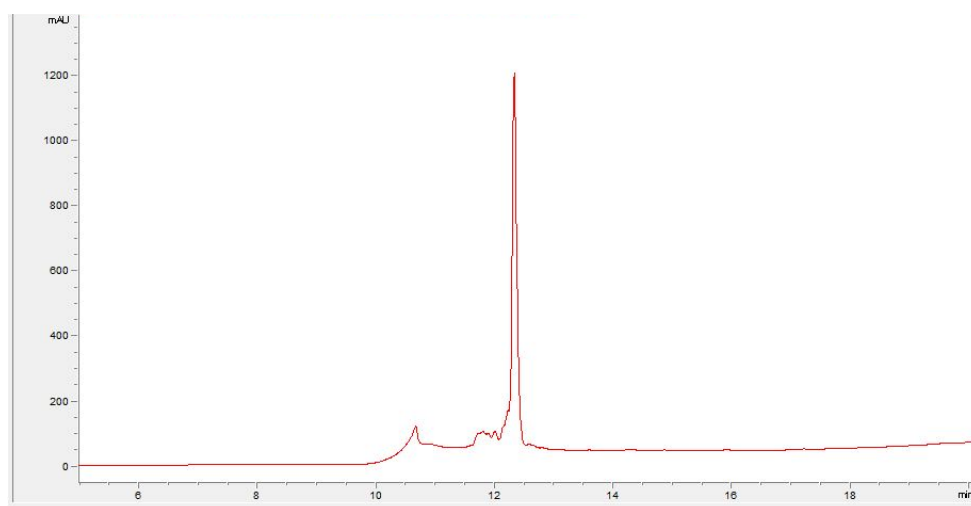
Figure S47: Analytical RP-HPLC C18 spectrum for **14**, 0-100% over 15 minutes (from 5-20 min) visualised at 220 nm.
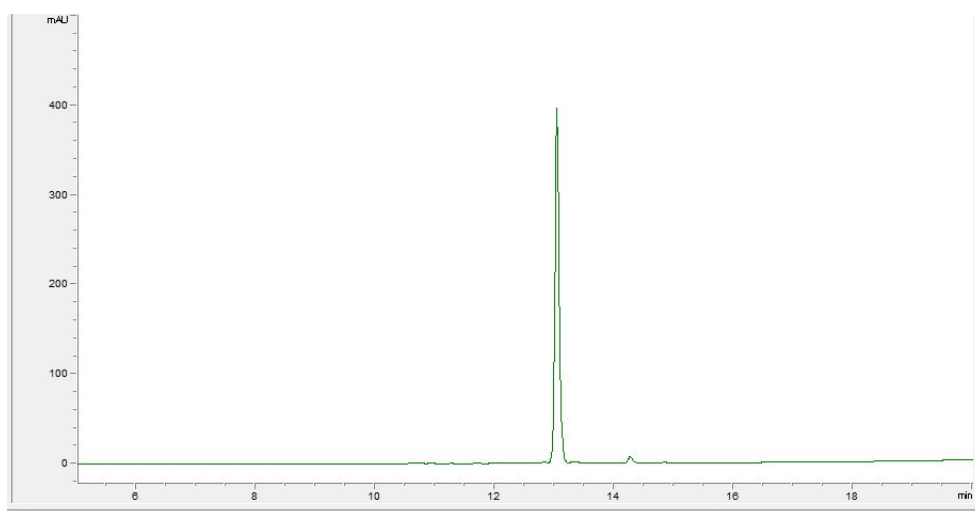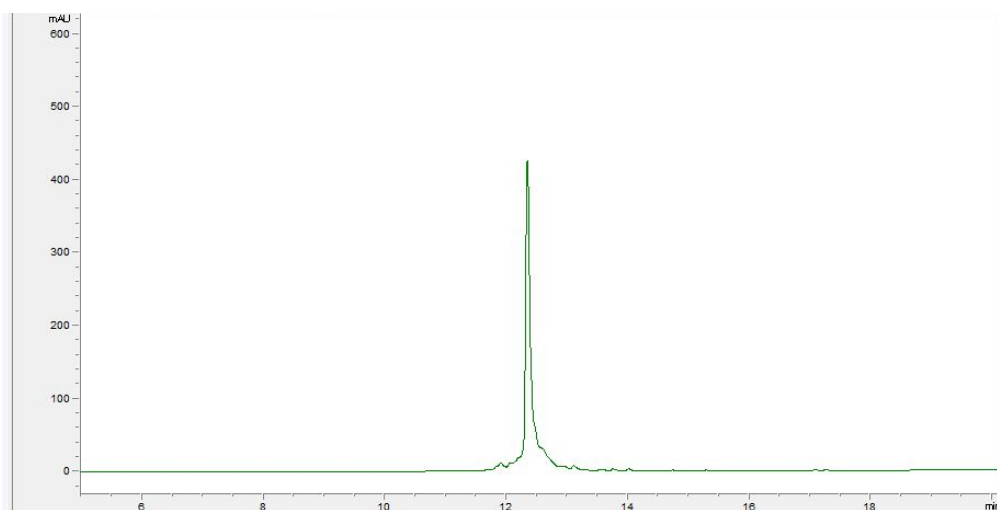

Figure S48: Analytical RP-HPLC C18 spectrum for **14m**, 0-100% over 15 minutes (from 5-20 min) visualised at 254 nm.
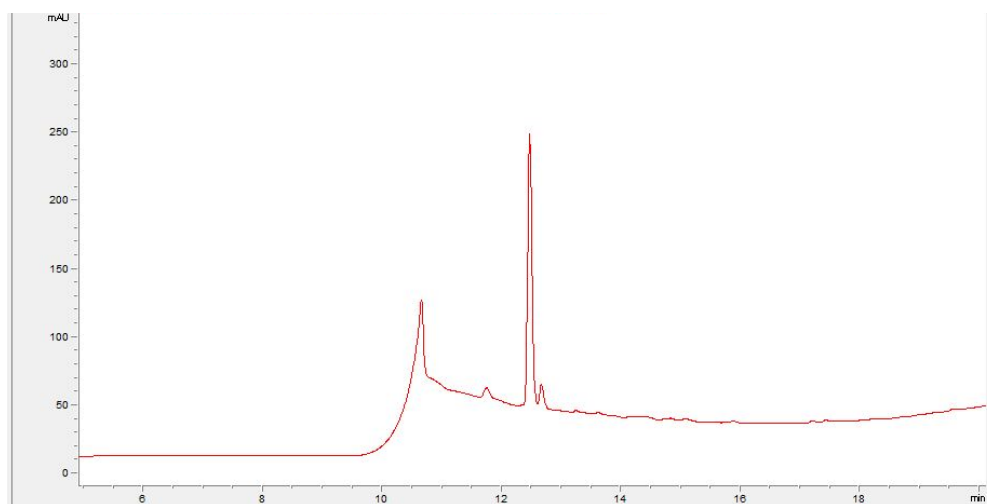
Figure S49: Analytical RP-HPLC C18 spectrum for **15**, 0-100% over 15 minutes (from 5-20 min) visualised at 220 nm.
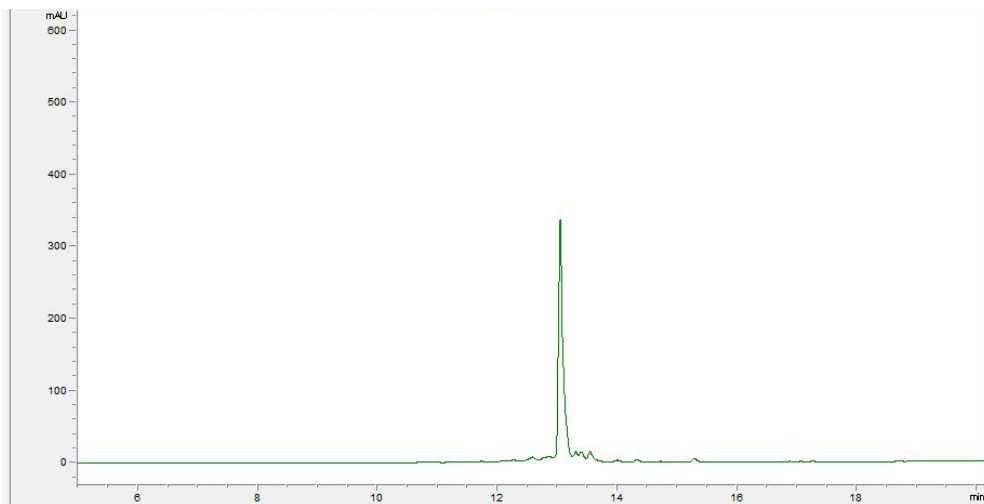
Figure S50: Analytical RP-HPLC C18 spectrum for **9**, 0-100% over 15 minutes (from 5-20 min) visualised at 254 nm.
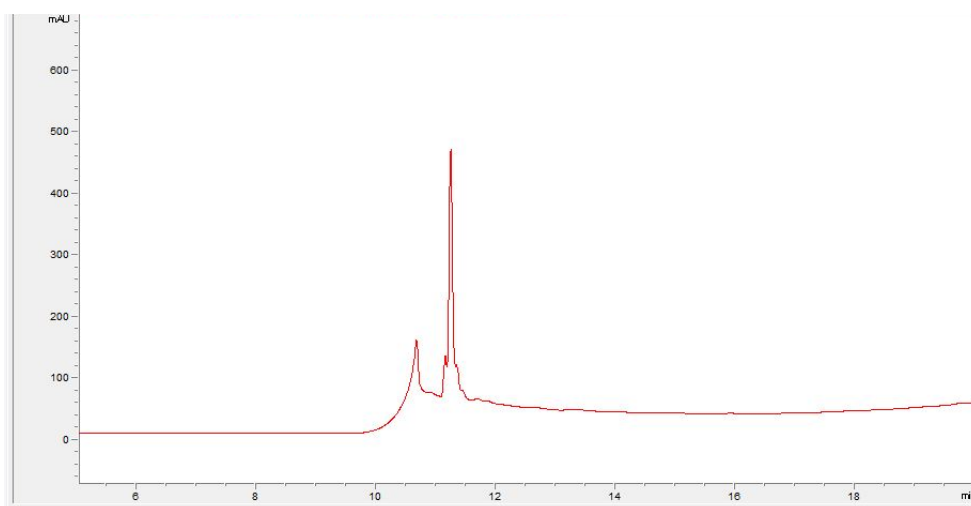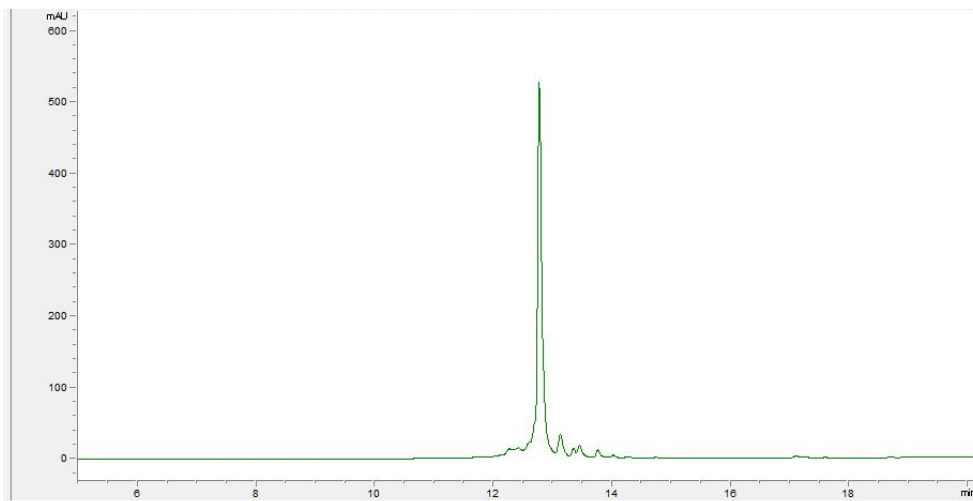

Figure S51: Analytical RP-HPLC C18 spectrum for **16**, 0-100% over 15 minutes (from 5-20 min) visualised at 220 nm.
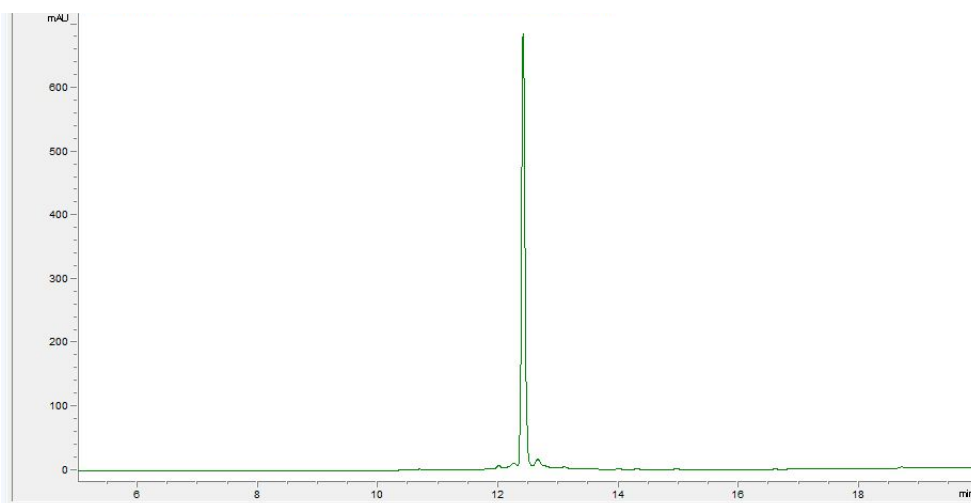
Figure S52: Analytical RP-HPLC C18 spectrum for **16d**, 0-100% over 15 minutes (from 5-20 min) visualised at 254 nm.
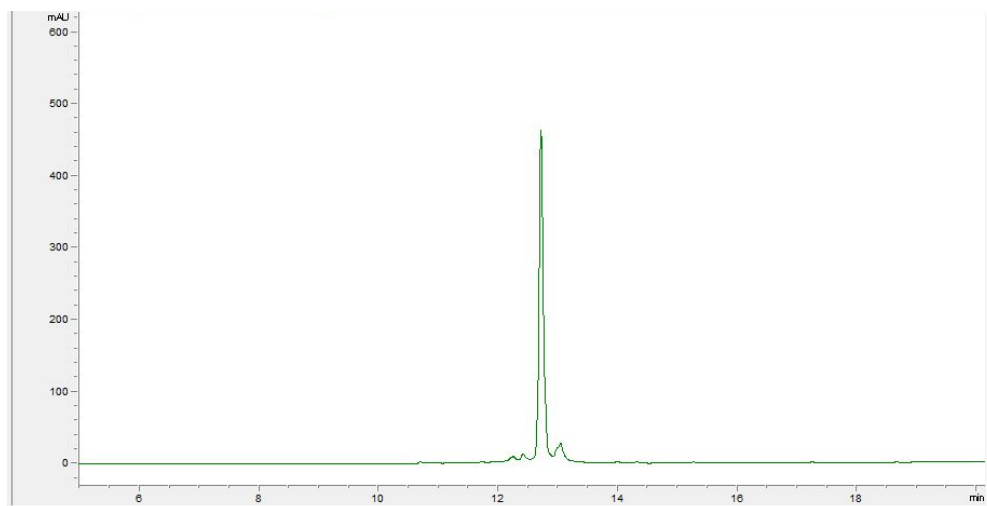
Figure S53: Analytical RP-HPLC C18 spectrum for 17d, 0-100% over 15 minutes (from 5-20 min) visualised at 254 nm.
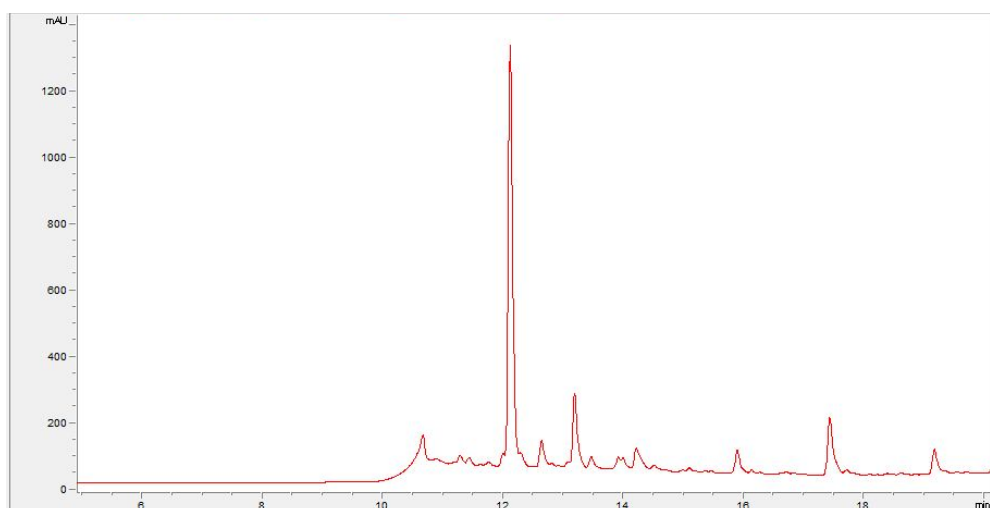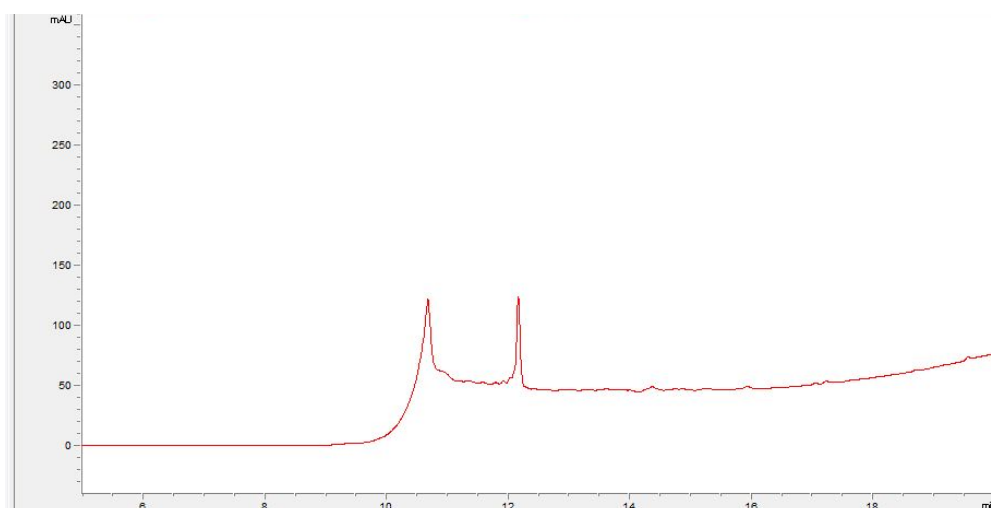

Figure S54: Analytical RP-HPLC C18 spectrum for **18**, 0-100% over 15 minutes (from 5-20 min) visualised at 220 nm.
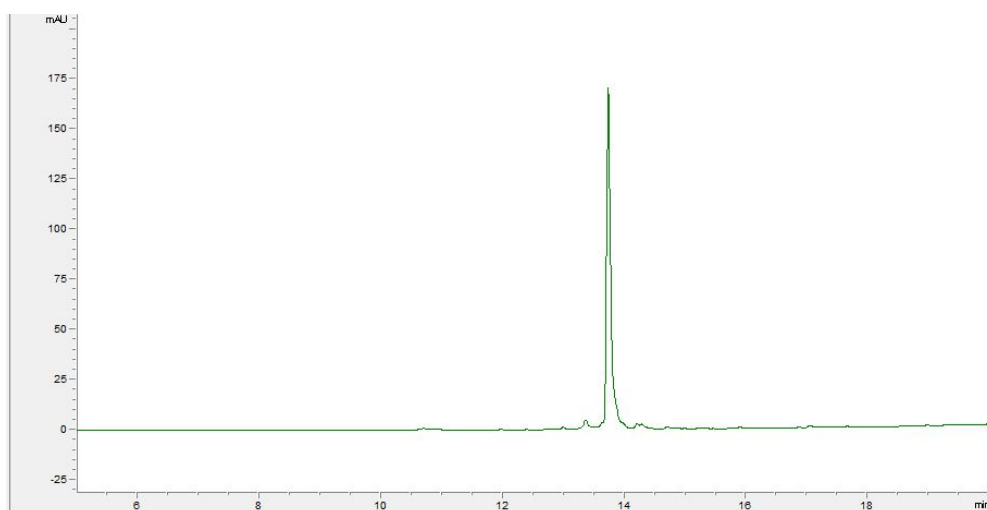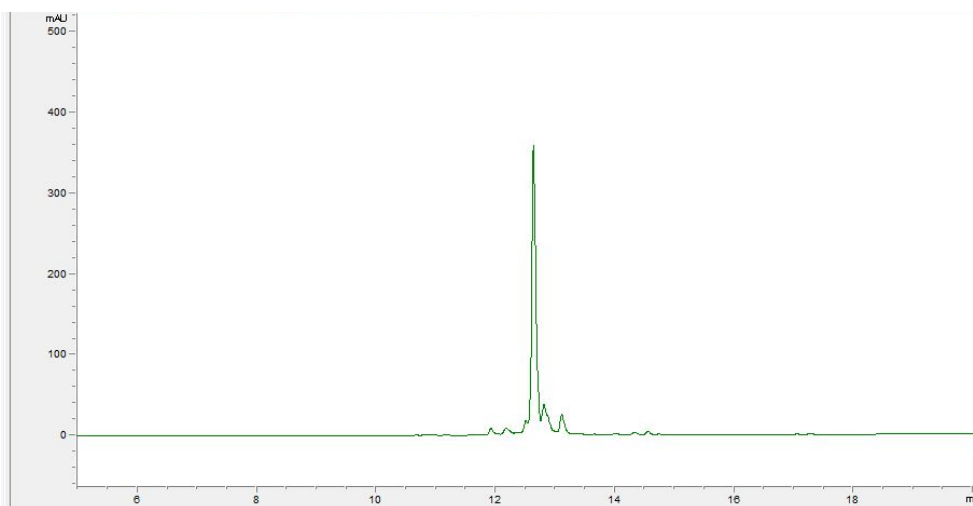

Figure S55: Analytical RP-HPLC C18 spectrum for **18d**, 0-100% over 15 minutes (from 5-20 min) visualised at 254 nm.

Figure S56: Analytical RP-HPLC C18 spectrum for **19**, 0-100% over 15 minutes (from 5-20 min) visualised at 220 nm.

Figure S57: Analytical RP-HPLC C18 spectrum for **19m**, 0-100% over 15 minutes (from 5-20 min) visualised at 254 nm.
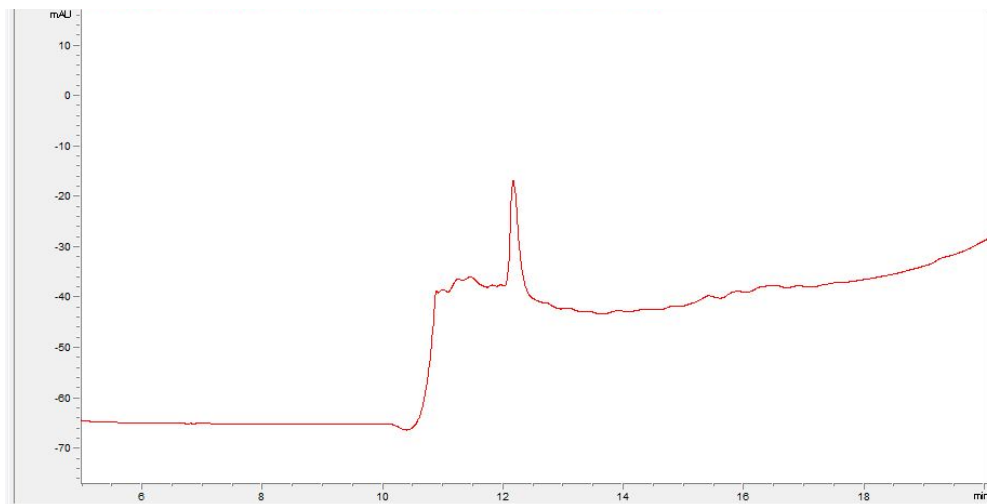

Figure S58: Analytical RP-HPLC C18 spectrum for **20**, 0-100% over 15 minutes (from 5-20 min) visualised at 220 nm.
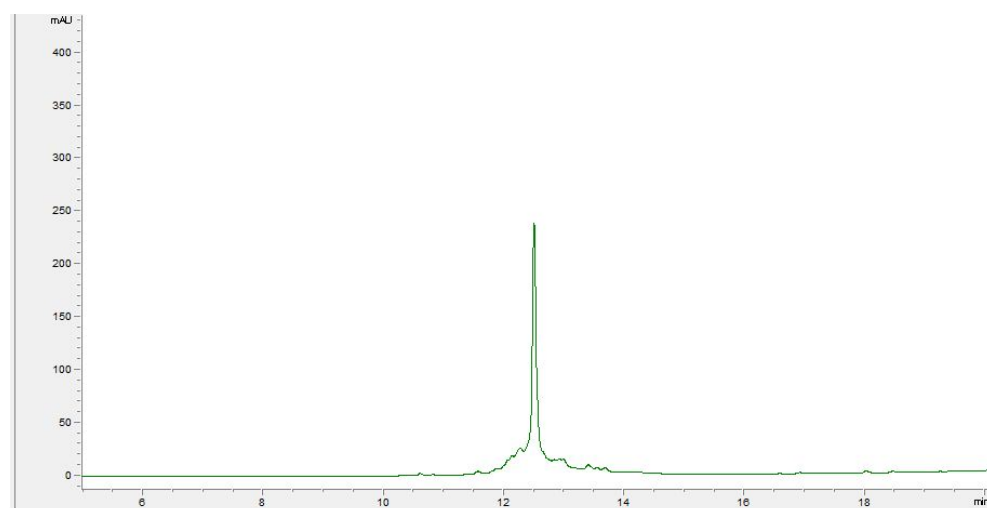
Figure S59: Analytical RP-HPLC C18 spectrum for **20m**, 0-100% over 15 minutes (from 5-20 min) visualised at 254 nm.

Figure S60: Analytical RP-HPLC C18 spectrum for **21**, 0-100% over 15 minutes (from 5-20 min) visualised at 220 nm.

Figure S61: Analytical RP-HPLC C18 spectrum for **21d**, 0-100% over 15 minutes (from 5-20 min) visualised at 254 nm.
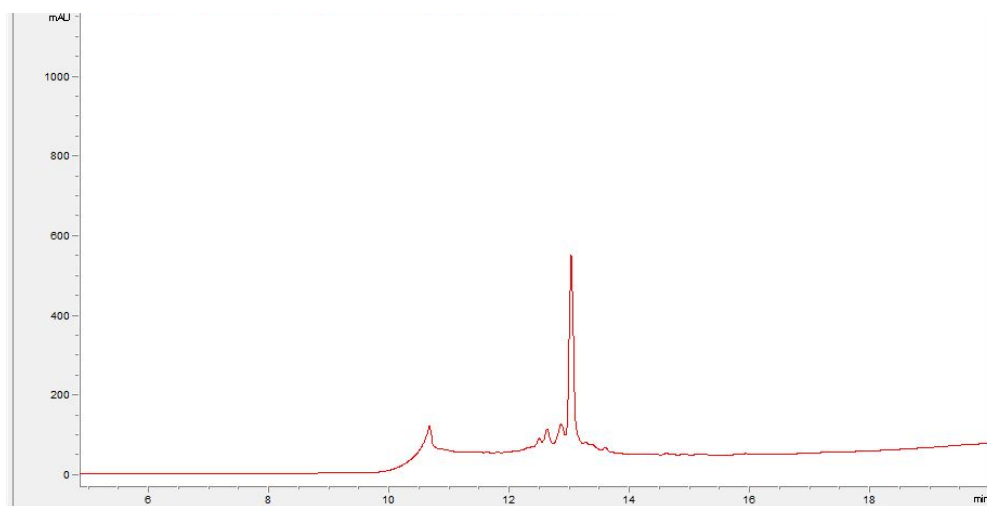
Figure S62: Analytical RP-HPLC C18 spectrum for **22d**, 0-100% over 15 minutes (from 5-20 min) visualised at 254 nm.

Figure S63: Analytical RP-HPLC C18 spectrum for **23**, 0-100% over 15 minutes (from 5-20 min) visualised at 220 nm.
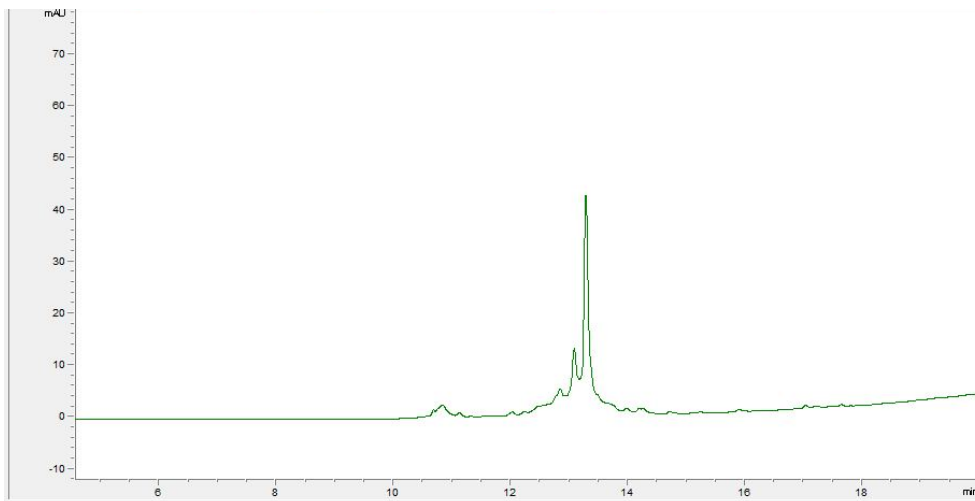

Figure S64: Analytical RP-HPLC C18 spectrum for **23m**, 0-100% over 15 minutes (from 5-20 min) visualised at 254 nm.

Figure S65: Analytical RP-HPLC C18 spectrum for **26**, 0-100% over 15 minutes (from 5-20 min) visualised at 220 nm.

Figure S66: Analytical RP-HPLC C18 spectrum for **26d**, 0-100% over 15 minutes (from 5-20 min) visualised at 254 nm.
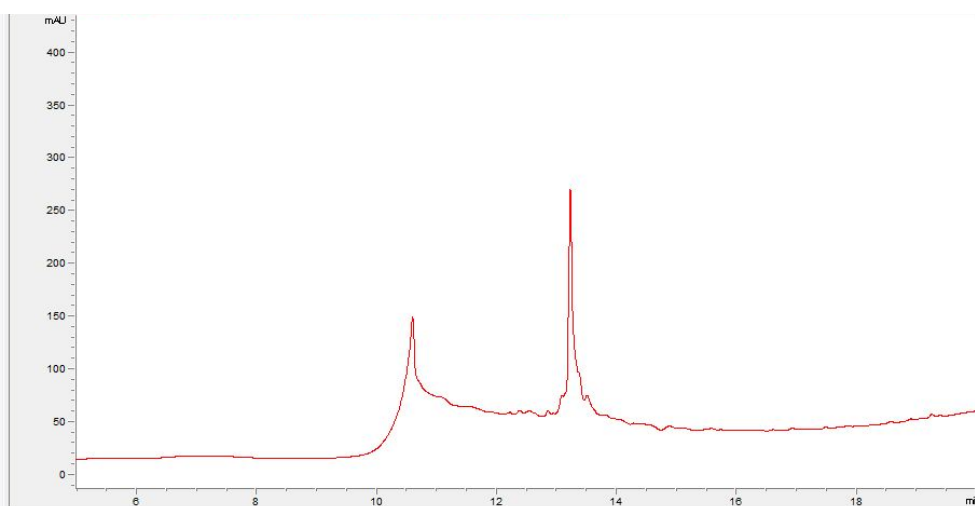

Figure S67: Analytical RP-HPLC C18 spectrum for **27**, 0-100% over 15 minutes (from 5-20 min) visualised at 220 nm.
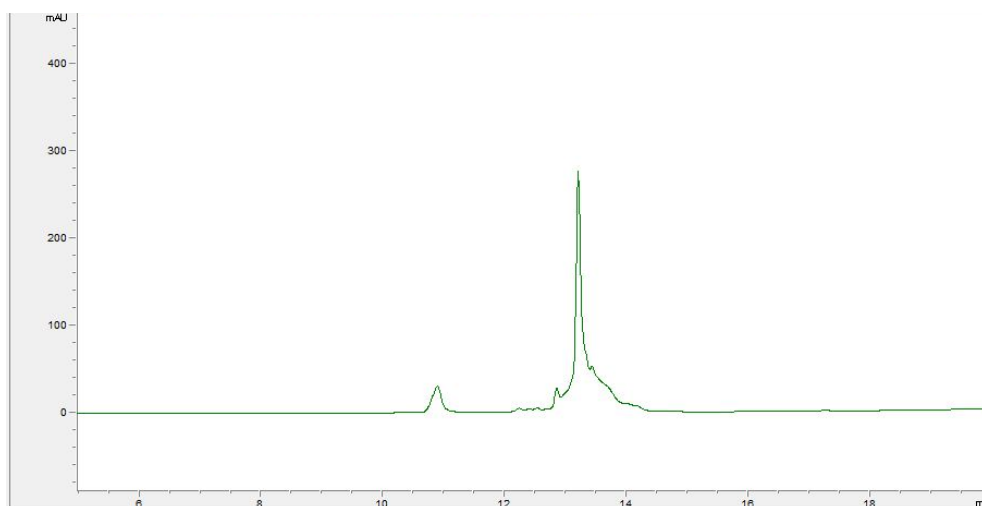
Figure S68: Analytical RP-HPLC C18 spectrum for **27d**, 0-100% over 15 minutes (from 5-20 min) visualised at 254 nm.

Figure S69: Analytical RP-HPLC C18 spectrum for **28**, 0-100% over 15 minutes (from 5-20 min) visualised at 220 nm.

Figure S70: Analytical RP-HPLC C18 spectrum for **28d**, 0-100% over 15 minutes (from 5-20 min) visualised at 254 nm.
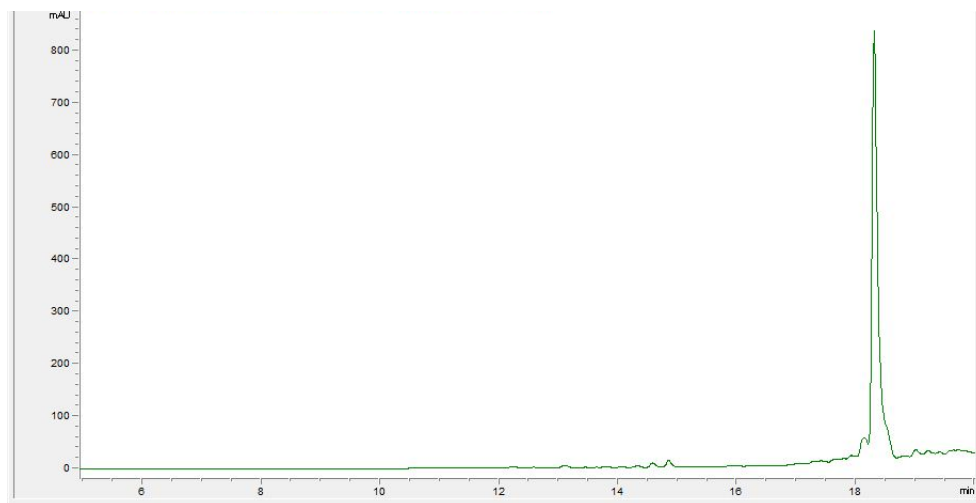
Figure S71: Analytical RP-HPLC C18 spectrum for **29d**, 0-100% over 15 minutes (from 5-20 min) visualised at 254 nm.
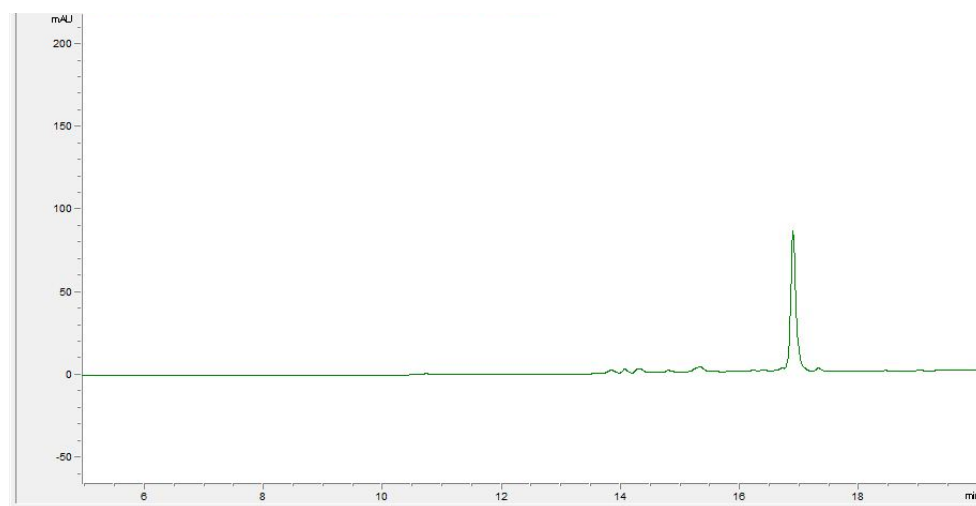

Figure S72: Analytical RP-HPLC C18 spectrum for **30d**, 0-100% over 15 minutes (from 5-20 min) visualised at 254 nm.